DIFFERENTIATION OF BONE MARROW DERIVED MESENCHYMAL STEM CELLS (BM-MSCs) USING ENGINEERED NANOFIBER SUBSTRATES

MICHELLE NGIAM LIMEI

(BACHELOR OF BIOMEDICAL MATERIALS SCIENCES, UNIVERSITY OF BIRMINGHAM, ENGLAND)

A THESIS SUBMITTED

FOR THE DEGREE OF DOCTOR OF PHILOSOPHY

NUS GRADUATE SCHOOL FOR INTEGRATIVE SCIENCES AND ENGINEERING

NATIONAL UNIVERSITY OF SINGAPORE

2010

Acknowledgements

I would like to give my heartfelt thanks to Prof. Seeram Ramakrishna for his tremendous encouragement, guidance and supervision throughout my PhD study. His zest for research excellence and knowledge often spurred me on to soar greater heights. In spite of his busy schedule, he always makes time for students and I am always amazed how promptly he replies to emails! He is a role model to me in more ways than one.

To Prof. Casey Chan, I am grateful to you for molding me into the person I am today. Amidst challenging times, Prof. Chan has been giving me his unconditional support and help. I have learned so much from Prof. Chan, to cultivate a thirst for knowledge and have a lifelong learning attitude. It is this man who gave me the opportunity to work under him. Without him, I might not even be making such a glorious exit from NUS. Indeed, I am one of the few who have worked under the very best, both Prof Chan and Prof Seeram. To Joan, thank you for being the sweet person that you are. I am blessed to know both of you and Prof Chan. I would also like to extend my sincere gratitude to Dr. Susan Liao, who has been such a great mentor and a friend to me. She has been such a joy to work with. The excitement of showing her my experimental results first-hand never fails me because she always see potential in my results, regardless of whether I think they are breakthrough or not! Her dedication and diligence in her work motivates me. It is amazing that she always seem to have the answers to any of my questions!

Special thanks to Miss Charlene Wang for her wonderful and constant assistance in the last but critical stage of my PhD study. Besides being my trusted assistant for my animal work experiments, she is also a friend. I would also like to thank Mr. Teo Wee Eong for his help and constructive suggestions for my project. To Miss Cheng Ziyuan, for teaching me some of the cell culture techniques. I would also like to thank the following people: Dr. Molamma P Prabhakaran and Dr. Jayarama Reddy Venugopal for their help whenever I am in doubt; Mr. Le Viet Anh, who spent over an hour trying to fix the wires of the electrospinning apparatus, despite him being busy with experiments and Miss Nguyen Thi Hien Luong, who worked along side with me in the bone research project. To the rest of the members of the Healthcare and Energy Laboratories, who have helped me in one way or another and for their friendship, Miss Anitha Panneerselvan, Miss Satinderpal Kaur, Miss Rajeswari Ravichandran, Miss Shayanti Mukherjee, Mr. Kai Dan, and Mr. Jin Guorui. To those who have left the lab, special thanks to Mr. Lennie Teng., Ram, Yixiang, Abhishek, Yingjun, Bojun and Tianfan, all of whom have helped me on various occasions. In addition, I am thankful to Yixiang who have introduced me the techniques of PCR techniques. I am very grateful to Dr Ralph M. Bunte for helping me with the histological analyses.

To my personal dear friends, Ma Kun and Huishan, thank you for your precious friendship and the invaluable work discussions we had. I will always relish the times we had in the lab. Soh Zeom and Priscilla, who are dear friends to me whom I would like to acknowledge. I would also like to extend my appreciation to Prof CT Lim's lab members,

such as Yuan Jian, Swee Jin, Sun Wei, Qingsen, Shi Hui etc., for always inviting me over to their lab during any celebratory events or outings.

I am grateful to NUS Graduate School (NGS) for Integrative Sciences and Engineering for the scholarship funding. My sincere appreciation to Prof. Michael Raghunath and Prof. James Goh for their efforts in helping me. To the administrative staff, such as Miss Irene Chuan, Mr. Marcus Chan, Mr. Steffen Ng, Miss Jasmin Lee and Miss Pang Soo Hoon, who have done a wonderful job in assisting me in all administrative matters.

Without my parents, I would not be where I am today. I am eternally indebted to them. Their unwavering spirit of love has sustained me throughout this period. Pa, Mummy, I love you both dearly. I am blessed to be your daughter. My brother, Shawn who has tolerated my antics all this years, thank you for being so accommodative to me and still loving me. The constant support, encouragement and understanding from my beloved boyfriend, Harville, who has made my life so much more enjoyable. Thank you for seeing me through good and tough times.

This dissertation is specially dedicated to my Lord Jesus Christ, who is the tower of my strength. It is He who made all things possible for me. He is the author and finisher of my faith, in the glorious completion of my PhD studies.

Publications

Journal Papers

1. **Michelle Ngiam**, Susan Liao, Timothy Ong Jun Jie, S. Ramakrishna, Casey K. Chan. Effects of mechanical stimulation in osteogenic and chondrogenic differentiation of bone marrow-derived mesenchymal stem cells on nanofibrous scaffolds. Journal of Bioactive and Compactable Polymers, Vol 26, 56-70, 2011.
   Impact Factor: 2.8

2. Dong Yixiang, Susan Liao, **Michelle Ngiam**, Casey Chan, S. Ramakrishna. Degradation behaviors of electrospun resorbable polyester nanofibers. Tissue Engineering B Rev, Vol 15(3), 333-351, 2009
   Impact factor: 4.582

3. **Michelle Ngiam**, Susan Liao, Avinash J. Patil, Ziyuan Cheng, Casey K. Chan, S. Ramakrishna. The fabrication of nano-hydroxyapatite on PLGA and PLGA/Collagen nanofibrous composite scaffolds and their effects in osteoblastic behavior for bone tissue engineering. Accepted in Bone. Fig.3b was selected for cover-art for July issue of Bone. Bone, Vol 45, 4–16, 2009
   Impact factor: 4.089

4. Susan Liao, **Michelle Ngiam**, Casey K. Chan, S. Ramakrishna. Fabrication of nano-hydroxyapatite/collagen/osteonectin composite for bone graft applications. Biomedical Materials, Vol 4(2), 25019-25027, 2009.
   Impact factor: 1.963

5. **Michelle Ngiam**, Susan Liao, Avinash J. Patil, Ziyuan Cheng, Fengyi Yang, Miguel J. Gubler, S. Ramakrishna, and Casey K. Chan. Fabrication of mineralized polymeric nanofibrous composites for bone graft materials. Tissue Engineering A, Vol 15(3), 535-546, 2009.
   Impact factor: 4.582

6. Liumin He, Susan Liao, Daping Quan, **Michelle Ngiam**, Casey Chan, S. Ramakrishna, Jiang Lu. The influence of laminin-derived peptides conjugated to Lys-capped-PLLA on neonatal mouse cerebellum C17.2 stem cells. Biomaterials, Vol 30(8), 1578-86, 2009.
   Impact factor: 7.365

7. Liumin He, Yanqing Zhang, Chenguang Zeng, **Michelle Ngiam**, Susan Liao, Daping Quan, Yuanshan Zeng, Jiang Lu, S. Ramakrishna. Manufacture of PLGA multiple-channel conduits with precise hierarchical pore architectures and in vitro/vivo evaluation for spinal cord injury. Tissue Engineering C, Vol 15(2), 243-55, 2009.
   Impact factor: 4.582

8. **Michelle Ngiam**, S. Ramakrishna, Casey K. Chan
   Patenting trends in nanofiber technology
   Recent Patents on Nanotechnology, Vol 1, 137-144, 2007.
   Impact factor: N/A.

9. Susan Liao, **Michelle Ngiam**, Fumio Watari, S. Ramakrishna, Casey K Chan
   Systematic fabrication of nano-carbonated hydroxyapatite/collagen composites for biomimetic bone grafts
   Bioinspiration and Biomimetics, Vol 2, 37–41, 2007.
   Impact factor: 1.367

10. Susan Liao, Fumio Watari , Guofu Xu , **Michelle Ngiam**, S. Ramakrishna , Casey K. Chan
    Morphological effects of variant carbonates in biomimetic hydroxyapatite.
    Materials Letters, Vol 61, 3624-3628, 2007.
    Impact factor: 1.940

11. Linda L. Lee, Casey K. Chan, **Michelle Ngiam**, S. Ramakrishna
    Nanotechnology patent landscape 2006
    Nano, Vol 1(2), 101–113, 2006.
    Impact factor: 1.008

12. Casey K. Chan, T.S Sampath Kumar, Susan Liao, Ramalingam Murugan, **Michelle Ngiam**, S. Ramakrishna
    Biomimetic nanocomposites for bone tissue graft applications
    Nanomedicine, Vol 1(2), 177-188, 2006.
    Impact factor: 5.982

Book Chapter

1. **Michelle Ngiam**, Susan Liao, Casey Chan, S. Ramakrishna
   Chapter 16 "Cell-based Nanocomposites and Biomolecules for Bone Tissue Engineering" published in "Advanced Biomaterials: Fundamentals, Processing and Applications", edited by Dr. Bikramjit Basu, Dr. Dhirendra S. Katti and Dr. Askok Kumar. Published in John Wiley & Sons, Inc., USA. pp 551-588.

Conferences

1. **Michelle Ngiam**, S. Ramakrishna. Biomimicking extracellular matrix proteins-Using nanoscale composites for tissue regeneration. *The 8th Pacific Rim Conference on Ceramic & Glass Technology*, 31 May-5 June 2009 in Vancouver, Canada (Invited oral presentation).

2. **Michelle Ngiam**, Susan Liao, Ziyuan Cheng, S. Ramakrishna, Casey K. Chan. Mineralized nanofiberous composite scaffolds for bone tissue engineering. *Orthopaedic Research Society (ORS) 55th Annual Meeting*, 22-25 February 2009 in Las Vegas, U.S. (Poster presentation)

3. Susan Liao, **Michelle Ngiam**, Timothy J.J Ong, Yixiang Dong, S. Ramakrishna, Casey K. Chan. Effects of Mechanical stimulation on bone marrow-derived mesenchymal stem cells. *Orthopaedic Research Society (ORS) 55th Annual Meeting*, 22-25 February 2009 in Las Vegas, U.S. (Poster presentation)

4. Casey K. Chan, Susan Liao, **Michelle Ngiam**, James W. Larrick, S. Ramakrishna, Michael Raghunath. Electrospun nanofibers for rapid capture of bone marrow-derived mesenchymal stem cells. *Orthopaedic Research Society (ORS) 55th Annual Meeting*, 22-25 February 2009 in Las Vegas, U.S. (Poster presentation)

5. **Michelle Ngiam**, Susan Liao, Ziyuan Cheng, Casey K. Chan, S. Ramakrishna. Fabrication of mineralized PLGA and PLLA based nanofibrous composites for bone tissue engineering. The 10th International Symposium on Biomineralization, 30 August- 4 September 2008 in Liangyungang, China (Invited oral presentation).

6. Susan Liao, **Michelle Ngiam**, Wee-Eong Teo, Casey K. Chan, S. Ramakrishna. Development of biomimetic nanocomposite scaffolds for bone tissue engineering

by electrospinning and mineralization *in vitro*. *8th World Biomaterials Congress*, 28 May - 1 June 2008 in Amsterdam, The Netherlands (Oral presentation).

7. **Michelle Ngiam**, Susan Liao, Casey Chan, S. Ramakrishna. Fabrication of mineralized electrospun polymeric nanofibrous composites for bone tissue engineering. *Tohoku-NUS Student Joint Symposium*, 10-12 May 2008 in Tokyo and Sendai, Japan (Oral presentation and conference proceeding).

8. **Michelle Ngiam**, Susan Liao, Casey Chan, S. Ramakrishna. Fabrication of mineralized polyglycolic acid nanofibers for bone tissue engineering. *Graduate Student Symposium in Biological and Chemical Engineering*, 14 September 2007, National University of Singapore (Oral presentation and conference proceeding).

9. **Michelle Ngiam**, Susan Liao, Casey K. Chan, and Seeram Ramakrishna. Biomimetic Polylactic Acid (PLLA) Nanofibers Composite for Bone Substitutes. International Conference on Materials for Advanced Technologies 2007 (ICMAT 2007), 1-6 July 2007, Singapore (Conference proceeding)

10. **Michelle Ngiam**, Tom R.Hayes, Santanu Dhara, Bo Su. Biomimetic Apatite/Polycaprolactone (PCL) Nanofibres for Bone Tissue Engineering Scaffolds. Bioceramics 19, *19th International Symposium on Ceramics in Medicine, The Annual Meeting of the International Society for Ceramics in Medicine*,10-13 October 2006 in Chengdu, China (Oral presentation). Proceedings of the 19th International Symposium on Ceramics in Medicine, 991-994, 2007 (Conference proceeding)

Table of Contents

Acknowledgements

Publications

Chapter 1: Introduction

Chapter 2: Literature Review

Chapter 3: Fabrication of mineralized polymeric nanofibrous composites for bone graft materials

Chapter 4: Osteogenic differentiation of bone-marrow derived mesenchymal stem cells on PLLA nanocomposites fibers

Chapter 5: 3D nanofibrous scaffold enriched with bone marrow stem cells for bone repair in critical size defects

Chapter 6: Bone regeneration in a rabbit ulnar model using novel 3D mineralized and non-mineralized PLLA/Col nanofibrous scaffolds

Chapter 7: Conclusions and recommendations

Summary

Bone loss caused by trauma or disease often renders the use of bone graft materials to facilitate bone healing. Autografts are still the gold standard treatment option. However, there are several drawbacks that are associated with the use of autografts such as patient site morbidity and limited availability of healthy bone especially in younger patients and elderly patients who might suffer from osteoporosis. As such, the use of bone graft substitutes (such as coralline hydroxyapatite (HA), bioglass, calcium-based materials etc.) provides an attractive alternative. However, such materials usually act as passive scaffolding, leading to the lack of bone remodeling. A myriad of research has focused on developing tissue-engineered bone grafts with the aim to replace the use of autologous bone grafts and improving on the clinical performance of the current state of bone graft substitutes. In this project, it was hypothesized that biomimetic mineralized nanofibrous scaffolds (NFS) mimicking natural extracellular matrix (ECM) provided efficient cell attachment and enhanced osteogenic differentiation to promote bone regeneration.

Structurally, bone encompasses fiber bundles that are made up of collagenous nanofibrils laced with HA nanocrystals. Electrospinning was used to produce the NFS to mimic the structure of the bone nanofibrils. The choice polymer used to fabricate the NFS was poly-l-lactide acid (PLLA). A biomimetic approach of nano-hydroxyapatite (n-HA) mineralization was employed on the NFS to attempt to mimic the native ECMin bone. Co-blending type I collagen (Col) with PLLA had shown to enhance n-HA deposition, due to the presence of nucleation sites for n-HA mineralization. Such rapid n-

HA deposition was achieved at room temperature. It was demonstrated that mineralized NFS enhanced early cell capture of osteoblasts within 30 minutes.

The osteogenic differentiation potential of bone marrow derived mesenchymal stem cells (BM-MSCs) was achieved by manipulating the physical, biochemical and environmental conditions. The nanoscale topography on the mineralized NFS was able to stimulate osteogenic BM-MSC differentiation without the use of any osteogenic supplements. Cell mineralization, a late osteogenic differentiation marker, which usually occurred on day 28 in culture, was seen after 14 days on mineralized NFS, where the BM-MSCs secreted bone nodules. The Ca/P ratio of the bone nodules was comparable to that of native HA in bone.

Since cells are subjected to different nanotextures within a 3D ECM niche *in vivo*, 3D NFS (nanoyarns) can be an effective carrier for rapid cell capture, which can provide an *in-situ* therapeutic bone graft option for bone regeneration. Mineralized nanoyarns were enriched with bone marrow aspirate and the cell capture rate was 80%. Biomimetic mineralized nanoyarns could augment bone healing due to its high resemblance to the native bone fibrils as seen in a rabbit model. Speckles of bone was observed within the defect site, suggesting that the presence of n-HA alone could elicit an osteoinductive bone formation process. Therefore, this study suggested that there was great potential for NFS to become efficient bone grafts.

List of Tables

List of Figures

List of Appendices

List of Abbreviations

Ab: Antibody

ALP: Alkaline phosphatase

AFM: Atomic Force Microscopy

ANOVA: Analysis of Variance

ARS: Alizarin red staining

BM-MSCs: Bone Marrow derived Mesenchymal Stem Cells

BCA: Bicinchoninic Acid

BET: Brunauer, Emmett and Teller analysis

α-TCP: Alpha-Tricalcium Phosphate

β-TCP: Beta-Tricalcium Phosphate

BM: Bone marrow

BMP: Bone Morphogenetic Protein

BSA: Bovine Serum Albumin

Ca-P: Calcium Phosphate

CFU-F: Colony Forming Unit-Fibroblasts

CFU-AP: Colony Forming Unit-Alkaline Phosphatase positive

COL: Collagen

CBAF-1: Core-Binding Alpha Factor-1

DAPI: 4',6-diamidino-2-phenylindole, dihydrochloride

DBM: Demineralized Bone Matrix

DCPD: Dicalcium Phosphate Dihydrate

DEX: Dexamethasone

DMEM: Low Glucose Dulbecco's Modified Eagle's Medium

ECM: Extracellular Matrix

EDX or EDS: Energy Dispersive X-ray Spectroscopy

FBS: Fetal Bovine Serum

FGF: Fibroblast Growth Factor

FTIR: Fourier Transform Infrared Spectroscopy

FDA: Food and Drug Administration

GFD: Growth Differentiation Factor

HA: Hydroxyapatite

H&E: Hematoxylin and Eosin

HFP: 1,1,1,3,3-hexafluoro-2-propanol

IGF-1: Insulin-like Growth Factor 1

LYM: Lymphocyte

MicroCT: Microcomputed tomography

MNGC: Multi-Nucleated Giant Cell

MSCs: Mesenchymal Stem Cells

n-HA: Nano-Hydroxyapatite

NFS: Nanofiber Scaffolds

PBS: Phosphate-Buffered Saline

PCL: Polycaprolactone

PLGA: Poly (D,L)-lactic-co-glycolic Acid

PLLA: Poly(L)-lactic Acid

RGD: Arginine-Glycine-Aspartic

rhBMP: Recombinant Bone Morphogenetic Protein

RT: Room Temperature

SEM: Scanning Electron Microscopy

TCP: Tissue Culture Polystyrene

TEM: Transmission Electron Microscopy

TGA: Thermal Gravimetric Analysis

TGF-β: Transforming Growth Factor-β

VEGF: Vascular Endothelial Growth Factor

VK: Von kossa

XRD: X-ray Diffraction

3D: Three-dimensional

2D: Two-dimensional

Chapter 1

Introduction

1.1 Background

Bone is the second most common transplantation tissue after blood. Globally, at least 2.2 million of bone grafting procedures are performed annually and approximately 500,000 of such procedures are done in the U.S. alone [3-5]. Fig. 1.1 shows the orthopaedic industry by market segments in the U.S [6]. As seen in Fig. 1.2, it is estimated that the orthopaedic market is set to generate revenues of over US$20 billion in 2010. The U.S., being the biggest player, is said to contribute 59% of the total world orthopaedic market share [6].

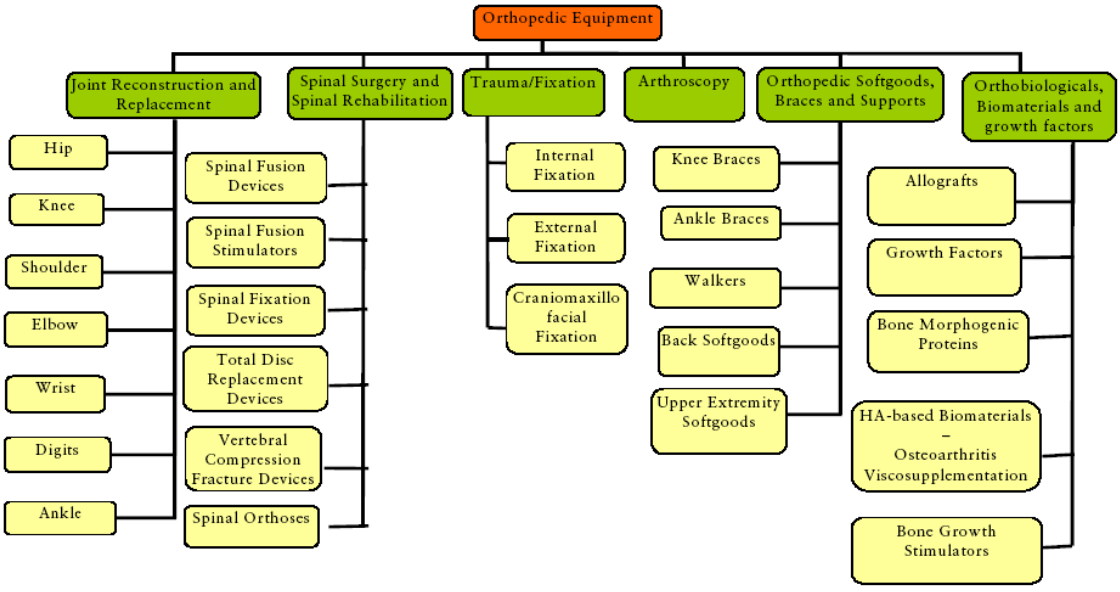

Fig. 1.1: Orthopaedic industry by market segments in the U.S. (Reprinted from [6], Copyright 2008, with permission from Frost & Sullivan)

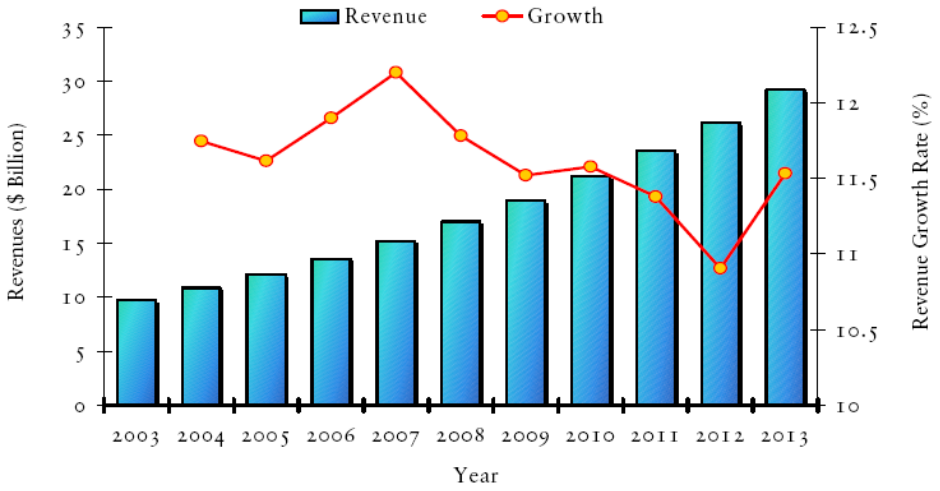

Fig. 1.2: Revenue forecasts in the orthopaedic market (U.S.) from 2003-2013. (Reprinted from [6], Copyright 2008, with permission from Frost & Sullivan)

The bone graft market alone is valued over US$2.5 billion [7]. Fig. 1.3 shows the overview of the revenue forecasts of bone grafts in the U.S., with allografts being the most popular choice [6]. This class of material is estimated to have a compound annual growth rate (CAGR) of 22.8%.

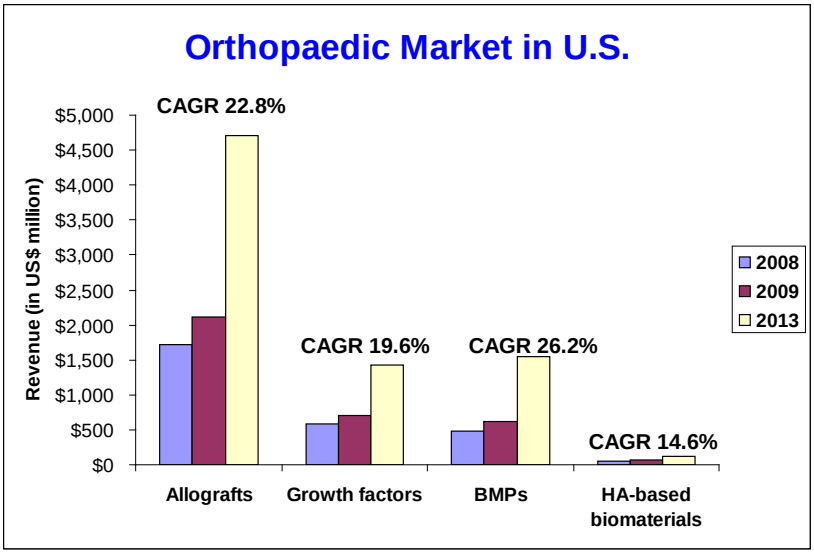

Fig. 1.3: Revenue of various segments of the orthopaedic market in the U.S., showing the compound annual growth rate (CAGR) for each segment. (Reprinted from [6], Copyright 2008, with permission from Frost & Sullivan)

Allografts are obtained from humans other than the patient's own tissue and the main advantages of allografts are their natural nanostructural assembly and the avoidance of donor site morbidity. Thorough disease screening needs to be done in order to reduce the risk of viral or bacterial infection transmission. Freeze-dried allografts usually have little osteogenesis as most of the osteogenic cells are destroyed, therefore synthetic bone grafts (usually calcium phosphate-based) provide an alternative bone graft option. Growth factors [e.g. bone morphogenetic protein-2 or -7 (BMP-2, BMP-7)] can be incorporated to improve their osteoinductive capabilities. The main drawbacks of these synthetic materials are that they are brittle, possess low mechanical strength, and depending on their fabrication methods, they can be highly crystalline (due to sintering at very high temperatures of more than 1000ºC). In addition, their structural and composition properties do not resemble natural bone.

The ideal bone graft should possess the three properties namely osteoconductivity, osteogenicity and osteoinductivity [8]. Osteoconductive graft materials provide biocompatible scaffolding that helps support new bone formation and growth. Osteogenic bone materials contain cellular elements (osteoprogenitor cells) which are at some stage of osteoblastic differentiation and these cells are able to synthesize new bone at the fusion site to form new bone directly. Lastly, osteoinductive graft materials facilitate the recruitment and differentiation of stem cells into osteoblasts. Understanding the composition, architectural, biophysical and mechanical properties of native bone would provide great insights in designing bone grafts for various applications.

Nanostructured materials are gaining new impetus owing to the advancements in material fabrication techniques, their unique properties (their nanosize/assembly/pattern effects on cellular behaviour) and breakthroughs in stem cell biology. The isolation of mesenchymal stem cells (MSCs) from various tissue sources has resulted in the interest to study the multiple differentiation lineages for various therapeutic treatments. The explosion in tissue engineering research has revolutionized our understanding in modulating stem cell fate and behavior, translating into potential clinical applications for regenerative medicine. Such nanostructured materials mimic the subtleties of extracellular matrix (ECM) proteins, creating artificial microenvironments which resemble the native niches in the body.

The understanding of material science, stem cell biology and signaling pathways (e.g. mitogen-activated protein kinase (MAPK) and phosphatidyl inositol-3-kinase (PI3K) etc.) is important to expedite expansion and differentiation of stem cells into tissue-specific lineages without changing the plasticity nature of the stem cells. Various biomaterial fabrication techniques aim to construct a microenvironment or niche similar to that in the body. During trauma and disease conditions, loss of tissue may occur and instead of being in homeostasis state, the stem cells migrate out of the niche and start their proliferative and differentiation work at the damaged site. Stem cells stored in the niche are exposed to an array of soluble chemokines, cytokines, growth factors, as well as insoluble transmembrane receptor ligands and ECM proteins [9].

In tissue engineering, material design is of utmost importance. Attempts have been made to fabricate scaffolds to mimic the chemical composition and structural properties of ECM because a tissue-engineered scaffold with these characteristics will have a better chance at enhancing tissue regeneration in the body. Structural proteins for example collagen are in the nanometer range and this nanotopography is said to affect cellular responses such as adhesion, proliferation, growth and differentiation.

1.2 Motivation

There is a central concept that cells attach and organize well on fibers that have diameters smaller than that of the diameter of the cells [10]. One of the key components of bone tissue engineering is the concept of ECM. ECM not only provides the structural and functional aspects of bone, it also provides key regulatory signals for cell proliferation and differentiation by cell-receptor interactions, mediating the diffusion of soluble growth factors and transmitting and attenuating mechanical signals [11].

Since the conceptual approach is to mimic native ECM, electrospinning technique is often employed to fabricate nanofibrous scaffolds (NFS). The nanofibrous meshwork mimics the protein nanofibrils in the native ECM. Moreover, the high surface area-to-volume ratio and its high porosity (with small pore sizes) allow efficient nutrient delivery, gas exchange and waste excretion. One of the characteristics of nanoscale scaffolds is the enhanced absorption of biomolecules such as vitronectin on the scaffolds due to a high surface area-to-volume ratio [12], which is important for e.g. wound healing, thereby creating a more favorable environment for cellular interaction. In addition,

biomineralization was significantly increased on NFS compared to solid-walled scaffolds [13]. For instance, when osteoblasts (bone cells) were seeded on both types of scaffolds, early bone markers such as runt-related transcription factor 2 (RUNX-2) protein and alkaline phosphatase (ALP) and middle-stage bone marker bone sialoprotein were higher on the NFS than on solid-walled scaffolds. Furthermore, the nanofibrous substrates seemed to promote protein adsorption such as fibronectin and vitronectin. Integrins that were associated with fibronectin ($\alpha v\beta 3$), vitronectin ($\alpha v\beta 3$) and collagen-binding ($\alpha 2\beta 1$) were also enhanced on NFS compared to solid-walled scaffolds. This implied that substrates had an influence on osteoblastic phenotype and cellular signaling, suggesting the superiority of NFS over solid-walled materials [13].

To mimic the nanocomposite nature of bone, efforts to develop newer compositions of synthetic bone graft substitutes to resemble the nano-hydroxyapatite (n-HA) and collagen fibrils composition of natural bone have been attempted. Collagen (Col), as one of the ECM proteins, plays critical role in bone mineralization, thus Col is a prime candidate material for tissue-engineered graft material. Type I Col has proven to be a good substrate for the binding of BMPs [14] and is also chemotactic to fibroblasts, because of its high affinity cell-binding domains [15]. Collectively, the activation of type I Col-specific integrins is said to have an osteogenic response to a bone cell line [16] and human bone marrow stem cells (BM-MSCs) [17] . In addition, collagen has been used in several commercial products such as Collapat II (Biomet Inc.), Collagraft (Zimmer Inc.) and Healos (DePuy Spine Inc.). Note that the above-mentioned commercial products are not tissue-engineering NFS. As collagen has a rapid adsorption rate and possess weak

mechanical strength, other polymers are often incorporated to enhance the mechanical properties of the material constructs. Besides, polymers lack cell recognition signals [18], and the addition of collagen provides the necessary binding sites for cell-material interactions. Polymer and collagen can be co-blended and then fabricated into NFS using the electrospinning method. In electrospinning, a high voltage field is applied to electrically-charge a liquid (the material of interest can range from polymers, collagen and salts that can be fully dissolved in the appropriate solvents), resulting in nanofibers. Calcium salts such HA [19], β-tricalcium phosphate (β-TCP) and calcium carbonate ($CaCO_3$) [20] can also be incorporated to improve the osteoconductivity of the material construct.

The importance of closely mimicking the natural composition (collagen and n-HA) of bone can be delineated in several studies [19,21,22]. For instance, enhanced mineral deposition (57% higher) was observed when osteoblasts were grown on poly-l-lactic acid/Collagen/HA (PLLA/Col/HA) nanofibers compared to PLLA/HA nanofibers, suggestive of the synergistic effect of collagen and HA in driving osteogenic differentiation and bone mineralization [22]. Many studies have shown that BM-MSCs are capable of differentiating towards an osteoblastic lineage [11,23,24]. It was shown that when MSCs were cultured on HA surfaces, osteo-specific genes were up-regulated [24,25]. Not only the viability of human MSCs was not affected, the expression of ALP, osteogenic genes and calcium mineralization of the MSCs were elevated when the cells were cultured on blended poly(lactic-co-glycolic) acid (PLGA) and n-HA nanofibers [26].

It was speculated that when the cells interacted with HA, potent inductive substances were released. Using this conditioned media after the initial culture, uncommitted MSCs were then cultured without the presence of HA and the upregulation of osteo-specific genes were observed [24]. Biological factors are often considered as they are said to meliorate cellular functions. The use of growth factors such as bone morphogenetic protein (BMP), fibroblast growth factor (FGF) [14,27,28] and osteogenic supplements (e.g. dexamethasone, β-glycerophosphate, ascorbic acid, vitamin D) [29,30] aims to induce osteogenic differentiation. Nanoscale disorder is capable of stimulating osteogenic stem cell differentiation without the use of chemical treatments [31]. Such geometric cues have demonstrated a dominant effect on adhesion, spreading, growth and differentiation of MSCs in several studies which will be described in Chapter 2.

The unmet medical needs include unreliable fusion and non-union, leading to implant or graft failure. For single-level lumbar fusion, the non-union rate is about 10-40% and this rate increases when multiple levels of fusion are attempted [4,5]. Large segmental bone defects (size larger than critical size defect) are difficult to treat, because of the extensive loss of bone and in many cases, the periosteum is also damaged [32]. The critical-size defect is said to be the smallest bone defect size that does not heal spontaneously on its own [33]. For instance, defects measuring 20 mm in length are considered as the size of a critical size defect in rabbit femurs [34]. The size of such defects which do not heal spontaneously is said to be dependent on the skeletal location, bone structure and presence/absence of vascular supply, acting load or stress, age, gender,

species, general health of the animal or individual [33]. The periosteum is an outer membrane encircling bone and serves as a reservoir of osteoprogenitor cells. During trauma or diseased conditions, compromised bone is often inevitable and thus, the bone's natural load-bearing capacity can be greatly hindered [32]. Other reasons contributing to the undesirable performance of most biomaterials include the poor surface interaction with the host tissue, resulting in the lack of adequate tissue formation around the biomaterials [35]. As some materials act only as passive scaffolding, insufficient remodeling occurs [35]. Moreover, current bone graft systems are not suitable for large bony defects of more than 5cm. The existing materials are often not available in sufficiently large quantities (e.g. autografts), and/or provide no load-bearing capability. Furthermore, current bone graft systems are usually blended systems and mimic native bone only at a micro-level. In this respect, the ultimate success of any bone graft healing is determined by whether the bones will grow together to form a solid bone mass.

1.3 Hypothesis and objectives

Hypothesis

Biomimetic mineralized NFS mimicking natural ECM provide efficient cell attachment and enhance osteogenic differentiation to promote bone regeneration.

(a) Electrospinning can be employed to fabricate nano-scale architectures in tissue-engineered bone grafts to resemble the natural ECM structure.

(b) The incorporation of collagen in NFS will improve n-HA mineralization on the fibers to mimic natural bone fibrils without the need for pre-treatment of the NFS.

(c) The presence of n-HA will improve the mechanical properties of mineralized NFS.

(d) The nanotexture features of mineralized NFS can provide nanotopographical cues and biomolecular cell signals for cell-scaffold interactions to improve osteoblast attachment and osteogenic differentiation.

(e) The nanoscale topography on mineralized NFS can stimulate osteogenic BM-MSC differentiation without chemical supplements.

(f) Since cells are subjected to different nanotextures within a 3D ECM niche *in vivo*, 3D NFS can be an effective carrier for rapid cell capture, which can provide an *in-situ* therapeutic bone graft option for bone regeneration.

(g) Biomimetic mineralized nanoyarns can improve bone healing due to its high resemblance to the native bone fibrils.

Objectives

- Utilizing electrospinning technique to fabricate PLLA and blended PLLA and Type I collagen (PLLA/Col) and employing a biomimetic approach of mineralization on the NFS to achieve efficient attachment of osteoblasts and osteogenic differentiation on mineralized fibers.

- Confirm the osteogenic differentiation potential of BM-MSCs by inducing BM-MSCs towards an osteogenic lineage *in vitro* by manipulating the physical, biochemical and environmental conditions.

- Utilizing electrospinning technique to fabricate 3D NFS (nanoyarns) and employing a biomimetic approach of mineralization on the NFS to achieve efficient cell attachment from bone marrow aspirate.

- Demonstrate the efficiency and efficacy of the biomimetic nanoyarn with or without autologous cell composite in a rabbit model.

1.4 Research rationale and strategy

Biodegradable electrospun NFS namely PLLA and blended PLLA/Type I collagen (PLLA/Col) were fabricated using the electrospinning technique. The NFS were further modified by n-HA deposition to obtain mineralized PLLA and PLLA/Col scaffolds to enhance osteogenic differentiation of osteoblasts and BM-MSCs.

Electrospraying of n-HA with polymeric NFS was not considered as the n-HA-reinforced NFS did not resemble the native bone fibrils [36,37]. The mineralized and non-mineralized PLLA/Col NFS were then used as bone grafts in a rabbit model, where rabbit bone marrow aspirates were incorporated for the rich and fast capture of cells in a 3D material construct to promote bone healing. The rationale of using mineralized and non-mineralized NFS/cell composites as bone grafts for bone healing in this study are as follows:

- Rapid n-HA deposition on NFS can be achieved at room temperature without the need of pre-treatment or surface modifications of the NFS.

- The biomimetic n-HA resembles the composition of native n-HA in bone.

- Mineralized NFS resembles the structure and composition of native bone fibrils.

- The architecture of the NFS mimics the nano-scale protein fiber meshwork in native ECM. The high surface area-to-volume ratio of NFS is efficient for cell adhesion, proliferation, migration and differentiation.

- The n-HA on NFS can provide nanotopographical cues for early cell attachment and osteogenic differentiation of osteoblasts and BM-MSCs.

- BM-MSCs have the potential of improving bone regeneration by differentiating into the phenotypes of bone cells and/or enhancing repair by providing a microenvironment that enhances the *in-situ* regeneration of local cells.

- Mineralized NFS can serve as a rapid cell capture substrate and carrier for *in-situ* clinical applications such as the application of bone marrow aspirates.

- The rapid and rich cell capture from bone marrow by mineralized NFS can be achieved at room temperature to emulate the temperature in a surgical suite.

- Autologous BM-MSCs will not elicit immune rejection after transplantation, unlike allogeneic BM-MSCs with immunosuppressive properties.

- The NFS has a high porosity (at least 80%) which is necessary for the efficient nutrient delivery, gas exchange and waste excretion after implantation.

- The NFS provide as an attractive alternative to autologous bone grafts, thereby circumventing donor site morbidity.

1.5 Work scope

In this dissertation, a comprehensive literature review is presented in Chapter 2 which includes the bone healing process, current treatments, properties of BM-MSCs and electrospun NFS for bone regeneration. As described in Section 1.3, the objectives will be carried out in three phases as seen in the Fig. 1.4. Table 1.1 summarizes the project

scopes from Chapters 3 to 6. Conclusions and recommendations for future work are described in Chapter 7 of this dissertation.

Unmet Medical Needs

- Unreliable fusion and non-union, leading to implant or graft failure.
- Undesirable performance of most biomaterials includes poor surface interaction with the host tissue, resulting in the lack of adequate tissue formation around the biomaterials.
- Current calcium phosphate-based grafts are usually blended systems and do not resemble the structural and composition of native bone.

Phase I
Fabrication of 2D nanofibrous scaffolds (NFS)

Objective (a): Utilize the electrospinning technique to fabricate PLLA and blended PLLA and Type I collagen (PLLA/Col) and employing a biomimetic approach of mineralization on the NFS.
Objective (b): Understand the cellular behavior of osteoblasts.
Objective (c): Understand the cellular behavior of the BM-MSCs

Phase II
Development of 3D nanofibrous scaffolds (nanoyarns)

Objective (a): Utilize the electrospinning technique to fabricate PLLA and blended PLLA and Type I collagen (PLLA/Col) and employing a biomimetic approach of mineralization on the NFS.
Objective (b): Evaluate the cell attachment efficiency on mineralized 3D nanoyarns.

Phase III
Investigation of the efficiency and efficacy of the 3D nanofibrous scaffolds (nanoyarns) in a rabbit model

Objective (a): Demonstrate efficiency and efficacy of the biomimetic nanoyarn as a potential bone graft in a segmental ulnar bone defect in a rabbit model.

Fig. 1.4: Flowchart illustrating the outline and flow of the research

Table 1.1: Overview of project scope

Hypothesis	Objectives	Descriptions	Thesis Chapter
(1) Electrospinning can be employed to fabricate nano-scale architectures in tissue-engineered bone grafts to resemble the natural ECM structure. (2) The incorporation of collagen in NFS will improve n-HA mineralization on the fibers to mimic natural bone fibrils without the need for pre-treatment of the NFS. (3) The presence of n-HA will improve the mechanical properties of mineralized NFS. (4) The nanotexture features of mineralized NFS can provide nanotopographical cues and biomolecular cell signals for cell-scaffold interactions to improve osteoblast attachment and osteogenic differentiation.	Utilizing electrospinning technique to fabricate PLLA and blended PLLA and Type I collagen (PLLA/Col) and employing a biomimetic approach of mineralization on the NFS to achieve efficient attachment of osteoblasts and osteogenic differentiation on mineralized fibers	(1) PLLA and blended PLLA/Col were electrospun and underwent n-HA mineralization. (2) Mineralized and non-mineralized NFS were further characterized for their material properties such as morphology, fiber diameter, wettability, X-ray diffraction (XRD) characteristics etc. (3) The viability and cellular behaviour of osteoblasts on the mineralized NFS were analyzed.	Chapter 3
The nanoscale	Confirm the	BM-MSCs were	Chapter 4

topography on mineralized NFS can stimulate osteogenic BM-MSC differentiation without chemical supplements.	osteogenic differentiation potential of BM-MSCs by inducing BM-MSCs towards an osteogenic lineage *in vitro*.	induced towards an osteogenic lineage with expression of osteogenic differentiation markers by manipulating the physical, biochemical and environmental conditions.	
Since cells are subjected to different nanotextures within a 3D ECM niche *in vivo*, 3D NFS can be an effective carrier for rapid cell capture, which can provide an *in-situ* therapeutic bone graft option for bone regeneration.	(1) Utilizing electrospinning technique to fabricate 3D NFS (nanoyarns) and employing a biomimetic approach of mineralization on the NFS to achieve efficient cell attachment from bone marrow aspirate. (2) Demonstrate the efficiency and efficacy of the biomimetic mineralized nanoyarn/cell composite in a rabbit model.	(1) PLLA and blended PLLA/Col 3D nanoyarns were electrospun. (2) Mineralization of PLLA/Col was employed and the material properties such as morphology, fiber diameter and mechanical properties were analyzed. (3) Rabbit bone marrow was aspirated and used for rapid cell capture in the mineralized PLLA/Col nanoyarn and implanted in a rabbit model.	Chapter 5
Biomimetic mineralized nanoyarns can improve bone healing due to its high resemblance to the native bone fibrils.	Demonstrate efficiency and efficacy of the biomimetic nanoyarn as a potential bone graft in a rabbit model.	Animal studies were conducted to demonstrate the capability of the nanoyarns as bone grafts in a rabbit model.	Chapter 6

Chapter 2

Literature Review

2.1 Introduction

Degenerative bone disorders such as osteoporosis, osteoarthritis (OA) and Paget's disease are common in the elderly and often lead to fractures of the bone. It is estimated that 40% of women over the age of 50 will experience an osteoporotic fracture. Consequently, joint diseases are prevalent in older patients, of which half of all chronic conditions will be associated with patients aged 65 years and above [38]. Paget's disease is a localized disorder of bone remodeling, affecting 2-3% of those over the age of 60 in the U.S [39]. Bone disorders such as osteogenesis imperfecta (OI) or brittle-bone disease, fibrous dysplasia are some examples which also call for therapeutic treatments. The prevalence of OI was reported to range from 1 per 10,000 to 1 per 20,000 live births [40]. In such instances, bone grafts are employed to treat the ramifications of these diseases that is, to replace the loss of the natural bone. Other cases which involve the use of bone grafts are trauma caused by either accidents or falls, and injuries due to sports. Conventional biomaterials which involve metals, ceramics and non-degradable polymers are permanent implants as these materials do not get resorb in the body. Yet, the risk of implant failure is prevalent and remnants of the failed implant will elicit an inflammatory response, hampering bone repair. This calls for a new generation of materials for bone applications, particularly tissue-engineered bone grafts which will be dealt with in this chapter.

2.1.1 Bone functions, structure and composition

Bone is a type of dense connective tissue that has several functions namely to perform mechanical, biological and chemical functions such as structural support, protection, movement, blood production, protection and storage of growth factors and mineral ion homeostasis. Bone encompasses of several hierarchical levels over many length scales as seen in Fig. 2.1 [41]. They can be broadly classified into five levels namely: (1) macrostructure (cancellous and cortical bone), (2) microstructure (osteons with Haversian canals ranging from 10 to 500 μm), sub-microstructure (lamella ranging from 1-10 μm), nanostructure (collagen fiber assemblies of collagen fibrils ranging from a few hundred nanometers to 1 μm) and sub-nanostructure (bone mineral crystals embedded within collagen and non-collagenous proteins that are below few hundred nanometers) levels.

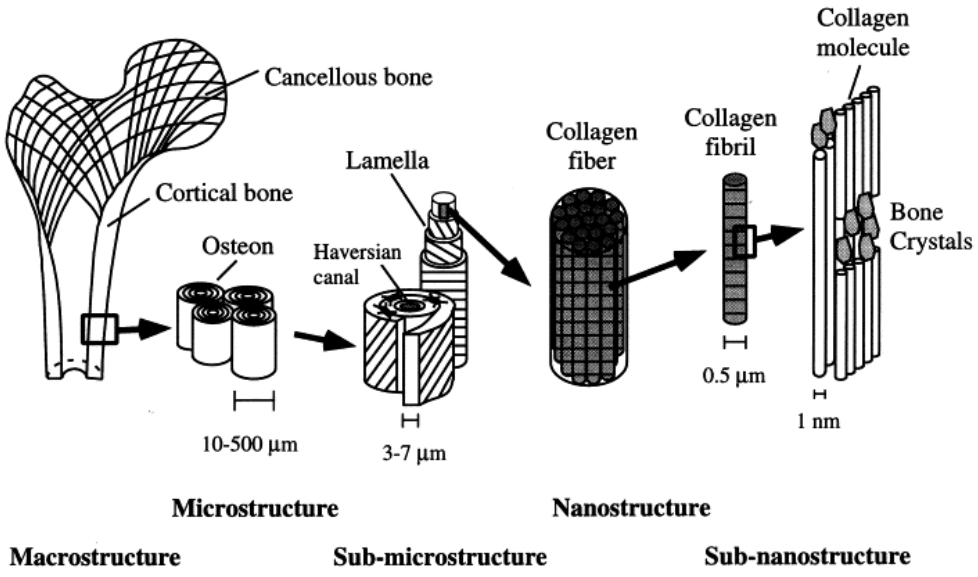

Fig. 2.1: Bone hierarchical architecture from macrostructure (cortical and cancellous bone), microstructure (osteons with Haversian canals), sub-microstructure (lamella), nanostructure (collagen fiber assemblies of collagen fibrils) and sub-nanostructure (bone mineral crystals embedded within collagen and non-collagenous proteins) levels. (Reprinted from [41] , Copyright 1998, with permission from Elsevier Limited)

As previously mentioned, bone is a nanocomposite with an intricate hierarchical structure, assembled through the orderly deposition of n-HA within a type I collagenous fibril matrix. Two-third of bone by weight is nanophase HA, which is the mineral constituent of bone [42]. Type I collagen is the main structural protein, contributing up to 30% of the dry weight of bone and 90-95% of the non-mineral (organic) content [42,43]. Collagen molecules are triple helices with a length of about 300 nm. The HA mineral crystals are embedded parallel to each other and parallel to the collagen fibrils, in a regularly repeating, staggered conformation (Fig. 2.2). Bone is a nanocomposite where cells reside on ridges, grooves, pores and fibers of the ECM. Besides collagen, non-collagenous proteins such as osteocalcin, osteopontin, osteonectin, bone sialoprotein etc. are part of the composition of bone. Other components also consist of calcium, phosphate, hydroxyl, carbonate, fluorine, sodium, magnesium, silicon, zinc and aluminum ions [42].

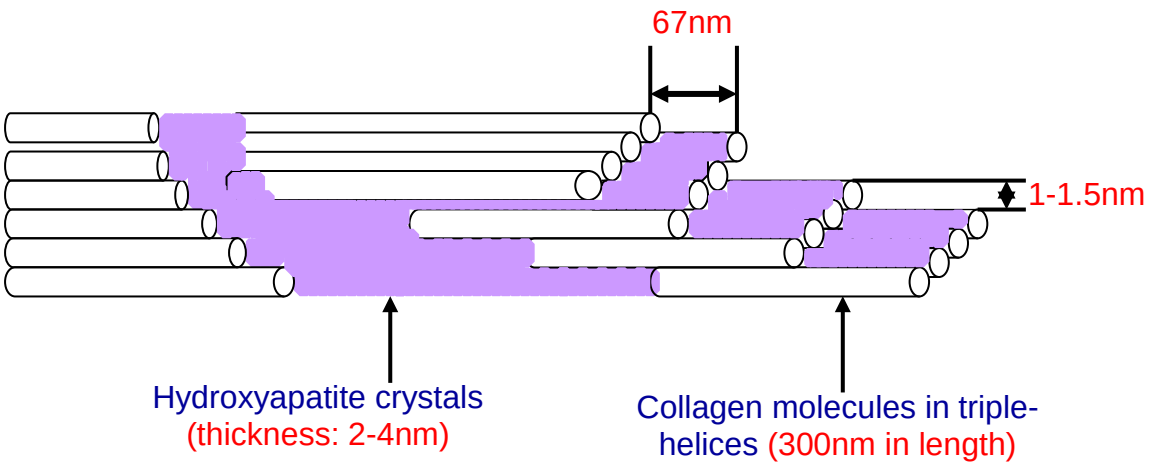

Fig. 2.2: Schematic of mineralized collagen fibrils of bone

The explosion in research towards designing nanocomposites for bone grafts are directed at polymeric nano-scale materials which closely mimicking the native bone

structure. One can envisage that cellular interactions and behavior such as adhesion, proliferation and differentiation on these nanotextured materials will be tremendously improve the osteogenic potential of these nanocomposites.

2.1.2 Bone regeneration *in vivo*

In bone remodeling, osteoclasts resorption precedes osteoblastic bone formation, thus the resorbed lacunae are filled with new bone produced by the osteoblasts. Fig. 2.3 shows the three phases of bone remodeling namely, initiation, transition and termination. Briefly, in the initiation stage, osteoclastic precursors are recruited followed by osteoclastic differentiation. In the transition phase, the multi-nucleated osteoclasts then resorb bone, which in turn induce osteoblastic differentiation. Secreted or membrane-bound molecules produced by osteoclasts act on osteoblastic precursors in order to stimulate bone formation. Some of the coupling effects can be seen in Table 2.1. In the resorbed lacunae, osteoclast apoptosis occur. Lastly, bone formation by the osteoblasts and osteocyte formation in the osteoid occur in the termination phase. Osteoblasts then become quiescent in the presence of sclerostin which is secreted through the osteocyte canaliculi. In addition, the osteoclastic differentiation is suppressed presumably by osteoprotegerin (OPG) produced by osteoblasts [44].

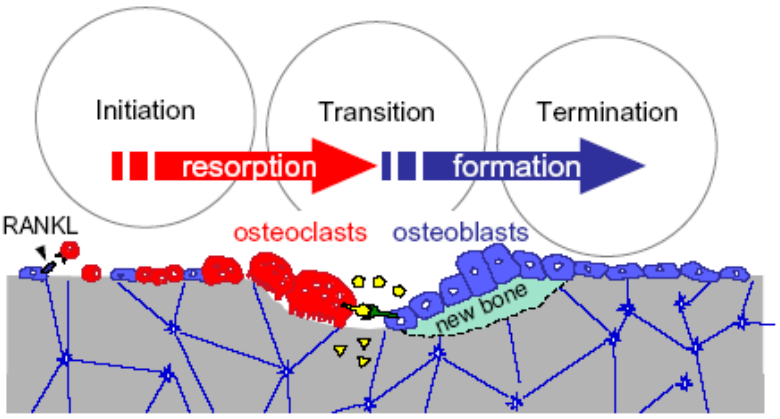

Fig. 2.3: Three phases in bone remodeling. In the initiation stage, hematopoietic precursors are recruited. Osteoblast lineage cells (blue) which express osteoclastogenic ligands (e.g. RANKL) elicit osteoclast differentiation. The osteoclasts (red) then form multi-nucleated cells to resorb bone. In the transition phase, osteoclastic resorption is followed by bone formation via coupling factors (e.g. membrane-bound molecules [yellow lollipops] and factors [yellow triangles]. Lastly in the termination stage, osteoblasts lay down new bone in the resorbed lacunae and forming a layer of lining cells over the newly-formed bone. Osteocytes (star-shaped) and canaliculi (blue lines) are within the bone matrix (gray) (Reprinted from [44], Copyright 2008, with permission from Elsevier Limited)

Table 2.1: Potential coupling factors produced by osteoclasts during the transition phase. (Reprinted from [44], Copyright 2008, with permission from Elsevier Limited)

Osteoclast		Osteoblast	Effects on osteoclast	Effect on osteoblast
TGF-β (matrix)[a]	→	TGF R	Various	Enhances bone formation
BMP (matrix)[a]	→	BMP R	Unknown	Enhances bone formation
IGF-II (matrix)[a]	→	IGF R	Unknown	Enhances bone formation
Cathepsin K	→	Unknown	Unknown	Enhances/inhibits bone formation
TRAP	→	GPC4 homolog, TRIP-1	Unknown	Enhances differentiation
Atp6v0d2	→	Unknown	Fusion	Suppresses bone formation
Sphingosine 1-phosphate (S1P)	→	S1P receptor	Attenuates differentiation (intracellular S1P)	Stimulates migration and survival, induction of RANKL (secreted S1P)
mim-1	→	Unknown	Unknown	Induces proliferation
PDGF BB	→	PDGF Receptor	Inhibits Differentiation by OPG	Suppresses Differentiation
HGF	→	HGF receptor	Stimulates migration and DNA replication	Stimulates DNA synthesis and proliferation
Wnt?	→	Frizzled, LRP5	Unknown	Enhances differentiation
OCIL	→	?	Unknown	Inhibits differentiation
?	←	OCIL	Inhibits differentiation	Unknown
c-Kit	←	SLF (membrane bound)	Suppresses differentiation	Enhances bone formation
ephrinB2	↔	EphB4	Inhibits differentiation	Enhances differentiation
Connexin	↔	Connexin	Regulates differentiation	Enhances differentiation and bone formation

→, signals from osteoclasts to osteoblasts. ←, from osteoblasts to osteoclasts. ↔, bidirectional.
[a] Embedded in bone matrix.

2.1.3 Acute healing *in vivo*

When bone undergoes trauma, leading to fractures, a combination of intramembranous and endochondral ossification takes place [45]. Subsequently, callus formation occurs. Immobilization by fixation prevents excessive motion at the fracture site, thereby minimizing the possibility of non-union. Intramembranous ossification happens when bone is formed directly without first forming cartilage from committed osteoprogenitor and undifferentiated MSCs that reside in the periosteum, further away from the fracture site. This results in callus formation. The bone marrow's contribution is vital during the early healing phase when the endothelial cells become polymorphic cells, thereby expressing an osteoblastic phenotype [46].

Endochondral ossification involves the recruitment, proliferation and differentiation of undifferentiated MSCs into cartilage which then gets calcified and subsequently replaced by bone. There are briefly six phases, namely (1) haematoma formation and inflammation, (2) angiogenesis and cartilage formation, (3) calcification of cartilage, (4) removal of cartilage, (5) bone formation and finally (6) bone remodeling. This type of fracture healing is contributed from the adjacent to the fracture periosteum and external soft tissues, giving rise to an early bridging callus [45].

There are several signaling molecules and cells that are involved in the initiation of the repair cascade such as pro-inflammatory cytokines, growth factors, platelets and MSCs [47] . Table 2.2 shows the list of signaling molecules that are involved in fracture healing.

Table 2.2: Various signaling molecules involved during fracture healing.
(Reprinted from [47], Copyright 2005, with permission from Elsevier Limited)

Signaling molecules	**Source**	**Function**	**Expression patterns**
Cytokines (IL-1, IL-6, TNF-α)	Macrophages and other inflammatory cells, cells of mesenchymal origin	Chemotactic effect on other inflammatory cells, stimulation of extracellular matrix synthesis, angiogenesis, recruitment of endogenous fibrogenic cells to the injury site, and at later stages bone resorption	Increased levels from days 1 to 3 and during bone remodeling
TGF-β	Degranulating platelets, inflammatory cells, endothelium, extracellular matrix, chondrocytes, osteoblasts	Potent mitogenic and chemotactic for bone forming cells, chemotactic for macrophages Targeted cells: MSCs, osteoprogenitor cells, osteoblasts, chondrocytes	Expressed from very early stages throughout fracture healing
PDGF	Degranulating platelets, macrophages, monocytes (during the granulation stage) and endothelial cells, osteoblasts (at later stages)	Mitogenic for mesenchymal cells and osteoblasts, chemotactic for inflammatory and mesenchymal cells Targeted cells: mesenchymal and inflammatory cells, osteoblasts	Released at very early stages of fracture healing
BMPs	Osteoprogenitor and mesenchymal cells, osteoblasts, bone extracellular matrix and chondrocytes	Differentiation of undifferentiated mesenchymal cells into chondrocytes and osteoblasts and osteoprogenitor cells into osteoblasts Targeted cells: mesenchymal and osteoprogenitor cells, osteoblasts	Various temporal expression patterns
FGFs	Monocytes, macrophages, mesenchymal cells, osteoblasts,	Angiogenic and mitogenic for mesenchymal and epithelial cells, osteoblasts, chondrocytes	Expressed from the early stages until osteoblasts

	chondrocytes	α-FGF mainly effects chondrocyte proliferation, β-FGF (more potent) involved in chondrocytes maturation and bone resorption Targeted cells: mesenchymal and epithelial cells, osteoblasts and chondrocytes	formation
IGFs	Bone matrix, endothelial and mesenchymal cells (in granulation stage) and osteoblasts and non-hyperthrophic chondrocytes (in bone and cartilage formation)	IGF-I: mesenchymal and osteoprogenitor cells recruitment and proliferation, expressed throughout fracture healing IGF-II: cell proliferation and protein synthesis during endochondral ossification Targeted cells: MSCs, endothelial cells, osteoblasts, chondrocytes	-
Metalloproteinases	Extracellular matrix	Degradation of the cartilage and bone allowing the invasion of blood vessels during the final stages of endochondral ossification and bone remodeling	-
VEGFs	-	Potent stimulators of endothelial cell proliferation	Expressed during endochondral formation and bone formation
Angiopoietin (1 and 2)	-	Formation of larger vessel structures, development of co-lateral branches from existing vessels	Expressed from the early stages throughout fracture healing

The expression profile of the various signaling molecules from the time of fracture to bone remodeling can be seen in Fig. 2.4. Certain growth factors such as bone morphogenetic protein-2 (BMP-2), FGF, transforming growth factor-β (TGF-β1) and insulin-like growth factor (IGF) were expressed from the onset of injury to the bone remodeling phase.

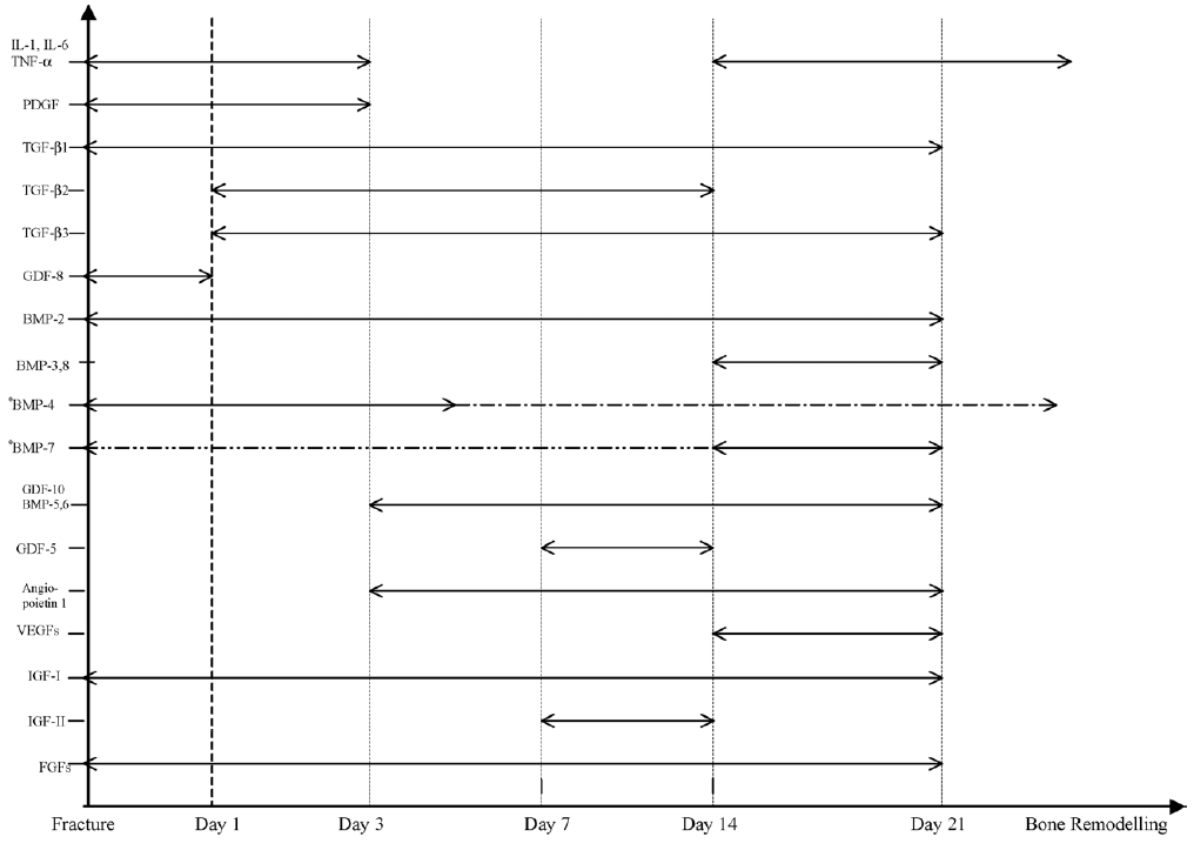

Fig. 2.4: Temporal expression patterns of various signaling molecules involved in fracture healing. Dashed lines represent differences in opinions by the scientists in terms of the timing of expression. (Reprinted from [47], Copyright 2005, with permission from Elsevier Limited)

2.1.4 Factors for bone regeneration

Besides diseases and trauma, there are several other factors which affect osteogenesis. In cell culture experiments, dexamethasone, ascorbic acid, β-glycerophosphate, 1,25-Dihydroxyvitamin D3 are supplements to formulate an osteogenic media to facilitate osteogenic differentiation of MSCs. For instance, dexamethasone stimulates proliferation and aid in the osteogenic lineage differentiation, ascorbic acid and 1,25-Dihydroxyvitamin D3 can be used for osteogenic induction, promotion of the deposition of matrix, increasing ALP activity and osteocalcin production [48]. Ascorbic acid plays a role in the conversion of proline residues in collagen to hydroxyproline. β-glycerophosphate acts as a form of phosphate supply and plays a role in mineralization and osteoblastic processes. Free phosphates can induce the expression of osteoblastic markers such as osteopontin [49]. Other functions of phosphates include the production and nuclear export of an important osteogenic regulatory gene called core-binding factor α-1 (Cbfa-1) [50]. Osteogenic supplements such as dexamethasone are often added in culture medium to direct osteogenic differentiation of either MSCs, progenitor cells or osteoblasts. Dexamethasone are bound to regulatory proteins and modulating the transcription of osteogenic genes [51,52]. Encapsulated human MSCs (hMSCs) exhibited an osteogenic effect when dexamethasone was released in a sustained manner over a month in a poly(ethylene glycol) (PEG) hydrogel due to the hydrolysis of the lactide ester bonds, where ALP and Cbfa-1 were enhanced [53]. Table 2.3 shows an overview of the effects of various culture media supplements for osteogenesis *in vitro* [54,55]. Some of the benefits of using differentiation medium are expansion of cell numbers, and cellular maturity, yet

there may be an increased risk of cell contamination during culture, cell aging, time loss in terms of direct application of cells into patient etc.

Table 2.3: Effects of Culture Media Supplements on Osteogenic Markers *In Vitro*
(Reprinted from [56], Copyright 2009, with permission from John Wiley & Sons Inc)

Cells	Function	References
Human bone marrow-derived primary osteoblasts	1. Dexamethasone enhanced ALP activity but not BMP-2 2. Dexamethasone caused the downregulation of Type I collagen 3. Osteocalcin synthesis was dependent on Vitamin D. Dexamethasone or BMP-2 alone had no effects on the basal osteocalcin levels but in the presence of Vitamin D and BMP-2 increased osteocalcin synthesis, whilst dexamethasone suppressed the production of osteocalcin 4. Parathyroid hormone-induced cyclic adenosine mono phosphate (cAMP) production was significantly increased with the treatment of dexamethasone 5. Mineralization was enhanced in cultures containing BMP-2 and dexamethasone elicited mineralization to a lesser degree 6. Dexamethasone significantly increased cell proliferation	[54]
Rat bone marrow stromal cells and osteoblastic MC3T3-E1 cells	**Bone marrow stromal cells** 1. Vitamin C was essential for doubling cell viability 2. Dexamethasone and β-glycerophosphate reduced the cell proliferation rate. On the other hand, BMP, TGF-β, vitamin D sustained the growth rate given by Vitamin C. 3. Vitamin C in Dulbecco's modified Eagle (DME) medium was vital for the rapid proliferation **MC3T3-E1 cells** 1. The incorporation of Vitamin C, Vitamin D, TGF-β and BMP did not give rise to a significant increase in cell proliferation	[57]

	2. Dexamethasone with Vitamin C and β-glycerophosphate increased the cell proliferation 3. There was no increase of cells in the samples treated with Vitamin C in DME medium	
Mouse embryo-derived NIH3T3 Fibroblasts	1. ALP activity was induced by 1 α, 25-dihydroxyvitamin D3 in a dose-dependent manner and enhanced in the presence of dexamethasone 2. Dexamethasone when used alone did not caused any detectable ALP expression 3. Osteocalcin and osteopontin were produced in the presence of 1 α, 25-dihydroxyvitamin D3 and dexamethasone 4. In the presence of β-glycerophosphate and L-ascorbic acid plus 1 α, 25-dihydroxyvitamin D3 and dexamethasone, extensive mineralization was observed 5. The expression of type I core binding factor alpha-1 (Cbfa-1) was not significant in samples treated with 1 α, 25-dihydroxyvitamin D3 and dexamethasone at 3, 10 and 20 days as compared to the controls No expression of type II or III Cbfa was seen regardless of time point or treatment	[58]
Adipose-derived stem cells	1. Vitamin D3, β-glycerophosphate and ascorbic acid were required for mineralization 2. Type I collagen secretion was upregulated by ascorbic acid and β-glycerophosphate 3. Vitamin D3 induced osteonectin, osteopontin and osteocalcin expression 4. Vitamin D3, β-glycerophosphate and ascorbic acid had a synergistic effect on sustained osteoblastic transcriptional gene expression such as RUNX-2 and transcriptional co-activator with PDZ-binding motif (TAZ). TAZ is a Runx2 transcriptional coactivator for osteocalcin expression.	[55]

BMPs are members of the TGF-β family that are potent stimulators of bone regeneration. For instance, BMP-2, BMP-7 etc. have been evaluated and it has been shown that they have the capability to heal bone defects *in vitro* and *in vivo*. One particular study demonstrated that by using recombinant adenoviruses expressing BMPs, besides BMP-2, BMP-6 and BMP-9 showed the highest osteogenic activity (to a lesser degree, BMP-4 and BMP-7) in both *in vitro* and *in vivo* settings. The osteogenic BMPs regulated a set of downstream target genes such as Ids, Dlx, and CTGF during the early stages of osteogenic differentiation [59]. Specifically, BMP-2 and BMP-7 are some of the predominant BMPs used and are able to induce osteogenic differentiation and bone healing. In a study involving 450 patients with acute, diaphyseal, open tibial fractures, the risk of secondary intervention was greatly decreased in the recombinant human BMP-2 (rhBMP-2) group as compared to the control group (standard of care for long bone repair) [60]. rhBMP-2 seeded on resorbable collagen sponge can be used in spinal fusion and open fractures in patients as it is FDA-approved. rhBMP-7 and bovine collagen or OP-1 are also FDA-approved and can be utilized as an alternative option to autografts in long bone non-unions and lumbar spinal fusion.

Despite the use of BMPs being potent inductors of osteogenic differentiation, the amounts of BMPs needed vary in humans and in animal studies. In humans, greater levels of BMPs are required for osteogenesis as compared to animals. It is evident that BMPs elicit a favorable response when added in culture medium or in material substrates. Yet there is variability in terms of patient response to BMP treatment and minute amounts of BMPs in the nanogram range are sufficient to trigger bone formation *in vivo*

[61-63]. Contrary, at least a magnitude of six orders was reported to result in osteogenesis in human with a matrix substrate [64]. A controlled delivery system of biomolecules or therapeutic agents can be achieved using tissue engineered biomaterials. Besides BMPs, other growth factors such as IGF-1, FGF-2 and vascular endothelial growth factor (VEGF) are also important for bone formation. Table 2.4 shows the types of growth factors used in polymeric substrates for bone repair [65,66].

Table 2.4: Types of Growth Factors Used in Various Materials for Bone Regeneration (Reprinted from [56], Copyright 2009, with permission from John Wiley & Sons Inc)

Materials	**Form**	**Growth Factors**	**Animal Model**	**References**
Collagen	Sponge	BMP-2	Goat, rat, rabbit	[67,68]
Gelatin	Hydrogel	BMP-2	Rabbit	[69]
		TGF-β1+IGF-1	Rat	[70]
Alginate	Hydrogel	TGF-β3+BMP-2	Mouse	[71]
PLGA	Scaffold	VEGF	Rat	[66]
		VEGF+BMP-4	Mouse	[65]
PLLA	Scaffold	TGF-β3	Sheep	[72]
HA/TCP	Porous implant	TGF-β2	Dog	[73]

Smad, Smurf and Tob proteins are also part of the intricate network of the osteogenic pathway [74]. The administration of such growth factors can be utilized in tissue-engineered constructs to induce bony formation. Certain secreting proteins such as Wnts are known to be involved in cellular differentiation such as osteogenesis [75].

Notch signaling had been said to have a non-promotive role in osteogenic differentiation of progenitor cells and ALP activity, osteocalcin, type I collagen and *in vitro* calcification were suppressive [76].

Heparan sulfate (HS) was assessed as a potential osteogenic agent in a rat model [77]. 5 µg of HS was incorporated in the fibrin glue scaffolds and the release kinetics were analyzed. Over 50% of HS was released with an initial burst phase in the first 4 hours, followed by a sustained release over 4 days at which 100% of HS was released. The released HS led to improved wound healing over a 3 month period and increased ALP, RUNX-2 and osteopontin gene expression. In contrast, minimal healing was seen in the absence of HS after 1 and 3 months of implantation [77]. Growth factors such as FGF-2 and BMP-2 were susceptible to proteolytic degradation [78]. As such, HS comes in handy as it binds to several soluble proteins such as heparin-binding growth factors, providing a protective shield from extracellular proteases and aiding specific binding to their respective cell surface receptors [79].

2.2 Types of materials for bone applications

There are a range of treatment options for bone regeneration. Autografts are often preferred as they are harvested from the patient's own body. In some instances where harvesting of autografts are not possible (e.g. inadequate supply of autografts, poor bone quality due to osteoporosis etc.), allografts and synthetic bone grafts can be considered.

2.2.1 Autografts and allografts

The gold standard for bone grafts is autologous bone grafts, also known as autografts, whereby healthy bone tissue is harvested from the patient and implanted in the diseased site. Some of the major advantages of autografts are that there is no immunological response due to host compatibility, the presence of osteoprogenitor cells and BMPs that are needed for bone regeneration. The main drawbacks are donor site immobility and risk of infection at the site of harvest. Allografts are grafts which are derived from another donor of the same species, often from cadavers that are freeze-dried. Some benefits of allografts include eliminating donor site morbidity caused by bone harvesting from the patient and a second operative procedure. One of the disadvantages of allografts is the possible immunological response in the patient as allografts are harvested from another donor. As such, there is a risk of disease transmission. Furthermore, donor shortage may also be an issue.

Demineralized bone matrix (DBM) is a processed product of allograft containing growth factors, collagen and proteins and it comes in various forms such as putty, injectable gel, granules or powder. Since DBM is further processed, the risk of disease transmission is reduced but it does not provide a strong framework for bone healing. Some researchers had attempted to combine autogenous bone grafts and DBM to treat tibial and femoral non-unions [80-82] whereby out of thirty femoral non-unions cases, twenty-four were healed within six months after surgical intervention. Four patients needed a second plate before healing took place and the remaining two cases were lost to follow-up. Others had shown that demineralized bone matrix gel could be used as a

supplement material to compensate the lack of autograft volume without compromising the fusion rates as of those who used autografts alone [83]. Different manufacturers have their own procurement, demineralization and sterilization procedures. Moreover, individual DBMs are often coupled with different carrier materials such as calcium sulfate, hyaluronic acid and glycerol. Donor variability is another concern in determining the osteoinductivity of the DBM material. It had been demonstrated that various commercially available DBMs exhibited different biological properties for the induction of spinal fusion in an athymic rat model [84]. As such, there is a medical need to address these pertinent issues by developing a new class of tissue-engineered bone grafts for orthopedic applications.

2.2.1.1 Drawbacks of current commercialized naturally-derived bone grafts

Table 2.5 lists the benefits and drawbacks of various naturally-derived bone graft materials.

Table 2.5: Properties of naturally-derived bone graft materials. (Reprinted from [85], Copyright 2006, with permission from Future Medicine)

Naturally derived bone graft materials	**Advantages**				**Disadvantages**
	Structural strength	Osteoconduction	Osteoinduction	Osteogenesis	
Autograft					Donor site morbidity
Cancellous	No	+++	+++	+++	
Cortical	+++	++	++	++	
Allograft					Risk of disease transmission

Cancellous	No	++	+	No	
Cortical					
Frozen	+++	+	No	No	
Freeze- dried	+	+	No	No	
Demineralized bone matrix (DBM)	No	No, depending on physical form	Variable	Variable	Bioactivity is highly dependent on the processing method
Bone marrow aspirate	No	No	+++	+++	Amount that can be extracted is limited. Cannot usually be used alone
BMP	No	No	+++	+++	Expensive. FDA-approved for limited applications

2.2.2 Synthetic bone grafts

To circumvent some of the deficiencies associated with autografts and allografts, scientists have come up with bone graft substitutes, which consist of systems based on DBM, bioceramics, BMPs, coral and composites. Although bioceramics such as tricalcium phosphate (TCP) and HA do not carry the risk of disease transmission, due to the lack of bioactive molecules, bone regeneration may be impeded or the repair may occur at a slower rate.

Calcium phosphate materials have been used as bone substitutes because they possess excellent biocompatibility and osteoconduction characteristics. Materials such as Bioglass®, TCP and HA are some bioactive ceramics used in orthopedic applications. Bioglasses consist of mainly silicon dioxide (mainly silicate), sodium oxide, calcium and phosphorus. Bioglasses exhibit both osteoconductive and osteointegrative properties [86].

Bioglass possesses bone bonding behavior, i.e. it can spontaneously bond to bone by forming a bone-like apatite layer on the surfaces. These materials are known to be bioactive ceramics. The formation of the apatite layer on the material/implant/bone surface is induced by functional groups such as Si-OH, Ti-OH, Zr-OH, -COOH and PO_4H_2 [87]. Calcium phosphates are usually used in bone defect filling in dental and orthopaedic applications. There are several calcium phosphates such as HA, TCP, octacalcium phosphate (OCP), dicalcium phosphate dehydrate (DCPD) and their properties depending on their Ca:P ratios, acidity and solubility. For example, the lower the Ca:P ratio, the higher are the acidity and solubility of the material. The acidity and solubility of the calcium phosphates reduce when the Ca:P ratios are closer to 1.67:1. The most commonly used and studied calcium phosphate is HA, as it resembles the mineral component of bone. HA can be used as coatings of joint prostheses to improve bonding properties. Other calcium phosphate materials include cements that can be resorbed and injected into the site of interest [42]. Table 2.6 summarizes the range of commercially available calcium-based bone graft materials. Some issues pertaining to these materials are inadequacies in bulk properties, lack of mechanical strength especially in load-bearing sites, problems in filling up large bony defects etc. Consequently, there is a medical need for a biomimetic material, which can be able to solve the above mentioned concerns, whilst improving bone formation *in vivo*.

Table 2.6: Various types of commercially available calcium-based bone graft substitutes. (Reprinted from [85], Copyright 2006, with permission from Future Medicine)

Product name	Company	Material
Allomatrix®	Wright Medical Technology	Demineralized human bone matrix in an osteosel medium (calcium sulfate powder). Injectable or malleable putty
CELLPLEX®	Wright Medical Technology	TCP synthetic cancellous bone
Collagraft®	Zimmer	Bovine collagen, HA and TCP available in granular and strip configurations
CONDUIT®	DePuy	Synthetic porous ceramic (TCP) granules
Endobon®	Merck KGaA	Sintered bovine cancellous bone blocks
NovaBone®	US Biomaterials	Bioactive glass (SiO_2 and minerals)
Osteosel®	Wright Medical Technology	Calcium sulfate pellets
Pro Osteon™	Interpore Cross	Coralline HA granules and blocks: 200, 500 and R forms. Harvested from marine coral exoskeleton that is hydrothermally converted to HA
SRS®	Norian	Calcium phosphate (carbonated apatite) injectable cement
TricOs™	Biomatlante	Biphasic calcium phosphate 60/40 HA/β-TCP granules
Vitoss®	Orthovita	Ultraporous β-TCP

Some researchers had successfully fabricated ceramic nanofibers such as HA and fluoro-hydroxyapatite (FHA) using an electrospinning technology [88]. The HA and FHA precursors were employed in sol-gel solutions and the solutions were subjected to aging and gelation processes. Subsequently, the sol-gel solutions were mixed with polyvinyl butyral (PVB) and used for electrospinning. By manipulating the sol concentration, the diameter of the fiber ranged from micrometers to nanometers in size (1.55 μm to 240 nm). Other processing factors which affected the fiber diameter to a lesser extent were the injection rate and field strength of the electrospinning parameters. Apatite polycrystallines (approximately 30 to 40 nm) were observed. The FHA nanofibers exhibited greater chemical stability than HA nanofibers [88] and the release of fluorine ions was said to be beneficial in dental restoration applications because fluorine

helped to prevent the dental caries formation and enhanced mineralization and bone formation [89,90].

Biphasic calcium phosphate scaffolds comprising of β-TCP matrix reinforced with HA nanofibers were produced by using a gel casting and polymer sponge techniques to improve material properties [91]. HA nanofibers were first synthesized via a biomimetic chemical precipitation method and incorporated with the β-TCP powder to make ceramic slurries. After polymerization of the monomers, a polyurethane foam with the desired shapes and sizes was then immersed into the ceramic slurries and subjected to sintering processes for the production of the nanocomposite scaffolds. The compressive strength and modulus increased as the HA nanofiber concentration increased. The HA nanofibers owing to their high surface energy could be easily diffused in the grain boundaries of the matrix during sintering. Scaffolds with 5wt% HA nanofibers had a compressive strength of 9.8 ± 0.3 MPa, comparable to the high end of the compressive strength of cancellous bone (2 – 10 MPa) [92].

In a separate study, bioactive glass nanofibers were electrospun with average diameters ranging from 85 to 400 nm [93]. The presence of polyvinyl pyrrolidone (PVP) and surfactant pluronic P123 (EO_{20}-PO_{70}-EO_{20}) resulted in the formation of smooth nanofibers and a reduction in diameter respectively. The nanofibers were subjected to simulated body fluid (SBF) whereby its ionic concentration was similar to human blood plasma and calcium phosphate nanoparticles were deposited on the nanofiber surfaces after six hours of SBF immersion. With increasing immersion periods, more apatite was

seen and after twenty-four hours of immersion, the bioglass nanofibers were entirely covered with apatite layers. Unlike conventional bioglass fibers, the induction of apatite was accelerated on the bioglass nanofibers and this could be explained by virtue of the fact that the nanofibers had a large surface area which promoted apatite deposition [93].

2.2.3 Tissue-engineered bone grafts

The principle of tissue engineering is to regenerate diseased/damaged tissue or organ by the use of biodegradable materials with or without biological factors. Through the extensive understanding of the structure and chemical composition of natural bone, bone grafts can be designed to mimic the native bone to achieve optimal performance.

The hype of fabricating nano-scale materials or the-like is due to the current advancement in nanotechnology, in areas such as electronics, filtration, catalysts, textiles, drug delivery etc. In particular, tissue engineering is making waves in the research and development arena because of the breakthrough discoveries of enhanced absorption of biomolecules such as vitronectin on the scaffold due to a high surface area-to-volume ratio [12], which can be useful for wound healing. Biodegradable materials are popular options for this new class of bone grafts. These materials can be either synthetic or natural polymers. Ultimately, researchers aim to develop bone grafts which surpass the status quo of existing bone grafts. A cocktail of growth factors and cells are usually integrated within the material as it is believed that the synergistic interactions between the material, cells and growth factors will improve the effectiveness of such regenerative therapies in bone repair as depicted in Fig. 2.5.

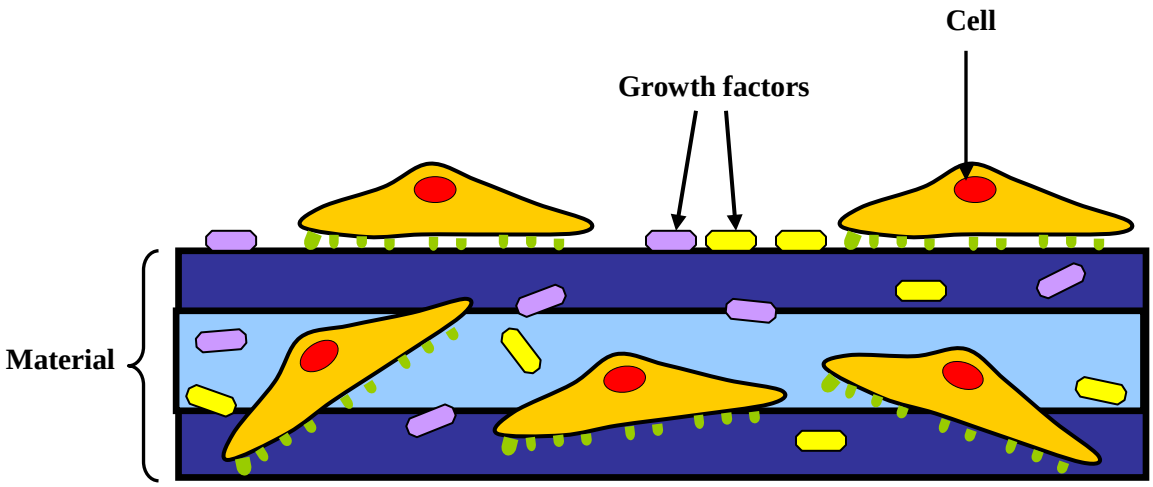

Fig. 2.5: A typical tissue-engineered material construct, with the addition of cells and growth factors (Reprinted from [56], Copyright 2009, with permission from John Wiley & Sons Inc)

It is of paramount importance that material selection should not be overlooked as the type of material plays a pivotal consideration of the success of bone tissue engineering as illustrated in this section of the chapter.

2.2.3.1 Types of polymers used for tissue-engineered bone grafts

2.2.3.1.1 Natural Polymers

Natural polymers such as collagen [23,94,95], gelatin [96], chitosan [97,98], alginate [96], hyaluronan [99], fibrin [100] and silk [101,102] are frequently used in bone tissue engineering. For instance, electrospun silk fibroin fibers were subjected to an alternate soaking method for nucleation and growth of apatite [102]. The fibers were first immersed in a calcium solution, followed by immersion in phosphate solution. Mineralization was achieved as apatite preferentially grew along the longitudinal direction of the fibers. The silk fibroin and acidic peptides allowed the controlled nucleation and growth of apatite minerals on the fibers [102]. In a separate study, porous

hyaluronan-based materials coated with fibronectin that were implanted in osteochondral defects in rabbits exhibited improved bone repair as compared to those without the implantation of the hyaluronan-based materials [99]. One of the drawbacks of natural polymers is the lack of mechanical properties and therefore, extensive investigations have been carried out in fine-tuning the material selection and design.

2.2.3.1.2 Synthetic Polymers

Synthetic materials are gaining popularity as alternative options because production scale-up is not an issue and they are mechanically better than natural materials. The commonly used synthetic polymers encompass poly(lactic-co-glycolic) acid (PLGA) [103,104], poly-l-lactide acid (PLLA) [105] and polycaprolactone (PCL) [106,107]. Polyglycolic acid (PGA) is often used in medical applications (such as sutures) because its degradable product, glycolic acid, is a natural metabolite. Glycolic acid can also be excreted out of the body as urine. Polylactic acid (PLA) is also used and it is generally more hydrophobic than PGA. PLA has three isomeric forms, namely d(-), l(+) and racemic (d, l). Poly(l)LA and poly(d)LA are semi-crystalline solids and have similar degradation rates as PGA. In general, the (l) isomer of lactic acid (LA) is preferred because it can be metabolized in the body. The degradation rate of PCL is slower than that of PLA and is a suitable material for long-term, drug delivery systems. One of the disadvantages of biodegradable synthetic polymers is the release of acidic by-productions during degradation [108]. Typically, a combination of ceramic-based materials is incorporated into the synthetic materials to aid in bone integration of the graft material to the native host tissue. n-HA/Col/ PLLA system was developed and it was shown that the

construct could support cell adhesion, proliferation and migration. Evidence of new bone formation and integration of the segmental defect in a rabbit model was also demonstrated [109].

2.2.3.2 Types of n-HA/Collagen-based composites used for tissue-engineered bone grafts

Calcium phosphate (CaP) coatings are commonly deposited on orthopedic implants to improve on the biological properties, especially at the bone-implant interface. Plasma spraying, laser deposition and ion beam deposition are some of the methods used to coat CaP on implants [110]. Studies had shown that nanoscale topography of materials favored cellular response. As such, the fabrication of nanophase HA has been evident in recent years. Electrostatic spray deposition, or electrospraying of n-HA is one such method, whereby n-HA particles were first synthesized via a precipitation reaction using calcium hydroxide ($Ca(OH)_2$) and orthophosphoric acid (H_3PO_4) with a Ca/P ratio of 1.67, similar to natural bone and subsequently, the n-HA particles were suspended in ethanol to form a ceramic slurry for electrospraying [111].

As natural bone is a nanocomposite, investigators explore the possibilities of fabricating nanocomposite materials to combine the properties of at least two individual materials. For instance, a composite was fabricated to act as a guided tissue regeneration (GTR) membrane for periodontal therapy [112]. This three-layered graded membrane consisted of one face of the material that was made of 8% nano-carbonated HA/Col/polylactic-co-glycolic acid (nCHAC/PLGA) porous membrane, the non-porous

opposite face that was made of pure PLGA and the middle layer that was made of 4% nCHAC/PLGA. The porous membrane allowed cellular penetration and the non-porous side of the membrane inhibited cellular adhesion. The composite was fabricated via a layer-by-layer casting method. As all three layers consisted of PLGA, the composite exhibited sufficient flexibility and mechanical strength. The nCHAC had the same constituent and had a nanocrystal size which was similar to that of natural bone [112]. As such, it could act as a template for mineralization to take place and attracting bone cells to the bone graft site during bone remodeling. PLGA is the choice polymer because it is biodegradable *in vivo*, and bone cells can deposit the osteoblastic components within the porous, degradable polymer over time, allowing it to be a suitable bone tissue engineered material, improving bone-biomaterial interface. Composites which do not contain collagen can be produced via a hot temperature method such as hot pressing. Recently, a biomimetic self-assembly method which has been developed is said to be suitable for fabricating collagen-containing composites because collagen degrades rapidly in environments higher than the body temperature of 37ºC [85]. In this method, illustrated in Fig. 2 [85], type I collagen was first dissolved in acetic acid. Aqueous solutions of Ca^{2+} and PO_4^- were added into the mixture for the initial nucleation of apatite. To adjust the pH of the solution, drops of sodium hydroxide were carefully added until the pH was approximately 8. At this time, calcium phosphates began to co-precipitate with the collagen. The precipitates were aged for 2 hours. n-HA could be retrieved via centrifugation [113,114].

The n-HA/Col nanocomposite had nano-sized bone like apatite, embedded in the collagen matrix. The three hierarchical levels namely the calcified collagen fibrils, collagen molecules and fibers showcased an example of a self-assembly biomimetic material, where the *c*-axes of the n-HA crystals were intimately aligned with the longitudinal axes of the collagen fibrils [113]. The n-HA and collagen molecules co-precipitated into mineralized collagen fibrils were approximately 6 nm in diameter and 300 nm in length as shown in Fig. 2.6 [113].

The presence of this bone-like mineral is one of the prerequisites of good interfacial bonding with the orthopedic implants with the host's bone (i.e. osteoconductivity) and may trigger osteogenic differentiation of progenitor or bone cells (i.e. osteoinductivity). Table 2.7 summarizes the various types of nanocomposites and their respective cellular responses [28,112,114,115].

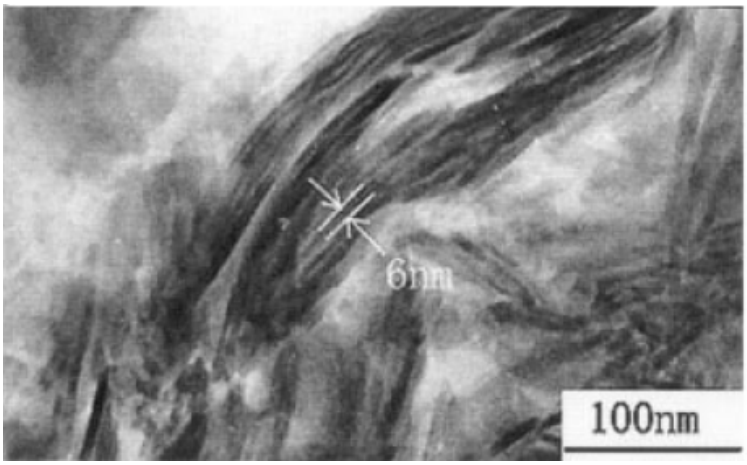

Fig. 2.6: Transmission electron micrograph of a biomimetic self-assembly n-HA/collagen composite (Reprinted from [113], Copyright 2004, with permission from Wiley InterScience)

Table 2.7: Biomimetic n-HA/collagen-based composite for bone tissue engineering (Reprinted from [56], Copyright 2009, with permission from John Wiley & Sons Inc)

Nanocomposite	**Cell/Growth factors**	**Tissue Reactions**	**References**
n-HA/Collagen	Osteogenic cells (*In vitro* and *In vivo*)	In a marrow cavity or bone fragment co-culture, interfacial bone formation at 2 weeks	[116-118]
n-HA/Collagen	Without/with BMP-2 (*In vivo*)	Resorbed by phagocytosis of osteoclast-like cells and form new bone in the surrounding area at 12 weeks	[119-121]
n-HA/Collagen	Chondroitin sulfate	No	[122-124]
n-HA/Collagen/PLA	Osteoblasts (*In vitro*)	In-growth 400μm depth of the porous scaffold	[125]
n-HA/Collagen/PLA	rhBMP-2 (*In vivo*)	8 weeks complete bone defect repair	[28,114]
n-HA/Collagen/PLGA	Osteoblasts (*In vitro*) (*In vivo*)	Enhance osteoblast and bone regeneration	[112,115]
n-HA/Collagen/Alginate	Fibroblasts/Osteoblasts (*In vitro*)	Positive affect on osteoblasts	[126]

The cell culture results were promising where osteoblasts adhered to the biomimetic PLA/Col/n-HA scaffolds within two days of culture and proliferated within the pores of the materials. Within a week, full confluence was achieved. The material

was then tested in an *in vivo* setting to evaluate its efficiency as a potential bone graft material [113]. A 15 mm segmental defect was made in the radius of twenty-four rabbits and the graft material was inserted into the defect with the incorporation of 0.5 mg of rhBMP-2. Observations were made at 4, 8, 12 and 16 weeks, with six samples at each time point. Histological observation also indicated that within 12 weeks post-implantation, complete healing occurred and double cortical bone was connected to the defect. Spherical cells adhered to the pores of the scaffold and appeared at the composite-new bone interface after 8 weeks. Trabeculae and bone marrow filled up the gaps left behind by the resorbed material. Furthermore, there was more trabeculae bone replacing the implant at 12 weeks than at 8 weeks. The n-HA/Col/PLA composite did not give rise to any acidic by-products unlike pure PLA materials as the pH value of the culture media did not change, enabling cellular processes to take place. Liao *et al* postulated that the mineralized collagen could play a role in neutralizing the acidic PLA products [113]. The porous nature of the scaffold provided a conducive environment for the deposition of bone matrix and mineralized collagen and could act as anchors for osteoblast adhesion. Further bone regeneration could be aided by the bone-cells in the scaffold [103,127,128]. Nutrient and waste transport were made possible via these pores as well. One study had reported that spinal fusion was achieved when rhBMP-2 in a collagen carrier was more homogeneous and underwent greater remodeling than when rhBMP-2 was in an autograft regardless of the presence of a collagen carrier. In addition, the incorporation of rhBMP-2 led to a stiffer and stronger spinal fusion than those using autologous grafts [129].

2.2.4 Potential of electrospun nanofiber scaffolds (NFS) as tissue-engineered bone grafts

The fibers or scaffolds being in nanometer scale (in diameter) are said to mimic the natural ECM, creating a more favorable environment for cellular interaction. For instance, electrospun NFS were fabricated from a mixture of PCL, type I Col and HA nanoparticles with an average fiber diameter of 180 ± 50 nm, was characteristic of the collagen fiber bundle diameter in native bone [130]. The presence of collagen in the nanofibers further improved the stiffness of the scaffold. In addition, the apatite particles were uniformly distributed on the fibers [130]. Electrospinning technology was also employed in producing hybrid membranes made of PLLA and HA [131]. The presence of HA particles enhanced the tensile strength of the hybrid membranes and the increased elastic modulus and lower strain at failure were indicative of the fact that HA nanoparticles had made the nanofiber matrix stiffer and less plastic in deformation [131]. Table 2.8 shows some examples of various types of nanofibrous composites that have been successfully fabricated using electrospinning [20,132,133].

Table 2.8: Electrospun Nanofibrous Composites with Calcium Salts (Reprinted from [56], Copyright 2009, with permission from John Wiley & Sons Inc)

Calcium Salts (Nanoparticles)	**Matrix**	**References**
Hydroxyapatite	Polyhydroxybutyrate-co-valerate	[132]
β-calcium phosphate	Polylactic acid	[134]
Hydroxyapatite	Polycaprolactone	[135]

Hydroxyapatite	Silk Fibroin	[133]
Calcium carbonate	Polycaprolactone	[20]

One of the advantages of NFS was that biomineralization was significantly enhanced on NFS than on solid-walled scaffolds [13]. Nanofibrous PLLA scaffolds with interconnected pores were made using a phase separation method. Osteoblasts were seeded on the scaffolds and higher alkaline phosphatase activity and an earlier and enhanced expression of Runx-2 protein and bone sialoprotein were observed on the NFS than on solid-walled scaffolds. In addition, the NFS seemed to promote the adsorption of proteins such as fibronectin and vitronectin as integrins associated with fibronectin ($\alpha v\beta 3$), vitronectin ($\alpha v\beta 3$) and collagen-binding ($\alpha 2\beta 1$) were present at higher amounts than those grown on solid-walled scaffolds. These observations seemed to have an impact on osteoblastic phenotype and cellular signaling, suggesting that nanofibrous materials were superior to solid-walled materials [13]. Improved mechanical properties and wettability were demonstrated on electrospun gelatin/PCL fibrous membranes as compared with pure gelatin or PCL membranes [136]. Not only bone marrow stromal cells were favorably attached on the gelatin/PCL, the cells migrated into the scaffolds up to 114 μm after 1 week of culture [136].

2.2.4.1 Techniques of fabricating NFS

Since the native ECM are of a nanofibrous structure, several methods have been developed to make nanofibers or NFS such as drawing, template synthesis, phase

separation, self-assembly and electrospinning. Table 2.9 shows the advantages and disadvantages of each technique. Briefly, drawing involves a micropipette that is submersed in a droplet of solution and withdrawn to draw a fiber. In template synthesis, the polymer is extruded through a porous membrane into a solidification solution for nanofiber formation. Phase separation is one method whereby separation of at least two different phases takes place, by the incorporation of polymer into a particular solvent; subsequently the freezing and freeze-drying processes give rise to a gel-like structure. For self-assembly method, smaller molecules act as building blocks to self-assemble fibers using specific bonds. Lastly, electrospinning uses a high voltage electric field to draw fibers out of a needle tip where the syringe is loaded with polymer solution as seen in Fig. 2.7 [137-140].

Table 2.9: Comparison of various fabrication methods of nanofibers (Reprinted from [141], Copyright 2007, with permission from Bentham Science Publishers Ltd.)

Method	Process	Comments
Drawing	A micropipette is submersed into a droplet of solution and withdrawn at a certain speed (e.g. 1 x 10^{-4} ms^{-1}) to draw a fiber	**Advantages** 1. Simple setup 2. Repeatability **Disadvantages** 1. Micro-sized fibers 2. Cumbersome 3. Not scalable
Template Synthesis	Extrusion of polymer through a membrane with nanosize pores into the solidification solution to form nanofibers	**Advantages** 1. Control of fiber diameter is possible 2. Ease of fabrication **Disadvantages** 1. Not scalable 2. Technically difficult to set up
Phase separation	Phase separation consists of the separation of at least two different phases by the	**Advantages** 1. Repeatability 2. Ease of fabrication

	addition of polymer into a solvent, followed by freezing and freeze-drying to obtain a polymeric gel-like structure	3. Simple setup **Disadvantages** 1. Not suitable for certain polymeric materials 2. Scaling up may be difficult
Self-assembly	Smaller molecules are used as building blocks for the self-assembly of fibers via specific bonds	**Advantage** 1. Smaller diameter nanofibers can be produced **Disadvantages** 1. Sophisticated process 2. Scaling up may be difficult
Electrospinning	This is a process which uses an electric field to draw fibers from the tip of a needle of a syringe which is loaded with a polymer solution to a collector plate	**Advantages** 1. Inexpensive equipment, therefore process is cost-effective in a lab setting 2. Long, continuous fibers with control of fiber diameter **Disadvantages** 1. Toxicity of solvent due to solvent evaporation 2. Instability of polymer jet causes collection of fibers difficult 3. Scaling-up is currently being solved

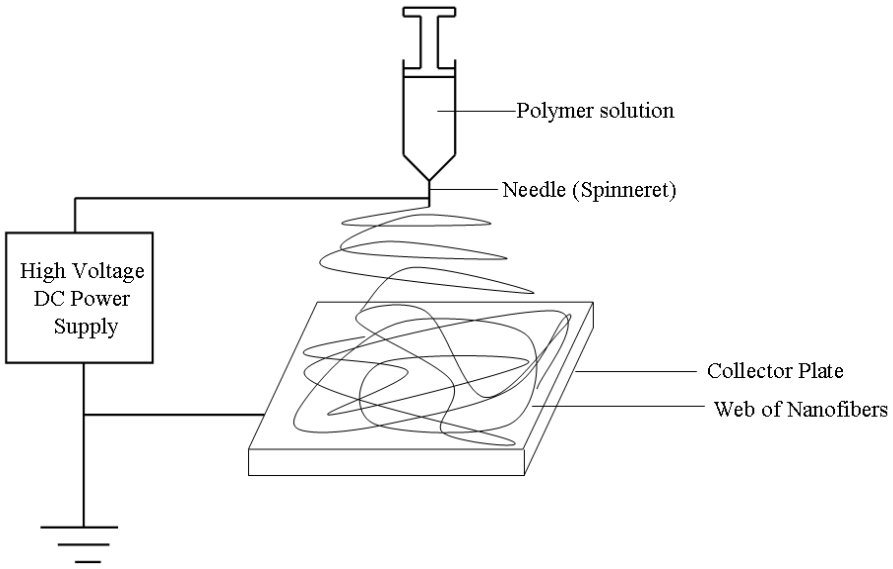

Fig. 2.7: Electrospinning set-up to fabricate nanofibrous mesh . (Reprinted from [141], Copyright 2007, with permission from Bentham Science Publishers Limited.)

Besides fabricating nanofibrous mesh, 3D nanofibrous conformation can be achieved using a modified electrospinning set-up as seen in Fig. 2.8 [142]. The aim of fabricating 3D scaffolds is to mimic the hierarchical structure of native tissues. The modified electrospinning set-up employs a liquid system where fibers are deposited directly onto the water surface and then subsequently drawn down the vortex into the collector (water tank) or a mandrel (Fig. 2.8). Liquid properties such as surface tension, viscosity and hydrodynamic interactions can be manipulated to achieve the desired nanofibers and various hierarchical organized nanofibrous assemblies can be obtained [143]. Bundles of aligned nanofibers and nanotexturing such as surface ridges and pores may be produced using this method of electrospinning [143].

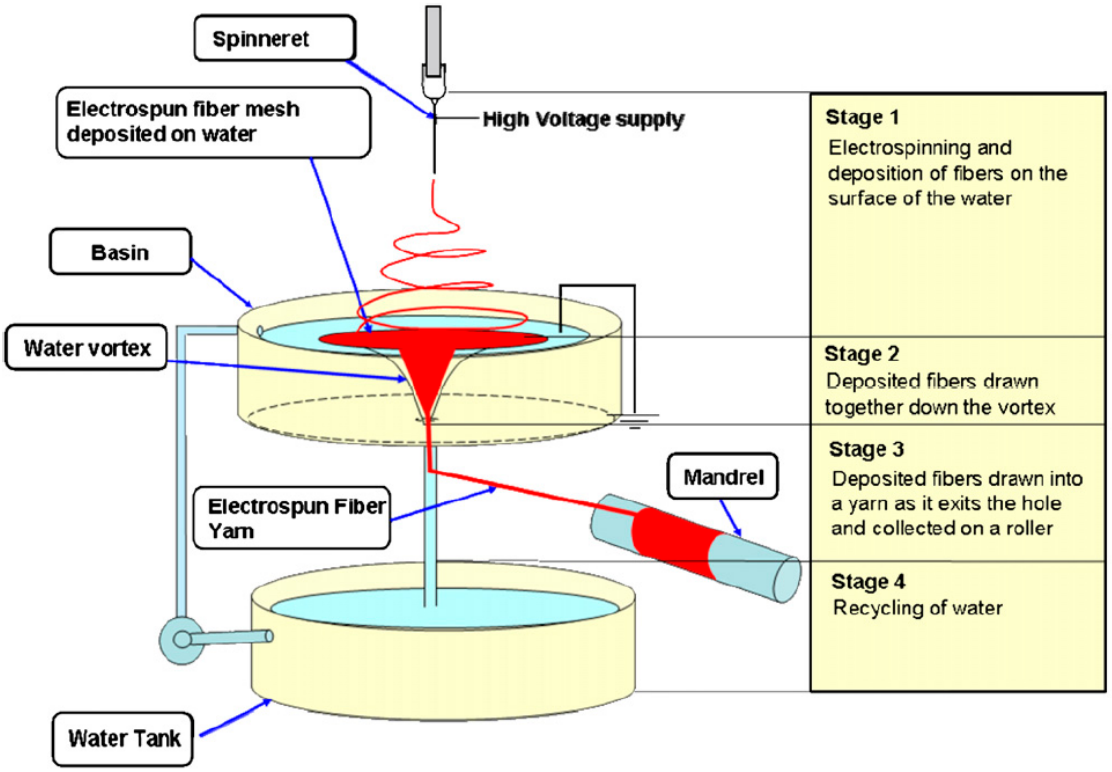

Fig. 2.8: Electrospinning set-up to fabricate 3D nanofibrous yarns or scaffolds. Bundles of fibers can either be collected on a mandrel or deposited directly into the water tank. (Reprinted from [142], Copyright 2007, with permission from Elsevier Limited)

The hierarchical assembly of a 3D scaffold aids to stimulate specific biological response such as cell attachment, proliferation, differentiation and maturation as it recreates the complex cellular microenvironment in the body. As such, there is a need for reproducible scaffolds to have specific and desired characteristics in order to modulate cell behavior. The surface topography and physical properties (or micro-architecture) such as the porosity, pore geometry and interconnectivity of the scaffold can affect cellular functions [144], thereby influencing tissue regeneration. Moreover, the 3D spatial organization affects the development and function of the tissues [145,146].

2.2.5 Peptide-based materials

In order to "coax" the native cells to adhere to the biomaterials, so that the cells would not view the material as a "foreign" object, peptides design and development have been gaining much attention, because these peptides contain adhesion domains of the ECM, thereby may have an impact on cell attachment, proliferation etc. and even inducing tissue formation.

Specifically, amphiphilic peptides with a carbon alkyl tail and other functional peptide motifs can be synthesized to form nanofibers via the self-assembly process [147,148]. Hosseinkhani *et. al.* demonstrated that the incorporation of the MSCs (that were isolated from the femurs of rats) into collagen sponge self-assembled peptide–amphiphile (PA) nanofiber hybrid scaffold in a bioreactor perfusion culture system had an impact on *in vitro* and *in vivo* osteogenic differentiation of the MSCs [149]. The hybrid material consisted of a hydrogel (PA) and a sponge (collagen sponge reinforced with polyglycolic acid (PGA) fiber). When the construct was subjected in a perfusion culture or static culture, bone formation was induced throughout the constructs, with those samples in the perfusion culture system exhibiting a greater and homogenous distribution of bone formation in a rat model. This was indicative that the flow velocity of the perfusion culture system accelerated the osteogenic differentiation of the MSCs [149].

A pivotal cell-binding domain of human Type I Col located in the α-1 (I) chain sequence (P-15) had been studied [150,151]. The P-15 peptide was said to facilitate bone formation, therefore this peptide had been used as a coating to mimic bone matrix components [152]. For instance, P-15 peptides were coated on anorganic bone mineral (ABM) particles and suspended in injectable hydrogels (such as hyaluronate (Hy), sodium alginate, carboxymethylcellulose) promoted cellular adhesion, osteoblastic activity and mineral deposition. Preferential adhesion of the osteoblast-like cells was observed on the hydrogels with P-15 peptide, with more cell coverage and scattering, suggestive that P-15 peptide had also reinforced cellular migration. In the presence of P-15 peptide on ABM (with or without hydrogel), more actin and stress fibers were seen as compared to ABM surfaces which had little cell spreading and stress fibers, indicative of the adhesive properties of P-15 peptide. The upregulation of gene expression (such as ALP, BMP-2 and BMP-7) was seen after ten days of culture and mineralized matrix deposition was more prominent after two weeks of culture in ABM/P-15/Hy than those in ABM/Hy [152].

From the above-mentioned observations, P-15 peptides seemed to stimulate bone repair and showed a synergistic effect on osteogenic inductors such as BMPs. Studies have shown that BMPs and TGF-β interact with collagen to promote osteoblastic processes [16,153]. Instead of using reconstituted collagen, some advantages of P-15 peptide include minimal batch variations, large scale production, ease of handling, greater stability etc [154,155]. One of the advantages of hydrogels is that they can be used in

any bony defect, regardless of size and shape, although one must be cautious about cell viability, and the possibility of hampering cell migration may occur.

To improve the osteoinductive properties of bioceramics, grafting of RGD-containing (Arg-Gly-Asp) peptides on HA by silanization, cross-linking and thiol bonding were done to mediate cell attachment [156] via the ligand-receptor interactions with ECM proteins such as collagen, fibronectin, vitronectin and laminin [157,158] . The advantage of using smaller peptides was that these peptides were more resistance to proteolysis and possessed greater affinities to integrin receptors [156]. Biomolecules such as peptides, proteins and other functional groups can be grafted onto the biomaterial's surface using plasma treatment without altering the construct's structural integrity and bulk properties, while improving the hydrophilicity of the material. Some groups had tried plasma-treatment as a form of surface modification on porous PLLA scaffolds to improve cell affinity [157]. A synthetic peptide derived from BMP-2 conjugated to a covalently cross-linked alginate gel was reported to show prolonged ectopic calcification, up to seven weeks in a rat model and inducing many osteoblast-like cells. Surprisingly, rhBMP-2 impregnated collagen gel showed maximum ectopic calcification after three weeks of implantation and the calcified products disappeared after five weeks. In addition, histological results showed that it induced many osteoclasts. Dense calcification was restricted in a particular region in the rhBMP-2 impregnated collagen gel, whereas the uniform calcification occurred in the BMP-2 peptide conjugated alginate gel. The results suggested that the peptide conjugated alginate gel

had greater stability than the rhBMP-2 impregnated collagen gel [159]. It was postulated that MSCs from the muscle tissue (implant site in the rat model) could have migrated into the alginate gel and osteoblastic differentiation occurred after the stimulation of the BMP-2 derived synthetic peptide. Subsequently, the osteoblasts then released phosphorus ions and the carboxyl functional groups of the alginate gel stimulated apatite nucleation, with the HA crystals being deposited on the gel [160]. Other synthetic peptides such as B2A2 which promoted rhBMP-2 bioactivity or B2A2-K-NS (an analog of B2A2) was said to improve osseous phenotypes in an osteoinductive environment [161,162].

2.2.6 Gene-based materials

Gene-based factor delivery systems can be designed in such a way that a gene encoding a target protein can be delivered. In this way, the upregulation and downregulation of a desired protein can be achieved. In bone repair, the upregulation of BMPs is generally favored.

Some of the drawbacks of delivering osteoinductive growth factors from the material constructs are that growth factors are easily degradable and the material processing may destroy them. Until now, there is no gold standard in terms of the optimal dose levels of growth factors to be added. By and large, the using of gene therapies in bone applications renders much attention as this facet of study provides an alternative option to bone repair. In essence, vectors are viral (e.g. retroviruses,

adenoviruses etc.) or non-viral (e.g. cationic lipid (CL) formulations etc.) tools that can be used for the delivery of recombinant proteins via the transfection, i.e. transfer of DNA to the cell nucleus, that are applicable in either an *in vitro* or *in vivo* setting. For instance, the delivery of a gene encoding for an osteoinductive factor to target the cell-of-interest can galvanize the cells to produce the necessary factors at the location of bone pathology. The *in vivo* approach of gene therapy is to inject the genetically-modified vector or plasmid into the patient, although there might be interferences such as the possibility of not being able to transfect the desired cell type or recombination with a wild-type vector. Alternatively, the patient's cells can be harvested and expanded *in vitro* prior to transfection before implantation. Nevertheless, this process is more cumbersome and time-consuming.

Bone marrow stromal cells that were isolated from rats were transfected with an adenovirus encoding cDNA for rhBMP-2 and seeded on PLGA/HA microspheres. In co-culture experiments (primary human MSCs and transfected cells), BMP-2 produced by the transfected cells promoted osteogenic differentiation and mineralization, with a significant increase in proliferation, ALP and calcium deposits than those MSCs which were co-cultured with non-transfected cells [163].

In another case, retrovirus encoding the CDNA for BMP-2 was used to transfect a murine stromal cell line and the transfected cells were cultured on the PLGA/HA material for a week [164]. The results showed that the transfected cells were attached onto the

material and proliferation was seen. BMP-2 was also continually expressed by the transfected cells. The material specimens were then implanted into the quadriceps muscle porch of severe combined immunodeficient (SCID) mice, with three sample groups namely PLGA/HA with 3 µg of rhBMP-2 (positive control), PLGA/HA with BMP-2 producing W-20 cells and PLGA/HA with non-transfected W-20 cells. No bone formation was observed in the PLGA/HA with non-transfected W-20 cells, unlike for the PLGA/HA with the BMP-2 producing cells and PLGA/HA with rhBMP-2 groups. This was indicative of the potential application of retroviral gene transfer in concert with an appropriate material for bone regeneration [164].

Non-collagenous molecules in bone such as dentin matrix protein 1 (DMP1) have been reported to be involved in apatite nucleation [165,166]. Using genetically-engineered silk DMPI, combined with SBF treatment, calcium-deficient carbonated HA was formed. It was found that the carboxyl terminal domain of DMP1 induced HA nucleation. HA was absent in samples with no carboxyl terminal domains of the DMP1. Such studies had shown that other macromolecules besides collagen, were involved in HA nucleation and deposition [165].

Recombinant collagen technology has also been investigated extensively. It has been shown that recombinant human-like collagen synthesized from *Escherichia coli* (*E.coli*) underwent mineralization when the collagen was subjected to a series of chemical treatments involving $CaCl_2$ and NaH_2PO_4 solutions [167]. n-HA crystals were deposited on the recombinant collagen fibrils, forming mineralized collagen fibers and

the crystallographic *c*-axis alignment of the n-HA crystals was parallel to the longitudinal axis of the collagen fibrils [167].

2.3 Types of cells used in bone tissue engineering for osteogenic differentiation

Work in the last decade includes evidence that stem cells possess self-renewal, multi-lineage differentiation and *in vivo* functional capabilities. The stem cells of interest include mainly embryonic stem cells (ESCs) and MSCs, although hematopoietic stem cells (HSCs) are extensively studied as well. ESCs are derived from the inner cell mass (ICM) of blastocyst-stage five-day embryo [168]. They possess high proliferative capability [169,170], are able to form three embryonic germ layers (endoderm, mesoderm and ectoderm) [168], produce germline chimaeras [171], exhibit differentiation in teratomas [168] and express specific ESC markers [168]. Human ESC (hESC) was isolated in 1994 [172]. Coincidentally, the generation of hESC lines [168] and human embryonic germ cell lines from aborted fetus [173] were established. ESCs are capable of becoming any specialized cells and can be useful for drug screening assays. However, the safety and efficacy of hESC lines may be a concern. These include technical issues such as potential of hESC rejection and the risk of tumorigenicity. There are also ethical and religious issues involving the harvesting of donor oocytes and destruction of the blastocyst. A recent study shows that the bone nodules that are formed by osteoblasts and MSCs exhibit the hallmarks of native bone, whereas those are formed by ESCs differ in terms of composition, stiffness and nano-architecture [174]. As such, MSCs provide an attractive alternative to ESCs and these cells can be readily obtained with less

controversy from bone marrow [175], umbilical cord blood [176] and adipose tissue [177]. More importantly, MSC has a versatile differentiation profile. Autologous MSCs surmount immune rejection and carcinogenesis is minimized. Several reports stated that MSCs facilitate bone repair [27,178,179] . In the light of the fact that the number of MSCs in bone marrow is low, the expansion of MSCs is often necessary prior to implantation. The number of MSCs in marrow was said to be approximately 1 in 100,000 cells [180]. Usually, about 100 to 500 attached bone marrow-derived MSCs are obtained from 50 to 100 million cells that are introduced into culture [181]. The minute number of MSCs (especially as donor age increases), tissue regeneration capability through self-renewal and proliferation are also limited. As such, to improve the proliferative and differentiation capabilities of MSCs, more attention has been devoted towards material selection and modification and/or the use of culture supplements and techniques.

2.3.1 Potential of mesenchymal stem cells (MSCs) for bone healing

MSCs are non-hematopoietic stem cells which have the ability to become many tissues such as bone, adipose, cartilage, skin, muscle and tendon etc. MSCs can be derived from several sources and comprehensive studies have been done in hope of determining the ideal source of MSCs for bone applications as discussed in the subsequent sections of this chapter.

2.3.2 Potential of bone marrow derived mesenchymal stem cells (BM-MSCs)

Pittenger *et. al.* indicated that by using stem cells from bone marrow aspirates from humans, the undifferentiated cells had the potential to differentiate into several lineages namely osteogenic, chondrogenic, adipocytic [175]. When expanded to colonies, the multi-linage potential of the cells were maintained. In one study by Xin *et. al*., they had showed that osteogenic and chondrogenic differentiation of human BM-MSCs (hMSCs) were observed when the cells were seeded on electrospun PLGA nanofiber scaffolds [104]. Note that these cells were treated with chondrogenic and osteogenic supplements.

hMSC from the vertebral bodies that were cultured in serum-free conditions seemed to have preferential response to treatment with certain BMPs, with regards to osteoinduction [182]. Amongst BMP-2, 4, 6 and 7, BMP-6 appeared to be a potent stimulus of osteoblastic differentiation and its gene expression was detected prior hMSC osteoblastic differentiation. The incorporation of BMP-6 to hMSC promoted the expression of osteoblastic genes such as type I Col, osteocalcin and bone sialoprotein. Furthermore, it stimulated key osteoblastic transcription factors such as core-binding factor α-1/runt-related transcription factor-2 (cbfa-1/Runx-2) and osterix. The synergistic effects led to an enhanced mineralization of ECM and HA deposition. It was found that the osteogenic growth factors such as IGF-1, FGF-β and vascular endothelial growth factor (VEGF) did not have direct osteoinductive effects on hMSC under serum-free media conditions. It was also suggested that the above-mentioned growth factors though essential in the function of osteoblasts or pre-osteoblasts and skeletal development, may not be sufficient in osteoblastic hMSC differentiation [182] . In a separate study, Boden

et al. showed that BMP-6 stimulated induced differentiation readily in rat calvarial cells, without glucocorticoid potentiation [183]. Similarly, the upregulation of BMP-6 production in rat calvarial cells in the presence of glucocorticoid was observed [182,184]. Conversely, the lack of sensitivity to BMP-2 and BMP-4 could be due to the expression of several families of secreted BMP antagonists, of which these antagonists could have a high affinity to BMP-2 and BMP-4, hindering their signaling, unlike BMP-6 and BMP-7 that had a lower affinity to the antagonists [182]. Another explanation as to the lack of responsiveness of MSCs to certain BMPs could be due to a dose-dependent issue, at which higher doses were essential for the induction of differentiation [185].

Surface chemistry was said to influence the MSC behavior on silane-modified surfaces in both basal and stimulated conditions [186], highlighting the importance of studying the minute details of material science such as surface area, porosity, local acidification, degradation properties etc. This phenomenon also pertains to other cell types as well.

Although for bone applications, bone marrow aspirates seem to be a "more" suitable choice for the extraction of stromal cells, the harvesting procedure for bone marrow is invasive and the number of stem cells from bone marrow varies from patient to patient, depending on the medical condition and age. Bone marrow stromal cells can be as little as 1 in 10^7 to 10^8 cells [51]. The numbers of osteogenic progenitor cells that are found in bone marrow decrease from 66.2 ± 9.6 cells for every 10^6 cells in patients who are under 40 years of age. The numbers of these cells further decrease to 14.7 ± 2.6 cells

per 10^6 cells in older patients [187]. In addition, the amount of bone marrow drawn from the patient is limited.

2.3.3 Potential of adipose-derived stem cells

To counter these issues associated with BM-MSCs, adipose tissue has been used as a source for stem cells as an enormous quantity of fatty tissue can be harvested. There are about 300 colonies per 100-mm dish for bone marrow samples and out of which, 1 MSC per 33,000 nucleated cells is present [188]. In other studies, typically there is 1 MSC in every 50,000 or 1 MSC in every 100,000 nucleated cells, which constitute to about a few hundred MSCs for every milliliter of bone marrow [187,189]. The number of adherent BM-MSCs is about 1 in 10^5 nucleated cells [190]. The confluency of the BM-MSCs took about five to seven days when the cells were plated between 20,000 to 400,000 cells/cm^2 [191,192]. Confluence was achieved within the same time period using the initial plating of 3,500 adipose derived stromal cells/cm^2 [193].

Immortal adipose stromal cell lines (ATSCs) was developed by transducing non-human primate-derived ATSCs with a retrovirus expressing TERT (catalytic protein subunit of the telomerase complex) [194]. The expression of TERT could be utilized for creating cell lines that could expand indefinitely while maintaining the multi-linage potential. The ATSC-TERT cells exhibited an increase level of telomerase activity and mean telomere length. These ATSC-TERT cells showed multi-lineage potential, at a lesser extent in untransduced cells *in vitro*. The duration of which calcium was produced

by ATSC-TERT cells was greatly shortened (one week of culture). However, calcium production occurred when native ATSCs was subjected to three to four weeks of culture in an osteogenic media. Enhanced expression of osteoblastic markers such as osteoblast-specific factor 2 and chondroitin sulfate proteoglycan was associated with ATSC-TERT cells. These observations suggested that telomerase expression could open new avenues for bone repair [194]. The use of T-box (Tbx) factors, in particular Tbx-3, was studied in human adipose-derived tissue stromal cells (hADSCs) by using a lentivirus si-RNA vector and it was proven that Tbx-3 played a role in proliferation and osteogenic differentiation of the stem cells [195].

2.3.4 MSCs derived from other sources

Umbilical cord blood (UCB), periosteum, synovium and muscle tissues are some of the alternate sources whereby MSCs can be derived [196-199]. Kern *et al* delved the characteristics of three different tissues (UCB, bone marrow and adipose tissue) as a human source of MSCs [196]. There were no significant differences in terms of morphology (fibroblastoid) and immune phenotype of the MSCs. All these sources portrayed a multi-potential differentiation ability with the capability of formation of colony-forming unit-fibroblast (CFU-F) and expression of a set of surface proteins (e.g. CD44, CD73, CD29, CD90, HLA-1). The success rate of isolating MSCs was 100% for both the bone marrow and the adipose tissue samples. Conversely, the isolation rate for umbilical cord blood was 63% [149]. This observation could be attributed to the fact that the MSCs could be circulating in the prenatal organism and residing in tissues of the

adult [153]. UCB showed the lowest colony frequency, whereas adipose tissue showed the highest colony frequency [196]. MSCs from UCB showed the longest culture period and the highest proliferation ability, but MSCs from bone marrow had the shortest culture period and lowest proliferation ability. Another noteworthy point to be elaborated was that MSCs from UCB did not show adipogenic differentiation capacity unlike those MSCs from bone marrow and adipose tissue which showed osteogenic, chondrogenic and adipogenic differentiation [196]. With regards to this, it was debated that a hierarchical or restricted differentiation capability of MSCs could be possible [175,200]. The proliferation rates of bone marrow, adipose and periosteum were similar after four, seven and eleven days of culture in a separate study [197]. Osteogenic and chondrogenic differentiation were achieved in all the MSCs. Using a rabbit model, it was demonstrated that bone-marrow and periosteum-derived MSCs had superior physeal arrest over adipose-derived MSCs [197].

For the comparative studies between bone marrow, adipose tissue, synovium, periosteum and skeletal muscle, bone marrow samples generated the greatest extent of calcification, followed by synovium, periosteum, adipose and muscle samples. For bone marrow samples, the colony number for every 10^3 nucleated cells was lower and cell number per colony was greater as compared to other tissue sources. The number of nucleated cells ($x10^3$) per volume or weight of tissue obtained was as follows: bone marrow (2,045±920), adipose tissue (22±21), synovium (3±4), periosteum (3±6) and muscle (2±1). Similarity in epitope profiles were found regardless of the tissue source [199]. One group had also evaluated on the immunological properties of bone marrow

stromal cells and adipose tissue derived MSCs and it was concluded that their properties were maintained during *in vitro* pre- and post-osteogenic induction and the results seemed to be similar in both tissues [201].

2.4 Cell-material constructs as bone grafts

After material selection, factors such as the type of pre-treatment of the substrate, choice of cells to be seeded and culture environment (dynamic/static conditions, cyclic/static loading) have to be considered. To create a more favorable environment for *in vivo* osteogenesis, many have attempted to pre-seed osteoblasts or MSCs on the bone graft materials. Essentially, bone is made up of two main cell types, namely osteoblasts and osteoclasts. These bone cells which are connected by gap junctions allow cellular communications between the bone surface and the mineral matrix. Osteoblasts are involved in the production of Type I Col and mineralization. The secretion of prostaglandin E_2 and interleukin-6 by osteoblasts stimulates osteoclasts, leading to bone resorption. MSCs seem to be an attractive cell source because they are capable of differentiating into an osteoblastic lineage when induced in the appropriate conditions. The ECM secreted by MSCs can involved in several cellular processes such as the recruitment, proliferation, differentiation and maturation of progenitor cells. Physiologically, MSCs differentiate into mature matrix-secreting osteoblasts, which progressively become osteocytes.

2.4.1 Mesenchymal stem cells (MSCs)-material constructs

For instance, coral which has a natural architecture that resembles spongy bone is said to be suitable as a bone graft material owing to its porosity (with an average pore size of 150 μm) because the blood vessels, ECM deposition and other cellular constituents can be intertwined within the graft, giving rise to an enhancement of material properties and stability. In a particular study, it was illustrated that the use of low level laser irradiation applied to a MSC/coral construct stimulated the proliferation and differentiation of MSC into an osteoblastic phenotype during the initial culture period and significantly induced *in vitro* osteogenesis over time [202]. Higher levels of calcium deposition was seen in irradiated-treated samples at early (days 3 and 6) and late culture periods (days 21 and 28). On the other hand, phosphate deposition was enhanced in those samples which were laser-treated in later culture periods (days 14, 21 and 28). In addition, ALP activity was observed. Laser-treated coral materials showed a significant level of ALP activity on day 2 of culture but at later culture stages (days 21 and 28), ALP activity was significantly reduced as compared to the control samples. These results implied that low level laser irradiation quickened the differentiation of MSC into an osteoblastic phenotype during bone formation processes in early culture periods, whilst at later stages, cellular response and bone maintenance by osteocytes were predominant [202]. Mygind and co-workers studied the effect of different pore sizes of the coralline HA scaffolds and found out that scaffolds with an average pore size of 200 μm showed a greater rate of osteogenic differentiation based on increased alkaline ALP and enhanced expression of osteogenic markers such as osteocalcin, BMP-2, BSP-I (bone sialoprotein-I) etc. than a 500 μm pore-sized scaffold [203] . They had also showed that slightly

fewer but more differentiated cells were found in the 200 μm pore sized scaffold. These scaffolds reached full confluency quicker than bigger pore-sized scaffolds owing to a higher degree of cell-to-cell communication, resulting in a higher rate of osteoblastic differentiation. Contrary, a significant number of less differentiated cells, i.e. higher proliferation, was associated with the bigger pore-sized scaffolds, possibly due to its higher surface area-to-volume ratio, which could have facilitated cellular adhesion on day 1 of culture. Other probable reasons were that more cells were needed to fill up the voids in the bigger pore-sized scaffolds for 3D confluency and the stimulated fluid flow aided in the proliferation process. By subjecting the constructs in a dynamic spinner flask as compared to a static cultivation, superior proliferation and differentiation of the cells within the scaffolds were demonstrated. Osteoblast matrix production was more prominent in constructs that underwent dynamic cultivation [203].

Chastain *et al.* showed that MSCs isolated from adult bone marrow in 3D poly(lactide-co-glycolide) acid (PLGA) scaffolds expressed and maintained greater osteocalcin gene expression than in PCL over a period of 5 weeks [204]. They hypothesized that the differential adsorption of certain ECM proteins in the serum-containing culture media and integrin-mediated attachment could be the reason of this difference. Type I Col seemed to favor MSC adhesion to PLGA. However, vitronectin enhanced the attachment of MSC to PCL. Greater ALP activity was observed for the PLGA group after two weeks, suggesting osteogenesis was more predominant in the type I Col-mediated attachment of MSC to PLGA (more osteoconductive) than in vitronectin-mediated MSC attachment to PCL. It was acknowledged that the conformation and

specific integrin-binding motifs in the ECM proteins and not just the identity of the ECM protein were some factors which modulated osteogenesis [204]. Other reasons for the preferential adsorption of the ECM proteins could be the wettability of the polymer, surface chemistry, nanotopography etc [205-208].

The MSC's fate to an osteogenic lineage was said to be dependent on certain cues such as cell shape which could be regulated by for example Rho A modulation [209]. hMSCs which were allowed to adhere and spread underwent osteogenesis. Local cues in the microenvironment and plating density were crucial for lineage-specific differentiation as seen in the activation of the Rho A-Rock signaling pathway [209].

2.4.2 Non-mesenchymal stem cells (Non-MSCs)-material constructs

Osteoblasts were seeded on hybrid membranes made of PLLA and HA [131]. It was evident that the number of viable cells on PLLA/HA hybrid membranes was greater than that of those on pure PLLA membranes. This was indicative that HA provided an osteoconductive environment for cell adhesion. SaOS-2 osteoblast-like cells underwent biomineralization when cultured in the presence of multi-phasic calcium phosphates which were synthesized via a self-propagating high temperature combustion synthesis (SHS) process, despite that culture conditions favored cell quiescence [210]. Membrane vesicles with calcium phosphate and porous plate-like calcium phosphate structures were found to be adjacent to the cells. Pseudopodia and a flattened morphology of the cells were observed, suggesting that the cells had a normal metabolism and anchored to the

heterogeneous calcium phosphates (mainly TCP and HA). The heterogeneous calcium phosphates had distinct crystalline regions as well as amorphous regions and the bulk porosity was spherical in nature. This heterogeneity and the hydrolysis of the amorphous phase resulted in the availability of calcium and phosphate, and resulting in enhanced biomineralization [210].

Nano-crystalline silicon-substituted HA (SiHA) coatings on titanium (Ti) substrates were produced by magnetron co-sputtering and increased Si content resulted in decreased crystallite size [211]. There was a significant increase in osteoblast cell growth density on coated SiHA Ti surfaces compared to uncoated Ti surfaces. Thian *et al* observed that flattened cells were attached on the coated surfaces with enhanced ECM synthesis. Moreover, a distinct and well-defined cytoskeleton with actin stress fibers was present on coated surfaces, whereas on uncoated Ti surfaces, the actin filaments were not present in the cytoskeleton structure. Rapid bone mineralization was seen in those coatings with a high Si content (4.9 wt% Si) by day 16 of culture. The drawback of high Si content was that rapid dissolution of the coating was apparent because of the small HA crystal size, thus the attachment of cells at very early stages may not be ideal. As such, it was found that 2.2 wt% Si was an ideal content for HA coatings [211].

2.5 Regulating osteogenic differentiation via nanotopographical characteristics

Regulating stem cell fate can be achieved through various means, such as chemical, topographical, mechanical and electrical or electromagnetic cues. This study focused on the topographical features and substrate characteristics for osteogenic

differentiation. For instance, lateral spacing geometry of TiO_2 nanotubes of 30-50 nm was reported to be the critical threshold for cell fate [212]. Diameter (<15 nm) and spacing (<30 nm) were considered to be the effective length scale for improving integrin clustering and focal contact formation. Good evidence showed that smaller diameter nanotubes (15 nm) were associated with greater focal contact formation, stress fiber (contractile actomyosin bundles or actin filaments) assembly, cell spreading and osteocalcin differentiation compared to larger diameter nanotubes (100 nm). On the other hand, larger diameter nanotubes (>50nm) resulted in the reduction in cellular activity, fewer focal contact and stress fibers and even programmed cell death [212]. In a separate study, it was shown that larger diameter nanotubes enhanced cell spreading compared to smaller diameter and flat substrates [213]. Increased MSC adhesion on smaller diameter nanotubes was said to be due to the increased protein aggregates such as fibronectin and albumin. Conversely, larger diameter nanotubes increased osteogenic differentiation as the cells were forced to elongate and stretch in search of protein aggregates, and such guidance and stressed-induced elongation resulted in osteogenic differentiation. Lower cell numbers were seen on larger diameter nanotubes within one day, but after seven days, the cell numbers for the different sized nanotubes were comparable, suggesting that the initial cell density could play a role in regulating the stem cell fate [213].

A landmark paper highlighted the importance of matrix stiffness and its influence in directing MSC commitment towards a specific lineage [214]. Briefly, soft matrices were associated with neurogenic differentiation, stiffer matrices were corresponded to myogenic differentiation and lastly rigid matrices were related with osteogenic

differentiation [214]. In a separate study, the stiffness of substrates (PEG-based materials) affected differentiation of pre-osteoblastic cells via mitogen-activated protein kinase (MAPK) activation [215]. It was reported that such ECM rigidity regulated osteogenic differentiation involving MAPK activation downstream of the RhoA-ROCK signaling cascade [216]. Early osteogenic differentiation markers, such as RUNX-2 and ALP expression were associated with stiffer materials [215,216]. The elasticity of the substrates also impinged upon cell proliferation, where stiffer substrates resulted up to ten-fold increase in cell numbers compared to lower stiffness substrates [217]. Interestingly, osteogenic differentiation of MSC was significantly increased on type I Col-coated substrates with the highest modulus [217], suggesting that substrate elasticity alone did not direct stem cell fate, but rather a network of factors such as the presence of integrins and integrin-receptor interactions was also likely at work. This highlights the importance of designing materials that are more closely related to the microenvironments found in native tissues.

Besides cell-substrate interactions, the presence of protein secretion by the cells would alter the chemistry of the material surface, thereby influencing osteogenic differentiation. The de novo synthesis and deposition of ECM proteins by the MSCs was said to modify the chemical characteristics of PLGA substrates, in turn affecting the MAPK and phosphatidyl inositol-3-kinase (PI3K) pathways which influenced osteogenic differentiation [218]. In addition, the attenuation in MAPK and PI3K pathways greatly inhibited MSC osteogenic differentiation [218]. Several studies have shown that the dimensionality of the substrate (2D vs. 3D) has an impact on cell fate and signaling

cascade. 3D scaffolds provide more precise, reproducible nano-topographical features and such nano-texturing is usually absent in 2D substrates. Certain stress mediators such as p38 and c-Jun N-terminal kinase (JNK) were significantly activated in 3D calcium phosphate scaffolds, thereby indicating that cells responsed to environmental signals, triggering certain signaling pathways such as MAPK cascade. This phenomenon was less evident in 2D calcium phosphate scaffolds [219].

2.6 Summary

In summary, although there are several bone graft materials in the market, there are huge differences in terms of graft performance and patient outcomes. Moreover, most of the calcium-based graft materials are blended systems and they do not mimic the composition and structure of native bone. Current research focuses mainly on developing bone graft materials that most likely constitute several strategies such as the use of biodegradable materials, functional cellular components and attempting to mimic the structure and properties of analogous ECM as described in this chapter. In this thesis, a biomimetic NFS was designed and developed by combining the functionality of electrospinning, biomineralization and physiologic activity of precursor cells such as BM-MSCs and osteoblasts. Here, biodegradable PLLA was the base material for electrospinning with the option of co-blending with type I Col. Biomimetic n-HA deposition was considered on both PLLA and PLLA/Col nanofibers for inducing osteogenic differentiation of osteoblasts and BM-MSCs. The efficiency of the resultant nanofiber/cell composite as bone grafts was further evaluated in a rabbit model. This strategy aimed to provide advanced bone graft materials that would by-pass the tedious

and time-consuming process of cell expansion to facilitate bone regeneration in the attempt to achieve better clinical outcomes.

(Note: Some of the text and results have been published and they are reprinted with permission in this chapter from the following publications: Casey K. Chan, T.S Sampath Kumar, Susan Liao, Ramalingam Murugan, **Michelle Ngiam**, S. Ramakrishna, Nanomedicine, Biomimetic nanocomposites for bone tissue graft applications, Vol 1(2), 177-188, 2006; **Michelle Ngiam**, S. Ramakrishna, Casey K. Chan, Recent Patents on Nanotechnology, Patenting trends in nanofiber technology, Vol 1, 137-144, 2007; **Michelle Ngiam**, Susan Liao, Casey Chan, S. Ramakrishna, Chapter 16 "Cell-based Nanocomposites and Biomolecules for Bone Tissue Engineering" published in "Advanced Biomaterials: Fundamentals, Processing and Applications", edited by Dr. Bikramjit Basu, Dr. Dhirendra S. Katti and Dr. Askok Kumar. Published in John Wiley & Sons, Inc., USA, 551-588, 2009

Chapter 3

Fabrication of mineralized polymeric nanofibrous composites for bone graft materials

3.1 Introduction

In bone tissue engineering, biomimetic mineralized collagen material, also known as n-HA/Col composite, can be prepared by various methods [116,121,220]. In an earlier study, n-HA/Col (nHAC)-based composite was prepared through a self-assembled co-precipitation method and its structure was similar to that of natural bone [121,220]. After mixing nHAC with PLLA solution via a phase separation technique, the nHAC/PLLA scaffold was prepared as a three-dimensional porous structure [113]. Osteoblasts were able to adhere and migrate into the inner part of the three-dimensional scaffold (nHAC/PLLA) [109]. When implanted in rabbits, these materials underwent remodeling with new bone formation [28,113,118]. Bone-like apatite was formed when the polymer substrates such as PLLA were subjected to SBFs [221]. In a separate study, nano-sized single crystalline HA fibers were synthesized using SBF as a solvent [222]. Co-precipitation methods were employed to fabricate a carbonate-substituted HA/chitosan-silk fibroin composite with improved compressive strength as compared to precipitated HA in the absence of any organic material due to the enhanced adhesion between HA and the organic matrix, whilst facilitating the distribution of stress transfer [223]. As such, a

combination of a polymeric material and bioceramic such as HA is often explored for future bone substitute materials.

The aim of this study was to develop a novel nanofibrous composite that would mimic the main components and nanofibrous characteristic of natural bone by combining the advantages of electrospinning and mineralization methods. Two types of polymers, namely PLLA and type I Col were chosen to be electrospun into nanofibrous scaffolds. Human bone derived osteoblasts were cultured on mineralized nanofibrous scaffolds over various time points to investigate cell affinity behavior. We hypothesized that there would be a preferential n-HA deposition on PLLA/Col nanofibers and improved early osteoblast attachment on mineralized nanofibers.

3.2 Materials and Methods

3.2.1 Processing of nanofibrous scaffolds by electrospinning

Type I Col (Koken Co. Tokyo, Japan) and a biodegradable polymer, PLLA (300,000 Da, Aldrich Chemical Company, Inc.) were used to prepare the scaffold. 3% of pure PLLA and a blend of PLLA/Col (50:50 w/w) solutions for electrospinning were prepared by dissolving the polymers in 1,1,1,3,3-hexafluoro-2-propanol (HFP, Aldrich Chemical Company, Inc.). Although the starting ratio for the preparation of the polymer solution was 50:50 w/w for PLLA/Col, the actual final ratio of the constituents was not determined in this study. For the preparation of 6.66% of pure electrospun collagen nanofibers, type I Col was dissolved in HFP solvent. Part of the electrospinning setup involved the connection of the syringe loaded with the polymer solution to a DC high

voltage power supply from Gamma High Voltage Research. A voltage was applied to the spinneret with a specified working distance, i.e. the distance from the tip of the spinneret to the surface of the collector plate. The voltage used for the preparation of the nanofibers was 15 kV (for PLLA and PLLA/Col nanofibers) or 12 kV (for collagen nanofibers). The working distance for the production of PLLA or PLLA/Col nanofibers and collagen nanofibers was 15 cm and 12 cm respectively. The spinneret used in our case was a BD 27G ½ needle which was ground to give a flat tip in order to produce smooth, continuous fibers. A KD Scientific syringe pump was used to provide a constant feed rate of 1 mL/hour. The entire electrospinning process was conducted under the controlled conditions; that is, at the room temperature of 25±1 ºC and at the relative humidity of 65%. The electrospun nanofibrous scaffolds were then vacuum dried overnight and sterilized with 70% ethanol for 10 minutes before mineralization was carried out.

3.2.2 Mineralization of electrospun nanofibrous scaffolds

PLLA and PLLA/Col nanofibrous scaffolds were mineralized using the modified alternate soaking method (Ca-P soaking) [224]. PLLA and PLLA/Col scaffolds were first immersed in 0.5 M of $CaCl_2$ (Aldrich Chemical Company, Inc.) for ten minutes. After rinsing with de-ionized (DI) water for a minute, the scaffolds were subsequently immersed in 0.3M of Na_2HPO_4 (Merck, USA) for 10 minutes. This denotes 1 cycle of Ca-P treatment. The DI water was then collected and centrifuged to collect the HA residues. After centrifugation, the HA was subsequently freeze-dried overnight before XRD analyzes. For PLLA scaffold, the material was subjected to five cycles of Ca-P treatment. For PLLA/Col scaffold, mineralization was achieved after three cycles of

alternate soaking. The mineralized scaffolds were subsequently freeze-dried for twenty-four hours.

3.2.3 Material characterization

The surface morphology of the electrospun scaffolds and the mineralized scaffolds were examined by using a field-emission scanning electron microscopy (FESEM) (Quanta 200F, FEI) with an accelerating voltage of 20 kV. The average fiber diameter of the scaffolds was determined from the FESEM micrographs using an image analysis software (Image J, National Institutes of Health, USA). The chemical functional groups of the (both Ca-P treated and non-treated) scaffolds were recognized by a spectroscopic method using a Fourier transform infrared (FTIR) spectrophotometer (Varian 3100 Excalibur Series). The crystallographic phase analyzes were carried out by powder X-ray diffraction (XRD) method using a Shimadzu XRD 6000 (Japan) diffractometer. The measurement was performed with the use of Ni filtered Cu $K\alpha_1$ radiation at the wavelength of 1.5406 Å, at a scan rate of 2° min^{-1}, at a sampling interval of 0.02° and in the 2θ range of 10°~80°. The data was analyzed using a XRD-6000 V2.5 software. Wettabilities of the nanofibers before and after mineralization were measured by sessile drop contact angle measurement using a VCA Optima Surface Analysis System (AST products, Billerica, MA). To quantify amount of HA on the fibers, thermogravimetry analysis (TGA) using TA Instruments TGA 2050 Thergravimetric Analyzer (Japan) was employed. The specimens (n=5) were heated up to 1000ºC, with a heating rate of 10ºC/min in air.

3.2.4 *In vitro* culture of osteoblasts

Scaffolds were imbedded in 70% ethanol twice for a period of 20 minutes at each time under UV light for sterilization purposes. The scaffolds were then washed with phosphate buffered saline (PBS) thrice to remove any residual ethanol. Human fetal osteoblast cells, hFOB 1.19 (ATCC, US), cultured until passage five, were seeded on the PLLA and PLLA/Col scaffolds , mineralized PLLA and PLLA/Col scaffolds, at a cell concentration of 10^4 cells/sample. For each material group, the sample size was three and tissue culture plastic (TCP) controls were used for all cell-related studies.

The constituents of the culture medium used include 1:1 mixture of Ham's F12 medium and Dulbecco's modified Eagle's medium (DMEM) without phenol red with 2.5 mM L-glutamine (Invitrogen, US), 0.3 mg/mL G418 (Sigma, US) and 10% fetal bovine serum (Invitrogen, US). The medium was changed every two days.

3.2.5 Cell attachment study

1 mL of the solution containing 10,000 osteoblasts was added to each of the wells containing the samples. The cells were incubated with the different test samples at room temperature for 10, 20, 30, and 60 minutes. At the end of the incubation period, the solutions containing the unattached cells were discarded and each well containing the test samples was washed thrice with 1 mL of PBS. For the purpose of cell counting, the nuclei of the attached cells were stained with DAPI (4', 6-diamidino-2-phenylindole, dilactate) (Invitrogen™) using the following protocol. Pre-chilled methanol was added to the wells containing the attached cells and allowed for fixation at room temperature for

10 minutes. Next, the nuclei of the attached cells were stained with 0.25 mL/well of 1 μg/mL DAPI for 30 minutes at room temperature. Each test sample was photographed using a fluorescence microscope (Leica DM IRB) at 100 times magnification. For each test sample, the number of cells in 5 predetermined rectangular areas (top, centre, bottom, left and right portions of the culture well) was counted based on the nuclei count. This cell count method was also used to calculate the cell number at the day 1, day 4 and day 7 of culture for cell proliferation quantifications.

3.2.6 Total protein assay

Osteoblasts (10,000 cells/sample) were seeded on non-mineralized and mineralized PLLA and PLLA/Col composite scaffold samples in three 24-well plates and cultured in osteoblast cell culture medium under standard cell culture conditions for 1, 4, and 7 days respectively. At the end of the prescribed times, the culture medium was removed from the culture wells and washed thrice with PBS. Samples were stained with bicinchoninic acid (BCA) protein assay working reagent (BCA Kit No.23225, PIERCE) at 37ºC for 30 minutes. Once room temperature was reached, the protein content was determined at 590nm using a FLUO Star Optima microplate reader (BMG Labtech GmbH). The total intracellular protein (expressed in mg) synthesized by the osteoblast cells cultured in the medium was determined from a standard curve of absorbance versus known concentrations of albumin by the BCA kit.

3.2.7 Alkaline phosphatase (ALP) activity assay

The prescribed cells were cultured on the materials and the alkaline phosphatase (ALP) activity was measured at day 1, 4, and 7 respectively. 400μL of *p*-Nitrophenyl Phosphate, Disodium Salt (PNPP) solution (Phosphatase Substrate Kit, No. 37620, PIERCE) was added to the 24-well culture plate and incubated at room temperature for 1 hour. The reaction of *p*-nitrophenol conversion to *p*-nitrophenylate ceased by the addition of 200μL of 2M of NaOH. Light absorbance of these samples was measured at 405nm on a FLUO Star Optima microplate reader.

3.2.8 SEM of cell morphology

Scaffolds with cells which were cultured for 1 day, 4 days and 7 days were fixed in 4% paraformaldehyde solution for 30 minutes at room temperature. Scaffolds were dehydrated in 50%, 70%, 95%, 100% (twice) (5 cycles with increasing concentrations of ethanol) for 10 minutes respectively. Samples were subsequently air-dried overnight and observed by SEM.

3.2.9 Mechanical Testing

After osteoblasts were cultured on the nanofibrous scaffolds for a period of time (1 day, 4 days and 7 days), the nanofiber/cell contracts were freeze-dried overnight at -60˚C. The nanofibrous scaffolds with or without cells were separated from the aluminium foil, using a paper frame with double-sided tape. The frame was designed to provide extra strength and support to the sample ends for proper fixation in the tensile

tester clamps and to ensure constant sizes of the samples being tested (10 mm width, 20 mm length). A micrometer (Mitutoyo) was used to measure the thickness of the membrane at three different positions and the average thickness was taken to calculate the cross sectional area of the specimen. Using a Tensile Tester (Instron Micro Tensile Tester 5848, USA) each sample (n=5 specimens) was subjected to a load of 2.5 Newton. Load deformation data was recorded at a deforming speed of 5 mm/min and a sampling rate of 100Hz. The E-modulus was calculated for low strain at the linear regime using numerical methods, which averaged the modulus using 40 data points.

$$\sigma = \frac{F}{A}$$

σ: stress (Pa), F: force (N), A: Cross-sectional area (m^2)

$$\varepsilon = \frac{L_{change}}{L}$$

ε: strain, L_{change}: change in length (m), L: original length (m)

$$E = \frac{\sigma}{\varepsilon}$$

E: E-modulus (Pa), σ: stress (Pa), ε: strain

3.2.10 Statistical analysis

Data was gathered at least in triplicate and expressed as mean ± standard deviation (SD). Statistical analyzes were carried out using one-way analysis of variance (ANOVA) testing by SPSS for Windows (SPSS Inc., Copyright1989-2002) version 11.5.0. Student's T-test (T-test) was applied to detect differences between the materials

groups. For all statistical tests, a value of $p < 0.05$ was considered to be a statistically significant difference.

3.3 Results

3.3.1 Nanofibrous and mineralized nanofibrous scaffolds

Uniform nanofibers of PLLA (Fig. 3.1a) and PLLA/Col (Fig. 3.1b) with average diameters of 287nm and 364nm respectively were fabricated by electrospinning. There were various definitions of "nanomaterials". It was widely accepted that nanomaterials refer to those materials with a nano-size topography or encompass of nano-size building blocks. The scale length/size/diameter of nanostructured materials, nanocrystals, nanocoatings, nanoparticles and nanofibers were typically in the range of 1-100 nm [110]. However, fibers that were above 100 nm but below 1000 nm were also described as "nanofibers" in several publications which had been cited in this document and in the public domain. After mineralization, the morphologies of both types of nanofibers were contrastive. The n-HA on PLLA nanofibers (Fig. 3.1c) was not formed in a continuous manner where there was a tendency for n-HA to be deposited at the cross points of at least two fibers, unlike those formed on PLLA/Col nanofibers (Fig. 3.1d) where the fibers were substantially covered with n-HA and no superior or enhanced mineralization at the cross points was seen.

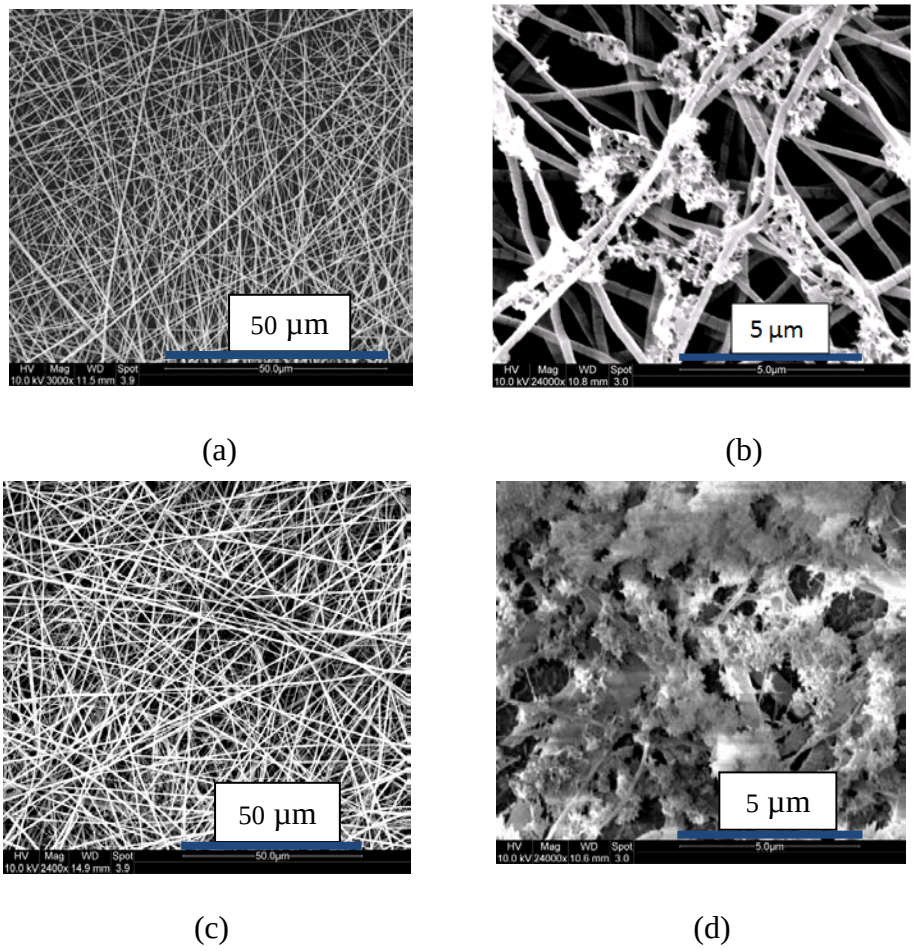

Fig. 3.1: SEM micrographs of (a) PLLA, (b) PLLA+n-HA; (c) PLLA/Col; (d) PLLA/Col+n-HA

From the XRD patterns, the formed minerals on PLLA and PLLA/Col were n-HA, with no impurities present. The n-HA obtained was similar to that of natural HA in human tooth (Fig. 3.2). All the diffraction peaks of PLLA+n-HA and PLLA/Col+n-HA were compared with the JCPDS (09-0432) standard for HA.

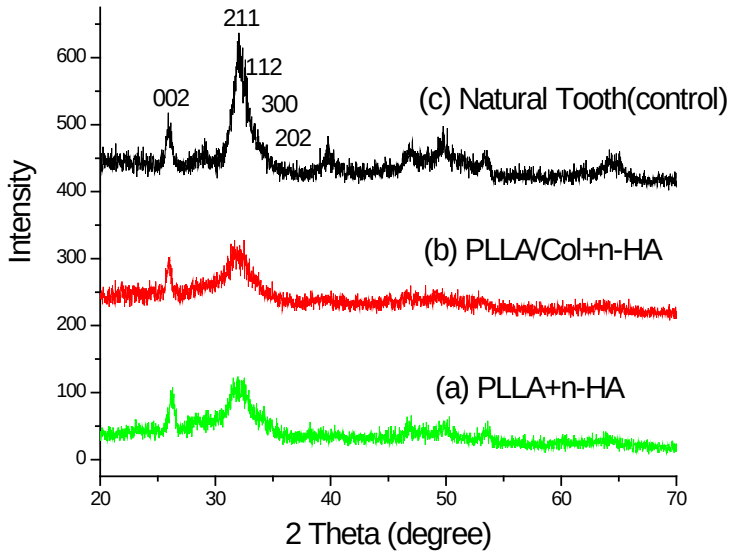

Fig. 3.2: XRD results of (a) mineralized PLLA nanofiber; (b) mineralized PLLA/Col and control (c) natural tooth of human, which identified that minerals on PLLA and PLLA/Col nanofibers are n-HA with same pattern as natural HA in human tooth. Note: Intensity in arbitrary (Arb) units.

Fig. 3.3 shows the FTIR results of the nanofibers. The spectrum of PLLA and PLLA/Col nanofibers (Figs. 3.3b and c) after mineralization exhibited typical absorption bands characteristic of carbonated hydroxyapatite, which was not seen in the spectrum of pure PLLA nanofibers (Fig. 3.3a). Peaks at 1755 cm^{-1} and 1086 cm^{-1} referred to carbonyl and C-O stretch in PLLA. Peaks at 1086 (ν3), 1033 cm^{-1} (ν3) and 558 cm^{-1} (ν4) referred to the phosphate group, and peaks at 1637 cm^{-1} (ν3), 866 cm^{-1} (ν2) referred to the carbonate group. For mineralized PLLA/Col nanofibers, amide I (1661 cm^{-1}) and amide II (1544cm^{-1}) were attributed to collagen although they were slightly overlapped by the carbonate group. Comparing the peak for carbonate group (866 cm^{-1}) in Figs. 3.3b and c, the n-HA on PLLA/Col nanofibers encompassed more carbonated component than that of PLLA nanofibers.

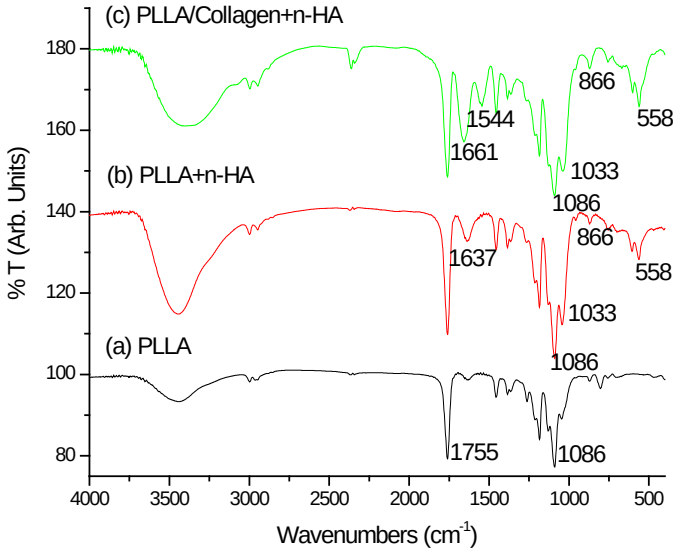

Fig. 3.3: FTIR spectra of (a) PLLA nanofibers; (b) mineralized PLLA nanofibers and (c) mineralized PLLA/Col nanofibers. Peaks at 1755 cm^{-1} and 1086 cm^{-1} referred to carbonyl and C-O stretch in (a) PLLA. Peaks at 1086, 1033 and 558 cm^{-1} in (b) and (c) referred to phosphate groups from nano HA. Although the absorption band (1086 cm^{-1}) from (a) PLLA overlapped with the vibration bands of the phosphate groups, the relative intensities of the phosphate groups were greater in (b) and (c). Peaks at 1637 and 866 cm^{-1} referred to carbonate groups from n-HA. Peaks at 1661 and 1544 cm^{-1} referred to amide I and II groups from collagen

As shown in Fig. 3.4, collagen improved the wettability of the nanofibers, from 115.5˚ (PLLA) to 41.5˚ (PLLA/Col). n-HA deposition on PLLA (PLLA/n-HA) (110.7˚± 5.2˚) did not significantly improve the wettability as compared to PLLA nanofibers (115.5˚±9.4˚). Conversely, the hydrophilicity property of PLLA/Col was significantly improved by the deposition of n-HA (16.4˚±4.2˚) compared to PLLA/Col (41.5˚±6.5˚) and the controls (pure collagen nanofibers, 53.8˚±7.1˚). The quantities of HA were established using TGA where PLLA and PLLA/Col contained 37.8 wt% and 30.2 wt% of HA.

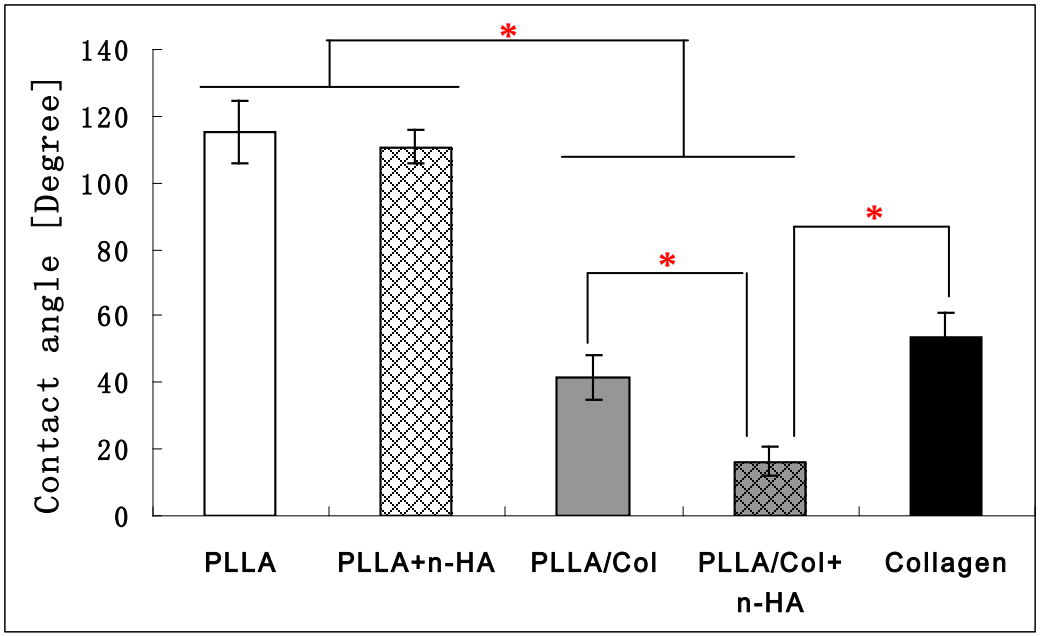

Fig. 3.4: Water contact angles of PLLA, mineralized PLLA, PLLA/Col, mineralized PLLA/Col and Collagen nanofibers (control). Significant difference between different groups were denoted as * (p<0.05)

3.3.2 Enhanced cell capture on mineralized nanofibrous scaffolds

Mineralization further enhanced the cell capture efficiency as shown in Fig. 3.5. The initial cell number for the cell capture study on each sample is 10,000. From 10 minutes to 60 minutes, approximately 10% of the cells were attached on TCP controls, which was lower than all the nanofibers. For PLLA and PLLA/Col nanofibers, mineralization significantly enhanced the cell capture efficiency, especially within 30 minutes. The prominent cell capture at 10 minutes was on PLLA+n-HA (35% ± 9%) and PLLA/Col+n-HA (37% ± 9%). The most desirable cell capture results at 20 minutes were on PLLA/Col+n-HA (61% ± 5%). At 30 minutes, there was no significant difference of cell capture between PLLA+n-HA (56% ± 8%) and PLLA/Col+n-HA (56% ± 9%).

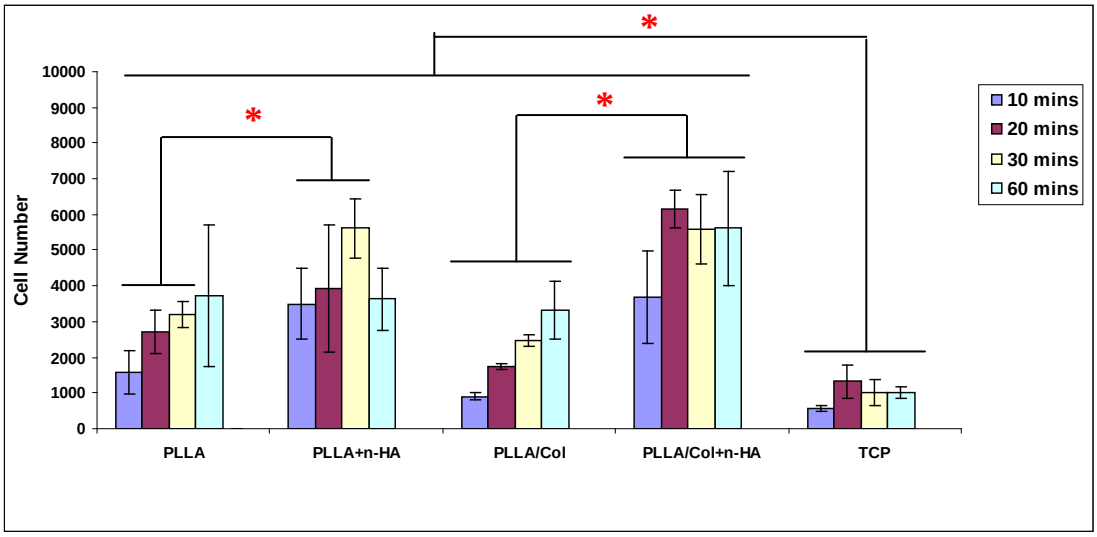

Fig. 3.5: Cell attachment on PLLA, PLLA+n-HA, PLLA/Col, PLLA/Col+n-HA and TCP (control) from 10 minutes to 60 minutes at room temperature. Significant difference between different groups were denoted as * (p<0.05)

3.3.3 Cell behavior on nanofibrous scaffolds

Cell proliferation, total protein assay and ALP expression were assessed on day 1, 4 and 7 of culture. Interestingly, the cell proliferation results were not in cognate with the results of the cell capture study as previously mentioned. Cell proliferation was greatest in the TCP control group as seen in Fig. 3.6. The increasing trend of cell proliferation was evident on non-mineralized nanofibers analogous to that on TCP. However, on mineralized nanofibers, there was no significant increase in cell proliferation. From day 1 to day 7, the number of attached cells on PLLA+n-HA and PLLA/Col+n-HA were maintained and the results from both material groups were comparable.

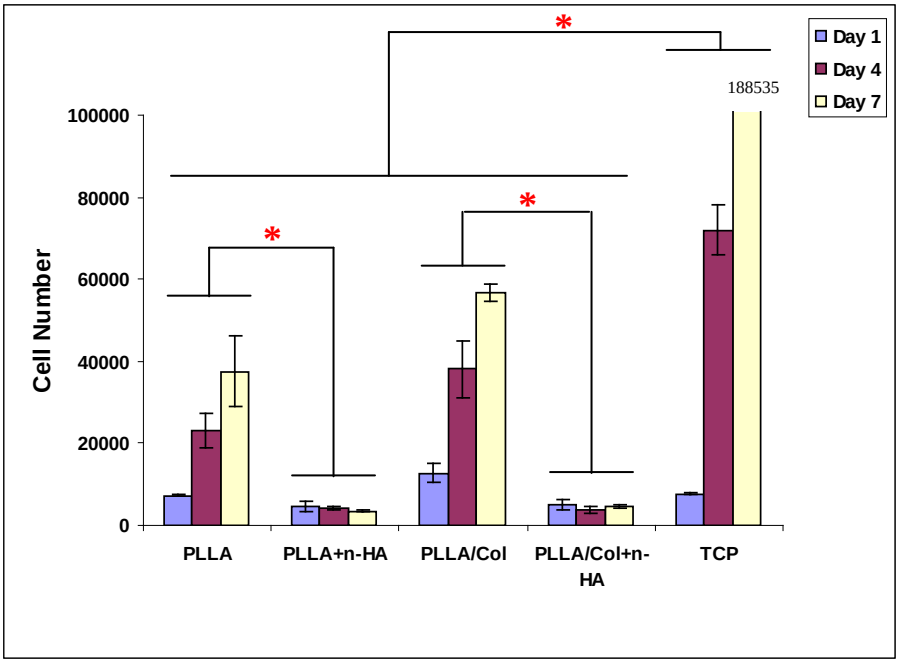

Fig. 3.6: Cell proliferation on PLLA, PLLA+n-HA, PLLA/Col, PLLA/Col+n-HA and TCP (control) from day 1 to day 7. Significant difference between different groups were denoted as * (p<0.05)

Fig. 3.7 shows the cell morphology and the observations are as follows: PLLA/Col+n-HA (Fig. 3.7d) was conducive for cell expansion than PLLA+n-HA (Fig. 3.7a) after day 1 of culture. In addition, there was a substantial increase in cell size on PLLA/n-HA nanofibers from day 1 to day 7 as seen in (Figs. 3.7a-c).

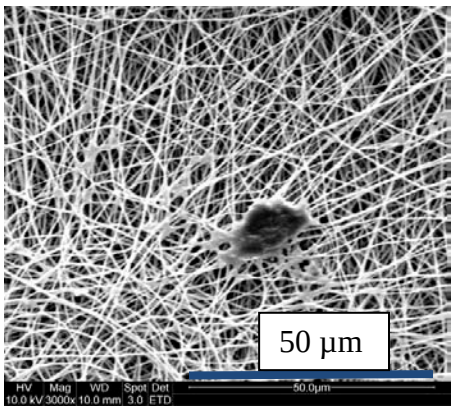

(a)

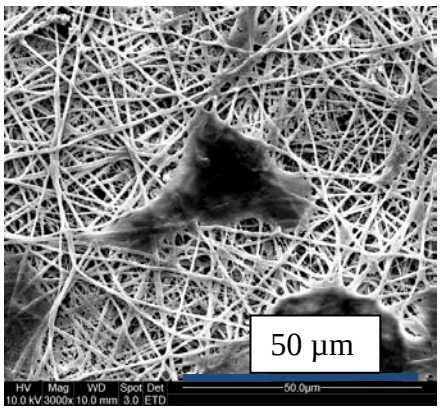

(d)

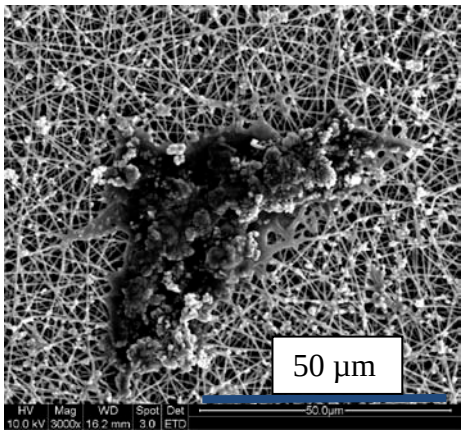

(b)

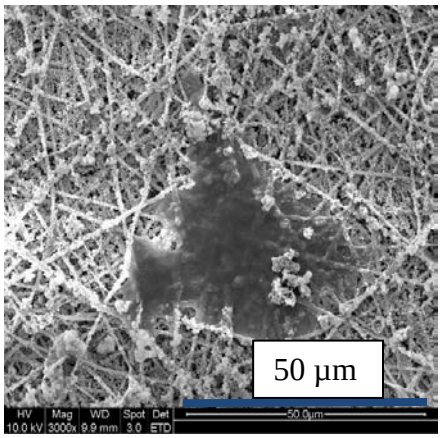

(e)

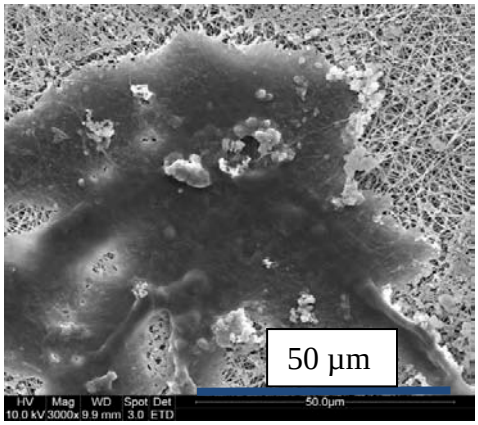

(c)

Fig. 3.7: SEM images of cells growing on mineralized nanofibers (a) PLLA+ n-HA for 1 day; (b) PLLA+ n-HA for 4 days; (c) PLLA+ n-HA for 7 days; (d) PLLA/Col+ n-HA for 1 day; (e) PLLA/Col+ n-HA for 7 days

The final protein concentrations synthesized by the cells depicted in Fig. 3.8 were obtained by dividing the initial results by the cell numbers (in Fig. 3.6). Here, the values of each expanded cell on the mineralized scaffolds performed at a higher level of function than each cell on non-mineralized scaffolds and TCP controls. Cells on mineralized nanofibers had higher protein amounts than non-mineralized nanofibers at day 1 and day 4 of culture. The ALP activity (Fig. 3.9) was comparable for all the material groups.

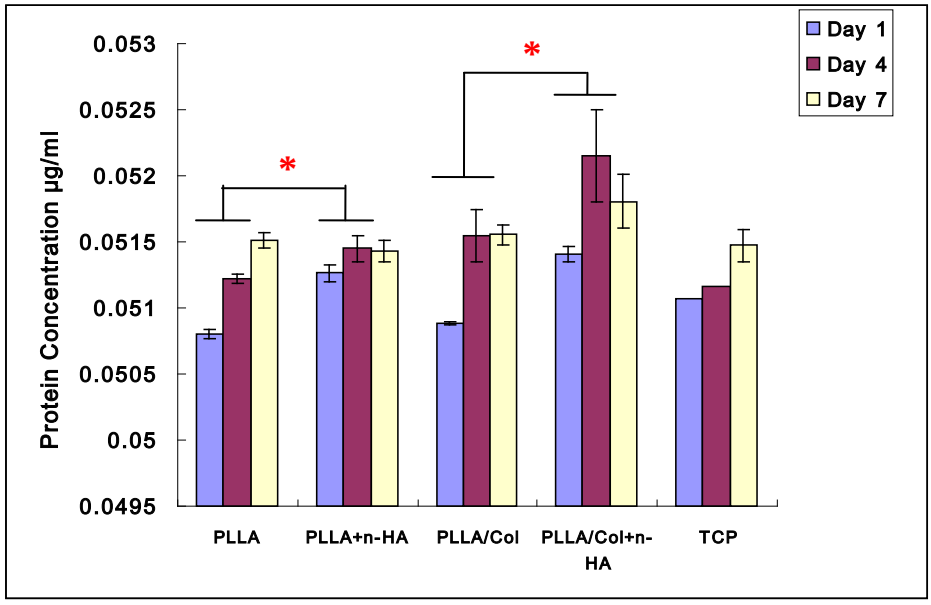

Fig. 3.8: Total protein assay of cells on PLLA, PLLA+n-HA, PLLA/Col, PLLA/Col+n-HA and TCP (control) from day 1 to day 7. Significant difference between different groups were denoted as * (p<0.05). Results shown have been normalized by the cell numbers

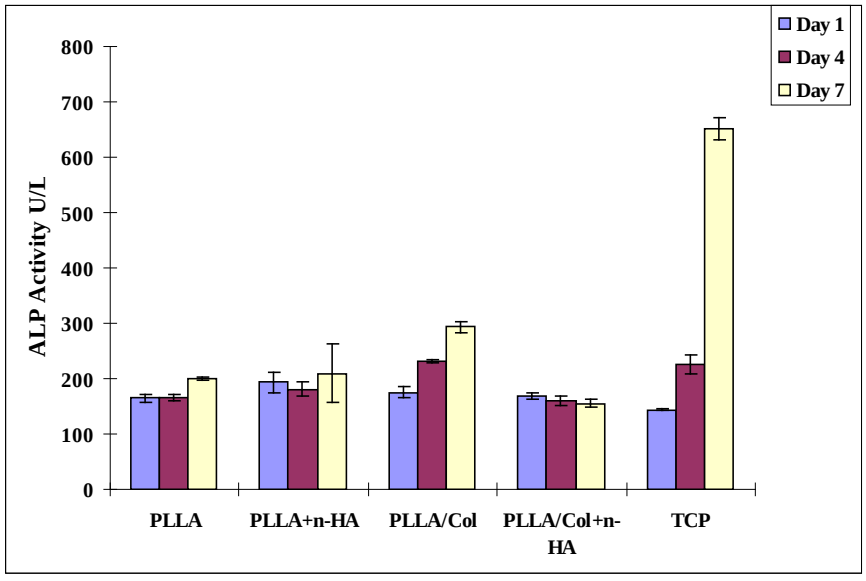

Fig. 3.9: Alkaline phosphatase (ALP) expression of cells on PLLA, PLLA+n-HA, PLLA/Col, PLLA/Col+n-HA and TCP (control) from day 1 to day 7. Results shown have been normalized by the cell numbers

Tensile testing was done on all the scaffolds (with or without cells). Fig. 3.10 shows the E-modulus of the scaffolds after day 1 and 4 of culture. No results were obtained for those cultured for 7 days because the samples were damaged during the separation of the fibers from the support material (aluminum foil) as the nanofibers were extremely "sticky". The increased tackiness could be due to the increased expression of ECM proteins secreted from the osteoblasts at day 7. Although there was no improvement in osteoblast proliferation on mineralized fibers after a week, the E-modulus of PLLA+n-HA with cells at day 1 and day 4 were significantly enhanced compared to PLLA+n-HA without cells (Fig. 3.10). On the other hand, the E-modulus of the PLLA/Col+n-HA nanofibers with cells at day 1 and day 4 was significantly decreased compared to those without cells.

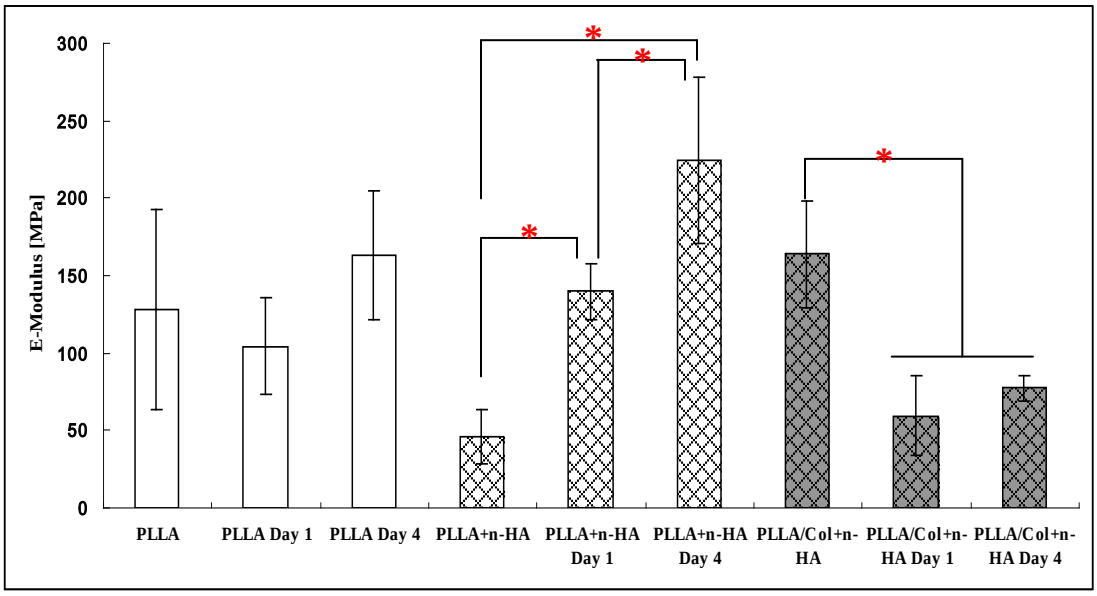

Fig. 3.10: E-modulus for PLLA, PLLA+n-HA, PLLA/Col+n-HA nanofibrous scaffold and various scaffold with cells after 1 day and 4 days of culture. Significant difference between different groups were denoted as * (p<0.05)

3.4 Discussion

The main objective of this study was to develop a novel nanofibrous composite using electrospinning and the alternate soaking methods. Various coating methods such as alternate dipping or SBF treatments [225-227] have been employed for apatite deposition on polymeric substrates for tissue engineering applications. The SBF strategy is to increase the concentration of Ca and P ions in the fluid by regularly replacing the solution with fresh SBF fluid. Studies have shown that the initial apatite nucleation by chemical means such as alkaline treatments to introduce functional groups such as carboxylate groups prior to SBF immersion is pivotal for the acceleration of apatite deposition. Apatite deposition was seen on PCL materials which were first treated with O_2 plasma followed by alternate dipping in calcium and phosphate solutions, subsequently subjected to SBF solutions for 24 hours [228]. PLLA scaffolds which were alkali-treated showed apatite deposition after 4 days in SBF [225]. However, the complete deposition of HA on the nanofibers occurred after 2 weeks of SBF soaking [225]. One of the advantages of our study was that the samples did not have to undergo any pre-treatment and successful apatite deposition occurred after a few rounds of alternate Ca-P dipping. From the results, n-HA deposition on pure PLLA nanofibers occurred at the cross points of at least two fibers. One possible reason was that the surface tension at these cross points was high and residual amounts of reactants of the Ca-P solutions during dipping could adhere to these sites, facilitating the initial nucleation process. Consequently, the higher supersaturation of Ca^{2+} ions at the cross points than the area of single nanofiber would in turn accelerate the induction of n-HA. This phenomenon had been reported during the mineralization of bioglass nanofibers [93].

As for the blended PLLA/Col nanofibers, n-HA was deposited more uniformly on the fibers and there was no preferential deposition at the cross points of the nanofibers. This was indicative that collagen was a good template for deposition, giving rise to uniform and accelerated mineralization of n-HA. About 11% of amino acid residues of collagen have carboxyl groups (-COOH). Those carboxyl groups ionized to $–COO^-$, which favored Ca^{2+} ion chelation [220,229]. The alternate soaking method for mineralization appeared to be effective and rapid n-HA formation on nanofibers was achieved by increasing concentrations of Ca and P ions that corresponded to the Ca/P ratio of 1.66 (equivalent to the ratio of natural bone).

Using our mineralization method of n-HA deposition, the n-HA on the nanofibers paralleled to that of natural HA in human tooth delineated in our XRD results. Moreover, the extensive broadening and overlap peaks were due to the extremely fine grain size of the crystal which was even lower than that of human teeth. Similarly to pure collagen molecules as templates for mineralization *in vivo*, nanofibers of PLLA and PLLA/Col could serve as templates for mineralization *in vitro*. It is commonly known that the HA phase which is present in natural bone, dentin and enamel contains approximately 7.4, 5.6, 3.5 wt% of carbonate respectively [230] and it is said that carbonated HA materials have excellent biocompatibility and properties, which can be favorably compared with those of hard tissue. In our study, phosphate and carbonate groups were present on our treated nanofibers. The carbonate content in the n-HA on the PLLA/Col nanofibers was more evident compared to PLLA nanofibers. The broad peaks could suggest the low crystalline apatite phase, which could be a mixture of amorphous calcium phosphate and

crystalline HA [231]. This could be beneficial as the major bone mineral was amorphous calcium phosphate (Young bone: 65%; Adult bone: 35%), which acted as a precursor to crystalline HA [232].

PLLA/Col nanofibers experienced lower contact angle results, suggesting that blending the polymer with collagen was an effective way to improve the hydrophilic property of synthetic polymer nanofibers [233]. The presence of n-HA on PLLA nanofibers did not significantly increase the hydrophilicity as compared to untreated PLLA nanofibers. Contrary to this observation, n-HA deposition significantly enhanced the wettability of blended PLLA/Col nanofibers than on PLLA nanofibers and the control (pure collagen nanofibers). In the light of these observations, one plausible explanation could be due to the distribution of n-HA on PLLA nanofibers than on collagen-blended PLLA nanofibers, leading to an increase in hydrophilicity in PLLA/Col+n-HA substrates. The TGA results showed that despite an increase in the number of treatment cycles in PLLA (five cycles) than in PLLA/Col (three cycles), the HA contents in both types of fibers were comparable, indicating that the presence of collagen favored HA deposition.

The objective of conducting a short-term cell attachment (named as cell capture, to emphasize this unique cell attachment on the nanofibers) study at room temperature was to explore the possibility of an attractive therapeutic approach in which scaffold with an enriched population of target cells could be achieved, i.e. direct cell seeding could be attained *in-situ* at the operating theatre. In this study, mineralization on the nanofibers improved the cell capture efficiency, especially at earlier time points. Principally, the n-

HA deposition on nanofibers could increase the surface roughness of the scaffold, thus mineralized nanofibers could provide more binding sites for cell attachment than pure nanofibers. Based on previous *in vivo* models, high osteoblast affinity was associated with n-HA based materials [28,113,118]. In one study, there was a significant increase in cell attachment on composite co-precipitated chitosan/n-HA microsphere-based scaffolds than on pure chitosan scaffolds after 30 minutes [234]. However after one and two hours, the number of cells that were attached to both scaffolds was comparable. Here, we attempted to provide a reasonable explanation and elucidate this point: n-HA may be able to attract the osteoblasts by enhancing the cell capture efficiency.

Cell proliferation and cell expansion were enhanced on collagen blended PLLA nanofibers. These results were consistent with other studies such that the introduction of collagen blending or coating aided endothelial cells proliferation on electrospun PLLA-CL nanofibers [233,235]. There was a significant enlargement in cell size on mineralized PLLA nanofibers. Taken together, osteoblast proliferation was significantly greater on n-HA than on conventional HA after 3 and 5 days as reported by Thomas J. Webster [228]. Greater cell proliferation measured by the total amount of dsDNA was observed on the chitosan/HA scaffolds than pure chitosan scaffolds after 5 and 7 days [234]. It is well-known that nanophase calcium phosphate is capable of enhancing osteoblastic proliferation and differentiation. However, other studies showed that while osteoblastic proliferation performed well on both chitosan and chitosan/powdered β-tricalcium phosphate scaffolds, no improvement was found when calcium phosphate was added [236]. In this case, the n-HA deposition actually prohibited the cell proliferation and

there was enhanced cell expansion if the substrate materials were PLLA or PLLA/Col nanofibers. Some studies reflected similar observations: cell proliferation was not significantly different after one and three weeks on pure freeze-dried chitosan and chitosan scaffolds mineralized with HA nanocrystals using a double-diffusion method [237]. They indicated that after one week, ALP activity was similar for both non-mineralized and mineralized scaffolds but after three weeks, the ALP production increased although similar cell proliferation was seen at the same time point [237]. As our cell culture work was only up to a week, it may not be facile to make any conclusive or concrete judgments. In our case, even though n-HA inhibited proliferation and similar rates were in cognate with both mineralized PLLA and PLLA/Col nanofibers, the ALP activity for all the material groups including the controls were comparable. Such studies highlighted the fact that although a material surface may favor certain cellular characteristics, some phenotypic expressions such as ALP activity and bone matrix formation may also be modified [238]. To expound on the above-mentioned phenomenon, PCL and PCL/HA scaffolds fabricated by fused deposition modeling (FDM) were treated with SBF [239]. HA deposition induced by SBF treatment failed to increase the osteoconductivity, i.e. cell attachment, proliferation, growth and mineralization were impaired. ALP activity peaked immediately upon seeding on day 1, but fell after 3 to 7 days of culture for all samples. From day 10 onwards, PCL and PCL/HA scaffolds exhibited an increasing trend in ALP production, peaking at day 17. Throughout the cell culture study, the ALP activity of SBF-treated samples was consistently lower than that of PCL and PCL/HA samples, where the difference increased substantially on day 10 onwards and a significant difference was observed on day 17 and

20. One probable explanation could be due to the increasing number of non-viable cells as the integrity of apatite layer was not optimal since flaking of the apatite was seen on the SBF-treated PCL scaffolds. Likewise, an increase in osteocalcin expression occurred on PCL and PCL/HA scaffolds after 10 days of culture but not for SBF-treated PCL scaffolds. Again, this could be due to the inability of the osteoblasts to attach properly on apatite-coated PCL samples, hence not able to produce ECM proteins [239]. Consequently, these findings allowed us to understand the importance of precise controllable deposition of n-HA, and the key function for n-HA was not to improve cell proliferation but to direct osteoblastic behavior at a single cell level. In contrast to tissue-engineered materials, osteoblastic attachment was reduced on titanium (Ti) surfaces with micro-rough rugosities compared to TCP or smooth Ti surfaces [240]. Cells that did attach showed reduced proliferation as well. Lohmann *et. al.* demonstrated that increased production of osteocalcin, transforming growth factor β-1 (TGF-β1), prostaglandin E_2 (PGE_2) was seen on surfaces with increasing roughness was caused by the greater synthesis per cell, i.e. lesser number of cells was synthesizing more proteins or cytokines [240]. In a separate study, ALP and enzymatic activities were also reduced on rougher Ti surfaces [241].

The presence of n-HA on the scaffolds had a greater influence on the functionality of the cells at early time points of the culture, i.e. day 1 and day 4 as there was an increase in intracellular protein produced by the cells. These results were in concordance with some studies which showed that the total protein content of mineralized scaffolds were significantly higher than non-mineralized specimens after 3 days of culture [242].

Enhanced protein adsorption was evident on n-HA/polymer composites fabricated via a thermally induced phase separation (TIPS) method [243]. Similarly, in our case, mineralization on both PLLA and PLLA/Col nanofibers increased the protein concentration, suggestive that n-HA was favorable in cellular conditions, where the quantification of HA on the nanofibers were analogous. The increased protein concentration could be due to a greater surface-to-volume ratio compared to non-mineralized nanofibers. This is important because the initial interactions of the cells and the material would affect the overall performance of the material in the host body. Our total protein concentration and ALP findings had been normalized by the cell numbers. The protein concentration results illustrated that HA improved the protein concentrations at early time points and the ALP results were comparable for all groups, even though our cell proliferation results decreased in the mineralized groups. This implied that the activity of the cells was not hampered even though there was less cell proliferation.

Good evidence showed that n-HA significantly enhanced the compressive modulus of n-HA/polymer composites [243]. Contrary to the above-mentioned study [243], n-HA surface deposition did not improve the E-modulus property of our materials. In addition, HA in electrospun PLLA/HA hybrid membranes contributed to higher tensile strength due to better integration of HA with the PLLA matrix [131]. Yet in a study done by Venugopal *et. al*., there was no improvement in mechanical properties (tensile strength and E-modulus) for electrospun blended PCL/HA nanofibers as compared to PCL nanofibers [244]. Tensile strength values were 3.37 and 1.07 MPa for PCL and PCL/HA nanofibers respectively. On the other hand, the E-modulus values were 10.82

and 3.52 MPa for PCL and PCL/HA nanofibers respectively. We suspected that the distribution of HA, be it surface coated or homogenously integrated in a bulk material could impinge upon on the type of mechanical property which may serve as a possible explanation in our case. Mechanical testing was done on unseeded control scaffolds and those explanted after 14 weeks *in vivo*, where the mean stiffness of PCL, PCL/HA and apatite-coated PCL was similar but the stiffness of the apatite-coated PCL samples after fourteen weeks of implantation was less than the control samples, possibly due to the poor attachment of cells on the weak apatite layer [239]. Contrary, after explantation, there was an increase in stiffness for PCL and PCL/HA scaffolds due to tissue in-growth and ECM formation. A different phenomenon was observed when osteoblasts were present on the nanofibers. The E-modulus of PLLA+n-HA seeded with cells was significantly higher than that of those without cells. One possible explanation that we postulated for this observation was that the cell expansion and secretion of ECM proteins were considered to be a major contributing factor for this improvement of mechanical strength. On the other hand, there was a significant reduction in E-modulus of mineralized PLLA/Col nanofibers with osteoblasts compared to those nanofibers without cells. This could be due to water absorption and the rapid biodegradation of collagen in nanofibers, thus despite the fact that ECM proteins were secreted by the cells, it was insufficient to compensate the strength provided by the blended collagen in the nanofibers. The influence of degradation was not explored in this short term study, but rendered future considerations in order to assess the duration of which the damaged bone tissue would need to repair itself and the appropriate mechanical stability provided by the scaffold. Although some published findings on the mechanical properties of tissue-

engineered constructs may appear more "promising" than others, the status quo may never be attained because the modulus of cortical bone ranges from 12.8-17.7 GPa and cancellous bone has a modulus of 0.4 GPa [245]. NFS had a variable pore-size distribution and the pore diameters could range up to 100nm [110]. Although the pore sizes of the NFS were small [36,37], the NFS substrates provided an excellent scaffolding structure for cells to adhere, proliferate, migrate and differentiate. The cells were able push the surrounding fibers aside as they migrated through the matrix. This was because the nanofibers provided minimal resistance to the amoeboid movement of the cells [110].

3.5 Conclusion

Rapid n-HA deposition was observed using the alternate dipping method. Blending collagen in PLLA polymer was an effective way to enhance the mineralization of nanofibers. n-HA significantly improved the hydrophilicity of PLLA/Col nanofibers. Moreover, n-HA deposition enhanced the cell capture efficacy within 30 minutes for PLLA and PLLA/Col nanofibers. Although there was no improvement of osteoblast proliferation by n-HA deposition in a week culture, the E-modulus of PLLA+n-HA with cells at day 1 and day 4 were significantly increased compared to PLLA+n-HA without cells due to the enhanced cell expansion and extracellular matrix secretion. Our findings, in correspondence to other published results demonstrated the possibility of misinterpreting the overall functionality of the material with regards to surface topography and chemistry on cellular response if we look at only certain characteristics whilst neglecting other important physiological parameters. As such, one must closely examine and strike a balance between optimizing material properties whilst improving

cellular response. In conclusion, mineralization of the nanofibrous scaffolds may provide a promising biomimetic method to exploit the advantages of early osteoblast capture although in-depth approaches can be further investigated and harnessed in future work. The final PLLA/Col ratio of the electrospun NFS can also be determined for future research.

(Note: The results have been published in *Tissue Engineering* and they are reprinted in this chapter from: **Michelle Ngiam**, Susan Liao, Avinash J. Patil, Ziyuan Cheng, Fengyi Yang, Miguel J. Gubler, S. Ramakrishna, and Casey K. Chan, Tissue Engineering, Vol 15(3), Fabrication of mineralized polymeric nanofibrous composites for bone graft materials, 535-546, 2009. Copyright 2009, with permission from Mary Ann Liebert Inc.)

Chapter 4

Osteogenic Differentiation of Bone-Marrow derived Mesenchymal Stem Cells on PLLA Nanocomposite Fibers

4.1 Introduction

MSCs are particularly popular because of its versatile differentiation profile and may be derived from several tissue sources such as bone marrow, adipose tissue, muscle and umbilical cord blood etc [175,246]. In addition, the use of autologous MSCs seems promising because chances of immune rejection and carcinogenesis are minimized.

Although MSCs are thought to be potential cell sources for autologous bone tissue engineering as it is said to facilitate bone repair in various bone defects [247], some drawbacks include the minute numbers of MSCs (especially as donor age increases), self-renewal and proliferative abilities are limited [247,248]. Since the relative frequency of MSCs in the marrow is approximately 1 in 100,000 cells, only a small population of these cells can differentiate into an osteogenic lineage [246-248]. As such, several attempts have been done to improve the proliferation and differentiation capabilities of the MSCs, either through material selection and modification and/or culture supplements and techniques.

Several reports have shown that cells are sensitive to the intrinsic properties of the materials such as composition, structure and elasticity they are exposed to. Nanofeatures (nanopits) of different symmetries and varying degrees of disorders on polymethylmethacrylate (PMMA) had showed to have an effect on osteogenic differentiation of MSCs, where nanoscale disorder stimulated MSC osteogenic differentiation bypassing the application of chemical means [31]. Moreover, rigid matrices were associated with osteogenic differentiation whilst soft and stiffer matrices were associated with neurogenic and myogenic differentiation respectively [214]. Furthermore, the geometry of the substrates influenced cell behavior. Larger diameter nanotubes (100 nm) coincided with more well-spread, cell elongation, lamellipodia and mobility compared to smaller diameter nanotubes [213]. In this study, we hypothesized that the nanotextured topography of n-HA on nanofibers would have a positive influence on osteogenic differentiation of MSCs without chemical treatment.

4.2 Materials and Methods

4.2.1 Fabrication of electrospun nanofibers and mineralization

Electrospinning was employed to fabricate our PLLA and PLLA/Col nanofibers as previously mentioned in Chapter 3. Similarly, n-HA mineralization on the PLLA and PLLA/Col nanofibers was done by employing a series of chemical treatments according to the same parameters as described in Chapter 3.

4.2.2 BM-MSC culture on nanofibers

Human MSCs were purchased (P2, Lonza, MD, U.S., Product No. PT-2501).

According to the technical sheet provided by Lonza, the MSCs were obtained from 21 year-old male African-Americans. The MSCs (P3) were cultured on PLLA, PLLA/Col, PLLA+n-HA and PLLA/Col+n-HA (10,000 cells/well/sample for all experiments) at various time points from 1 and 28 days in normal and osteogenic media and incubated at 37ºC in 95% humidified atmosphere and 5% CO_2. The normal media consisted of low-glucose Dulbecco's modified Eagle's medium (DMEM) (Aldrich Chemical Company, Inc., St. Louis, MO, U.S.), 10% fetal bovine serum (FBS) (Invitrogen, CA, U.S.) and 1% penicillin-streptomycin (PS) (Invitrogen, CA, U.S). The osteogenic media had the same constituents as the normal media, with the additions of 10 nM dexamethasone (DEX) (Aldrich Chemical Company, Inc., St. Louis, MO, U.S.), 0.05 mM ascorbic acid (Aldrich Chemical Company, Inc., St. Louis, MO, U.S.) and 10 mM β-glycerophosphate (Aldrich Chemical Company, Inc., St. Louis, MO, U.S.). The media was changed every 2 to 3 days to ensure a constant supply of nutrients. The cell morphology was observed using the fluorescence microscope (Leica DM IRB, Leica Microsystems GmbH, Wetzlar, Germany) at 100 times magnification.

4.2.3 Material characterization

The morphologies of the mineralized nanofibers were analyzed using the Atomic Force Microscope (AFM) in tapping mode (Dimension 3100 AFM, Veeco Instruments Inc., CA, U.S.) using a silicon tip (Pointprobe-Plus® silicon-SPM sensor, Nanosensors™, Switzerland) under ambient conditions with scanned areas of 800×800 nm. The images were recorded at a scan rate between 0.5 and 1 Hz. The cantilever tips had a tip radius of between 5 and 7 nm, with a resonance frequency of 315–369 kHz. The images were

scanned at five predetermined areas for each material (n=3). The specific surface area of each substrate (n=3-5) was determined using the Brunauer-Emmett- Teller (BET) Analyzer (NOVA-3000 Ver 6.07, Quantachrome Instruments, Florida, U.S.). The fibers were degassed at room temperature for a day before measurements were taken. After the predetermined time point of culture, the scaffolds with cells were fixed in fixed in 4% paraformaldehyde (Lancaster, England) solution for 30 minutes at RT. Subsequently, the cell/material constructs underwent a series of dehydration process in ascending concentrations of ethanol, i.e. 10 minutes in each solution at 50%, 70%, 95%, 100% (twice) respectively. The samples were then air-dried overnight prior to scanning electron microscopy (SEM) imaging. The topographies of the substrates were assessed using a field-emission scanning electron microscopy (FESEM) (Quanta 200F, FEI, Oregon, U.S.) at an accelerating voltage of 20 kV. The Ca-P ratios of the mineralized PLLA and PLLA/Col fibers and the bone minerals (n=10 measurements) secreted by the MSCs were measured using SEM-EDX (Energy Dispersive X-ray Spectroscopy, (JSM-5600LV, JEOL, Japan/Oxford EDX, INCA).

4.2.4 Cell proliferation

All samples were inoculated with MSCs (10,000 cells/sample) for a culture period of 1 day to 28 days. At the end of the stipulated time period, the medium was removed from each well and the wells were washed with PBS thrice. Next, 300 µL of pure DMEM and 30 µL of CCK-8 reagent (Scientific Resources) were added and the samples were incubated for 1.5 hours at 37ºC. After thorough mixing, the light absorbance was

measured at 490 nm using a FLUO Star Optima microplate reader (BMG Labtech GmbH, Offenburg, Germany) to arbitrate the number of cells.

4.2.5 Alkaline phosphatase (ALP) expression

ALP expression was measured at day 1 and 7, where the activity was normalized by cell number at the respectively culture time point. Using a Phosphatase Substrate Kit (No.37620, Pierce Biotechnology, IL, U.S.), 400 µL of *p*-Nitrophenyl Phosphate, Disodium Salt (PNPP) solution was added in each well and incubated for an hour at room temperature. Next, 200 µL of 2M NaOH was incorporated to terminate the reaction of *p*-nitrophenol conversion to *p*-nitrophenylate. Using a FLUO Star Optima microplate reader (BMG Labtech GmbH, Offenburg, Germany), the light absorbance was measured at 405nm.

4.2.6 Protein assay

At the end of each incubation period, the medium was removed and phosphate buffered saline (PBS) solution was used to wash the well thrice. The samples were treated with a bicinchoninic acid (BCA) protein assay working reagent (BCA Kit No.23225, Pierce Biotechnology, IL, U.S.) and incubated for 30 minutes at 37ºC. The protein content was quantified using a FLUO Star Optima microplate reader (BMG Labtech GmbH, Offenburg, Germany), set a wavelength of 590nm at RT. The total intracellular protein (expressed in milligrams) results were normalized by the respective cell numbers.

4.2.7 Immunostaining

4.2.7.1 CD29 staining of BM-MSCs

After 14 days of culture, CD 29, a human MSC marker, was incubated with the substrates and incubated with the secondary antibody goat anti-mouse antibody-fluorescein isothiocyanate (FITC) according to the protocol in 4.2.7.1. Confocal imaging (FV 1000, Olympus Corporation, Japan) was then carried out to ascertain that the cells used were MSCs.

4.2.7.2 Osteocalcin (OC) expression

After day 21 of culture, OC expression was assessed. The media was first removed and 4% formaldehyde with 1% sucrose was added and incubated at 37ºC for 15 minutes to fix the cells. After removal of the fixative solution, the wells were washed with PBS, followed by the addition of permeabilizing buffer (10.3g sucrose, 0.292g NaCl, 0.06g $MgCl_2$, 0.476g HEPES buffer, 0.5mL Triton X in 100ml water, pH 7.2) and then incubated for 5 minutes at 4ºC. After which, the permeabilizing buffer was removed and 1% bovine serum albumin (Sigma Aldrich Chemical Company Inc., St Louis, U.S.)/phosphate buffered saline (BSA/PBS) is added and the samples were incubated at 37ºC for 5 minutes. For OC staining, mouse monoclonal anti-osteocalcin (Invitrogen, CA, U.S.) was diluted 1:100 in 2%BSA/PBS and incubated at 37°C for 1 hour. After washing 3 times with PBS to remove the primary antibody, the samples were incubated at 37°C for 1 hour with goat anti-mouse antibody-fluorescein isothiocyanate (FITC) (Sigma Aldrich Chemical Company Inc., St Louis, U.S.) that was diluted in 1:100 BSA/PBS. Next, the wells were washed with PBS thrice and 300 µL of DAPI (Invitrogen, CA, U.S.)

(1:5000 diluted in PBS) was added and the culture plates were incubated at RT for 30 minutes. Samples were then observed using a confocal microscope (FV 1000, Olympus Corporation, Japan). Using an image analysis software (Image J, National Institutes of Health, Bethesda, U.S.), the intensities of the green fluorescence signals of the confocal images (n=10 to 19) were calculated for semi-quantifications.

4.2.8 Alizarin red staining (ARS)

ARS was carried out after day 14 and day 28 of culture. Briefly, chilled 70% ethanol was used to fix the cells and the samples were incubated at 4ºC for an hour. After which, DI water rinsing (twice) was done prior to the addition of 40 mM of ARS staining reagent (Sigma Aldrich Chemical Company Inc., St Louis, U.S.) and the samples were incubated for 30 minutes at RT. The staining reagent was then removed and the samples were again washed with DI water. Next, 10% cethyl pyridinium (CPC) (Sigma Aldrich Chemical Company Inc., St Louis, U.S.) was prepared by dissolving the CPC in sodium phosphate (Sigma Aldrich Chemical Company Inc., St Louis, U.S.) solution. 1 mL of 10% CPC was added in each well and left at RT for 1 hour. Subsequently, 100 µL of the CPC from each well was removed and diluted to 900 µL of pure CPC solution. The absorbance was then measured at 570 nm using a UV/VIS spectrophotometer (Unicam UV 300, Thermo Spectronic, WI, U.S.). ARS staining was also carried out on samples without cells to normalize absorbance readings of the mineralized substrates with cells.

4.2.9 Von kossa (VK) staining

After 28 days of culture, VK staining was conducted to assess the extent of

mineralization. According to conventional VK protocols, after cell fixation with 4% paraformaldehyde at RT for 1 hour, the samples were incubated with 5% silver nitrate (Sigma Aldrich Inc.) at RT for 1 hour with ultraviolet (UV) exposure. The samples were then rinsed with DI water and 5% sodium thiosulfate (Sigma Aldrich Inc.) was added. After a couple of minutes, DI rinsing was employed prior to the incorporation of nuclear fast red (Sigma-Aldrich Inc.) to stain the cell nuclei. After 5 minutes, the samples were rinsed with DI water before imaging. VK staining was also employed on the mineralized samples without cells to differentiate cell mineralization from n-HA of the scaffolds.

4.2.10 Statistical analysis

The data obtained (at least in triplicate) was expressed as mean ± standard deviation (SD). The Student's T-test (T-test) and two-way ANOVA were used and differences between the material groups are considered statistically significant at $p < 0.05$.

4.3 Results

4.3.1 Material characteristics of 3D nanoyarns

Fig. 4.1 shows the nanotextured surface of mineralized PLLA (Figs. 4.1b and c) and PLLA/Col (Figs. 4.1e and f). Our previous work showed that n-HA were attached along PLLA nanofibers and homogeneously dispersed on PLLA/Col nanofibers [19]. The Ca/P ratios for the mineralized PLLA and PLLA/Col fibers were 1.8 ± 0.12 and 1.7 ± 0.14 respectively, which was similar to hydroxyapatite (~1.67) [249] in native bone. The presence of n-HA on PLLA (22.7 ± 7.3 m^2/g) and PLLA/Col (25.2 ± 9.7 m^2/g)

significantly improved the specific surface area compared to pure PLLA (8.9 ± 3.5 m^2/g) and PLLA/Col (10.1 ± 2.4 m^2/g) fibers respectively.

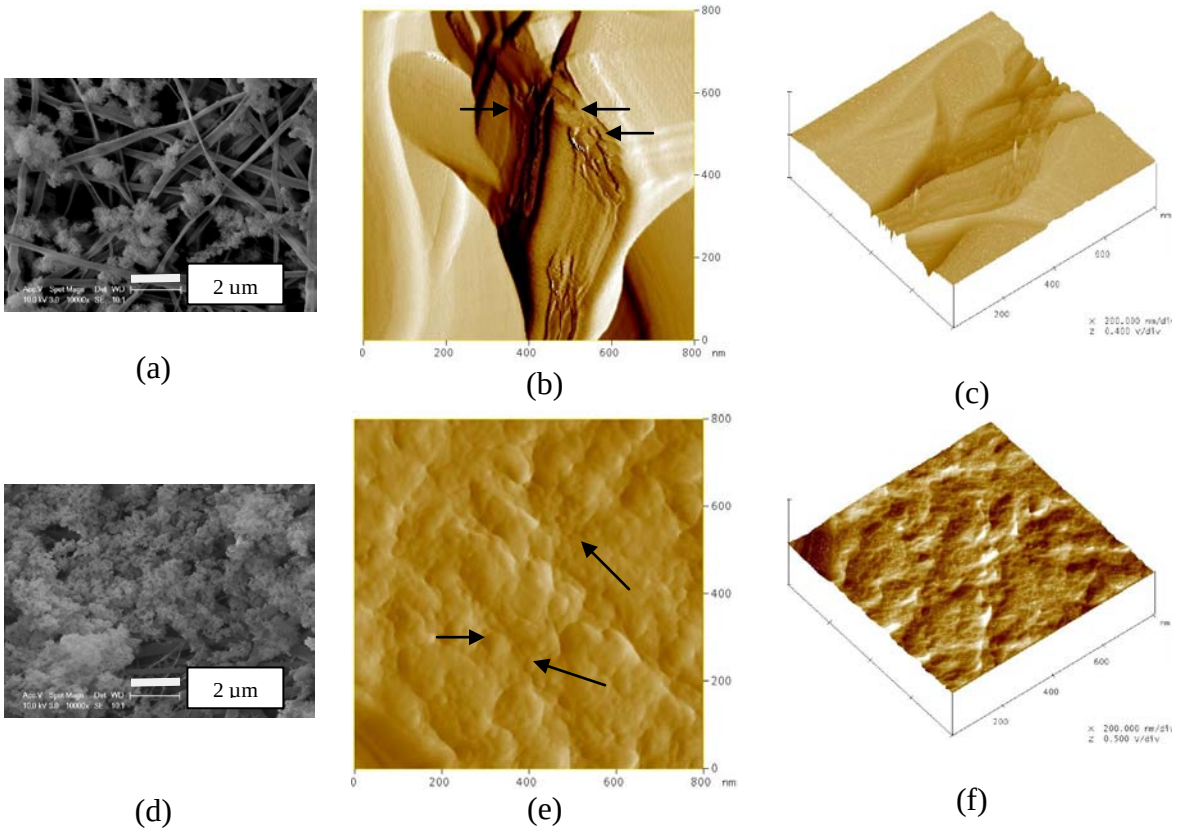

Fig. 4.1: SEM images of mineralized (a) PLLA and (d) PLLA/Col fibers. AFM images depicting the nanotexturing of mineralized fibers (b) PLLA+n-HA, (c) 3D surface topography of (b) PLLA+n-HA, (e) PLLA/Col+n-HA and (f) 3D surface topography of (e) PLLA/Col+n-HA. (Arrows represent n-HA on the fibers)

4.3.2 Cell morphology in normal and osteogenic media

From our results, MSCs cultured in the osteogenic media differentiated (Figs. 4.2b and d) to a greater extent (more elongated morphology) than those in normal media (Figs. 4.2a and c) after day 1 and 4 of culture.

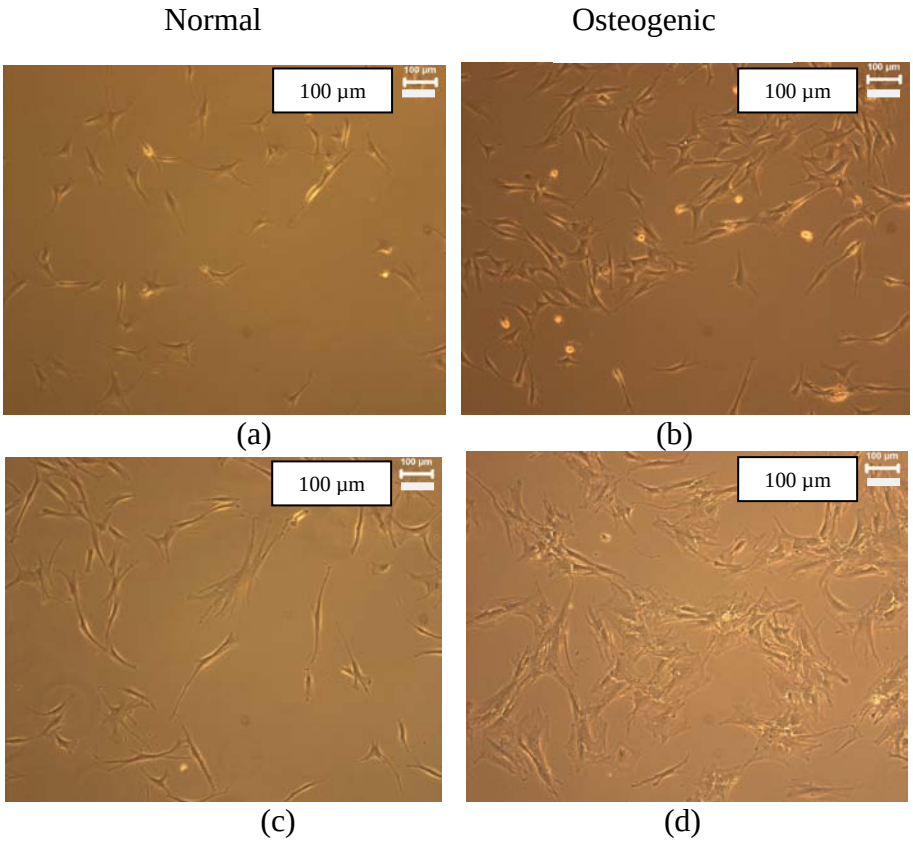

Fig. 4.2: Cell morphology of BM-MSC on tissue culture plastic (TCP) in either normal media or osteogenic media. (a) after 1 day in normal media, (b) after 1 day in osteogenic media, (c) after 4 days in normal media, (d) after 4 days in osteogenic media

4.3.3 Cell proliferation of BM-MSCs

Fig. 4.3 shows the cell proliferation on the NFS. In general, the cell proliferation levels in all the nanofiber groups were lower than the TCP controls. There was a reduction in the cell proliferation levels in the presence of n-HA, especially for mineralized PLLA/Col compared to their non-mineralized counterparts.

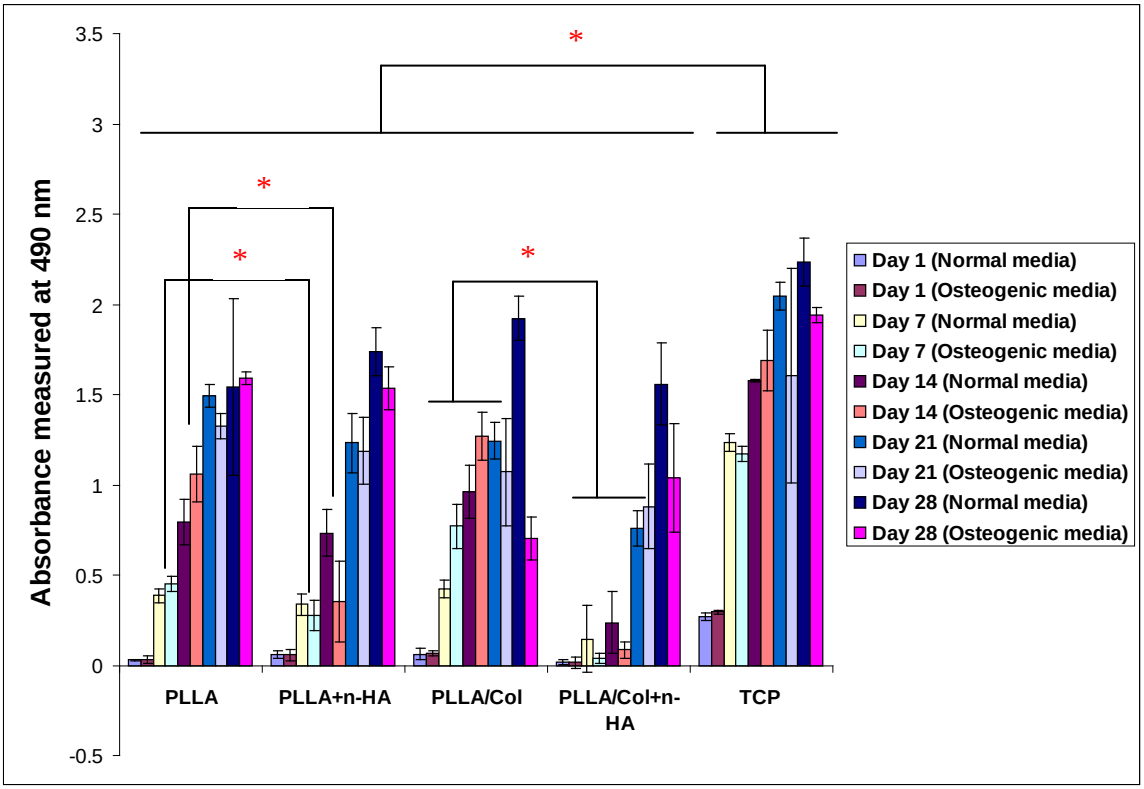

Fig. 4.3: Cell proliferation on various nanofiber substrates after 1 to 28 days of culture in normal and osteogenic media. Significant difference between different groups were denoted as * (p<0.05)

4.3.4 Protein concentrations of BM-MSCs on various NFS

Fig. 4.4 shows the protein concentrations after cell normalization. The protein concentrations for both mineralized PLLA and PLLA/Col substrates were significantly meliorated compared to their non-mineralized counterparts on both days except those cultured in osteogenic media on day 1. In general, all the nanofiber groups fared better than the TCP controls.

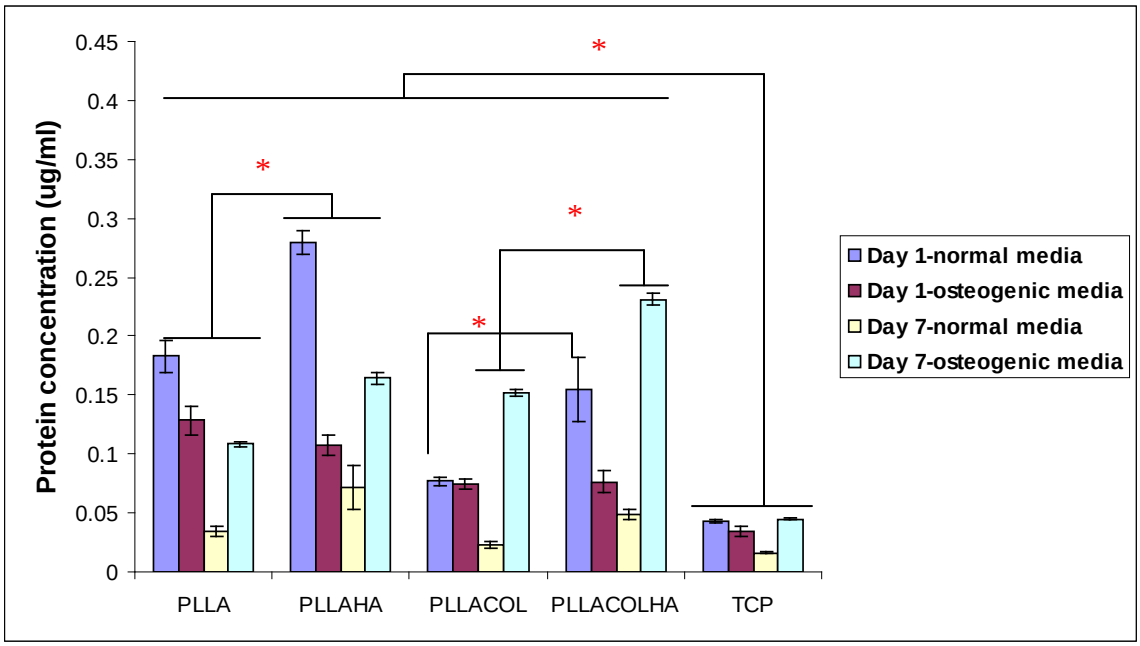

Fig. 4.4: Protein concentration of various nanofiber substrates after 1 and 7 days of culture in normal and osteogenic media. Significant difference between different groups were denoted as * (p<0.05)

4.3.5 Immunostaining of MSC marker on various NFS

CD29, a MSC marker was used to ascertain the presence of MSCs used on our nanofibers. Fig. 4.5 shows that all the material groups in different media conditions displayed CD29-positive signals.

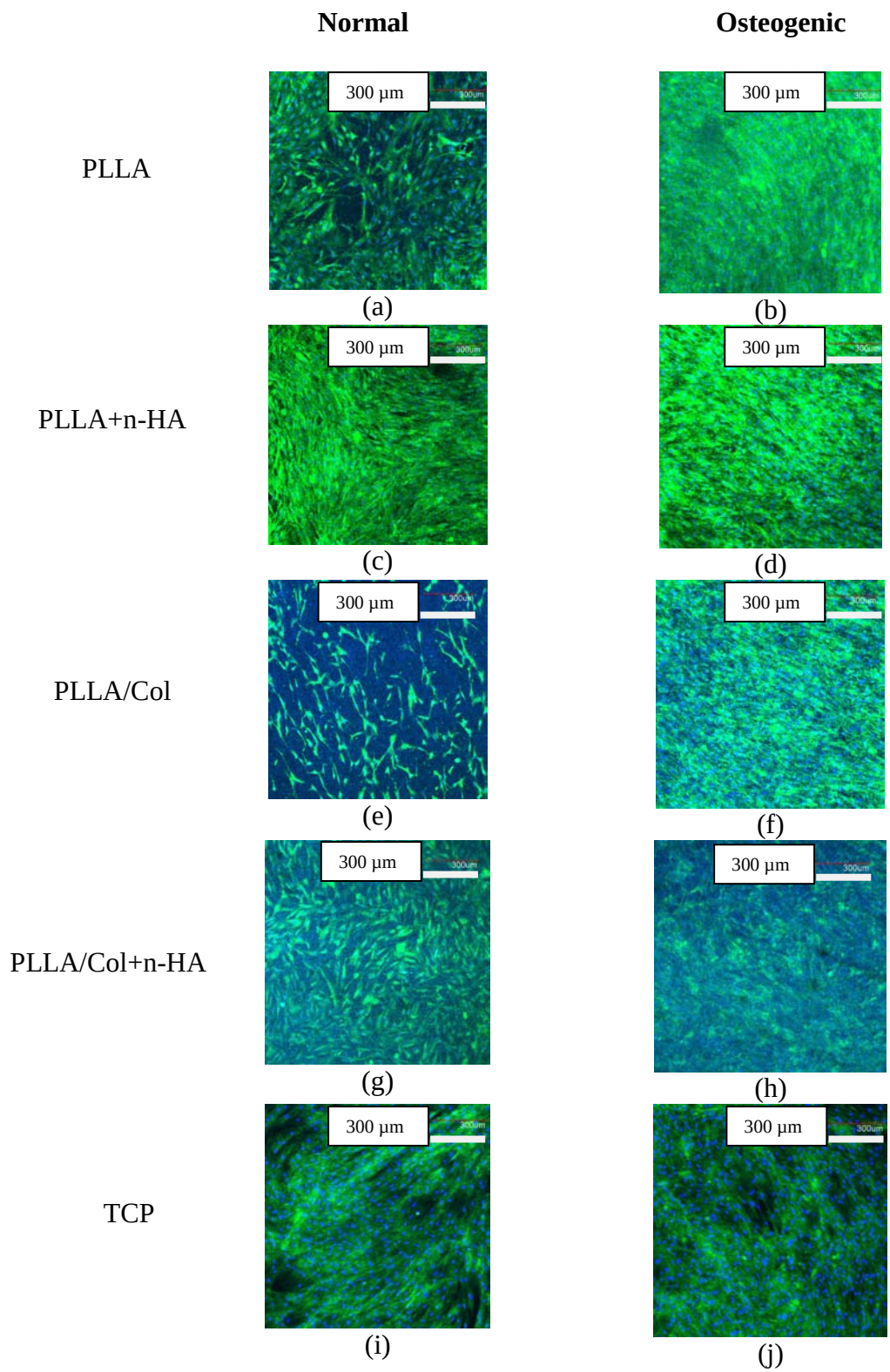

Fig. 4.5: CD29 staining of various substrates after 14 days of culture. Blue denotes DAPI-stained cell nucleus and green denotes CD29 expression. Scale bar for x10 is 300 µm

4.3.6 Osteogenic differentiation of BM-MSCs on various NFS

Fig. 4.6 illustrates the ALP (an early osteogenic differentiation marker) activities after cell normalization. There was a significant increase in ALP expression in mineralized PLLA substrates compared to non-mineralized PLLA substrates. The ALP level was raised in mineralized PLLA/Col compared to PLLA/Col in normal media after day 1, but the presence of n-HA and collagen did not significantly improve the ALP expression in osteogenic media conditions and at different time points.

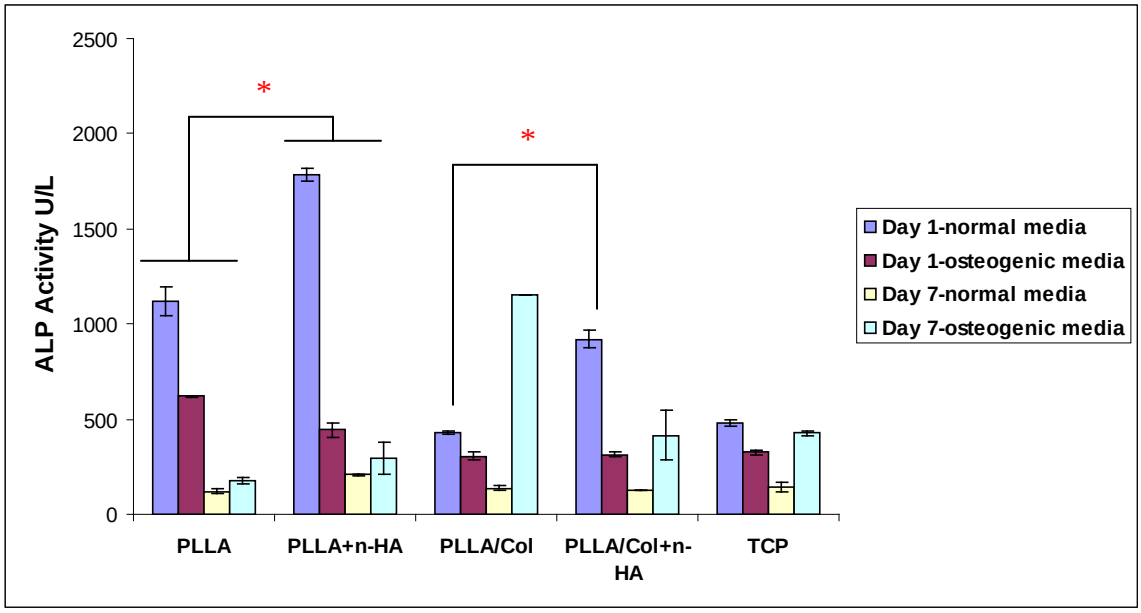

Fig. 4.6: Alkaline phosphatase (ALP) expression on various nanofiber substrates after 1 and 7 days of culture in normal and osteogenic media. Significant difference between different groups were denoted as * (p<0.05)

Osteocalcin, a middle-stage osteogenic marker, was used to determine the level of osteogenic expression. From the images (Fig. 4.7), osteogenic supplements enhanced

osteocalcin expression in PLLA and PLLA+n-HA nanofibers. It was noteworthy to highlight that OCN expression levels were comparable in both media conditions for mineralized PLLA and blended PLLA/Col nanofibers (Fig. 4.8), suggesting that n-HA or collagen alone was a potent inducer of osteogenic differentiation in the absence of osteogenic supplements. More importantly, the combination of n-HA and collagen significantly elevated OCN expression in normal media conditions compared to those in osteogenic media, which also implied that the n-HA aided in osteogenic differentiation. In general, the OCN levels of the nanofiber groups fared better than TCP controls regardless of media conditions.

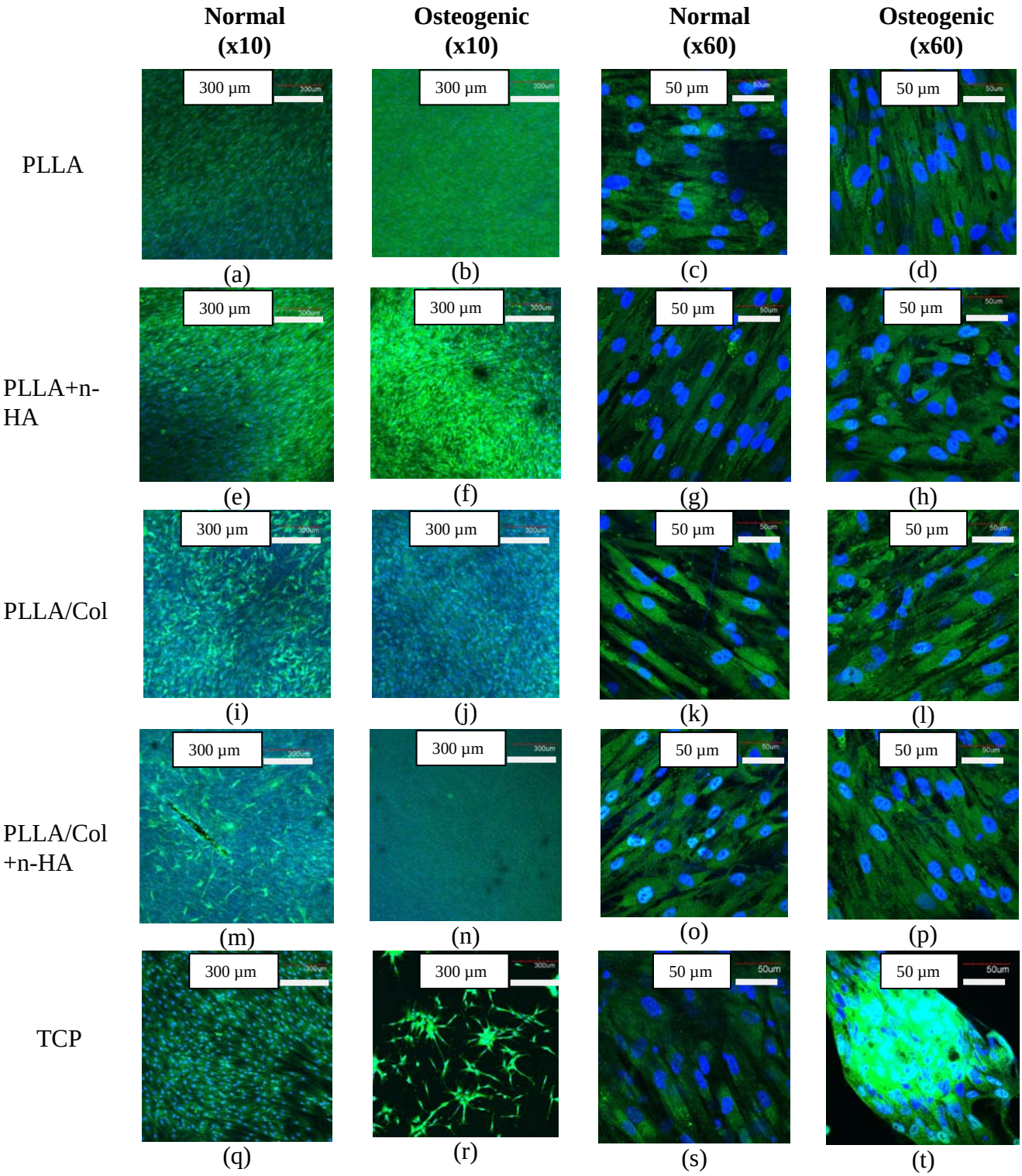

Fig. 4.7: Osteocalcin staining of various substrates after 21 days of culture. Blue denotes DAPI-stained cell nucleus and green denotes osteocalcin expression. Scale bars for x10 and x60 are 300 µm and 50 µm respectively

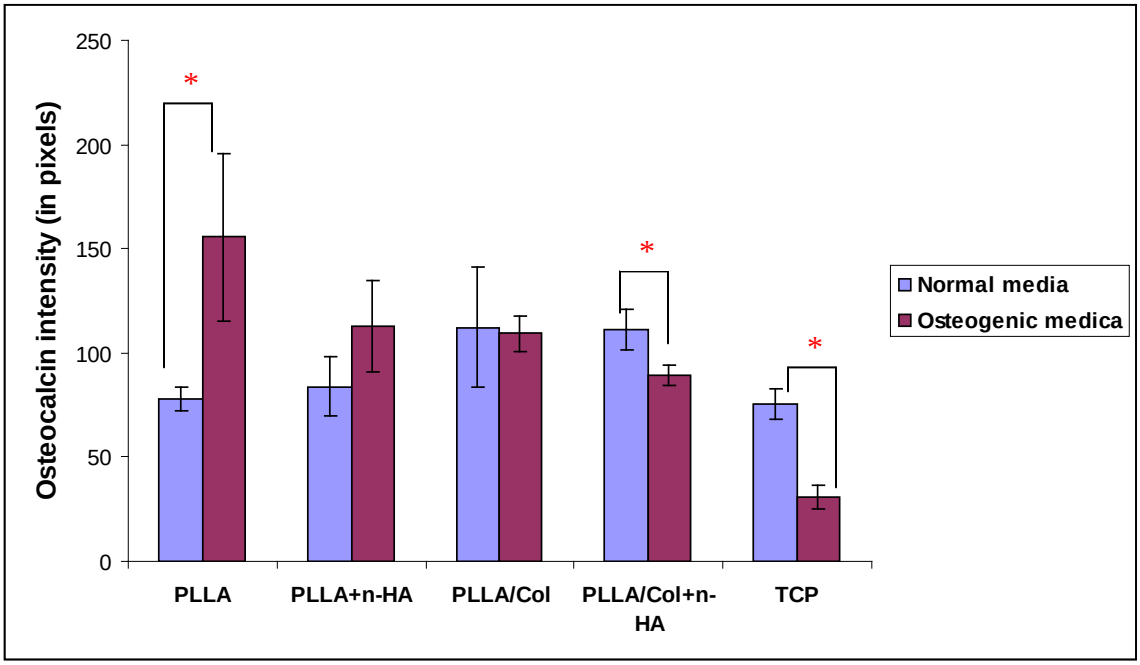

Fig. 4.8: Osteocalcin intensities of various substrates after 21 days of culture. Significant difference between different groups were denoted as * ($p<0.05$)

Fig. 4.9 shows the cell morphologies after 14 days of culture in normal media. Minerals secreted by the MSCs were observed on all the nanofiber groups except PLLA. More minerals were seen on mineralized PLLA and PLLA/Col. As mineralization is considered a late-stage osteogenic marker (usually seen after 28 days of culture and often aided with osteogenic supplements), our results are considered a breakthrough as minerals secreted by the cells were obtained just after 14 days without any osteogenic supplements. The extent of mineralization was more evident on both PLLA+n-HA and PLLA/Col+n-HA than on blended PLLA/Col. This implied that the nanotextured surface of mineralized substrates was capable of inducing osteogenic differentiation.

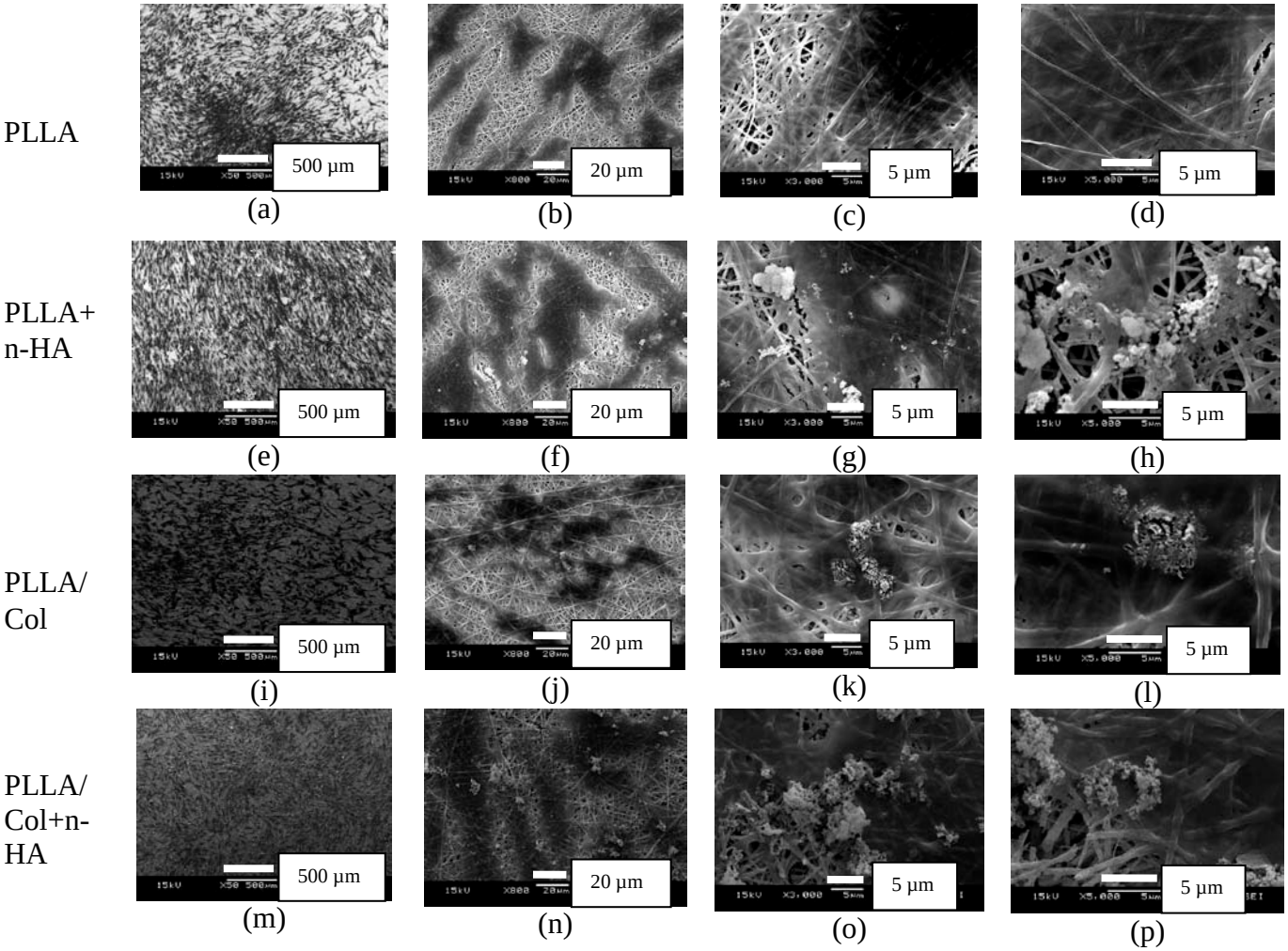

Fig. 4.9: MSC morphologies on mineralized and non-mineralized substrates after 14 days of culture in normal media at various magnifications. (a) to (d) PLLA, (e) to (h) PLLA+n-HA, (i) to (l) PLLA/Col and (m) to (p) PLLA/Col+n-HA

After 14 days in osteogenic media, minerals were seen on the cells in all the nanofiber groups (Fig. 4.10). A greater extent of minerals secreted by cells was noted on mineralized PLLA and PLLA/Col substrates compared to their non-mineralized counterparts, suggesting the benefits of the use of osteogenic supplements. The Ca/P ratios of the bone nodules secreted by the cells after 14 days of culture and the Ca/P

spectra for mineralized PLLA are presented in Table 4.1 and Fig. 4.11 respectively. With the exception of PLLA group in osteogenic conditions, the Ca/P ratios hovered between 1.5 to 1.85, which were within the acceptable range of Ca/P ratios of bone.

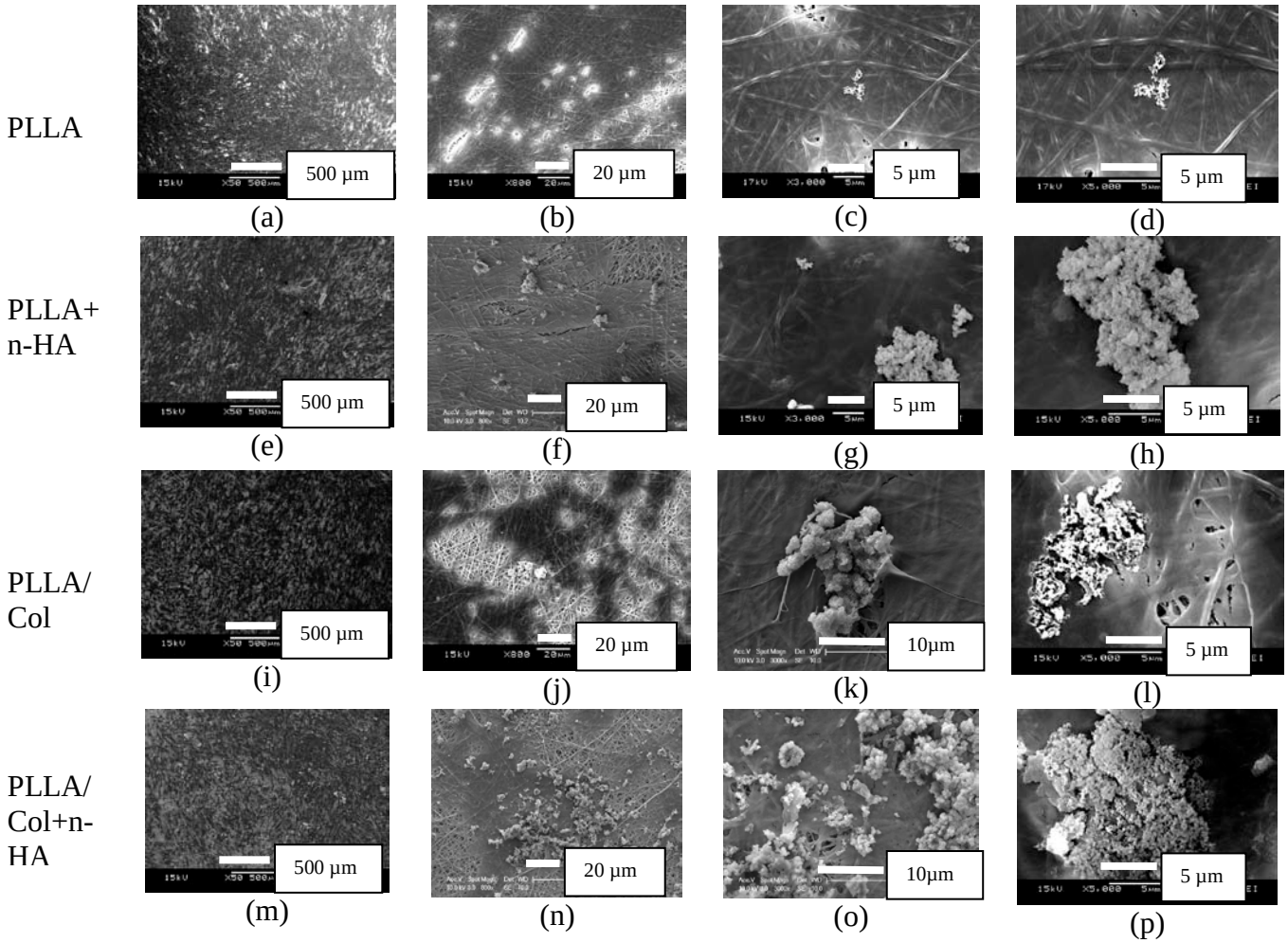

Fig. 4.10: MSC morphologies on mineralized and non-mineralized substrates after 14 days of culture in osteogenic media. (a) to (d) PLLA, (e) to (h) PLLA+n-HA, (i) to (l) PLLA/Col and (m) to (p) PLLA/Col+n-HA

Table 4.1: Ca/P ratios of bone minerals secreted by MSCs after 14 days of culture in normal and osteogenic media. NA: Not applicable.

	PLLA	**PLLA+n-HA**	**PLLA/Col**	**PLLA/Col+n-HA**
Normal	NA	1.7 ± 0.14	1.5 ± 0.31	1.83 ± 0.39
Osteogenic	2.36 ± 1.19	1.85 ± 0.46	1.58 ± 0.83	1.75 ± 0.23

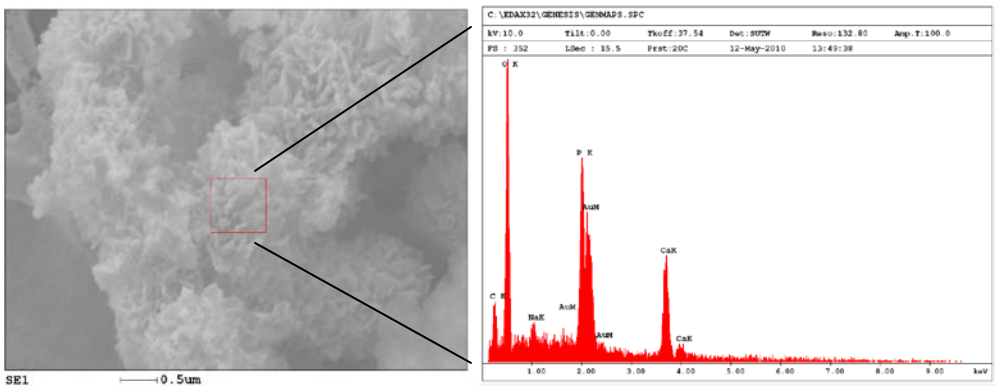

Fig. 4.11: EDX spectra of mineralized PLLA after 14 days in normal media

By day 21, the cells on pure PLLA began to secrete limited minerals without osteogenic media (Figs. 4.12a-d). Mineralized nodules by the cells on PLLA/Col (Figs. 4.12i-l), PLLA+n-HA (Figs. 4.12e-h) and PLLA/Col+n-HA (Figs. 4.12m-p) continued to increase and again, more minerals were evident on cells on mineralized substrates, proving our hypothesis that the nanotextured surface of n-HA on nanofibers was capable of driving MSCs towards a osteogenic lineage without any chemical and mechanical intervention.

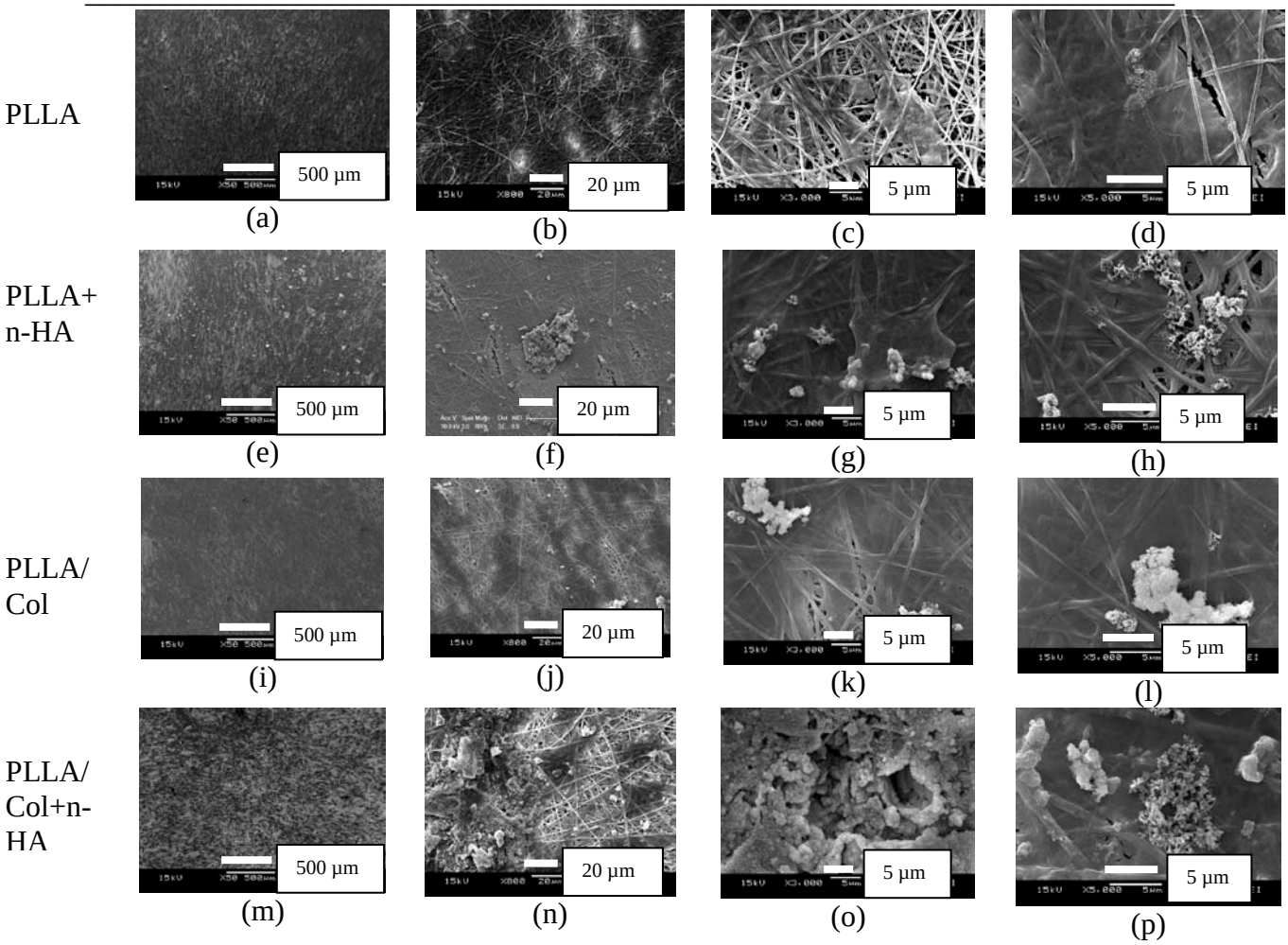

Fig. 4.12: MSC morphologies on mineralized and non-mineralized substrates after 21 days of culture in normal media. (a) to (d) PLLA, (e) to (h) PLLA+n-HA, (i) to (l) PLLA/Col and (m) to (p) PLLA/Col+n-HA

Further mineral enlargement was demonstrated in those cultured in osteogenic media (Fig. 4.13), again with a greater extent of bone nodules by cells on mineralized PLLA (Figs. 4.13e-h) and PLLA/Col (Figs. 4.13m-p) compared to non-mineralized substrates (Figs. 4.13a-d and 4.13i-l).

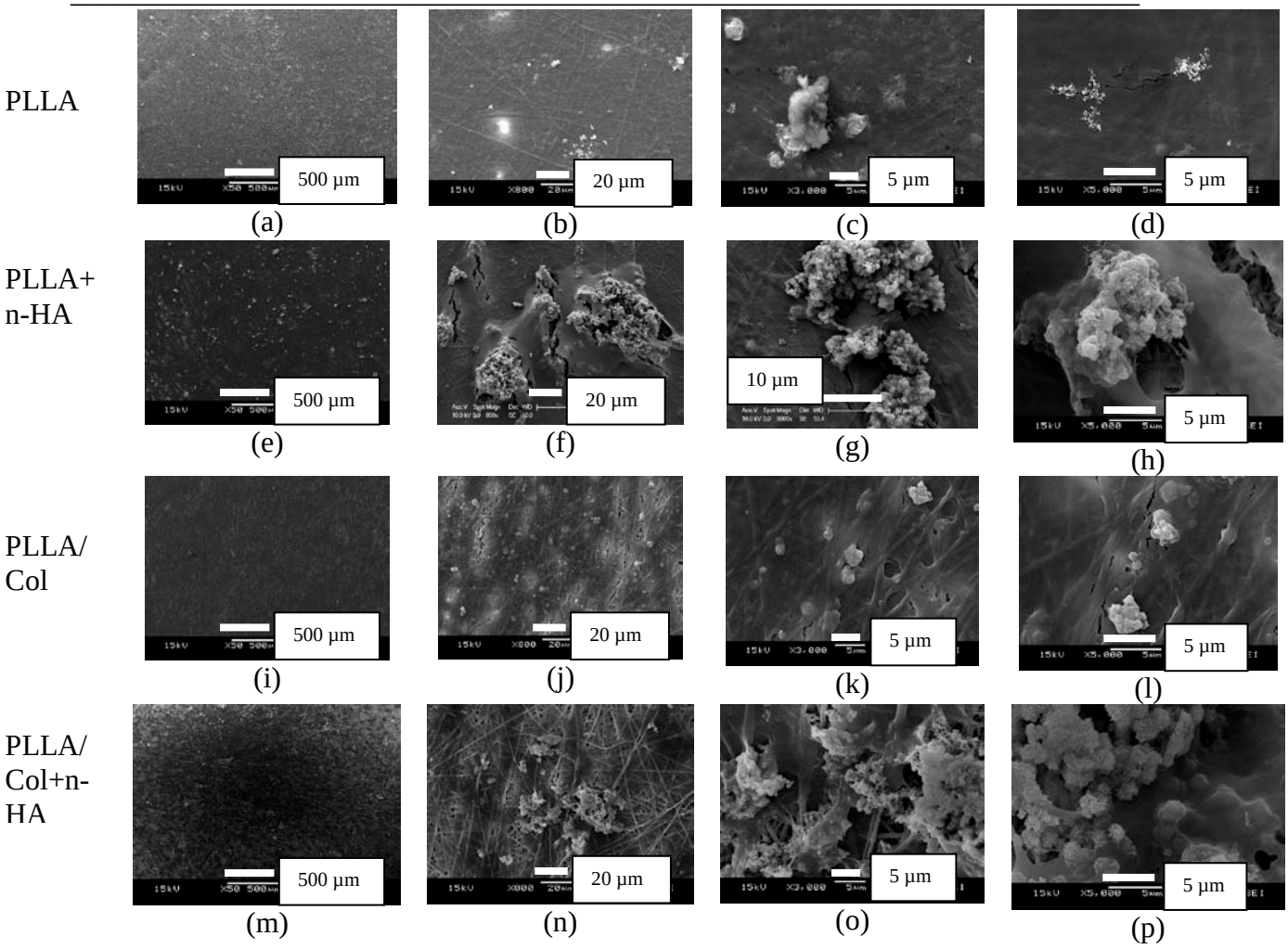

Fig. 4.13: MSC morphologies on mineralized and non-mineralized substrates after 21 days of culture in osteogenic media. (a) to (d) PLLA, (e) to (h) PLLA+n-HA, (i) to (l) PLLA/Col and (m) to (p) PLLA/Col+n-HA

The ARS absorbance levels were normalized with those without cells. Despite the reduction of cell numbers on the nanofibers compared to TCP at early time points, the ARS level was higher in all the nanofiber groups compared to TCP controls as shown in Fig. 4.14. The absorbance levels were negligible for PLLA/Col (normal media: day 14) and TCP controls (normal and osteogenic media: day 14). Osteogenic supplements aided the ARS absorbance level in PLLA on day 28, but with the presence of n-HA on PLLA,

the ARS absorbance levels were comparable at each time point regardless of media conditions. Besides, increased ARS level was seen in PLLA+n-HA than PLLA in normal media after 28 days. The synergistic effects of collagen and n-HA was evident as the ARS levels were significantly higher on PLLA/Col+n-HA than PLLA+n-HA at both time points. Interestingly, the presence of n-HA significantly expedited the ARS levels on PLLA/Col compared to pure PLLA/Col. In fact, n-HA on PLLA/Col ameliorated ARS levels without the assistance of osteogenic supplements on day 28. These results showed that n-HA alone was able to induce osteogenic differentiation of MSCs without chemical supplements.

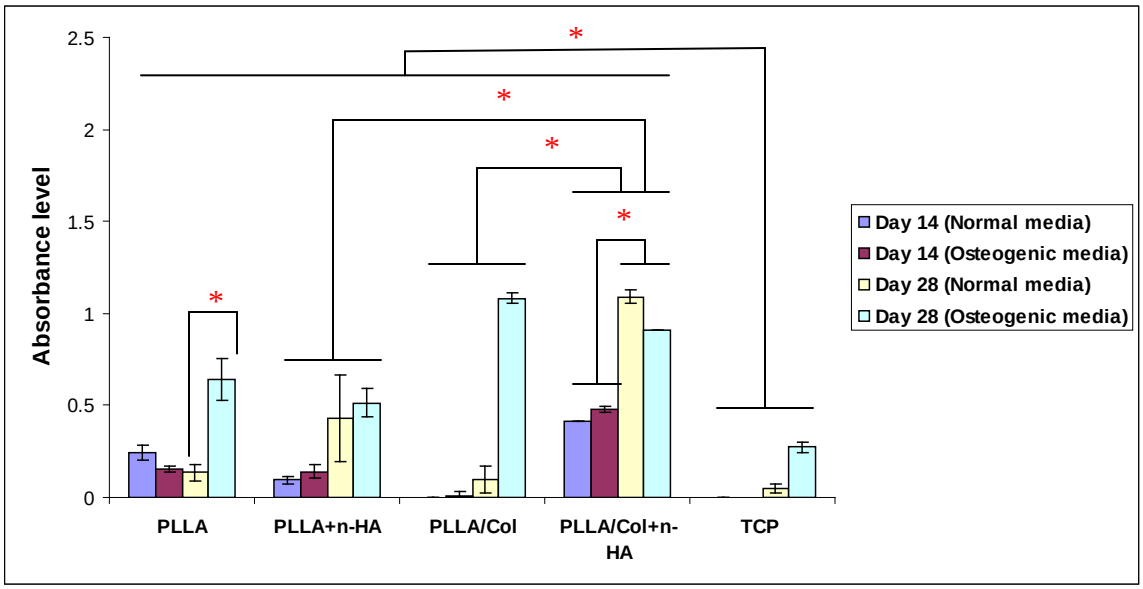

Fig. 4.14: Absorbance level of alizarin red stains of various substrates after 14 and 28 days of culture in normal and osteogenic media. * denotes significant difference between the groups. Note that the absorbance levels have been normalized with the substrates without cells

Figs. 4.15 and 4.16 showed the ARS stained substrates after 14 and 28 days of culture respectively. In both figures, osteogenic supplements hastened the ARS levels on PLLA, PLLA/Col nanofibers and TCP controls. The intensity was the strongest on mineralized PLLA/Col nanofibers at both time points compared to the other material groups. Not surprisingly, osteogenic differentiation was enhanced further after 28 days of culture (Fig. 4.16).

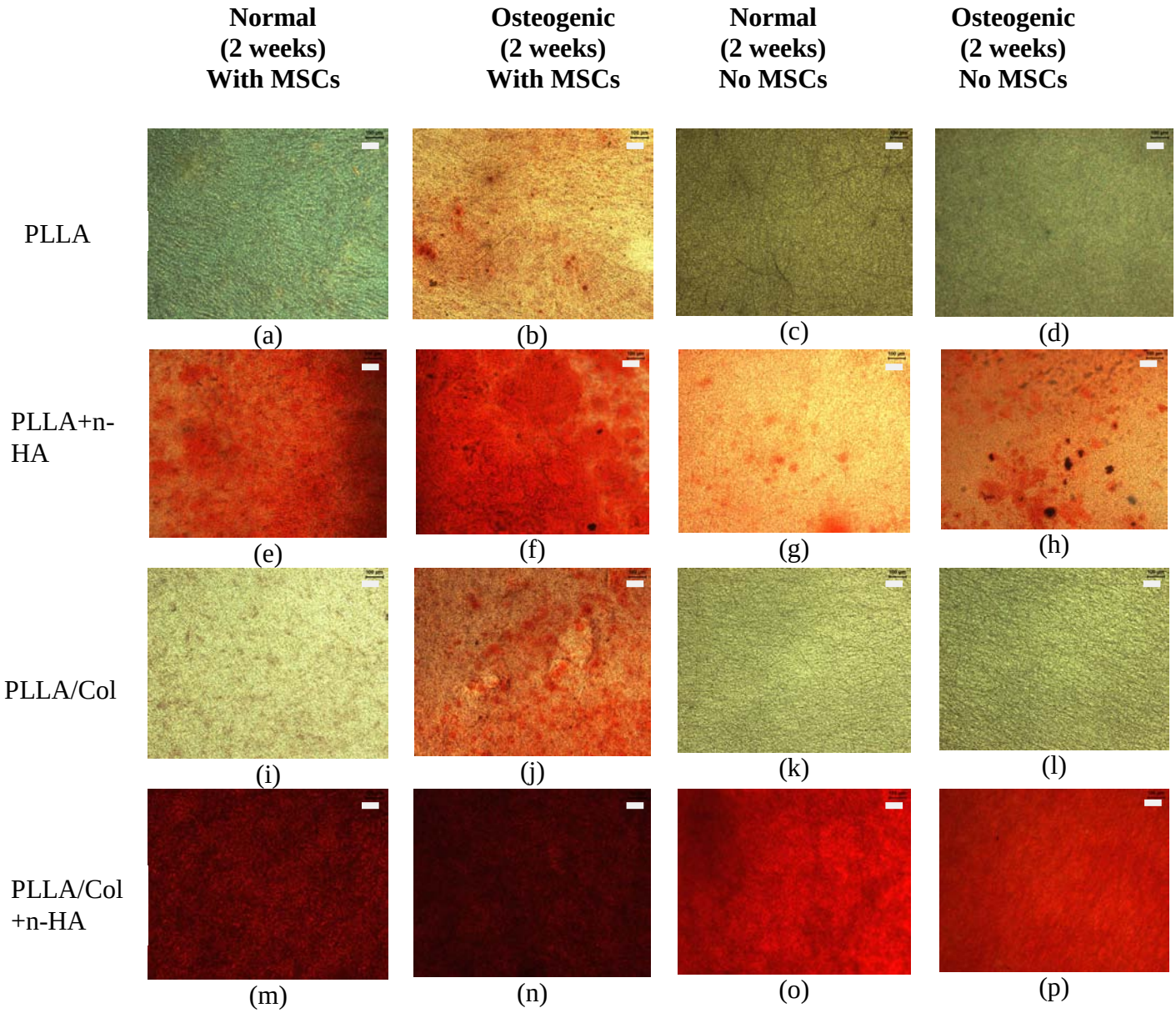

TCP

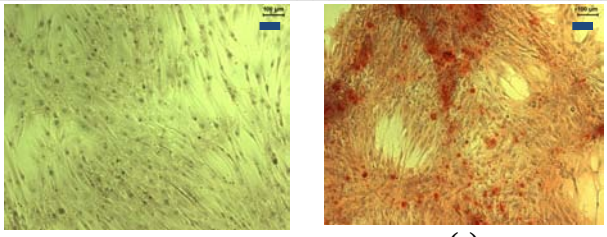

(q) (r)

Fig. 4.15: Alizarin red staining of various substrates after 14 days of culture in normal and osteogenic media. Scalebar: 100 µm

Normal (4 weeks) With MSCs

Osteogenic (4 weeks) With MSCs

PLLA

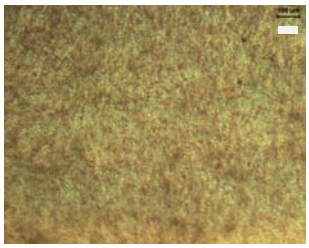

(a)

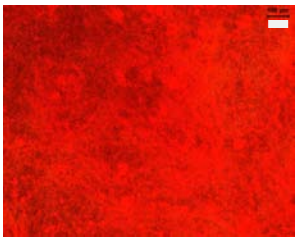

(b)

PLLA+n-HA

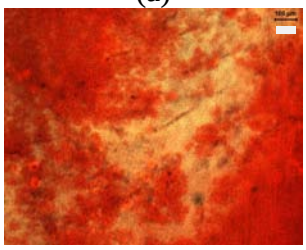

(c)

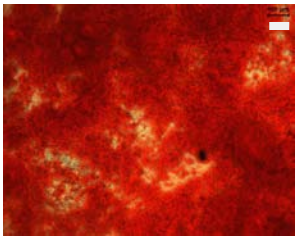

(d)

PLLA/Col

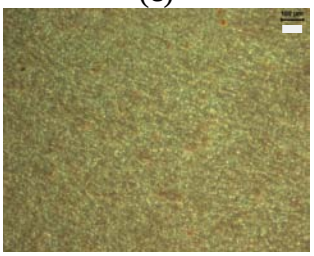

(e)

(f)

PLLA/Col+ n-HA

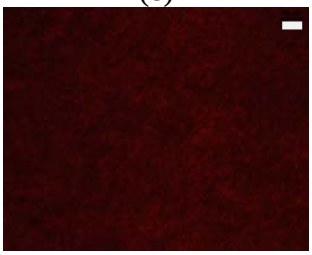

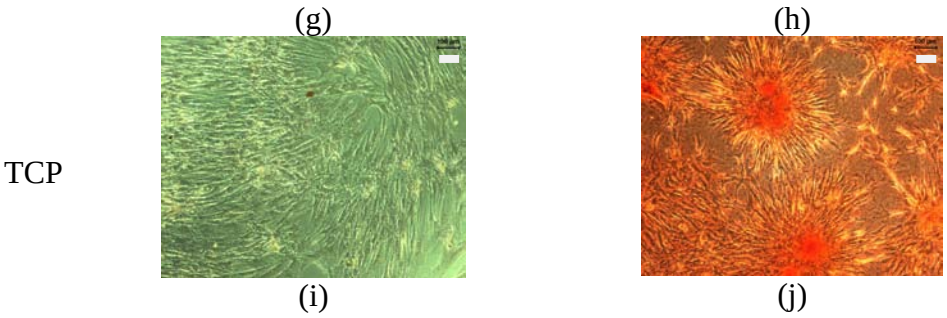

Fig. 4.16: Alizarin red staining of various substrates after 28 days of culture in normal and osteogenic media. Scalebar: 100 µm

Fig. 4.17 shows the von kossa staining of the nanofibers after 28 days of culture. Black deposits were seen on all the nanofibers. Osteogenic media enhanced the mineral deposition on PLLA and PLLA/Col compared to those cultured in normal media. The presence of collagen and n-HA promoted mineral deposition compared to mineralized PLLA nanofibers regardless of media conditions. Again, this shows that n-HA alone or the combination of n-HA and collagen is able to drive osteogenic differentiation of MSCs on nanofiber substrates avoiding the use osteogenic supplements.

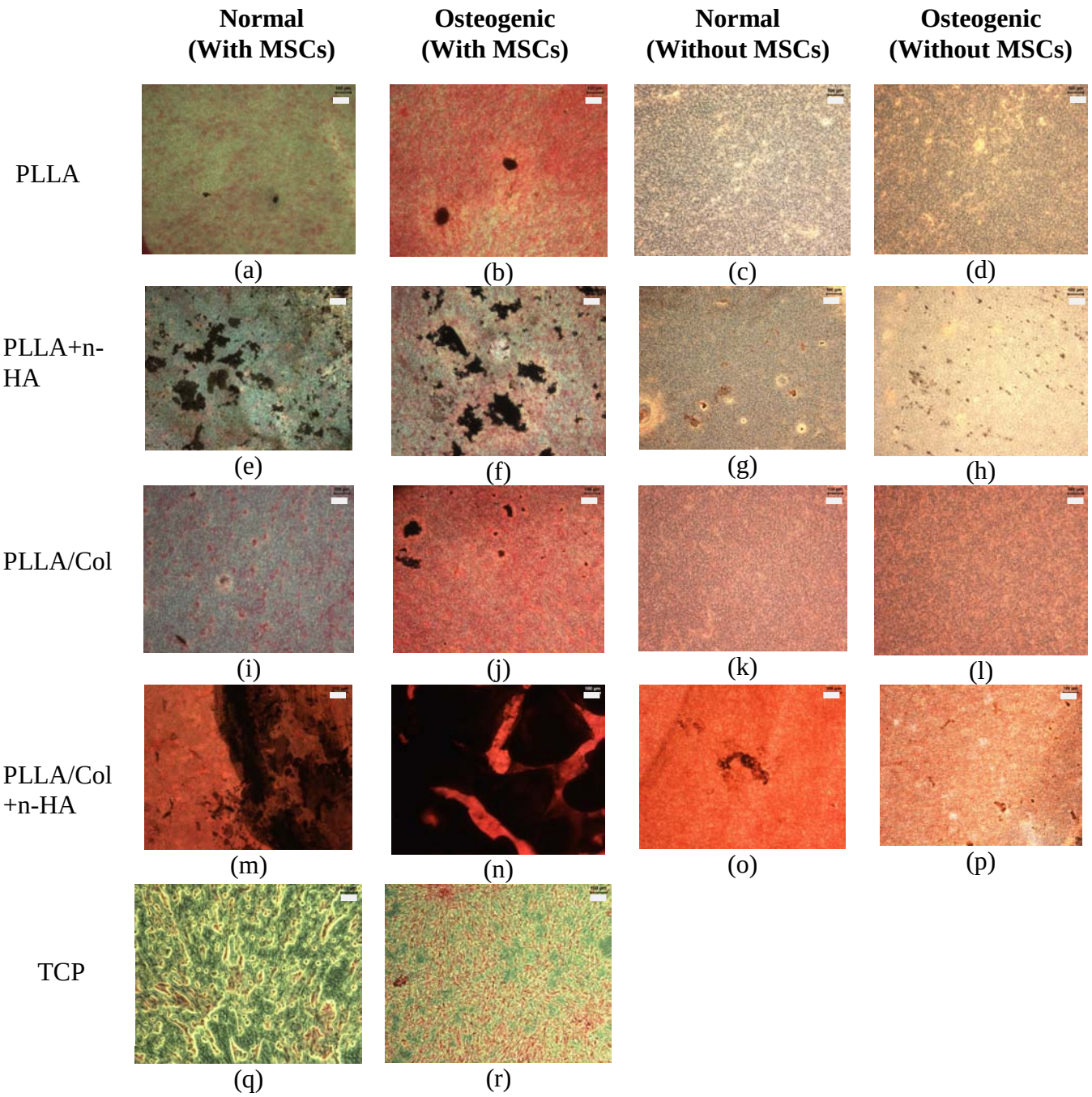

Fig. 4.17: Von kossa images of various substrates after 28 days of culture in normal and osteogenic media. Scalebar: 100 µm

4.4 Discussion

Studies have shown that BM-MSCs are able to differentiate into an osteoblastic lineage [11,24,25,250,251]. From our results, it was shown that the n-HA present on our nanofibers had a positive impact on cellular activity, as shown by the increase in ALP and protein expression, despite lower cell proliferation levels. Our results were in concordance with this study, where BM-MSCs cultured on mineralized Type I collagen membrane, had lower proliferation rates and increased in ALP activity [25]. The ALP expression of BM-MSC was promoted on calcium phosphate-based materials without the presence of osteogenic differentiation additives [252]. It was postulated that calcium phosphate surfaces enhanced osteogenic differentiation, in response to lower number and smaller focal adhesions, but with an increase mobility of focal adhesions [252]. An intracellular signal transduction was likely to be involved and induced by changes in the cell-ECM interaction. Firstly, the chemical properties of the material may induce selective adsorption of matrix proteins [253]. In addition, non-collagenous matrix protein such as osteocalcin and bone sialoprotein exhibit calcium and HA binding characteristics which are likely to preferentially be adsorbed onto a calcium phosphate-based material. Likewise, type I collagen, vitronectin and laminin were also able to support increase osteogenesis from MSCs [254,255]. The matrix protein composition serves as a substrate for cells for binding and activation of specific integrins. For instance, the binding of integrin $\beta 1\alpha 5$ is vital for osteoblastic differentiation and mineralization [256]. Not only do the material properties affect selective adsorption of proteins, the material characteristics also influence the structural organization of the matrix proteins, where alternations in integrin binding domains may occur. For example,

when the structure of the adsorbed fibronectin was modified by surface chemistry, the integrin biding activity was affected, in turn modulating osteoblastic differentiation [206]. Moreover, higher surface area was associated with mineralized substrates and this could in turn attribute to enhance the adsorption of soluble factors onto the substrate surfaces.

Nanofiberous scaffolds being in nanometer scale (in diameter) are said to resemble the ECM proteins, and such microenvironment is conducive for cellular interaction. Nanotexture is said to influence cell activity. Cells are subjected to topographical features such as protein folding, collagen bending within a niche *in vivo*. Nanoscale disorder has shown to stimulate osteogenic stem cell differentiation without chemical treatments [31]. Such geometric cues have demonstrated a dominant effect on adhesion, spreading, growth and differentiation of MSCs. Increase cell growth, cell numbers and osteogenic differentiation was also more evident 3D scaffolds with nanotextured surfaces compared to smooth 3D scaffolds [257], implying the importance of nanotopographical features in modulating cellular activities. In our study, the biophysical cues which aided in the osteogenic differentiation include the nanotopography of the fibers and the n-HA particles on the fibers. This is the first time that osteoinductivity is demonstrated on nanofibrous scaffolds without any osteogenic supplements. Bone nodule formation by the cells occurred at very early time point without osteogenic reagents, especially on mineralized substrates. The cells first undergo attachment, proliferation, ECM formation and lastly mineralization in an osteoblastic lineage [258]. Typically, mineralization usually occurs after 28 days. In osteogenic conditions, BM-MSCs and osteoblasts reached confluence at day 14, but bone nodules

were formed after 21 days [258]. Here, good evidence showed that the synergistic combination of collagen and n-HA greatly induced osteogenic differentiation as osteocalcin expression and ARS levels were meliorated in normal media but not in osteogenic media. Furthermore, the higher ARS levels were cognate with mineralized PLLA/Col compared to mineralized PLLA/Col regardless of media conditions.

When MSCs were cultured on HA surfaces, osteo-specific genes were up-regulated [24,25]. It was speculated that when the cells interacted with HA, potent inductive substances were released. Using this conditioned media after the initial culture, uncommitted MSCs were then cultured without the presence of HA and upregulation of osteo-specific genes were observed [24]. During bone remodeling, the mineral phase in bone undergoes a degree of bioresorption and cells such as MSCs and osteoblasts are recruited to the site of interest for the ossification process. As the n-HA on our fibers resemble the morphology and composition of natural n-HA in bone, we cannot rule out the possibility of a local release of Ca and P ions from the fibers in the media, which could in turn induce the cells towards an osteogenic lineage. Although some reports stated that HA induced osteogenic differentiation of MSCs and other cell types, there were also conflicting reports which saw an attenuation in osteogenic differentiation when cells were cultured on HA surfaces [259,260]. This could be due to the physical and chemical characteristics of the HA material such as crystallinity and particle size etc [260].

In vivo osteoinductivity in a rat model was attenuated when the MSCs were subjected to longer culture periods (16 days) compared to shorter culture period (4 days) in osteogenic media for expansion prior to seeding on titanium fiber meshes [261]. The meshes seeded with MSCs that were expanded in normal media for 6 days (as the control group) fared better than those cultured in osteogenic media for 16 days, but less bone formation was observed in the control group compared to those pre-cultured for 4 days in osteogenic stimulants. These observations implied that cell aging caused by prolonged osteogenic factors had a negative effect on osteoinductivity and high cell proliferative capability (control group) alone was not sufficient in elevating osteoinductivity, but rather the stimulated cells needed to be at the earlier differentiation phase in order to enhance the recruitment of new osteoprogenitor cells for optimal *in vivo* bone formation [261]. From these observations, the state of differentiation level and the type of MSC carrier are important considerations for the use of tissue-engineered constructs in *in vivo* situations [178].

4.5 Conclusion

Our results delineated the importance of nanotopography and nanotexturing in stimulating stem cell osteogenic differentiation, without compromising cell functions and material properties. By minimizing cell aging from extensive long culture periods, optimal cell functionality and regenerative process may be achieved. As our biomineralized nanofibrous composites are biomimetic and also scalable into 3D scaffolds, this further translates into potential clinical applications for bone regeneration.

Chapter 5

3D nanofibrous scaffold enriched with bone marrow stem cells for bone repair in critical size defects

5.1 Introduction

Large segmental bone defects are difficult to treat in clinical settings, because of the extensive loss of bone and in many cases, the periosteum is damaged [32]. In many clinical situations, compromised bone is often inevitable and thus, the bone's load-bearing capacity is greatly hindered. Despite the plethora of bone graft materials commercially available, there are concerted efforts to develop tissue-engineered substrates for bone graft applications to address problems associated with autografts such as donor site morbidity and limited supply. Allografts on the other hand, posed the risk of graft rejection and disease transmission. Although synthetic bone grafts provide a solution to address the shortage of autografts and allografts, the main disadvantages of these calcium-based systems are that they are brittle and have slow resorption especially HA.

Multiple reports have examined several 3D material fabrication techniques such as phase separation [262,263], solvent casting and particular leaching [264], and various rapid prototyping methods [265,266]. Although rapid prototyping produce scaffolds with controlled micro-architectures such as defined porosity and structural dimensions, precise micro and nanotexturing of the surface are often not present. Such surface features are

important and they serve as contact guidance, influencing cell adhesion behavior and cell growth. Cell attachment, proliferation, migration and differentiation are also strongly dependent on the chemical characteristics of the substrates. Several studies have shown that nanopatterns and topographical features affect cell fate [31,257]. Our previous work showed that the n-HA on nanofibers could modulate cell behavior [19,21]. It was demonstrated that nanofibers were effective in early cell capture. Since cells are subjected to different nanotextures within a 3D ECM niche *in vivo*, it was hypothesized that 3D nano-scaffold could be an effective carrier for rapid cell capture, which could provide an *in-situ* therapeutic bone graft option for bone regeneration.

5.2 Materials and Methods

5.2.1 Fabrication of 3D PLLA/Col nanoyarns

PLLA (300,000 Da, Aldrich Chemical Company, Inc.) and Type I collagen (Koken Co., Tokyo, Japan) were dissolved (w/w 50:50) in 1,1,1,3,3-hexafluoro-2-propanol (HFP, Aldrich Chemical Company, Inc., St. Louis, MO). The fabrication of 3D nanoyarns was described in our previous work [267]. Briefly, a dynamic liquid system was employed to create a vortex through a 5mm diameter hole at the centre of the collector basin as the water was pumped into the basin at room temperature (25±1ºC) and relative humidity of 65%. The syringe loaded with the polymer solution was connected to a direct current high-voltage power supply (Gamma High Voltage Research, Ormond Beach, Florida) and the applied voltage was 15 kV. The spinneret used was a BD 27G ½ flat-tip needle and the feed rate was set at 1ml/hour (KD Scientific syringe pump, Holliston, MA). The working distance was 15 cm. The fibers which were collected on

the surface of the water of the basin were then drawn through the vortex and collected at the bottom of the water tank, which supplied the flow of water to the basin through a pump. After an hour, the nanofibers were then collected and stored in DI water prior to n-HA mineralization. For non-mineralized scaffolds, the nanoyarns were immediately mounted into a mold (6 mm in diameter, 17 mm in length) and freeze-dried overnight.

5.2.2 Mineralization of 3D nanoyarns

The 3D nanoyarns were chemically treated in calcium and phosphate (Ca-P) solutions. Using the same treatment conditions in our previous studies [19,21], the nanoyarns were first subjected in 0.5M of $CaCl_2$ (pH 7.2) (Aldrich Chemical Company, Inc., St. Louis, U.S.) for 10 mins, following by deionized water (DI) rinsing for a couple of mins. The nanoyarns were then immersed in 0.3M Na_2HPO_4 (pH of 8.96) (Merck & Co. Inc., N.J, U.S.) solution for 10 minutes and then rinsed with DI water. This typified 1 cycle of treatment and the PLLA/Col nanoyarns underwent 3 cycles of Ca-P treatment. After n-HA mineralization, the nanoyarns were fitted into a mold (6mm in diameter, 17mm in length) and then subsequently freeze-dried overnight.

5.2.3 Material characterization of 3D nanoyarns

The morphologies of the nanoyarns and a commercial product (mineralized collagen fibers) were observed using a field-emission scanning electron microscopy (FESEM) (Quanta 200F, FEI, Oregon, U.S.) at an accelerating voltage of 10 kV or 20 kV. From the FESEM micrographs, the average fiber diameter of the nanoyarns (n=10 fibers)

was determined using an image analysis software (Image J, National Institutes of Health, Bethesda, U.S.). Scaffolds incubated with bone marrow were dehydrated by treating in increasing concentrations of ethanol (50%, 70%, 90%, 100% (twice)) for 10 minutes in each solution, followed by vacuum-drying for 2 days prior to SEM observation. Thermogravimetry analyzes (TGA) (TGA 2050 Thergravimetric Analyzer, TA instruments, Tokyo, Japan) were conducted to determine the amount of HA present on the mineralized nanoyarns. The fibers (n=5) were heated up to 1000°C, at a heating rate of 10°C/min in air conditions. The specific area of the nanoyarns was tested using the Brunauer-Emmett-Teller (BET) Analyzer (Nova-3000 Version 6.07, Quantachrome Instruments, Florida, U.S.). The nanoyarns (n=3-4) were degassed at room temperature for a day before measurements were taken [113,268]. Porosity assessment of the scaffolds (n=3) was determined by the liquid displacement method. Each scaffold was weighed prior to submersion in a known volume of water and a series of brief evacuation-repressurization cycles was performed to force the liquid into the pores of the scaffold. The liquid-impregnated scaffold was then weighed and the porosity was calculated as a percentage. The mineralized and non-mineralized nanoyarns (n=3-4), with a length of 6 mm and diameter of 6 mm were mechanically-tested under compressive conditions, at a strain rate of 3 mm/min, using an Instron 3345 single column test system (Instron, MA, U.S), with a load of 100N. Compressive results were analyzed by Instron Bluehill software (Version 2.16.635). The calcium and phosphate (Ca/P) ratios (n=10) were measured using the SEM-EDX (Energy Dispersive X-ray Spectroscopy, JSM-5600LV, JEOL, Japan/Oxford EDX, INCA).

5.2.4 Cell capture from rabbit bone marrow

Bone marrow was harvested in each of the tibia of the rabbit [269,270]. The bone marrow obtained from each tibia was mixed together and separated into two equal portions consisting of 5 mL, one portion for determining the cell number (control) and the other portion for cell capture. For the first portion, 20 mL of Hank's balanced salt solution (HBSS, Invitrogen, CA, U.S.) was added to the 5 mL of bone marrow to make up a total volume of 25 mL. This mixture was then gently overlaid onto a separate tube containing 20 mL of Histopaque 10771 (Sigma-Aldrich, U.S.). After centrifugation at 1800 RPM for 30 minutes at room temperature, the cell layers at the 20-25 mL mark of the tube was collected after removing the top layer of solution (from the 25 to 45mL mark of the tube). The 5 mL of cell layer was then transferred to a tube containing 15 mL of HBSS and then centrifuged at 1000 RPM for 10 minutes at room temperature. After which, the cell pellet was collected and then mixed with 15 mL of HBSS and centrifuged again, at 1000 RPM for 10 minutes at room temperature. The supernatant was removed and the cell pellet was diluted with cell media consisting of α-MEM (Invitrogen, CA, U.S.), 10% fetal bovine serum, 1% penicillin-streptomycin and 10 nM of dexamethasone for cell counting using a hemocytometer. The second portion of the fresh bone marrow was gently and slowly flushed through a 5 mL syringe containing the 3D mineralized nanoyarn scaffold for a series of ten times (i.e. suction and plunging marrow through syringe equates one time). Subsequently, the nanoyarn scaffold was incubated at room temperature for 20 minutes. After which, the nanoyarn was immediately fixed with 4% paraformaldehyde for 30 minutes at 37ºC and the residual bone marrow was collected, diluted with HBSS and centrifuged according to the protocol

as previously mentioned. The number of cells in the residual marrow (effluent) which was obtained after incubation with the scaffold was also determined using the hemocytometer. After fixation, the nanoyarn scaffold was washed with phosphate buffered saline (PBS) thrice and then blocked with 2% bovine serum albumin (Sigma Aldrich, U.S.) diluted in PBS (BSA/PBS) for 40 minutes at 37ºC. After rinsing with PBS thrice, the scaffold was incubated overnight at 4ºC with rabbit CD44 (SM 607 from Acris GMBH, Germany) that was diluted in 2%BSA/PBS (1:100). Subsequently, the scaffolds were incubated at 37°C for 1 hour with goat anti-mouse antibody (FITC) (Invitrogen, CA, U.S.) that was diluted in 2% BSA/PBS (dilution of 1:100). DAPI diluted in PBS (1:5000) was then incorporated and this incubation was done at room temperature for 30 minutes. To test for non-specific antibody binding, some scaffolds were not incubated with primary antibody CD44 but incubated with FITC and DAPI. The nanoyarns were then observed using a confocal microscope (Olympus FV 500, Olympus Corporation, Tokyo, Japan). The sample size for cell capture studies was five. The cell morphology on the nanoyarns was also observed using SEM. As it was almost an gargantuan task to quantify the total number of nucleated cells and MSCs captured in the 3D scaffolds, we plated the cells from the control and effluent samples onto three wells of 24-well tissue culture plates and incubated for 1 hour at 37ºC prior to DAPI and CD44-FTIC staining. Confocal images (at least 20-30 images) were taken and the number of MSCs was calculated from these images to ascertain cell capture results based on hemocytometer. Note that one sample (control and effluent) was based on marrow obtained from one rabbit.

5.2.5 Colony-forming unit (CFU) study

After cell counting of the control (without flushing through scaffold) and residual/effluent marrow (obtained after flushing through scaffold), each of these marrow samples (n=3) were plated onto the 6-well plate and cultured in α-MEM (Invitrogen, CA, U.S.), 10% fetal bovine serum, 1% penicillin-streptomycin and 10 nM of dexamethasone. Media was changed on the 6^{th} day. After 13 days of culture, the media was removed and rinsed with DI water. 2 mL of CFU staining reagent (120 mM Tris buffer (BioRad Laboratories, CA, U.S.), containing 0.9 mM Naphthol-AS-MX phosphate (Sigma-Aldrich, U.S.), 1.8 mM Fast Red TR (Sigma-Aldrich, U.S.) in DI water) was added in each well and incubated for 30 min at 37% degrees in 5% CO_2. The staining reagent was then removed and the culture plates were rinsed with DI water once before colony counting. The number of CFUs (eight or more cells in a cluster) that were expressing alkaline phosphatase activity was considered [271]. Images were taken using a fluorescent microscope (Leica DM IRB, Leica Microsystems GmbH, Wetzlar, Germany) at x100 magnification and a digital camera.

5.2.6 Implantation of mineralized 3D PLLA/Col nanoyarns enriched with bone marrow in a rabbit model

The mineralized PLLA/Col nanoyarn (6mm in diameter, 17mm in length) treated with rabbit bone marrow was implanted in the midshaft of the rabbit ulna (n=3). The rabbit was anesthetized using ketamine 50mg/kg (i.m) + Xylazine 10mg/kg (i.p). We also administered pre-op antibiotics and analgesic, Baytril @ 5mg/kg (i.m) + Rimadyl @

2mg/kg (s.c). Prior to implantation, 5 mL bone marrow (inclusive of 0.5 mL of heparin of 5000 IU/ml) was harvested from the proximal right tibia of the rabbit using a 13G aspiration needle and collected in a 10 mL syringe. The bone marrow was then placed in a kidney dish. The mineralized PLLA/Col nanoyarn was placed in the interior of a separate 5 mL syringe and bone marrow was slowly flushed through the syringe containing the material for ten times (i.e. suction and plunging marrow through syringe equates one time). The nanoyarn was then incubated with the marrow at room temperature for 20 minutes whilst the bony defect was created. The effluent marrow was collected for cell counting. The bony defect of 15 mm was created using an oscillating saw under continuous saline cooling. The entire bone block was removed with the periosteum and the bone ends were cleaned with a bone rongeur. The defect site was then copiously irrigated with saline to remove any bone debris. Our mineralized PLLA/Col treated with bone marrow was then removed from the syringe and implanted into the defect. Post-surgery, the rabbit received Baytril @ 5mg/kg (i.m) - 5 days postop+ Rimadyl at 2mg/kg (s.c) - 3 days postop.

5.2.7 MicroCT analyzes

The explant was removed after three months of implantation. The explant was immediately fixed in 10% neutral buffered formalin. The explant was scanned through 360º with a rotation step of 3º/s, at a spatial resolution of 27 µm x 27 µm x27 µm using a microCT machine (SMX-100CT X-ray CT Sys, Shimadzu, Japan). The parameters used were: X-ray voltage (47 kV), X-ray current (50 µA), detector size (9”) and scaling

coefficient (50). No filter was used during the scanning. The scan files were then reconstructed using a modified Feldkamp algorithm (Skyscan, Belgium), at a step size of 27 µm. The microCT software (VGStudioMax, version 1.2, Volume Graphics GmbH, Germany) was used to construct the 3D image of the explant. Bone volume values were determined by using the reconstructed 3D image where the gray value range for bone were set at 225-255 (CTAnalyser, version 1.9, Skyscan, Belgium).

5.2.8 Statistical analyzes

Student's T-test was employed to assess statistical differences between the material groups for TGA, compressive and cell capture tests. Difference was considered to be of statistically significance at $p < 0.05$.

5.3 Results

5.3.1 Morphology of 3D mineralized and non-mineralized nanoyarns

3D mineralized nanofibrous yarns (nanoyarns) were successfully fabricated which highly resemble the characteristics of native bone which has a nano to macro hierarchical assembly. Depending on the defect size, the 3D nanoyarns can be molded in a cylindrical form (Fig. 5.1a), blocks, fibrils or granules for various applications. Using electrospinning technique, bundles of yarns encompassing continuous, smooth nanofibers were generated by direct freeze-drying of PLLA/Col (Fig. 5.1b).

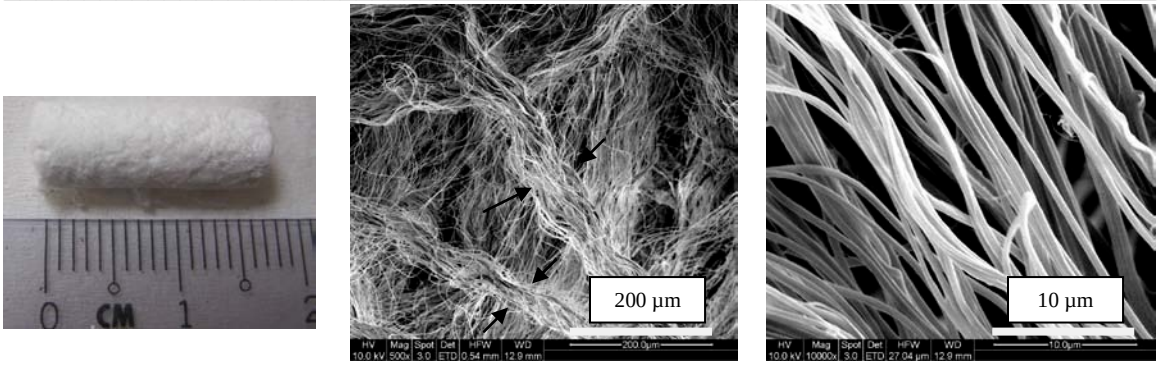

(a) (b) (c)

Fig. 5.1: 3D pure PLLA/Col nanoyarn. (a) Gross image and (b) to (c) SEM micrographs of pure nanoyarn at different magnifications. Arrowheads denote the bundles of yarns (collection of nanofibers).

PLLA/Col was used as the base material for n-HA deposition and interestingly, the individual fibers in each yarn bundle were uniformly mineralized with n-HA (Fig. 5.2). At higher magnifications (Figs 5.2d and 5.2e), the mineralized fiber morphology resembles to that of native bone (Fig. 5.2f from Fantner's Nature's paper [1]). The calcium-phosphate (Ca/P) ratio was 1.67 ± 0.11, similar to that of n-HA in native bone.

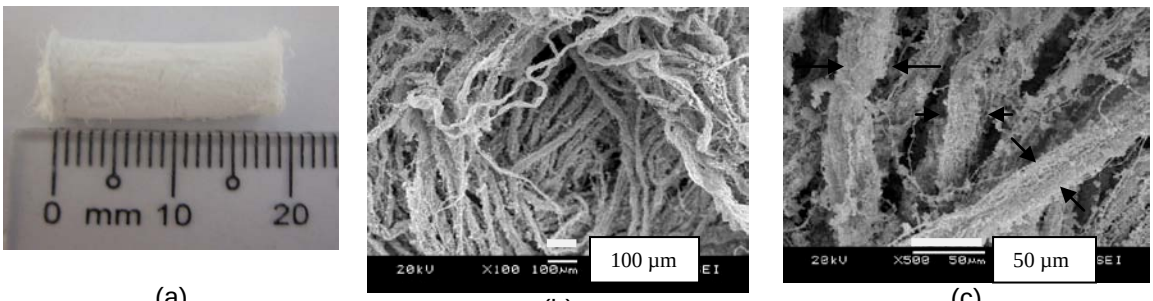

(a) (b) (c)

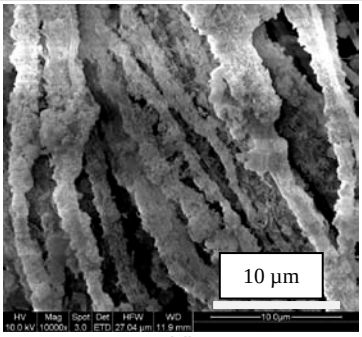

(d)

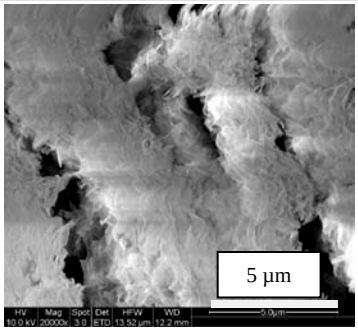

(e)

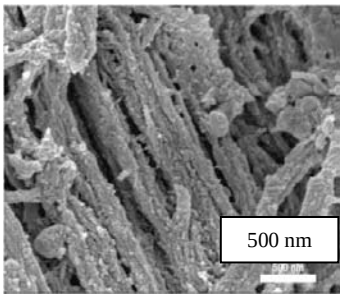

(f)

Fig. 5.2: 3D mineralized PLLA/Col nanoyarn. (a) Gross image, (b) to (e) SEM micrographs of mineralized nanoyarn at different magnifications and (f) SEM micrograph of native bone [1]. Note that n-HA is uniformly distributed on individual fibers. The yarn structure is maintained after n-HA mineralization as represented by the arrowheads in (c)

From the SEM micrographs, the average diameters of the mineralized PLLA/Col and pure PLLA/Col nanoyarn were 563 ± 76 nm and 450 ± 34 nm respectively. Furthermore, the morphology of our mineralized fibers closely mimicked native bone fibers compared to a commercial product which was also mineralized fibers (Fig. 5.3). The Ca/P ratio for the commercial mineralized fibers was 4.94 ± 2.15, which was not similar to that of native bone.

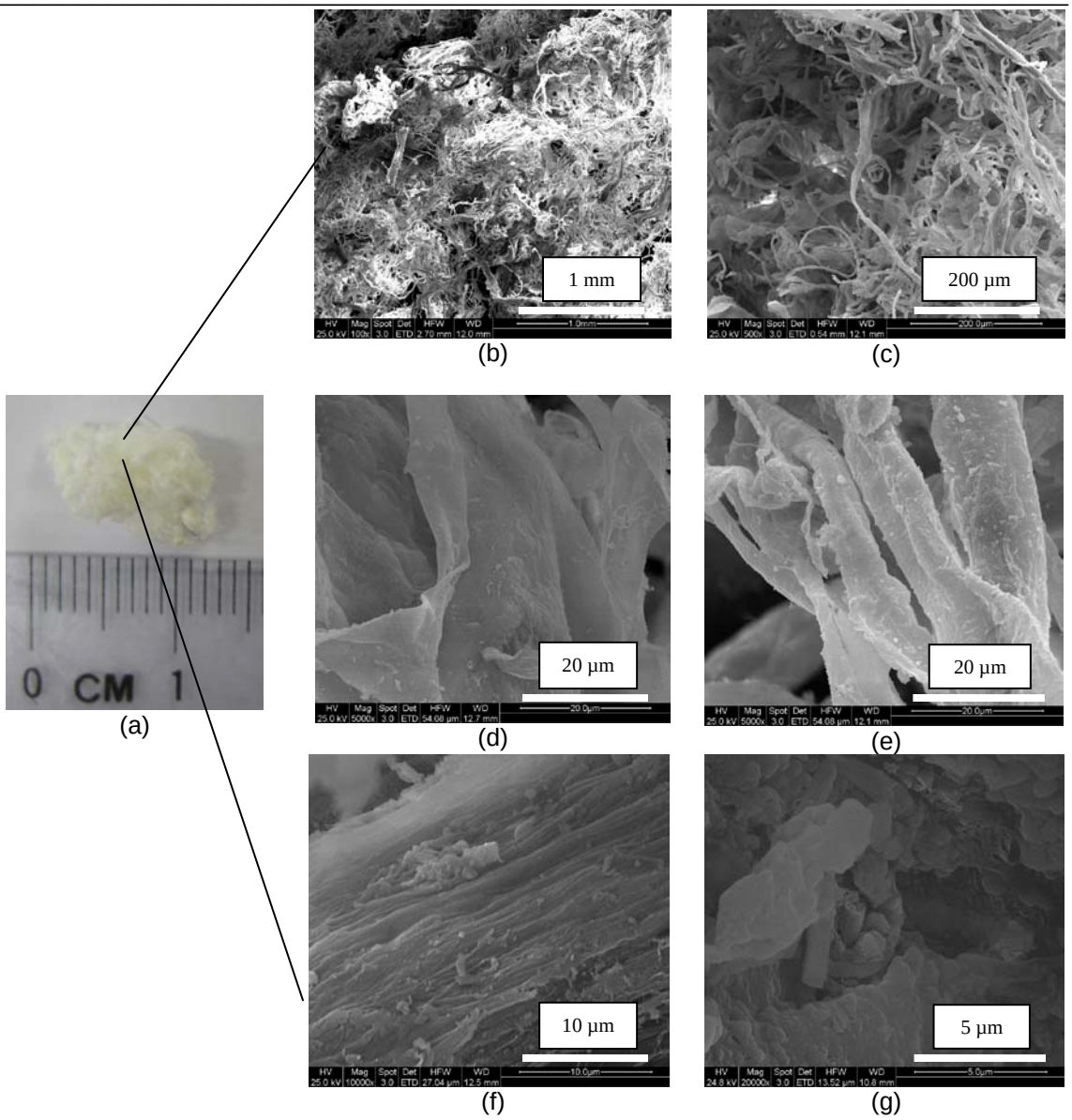

Fig. 5.3: Commercial product (mineralized collagen fibers). (a): Gross image and (b) to (g) are the SEM micrographs at different magnifications

5.3.2 Porosities of 3D nanoyarns

The porosities of non-mineralized and mineralized 3D scaffolds were 82.0 ± 6.1% and 88.3 ± 3.8% respectively. Enhanced cell capture could also be attributed to the

hierarchical structure of the mineralized nanoyarn, where its specific surface area (30.67 ± 4.29 m^2/g) was higher than that of non-mineralized nanoyarn (11.23 ± 3.39 m^2/g).

Based on our previous work, the alternate dipping method was effective in depositing n-HA on PLLA [19] and poly(lactide-co-glycolide) acid (PLGA) [21] NFS. The 3D PLLA/Col fibrous structure (68.91 ± 0.94 wt%) significantly improved n-HA deposition compared to 2D PLLA/Col structures (30.2 ± 9.98 wt%). Strikingly, the amount of n-HA on our 3D nanoyarns were comparable to that of native bone, where the mineral part of natural bone constituted approximately 67% of nanophase HA. This could be attributed to the spatial 3D organization of our scaffolds, allowing n-HA deposition to occur throughout the fiber surfaces. Pre-treatment of the substrates are often considered in order to incorporate functional groups for initial apatite nucleation. Some of the pre-treatment methods include alkaline treatment [225], and surface modification such as plasma surface treatment [226,272]. In this study, such pre-treatment methods were not required. Compared to using SBF where the induction of HA deposition occurs over a period of a few days [273], sufficient HA deposition is accomplished within an hour using our method.

5.3.3 Mechanical properties of 3D nanoyarns

From a biomechanical standpoint, most tissue-engineered constructs possess mechanical properties several orders of magnitude lower than native bone. Besides morphological and compositional similarities to bone, our mineralized nanoyarns had

compressive strength of 1.035 ± 0.22 MPa, which was the lower limit of the compressive strength of human cancellous bone (1 - 100 MPa) [274]. The presence of n-HA improved the mechanical property, where the compressive strength of non-mineralized nanoyarns was 0.58 ± 0.31 MPa. This improvement of 44% in compressive strength of the mineralized nanoyarns was possibly due to the interlocking of the fibers by the n-HA. In a separate study, 3D PLGA scaffold reinforced with 20 wt% grated L-lactic acid oligomer HA nanoparticles showed the maximal compressive strength of 2.31 MPa [275], whereas those scaffolds reinforced with 5, 10 and 40 wt% of HA had compressive strength values of less than 1 MPa. This suggests that increasing the HA content past its threshold can potentially compromise the compressive properties as it would make the material weaker. Besides, more micropores which were present in the pore walls were associated with scaffolds with higher HA content, coinciding with the decrease in compressive strength [275].

5.3.4 Rapid cell capture from bone marrow on mineralized 3D nanoyarns

To demonstrate the effectiveness of our 3D mineralized nanoyarns for rapid cell capture, rabbit bone marrow was flushed through the scaffolds. The average nucleated cell count in 5 mL of marrow prior to marrow flushing was 1,145,500 ± 300,710 cells. The average amount of effluent marrow left after flushing was 3.04 ± 0.36 mL. In addition, the average number of nucleated cells in the effluent was 203,500 ± 92,679 cells. This was significantly lower than the number of nucleated cells of the bone marrow prior to flushing (control samples).

This is the first report that shows that high cell capture from bone marrow is achievable in a 3D biomineralized nanofibrous construct in less than an hour. The nucleated cell capture was 80.2 ± 10.9% (Fig. 5.4) after 20 minutes. Fig. 5.5 shows the nucleated cell count of the control and effluent samples.

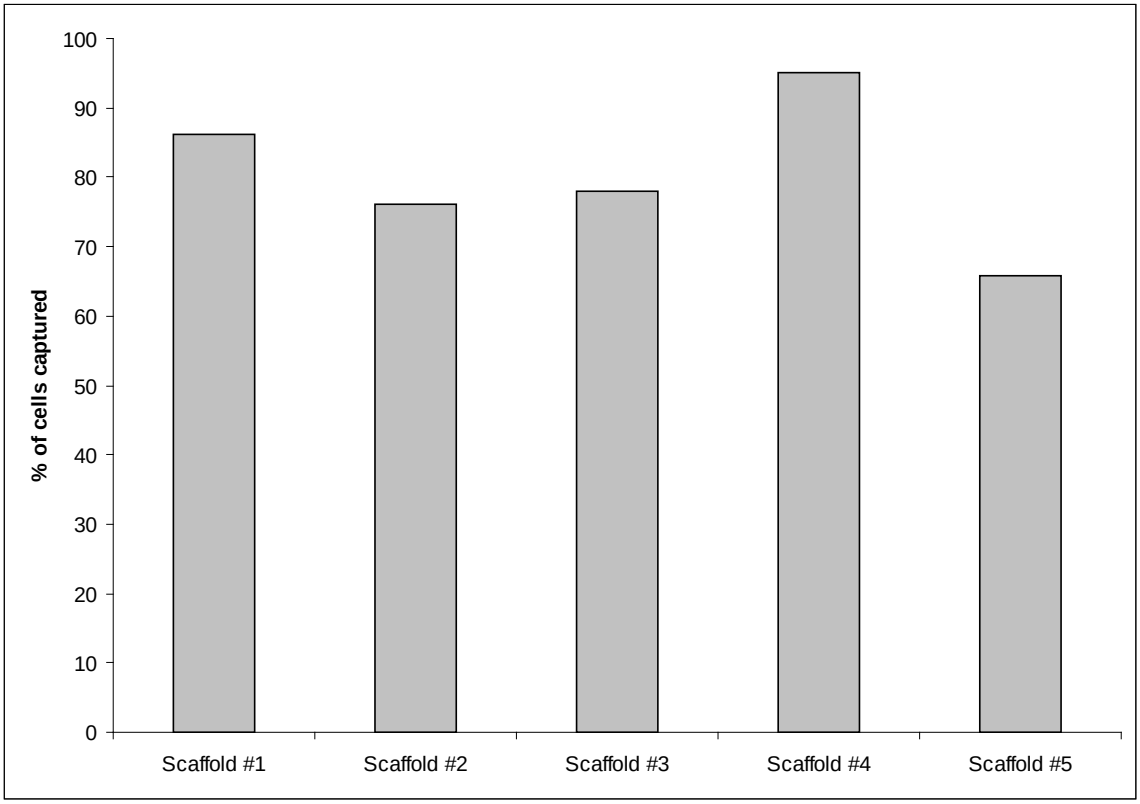

Fig. 5.4: Percentage of cell capture in 3D mineralized nanoyarn scaffolds after 20 minutes of incubation in rabbit bone marrow. Note that cells were captured in scaffolds in *in vitro* settings

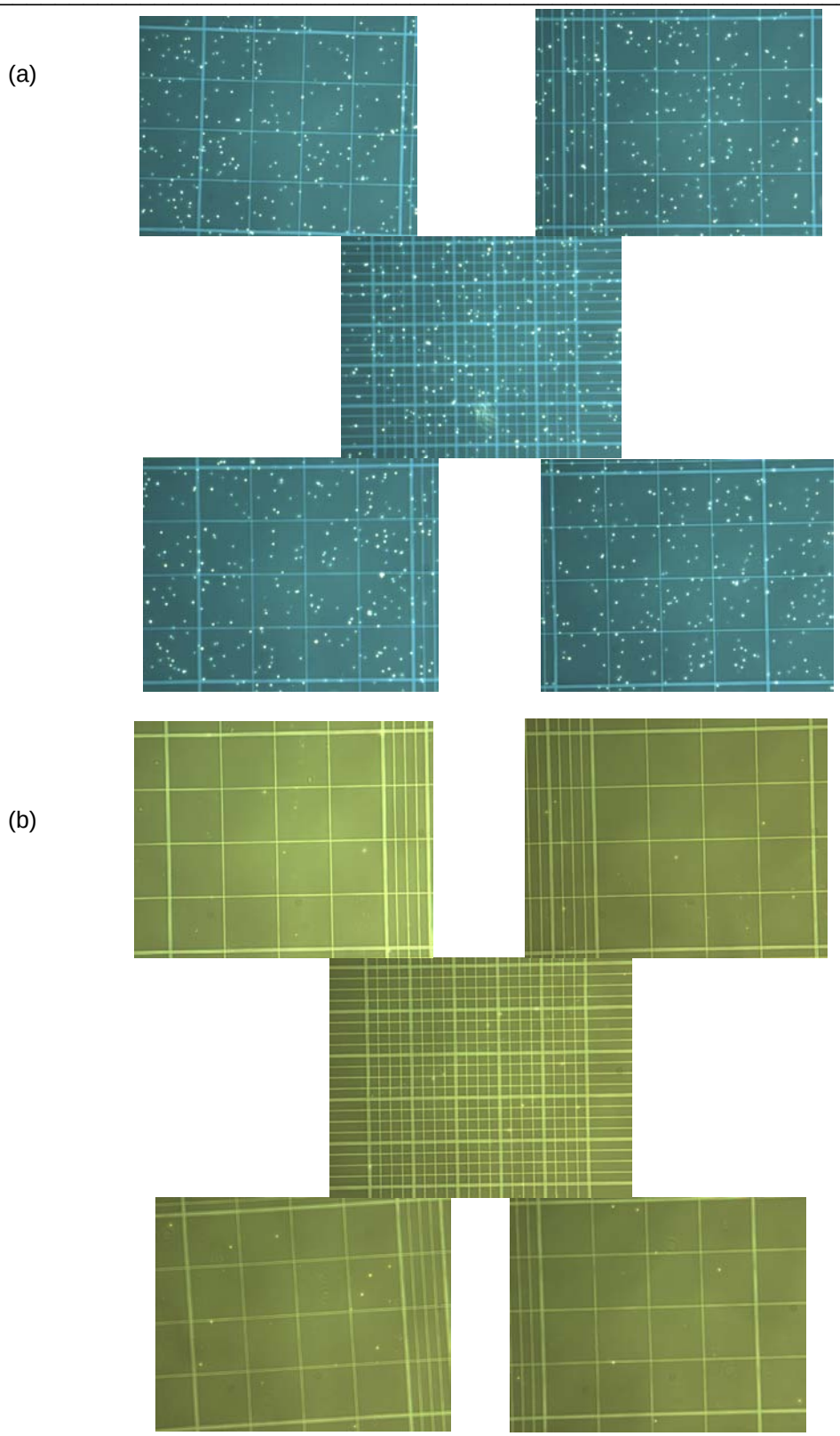

Fig. 5.5: Nucleated cell count using the hemocytometer. (a) Control: 5 mL of marrow without flushing through the scaffold. (b) Effluent: Residual marrow left after flushing through the scaffold

To assess the average number of MSCs captured by the scaffold, the nucleated cells in the bone marrow (before flushing, i.e. control samples) and the nucleated cells in the effluent were stained with an antibody, CD44 and counted using a predetermined number of confocal images. CD44 is one of the MSC markers [276]. The average proportion of the MSCs captured in the scaffold was 76.1 ± 15.2% (Table 5.1). This proportion was similar to the total number of nucleated cells captured in the scaffolds. As such, we could infer that a large proportion of MSCs were captured in our nanoyarns.

Table 5.1: Average of number of MSCs before flushing through the scaffold (control) and after flushing through the scaffold (effluent)

	Sample 1	**Sample 2**	**Sample 3**
Average number of MSCs (CD44-FITC positive) in control	9.45	9.68	3.41
Average number of MSCs (CD44-FITC positive) in effluent	1	3.91	0.71
% of MSC capture	89.42	59.56	79.27

5.3.5 Colony-forming units (CFU) study

In order to determine the number of osteoblastic progenitor cells, colony-forming assays can be employed. These assays can be used to determine the number of colonies formed after culture and these colonies include cells that can differentiate towards an osteogenic lineage or other types of lineages such as fat, muscle, cartilage etc. Such tissue-derived cells can be broadly classified as connective tissue progenitor cells [277]. ALP is an early osteoblastic differentiation marker. Colony-forming units (CFUs) that express ALP activity denote the presence of the osteogenic progenitor cells. Fig. 5.6 shows the colony-forming units-alkaline phosphatase positive (CFU-ALP) of the marrow

obtained before flushing (control) and after flushing through scaffold (effluent). The number of CFU-ALP was significantly higher in our control samples (27 ± 21) than in the effluent samples (0 ± 1). This was consistent with the nucleated cell capture results, where the total cell numbers in the marrow prior to flushing were greater the cell numbers in the effluent samples. Table 5.2 shows the absolute number of CFU-ALP of individual samples before and after marrow incubation.

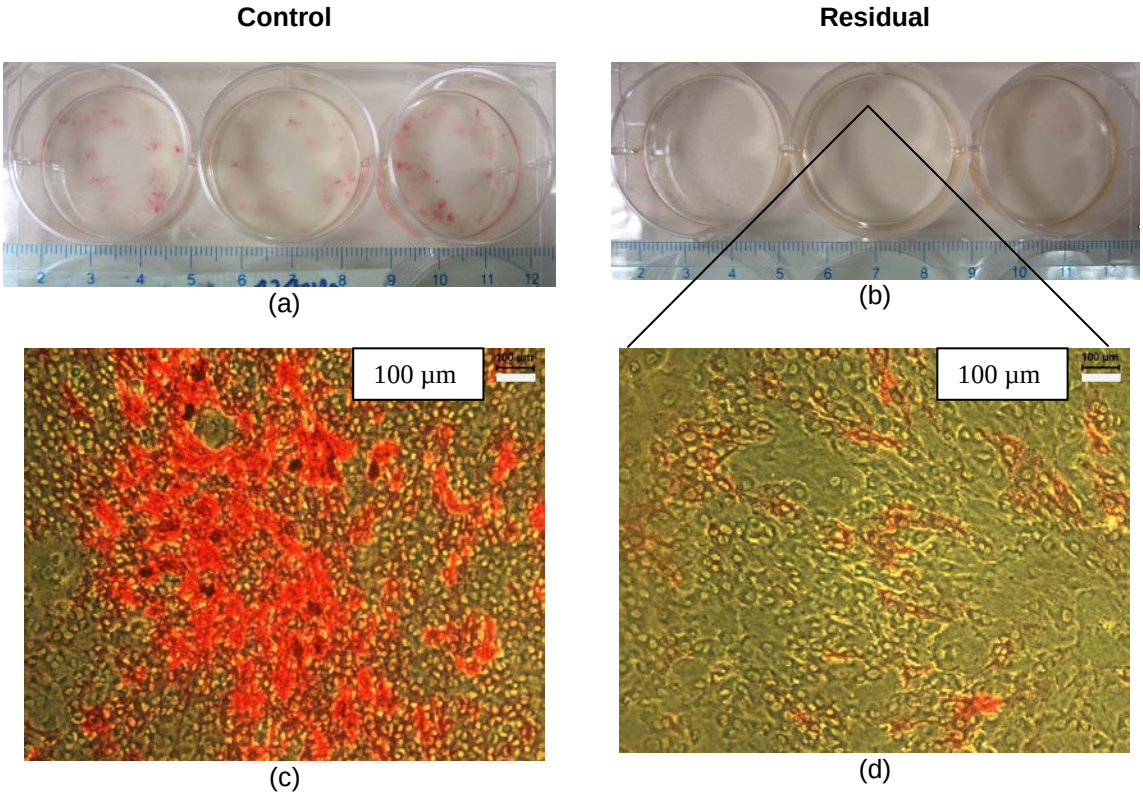

Fig. 5.6: Colony-forming units-alkaline phosphatase positive (CFU-AP) after 13 days of culture. Gross images of (a) control (without flushing through the scaffold), (b) effluent (after flushing through the scaffold) and light micrographs of CFU-AP colonies in (c) control and (d) effluent samples

Table 5.2: Number of colony-forming unit-alkaline phosphatase positive (CFU-AP) in the control and effluent samples. Note that marrow used for the control and effluent samples was obtained from the same rabbit

Sample ID	No of CFU-AP in control	No of CFU-AP in effluent
Sample 1	124	0
Sample 2	3	0
Sample 3	34	1

5.3.6 Immunostaining of mineralized 3D nanoyarn enriched with cells

Confocal images showed that the nanoyarn captured a substantial number of cells, as indicated by the DAPI-stained (blue) nucleated cells (Figs. 5a, 5d, 5g). Interestingly, despite a short cell incubation period, cells were able to penetrate through the nanoyarn as seen in the cross-section of the construct (Fig. 5.7g-i). Immunostaining of the primary rabbit antibody CD 44 (green fluorescent signal) showed the presence of CD44-positive cells (MSCs) on both the surface (Fig. 5.7e-f) and the cross-section (Fig. 5.7h-i) of the nanoyarns.

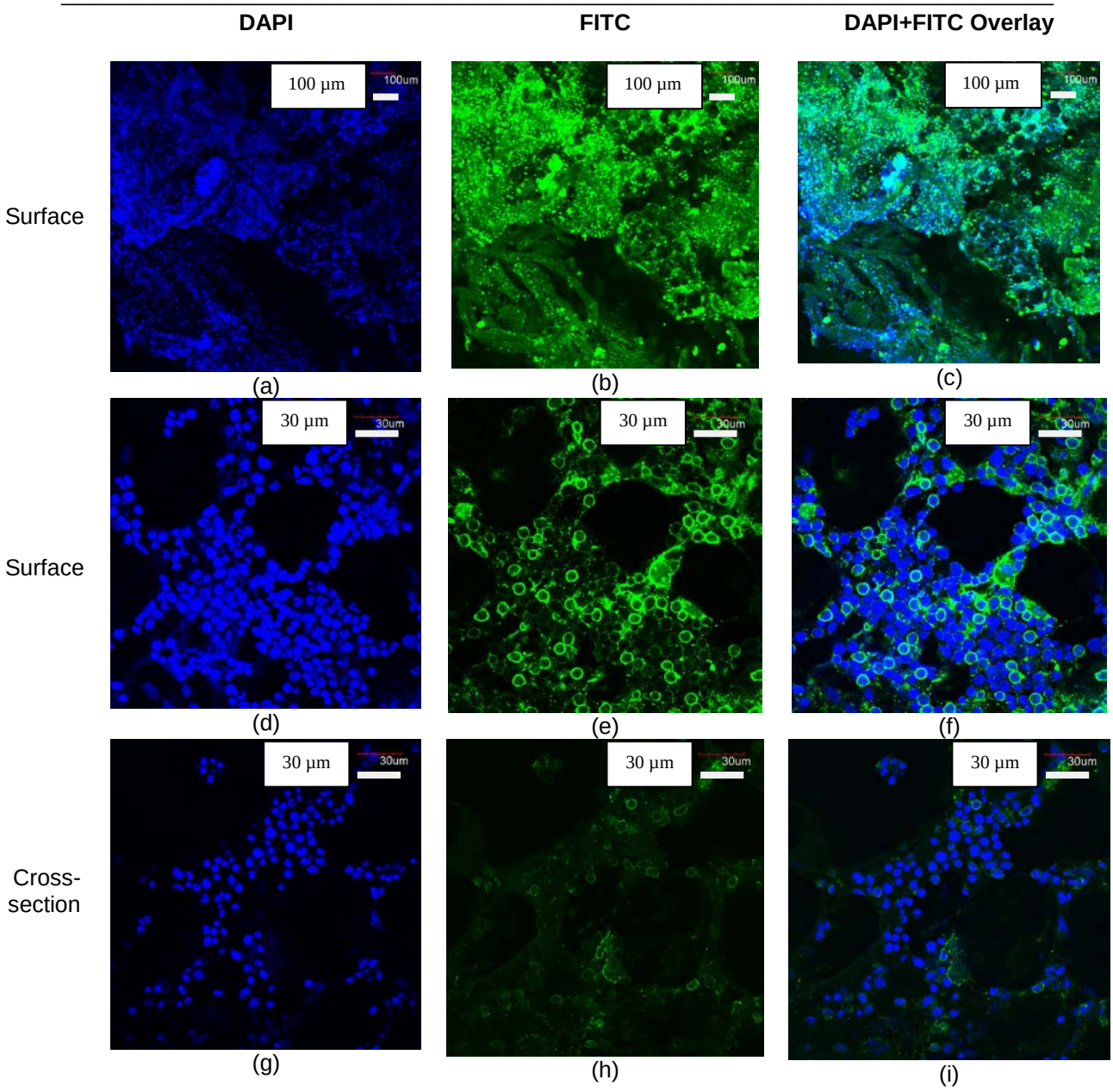

Fig. 5.7: Immunostaining of 3D mineralized nanoyarn scaffolds with primary antibody CD 44. (a) to (c) Surface of scaffold (x10), (d) to (f) Surface of scaffold (x60), and (g)-(i) Cross-section of scaffold (x60). Note that there are more nucleated cells (blue DAPI-stained) cells on the surface than in the cross-section region of the scaffold

It is important to ascertain if the primary antibody CD 44 is cell-specific or physically absorbed onto the scaffold. As such, another scaffold was incubated with only the secondary antibody FITC and without CD44, as seen in Fig. 5.8. Both Figs. 5.7 and 5.8 showed that the scaffold surface was saturated with nucleated cells, with some nucleated cells being captured in the interior of the scaffold. In addition, the green signals (in Fig. 5.8) were weaker. This corroborated that both nucleated cells and MSCs from bone marrow were captured in the mineralized nanoyarns.

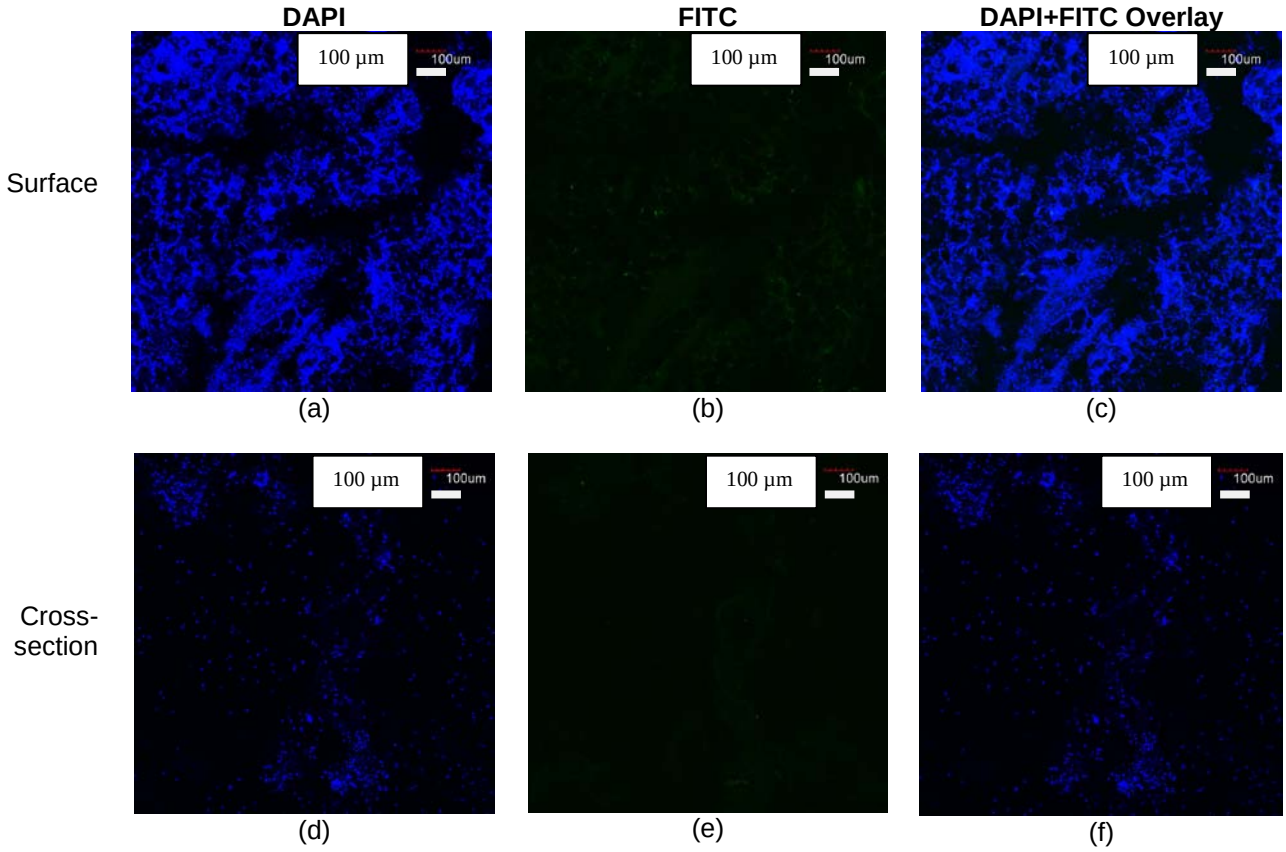

Fig. 5.8: Immunostaining of 3D mineralized nanoyarn scaffolds without the primary antibody CD 44. (a) to (c) Surface of scaffold (x10) and (d) to (f) Cross-section of scaffold (x10). Green signals (b) and (e) are very much weaker compared to samples (Fig. 5.7) which were incubated with CD44 MSC marker

Confocal z-stacking of 3D mineralized nanoyarn as seen in Fig.5.9 where the nucleated cells and MSCs were distributed in the multiple layers of the scaffolds.

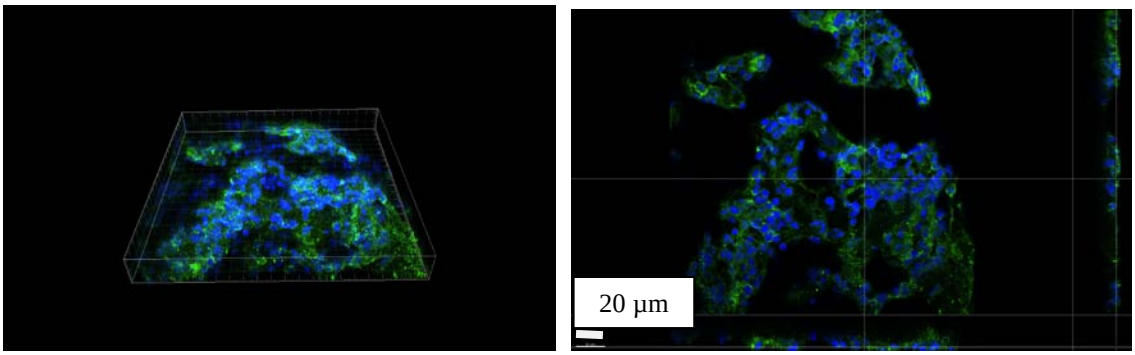

Fig. 5.9: 3D confocal imaging of the surface of the scaffold with CD44 at magnification of 60x

5.3.7 Cell morphology on 3D mineralized nanoyarns

The SEM images showed that the surface (Fig. 5.10a-j) and the cross-section (Fig. 5.10 k-t) of the scaffolds were inoculated with cells. In some cases, the cells underwent morphological changes as they began to stretch, which was evident on both the interior and the exterior of the scaffold.

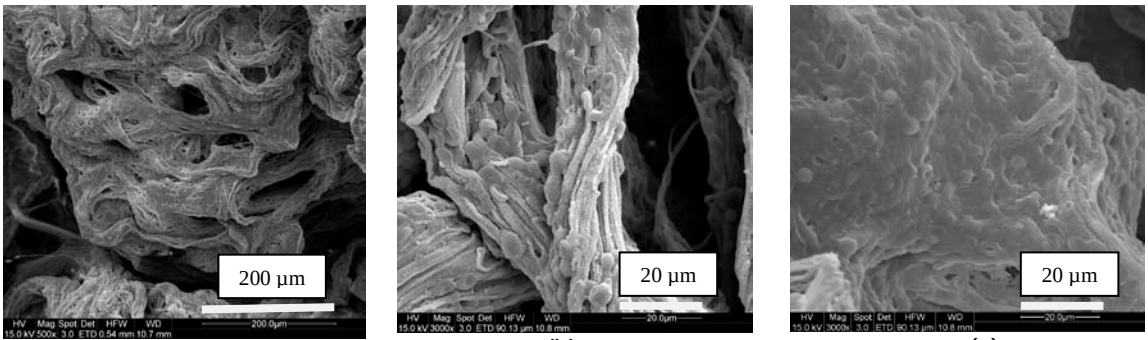

(a) (b) (c)

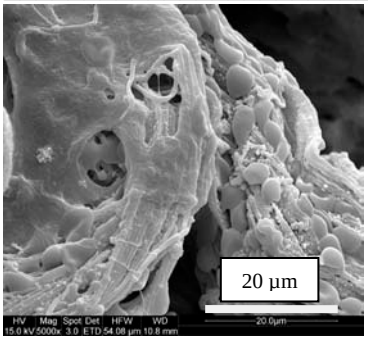

(d)

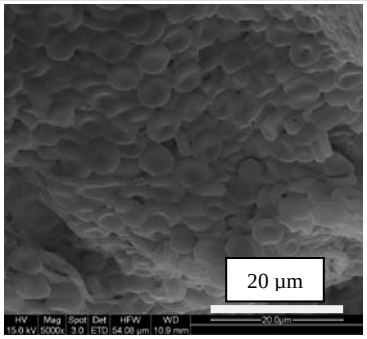

(e)

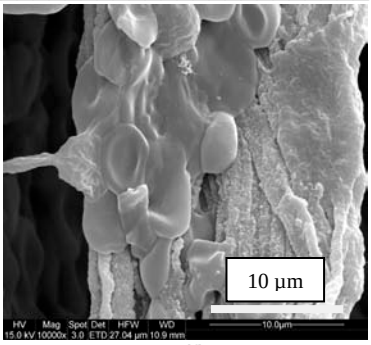

(f)

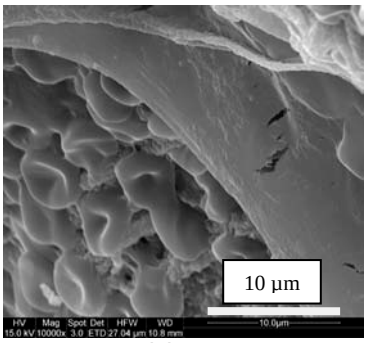

(g)

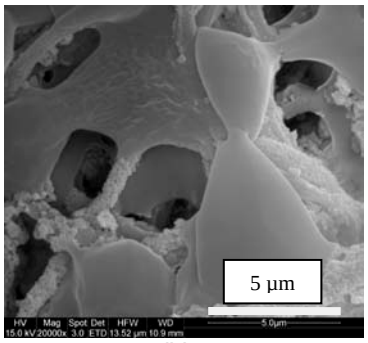

(h)

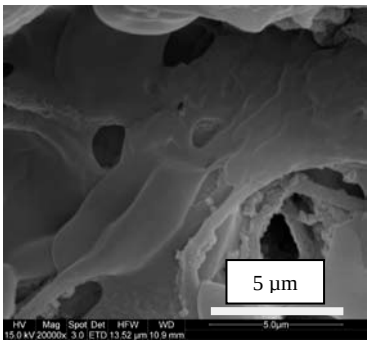

(i)

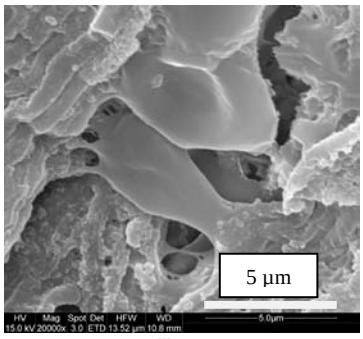

(j)

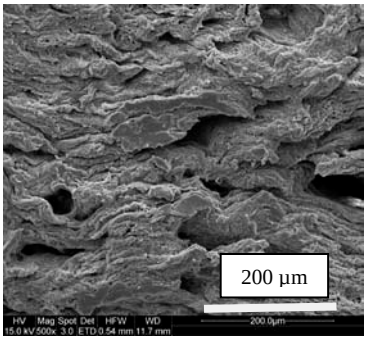

(k)

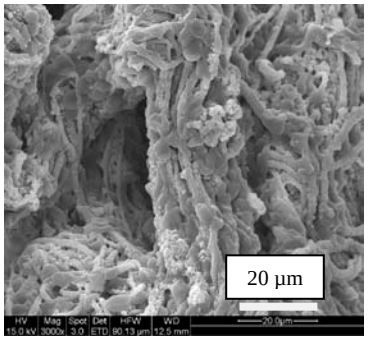

(l)

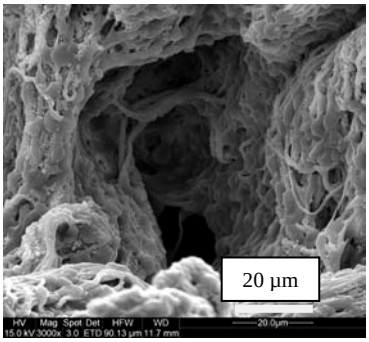

(m)

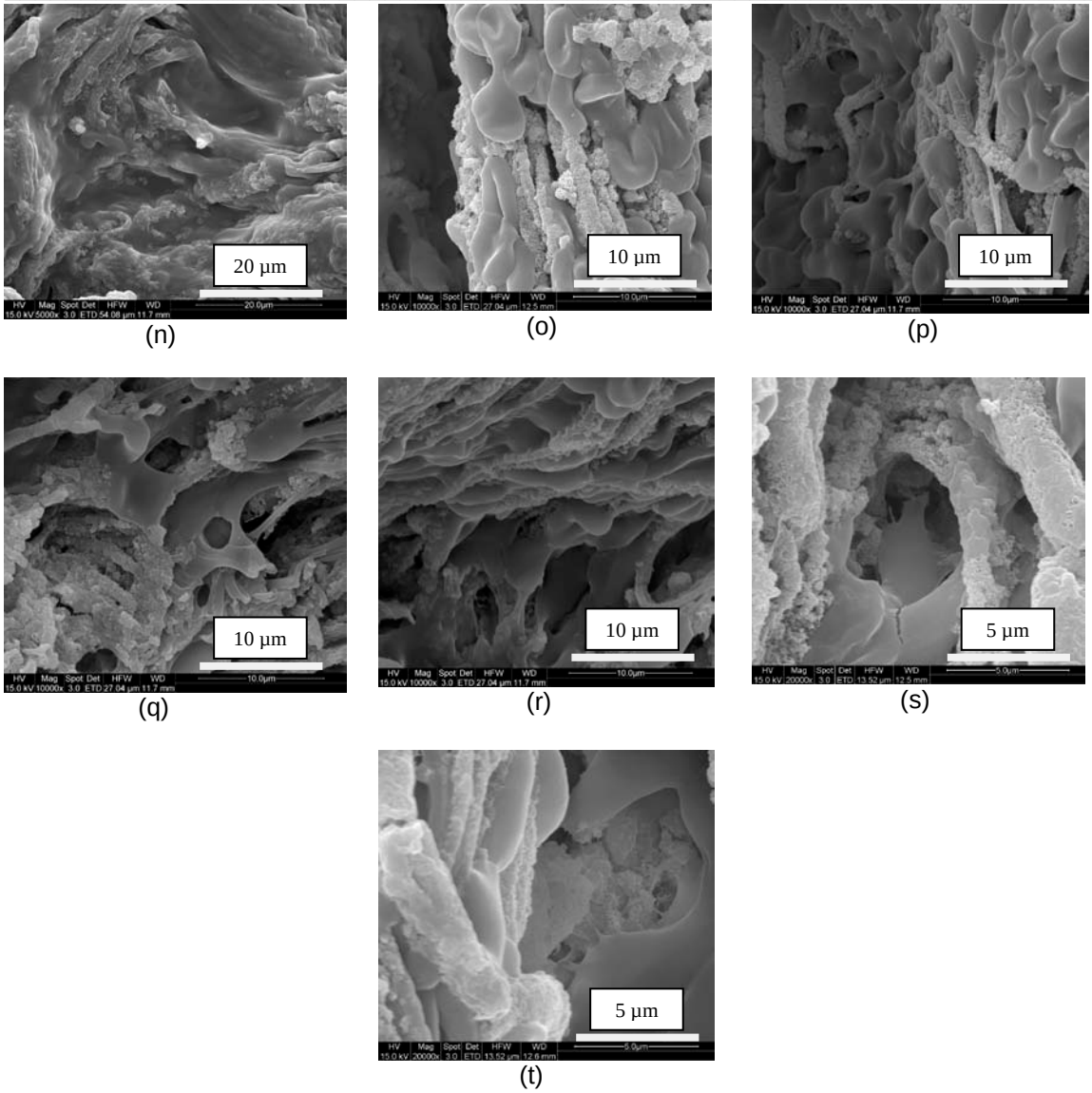

Fig. 5.10: SEM micrographs of mineralized nanoyarns which were inoculated with bone marrow and then incubated for 20 minutes. (a) to (j) show the surface and (k) to (t) show the cross-section of scaffold. Note that the fibers were inoculated with cells and cell morphological changes (e.g. cell stretching) was observed in both the surface and cross-section regions of the scaffolds after 20 minutes of incubation.

5.3.8 Rapid cell capture from rabbit bone marrow in implanted 3D mineralized nanoyarns

The mineralized nanoyarns enriched with bone marrow cells were tested in a rabbit model. Using the same bone marrow incubation conditions, the cell capture in the implanted scaffolds was 78.73 ± 6.95% (Fig. 5.11). This was consistent with the *in vitro* results in this study.

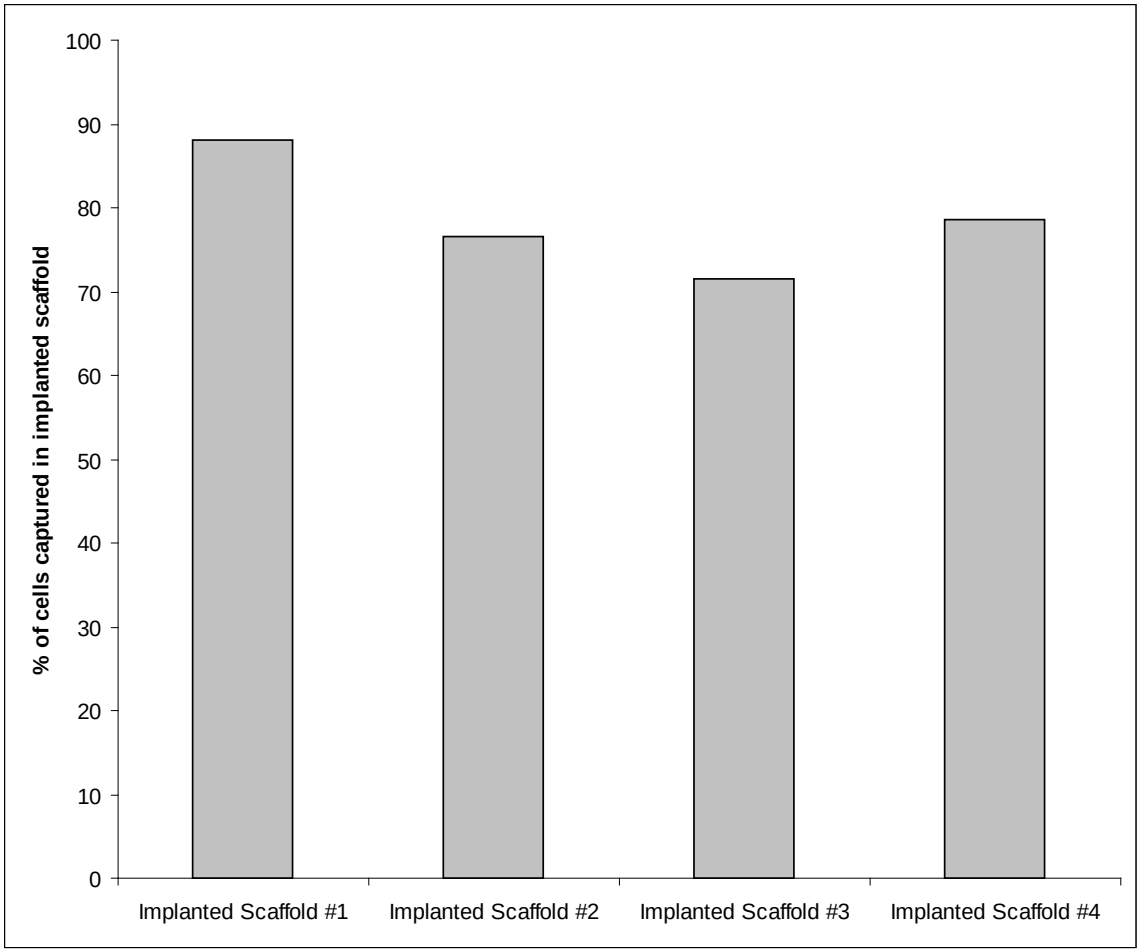

Fig. 5.11: Percentage of cell capture in 3D mineralized nanoyarn scaffolds after 20 minutes of incubation in rabbit bone marrow before implantation

5.3.9 MicroCT analyzes

The microCT results (Fig. 5.12) showed that bone formation was distributed uniformly at the defect site, suggesting that the enrichment of bone marrow cells in the mineralized scaffold could have an osteoinductive effect. The amount of bone regeneration was 63.8 ± 20% based on micro-CT results.

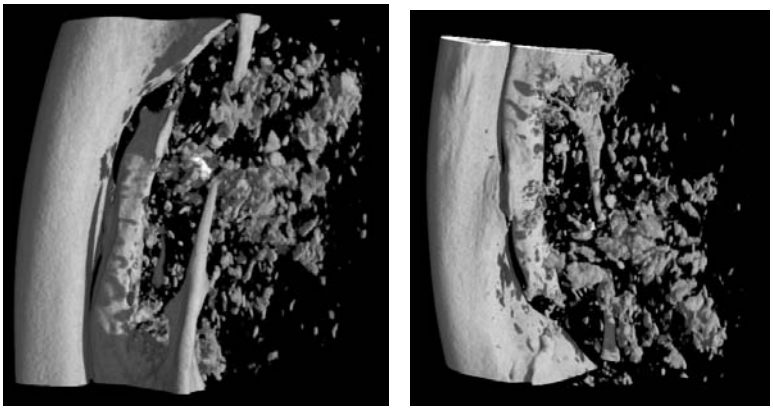

Fig. 5.12: Micro-CT images of segmental ulnar defect site of the rabbit where 3D mineralized nanoyarn enriched bone marrow cells was implanted. Bone formation was evident throughout the defect site.

5.4 Discussion

Tissue-engineered scaffolds have been considered as potential bone graft materials. In order to improve the performance of the graft material, bone marrow is often used with the graft material as the marrow contains osteoblastic progenitor cells, MSCs, HSCs and other potent inductive substances such as growth factors, which are necessary for bone healing. It was reported that the intraoperative processing of bone marrow can be used to concentrate the bone marrow-derived cells in order to enhance the graft performance [278]. Furthermore, the percutaneous injections of bone marrow were successful in the treatment of eighteen of twenty tibial non-unions, with the combination

of either the use of a cast or fixation [279]. As such, enriched biomineralized NFS provide a means of a quick, easy, safe and cost-effective strategy of facilitating cell attachment, cell delivery and migration of the desired cell population at the injury site. The incubation period of twenty minutes was chosen in this study because the duration of marrow incubation with the graft was twenty minutes prior to cell counting or implantation in several studies [280,281].

Studies have shown that the efficiency of cell attachment from canine bone marrow in mineralized and demineralized cancellous bone chips were 49 ± 8% and 44 ± 19% respectively [281]. In a separate study, demineralized canine cortical bone powder was used as a matrix for cell attachment, where the cell capture efficiency was 23 ± 8%. These studies show that the enrichment of bone marrow-derived cells in a material carrier enhances spinal fusion in a canine model [281,282]. Other material substrates used for cell capture from bone marrow include coralline HA and demineralized human cancellous bone [283,284]. It was reported that the percentages of nucleated cells from human bone marrow that were retained in coralline HA and demineralized human cancellous bone were 47% and 24% respectively [283,284]. By employing a 3D material matrix to act as a means of cell selection and enrichment from bone marrow, bone healing can be further promoted as a conducive and biological environment containing the appropriate cell populations and inductive stimuli is created. In this way, the potential of proliferation and differentiation of the cells may be enhanced. Pre-

existing cells in the graft may also induce further cell recruitment at the injury site necessary for bone healing and revascularization.

As the motivation was towards *in situ* application of bone marrow in this study, the 3D biomineralized NFS was considered as a substrate to facilitate the rapid cell attachment from bone marrow. In this way, cell expansion can be avoided. This strategy would improve on the efficiency in which osteoprogenitor cells, primary MSCs, or other bone marrow-derived cells can be seeded, expanded and differentiated on an implantable graft material.

Some cells are able to migrate through the scaffold as they are able to push the surrounding nanofibers aside as these fibers have very little resistance to the amoeboid movement of the cells [110]. The 3D nanofibrous conformation provides spatial and temporal hierarchical levels to mimic the ECM, thereby modulating cell behavior. Besides, such nanoscale materials are biologically preferred [228] . Moreover, nanoscale materials are said to have an increased number of atoms and crystal grains on their surfaces and have a higher surface area-to-volume ratio compared to microscale materials. These differences in surface topography can affect the surface energy for protein adsorption [110]. Protein interactions in the native tissues control the cell functions such as proliferation, migration and ECM production [285]. Consequently, the nanotopographical features and surface characteristics such as roughness, surface charge, surface chemistry, wettability etc. will in turn affect protein adsorption [286]. In addition, cumulative adsorption and bioactivity of adhesion proteins was reported to be

significantly higher on nanophase materials. For instance, enhanced adsorption, conformation and bioactivity of vitronectin on nanophase alumina were correlated with the increase of osteoblast adhesion on the substrates [208]. The 3D organization and nanotextured surfaces could have an effect on protein adsorption. At this point, we could not completely rule out the possibility that there could be a synergistic effect on surface topographical and chemical cues on the initial cell adhesion and cell stretching. One study suggested that surface chemical cues (caused by pre-adsorption of fibronectin) influenced initial cell-substrate contact, whereas surface topographical signals dictated cell morphology within one day [287]. Several studies have shown that surface nanotopography elicited different biological response. For example, nanoporous fibers significantly increased BM-MSCs proliferation and cell spreading compared to smooth nanofibers [288]. Furthermore, nanotopography had an effect on integrin-mediated focal adhesion and focal adhesion kinase expression [289].

To assess the efficacy of a material-cell construct as a bone graft, Quarto *et al.* [290] was the first to report the repair of large bone defects (4-7cm) in humans using a porous ceramic scaffold with *in vitro* expanded autologous MSCs. However, it would be an attractive option to be able to circumvent the need for the expansion of MSCs prior to implantation. It was reported that increased cell growth, cell numbers and osteogenic differentiation was associated with 3D scaffolds with nanotextured surfaces compared to smooth 3D scaffolds [257], highlighting the importance of nanotopographical signals in controlling cell functions.

5.5 Conclusion

A 3D NFS was developed in the form of bio-mineralized 3D nanoyarn with high resemblance to native bone, in terms of morphology, composition and compressive strength. A dynamic liquid electrospinning system and nano-hydroxyapatite (n-HA) deposition technique was employed to fabricate the mineralized 3D scaffold. The unique 3D nanostructural facilitated early cell capture (in less than 30 minutes), where up to 80% of the cells were captured when rabbit bone marrow was flushed through the scaffold. The current work showed that human MSCs were able to secrete bone minerals at very early time point on mineralized PLLA and more evidently on PLLA/Col nanofibers in the absence of osteogenic media, suggesting that osteoinduction can be modulated by the material characteristics of our biomimetic nanocomposites. The mineralized nanoyarn enriched with bone marrow cells was implanted in a ulnar critical size defect in a rabbit model. There was evidence of bone regeneration after three months. These observations provide good evidence that such tissue engineered nanofibrous scaffolds could be employed in today's clinical settings. In summary, these results delineated the importance of 3D organization and nanotopography for enriched cell capture. At this stage, it would be inappropriate to claim that osteoinduction was solely controlled by the 3D biomimetic nanocomposites alone or by the interplay between the enriched cell population and biophysical cues directing osteogenic differentiation *in vivo*. The physiological and regenerative strategy needs to be further elucidated in order to achieve effective clinical outcomes.

Chapter 6

Bone regeneration in a rabbit ulnar model using novel 3D mineralized and non-mineralized PLLA/Col nanofibrous scaffolds

6.1 Introduction

Calcium phosphates are often sintered at extremely high temperatures (> 1000ºC) and are highly crystalline. Not only do they differ in structure and composition of native n-HA, the osteointegration rates vary according to their crystalline size and stoichiometry [291]. As such, tissue engineered scaffolds are touted to be the next generation of bone grafts [108].

Besides improving on the osteoconductive properties of the graft material to support bone healing, osteoinductivity is also important as the active recruitment of host MSCs from the surrounding tissues to the graft site help to differentiate into bone-forming osteoblasts. BMPs are growth factors in the TGF-β group of proteins which are involved in several signaling pathways such as hedgehog pathway and the TGF-β signaling pathway [292]. These potent proteins are capable of stimulating and hastening bone growth. Currently, rhBMP-2 and rhBMP-7 (or osteogenic protein 1 [OP-1]) are routinely used, with excellent clinical outcomes. Typically, BMPs are loaded onto carrier materials (such as INFUSE, rhBMP-2 on type I collagen sponge [293] and OP-1, rhBMP-7 also on type I collagen material [294]) for effective administration into the targeted

sites. As such, tissue-engineered scaffolds are often impregnated with BMPs because of their highly osteoinductive prowess.

Current bone grafts only mimic native bone at a micro-level and are usually blended systems. This gave us the motivation to develop biomimetic n-HA/polymeric nanofibrous scaffolds. We have shown that the n-HA on our scaffolds mimic native bone which was similar in nanostructure and composition [19,21]. In this study, we attempted to examine the *in vivo* response of our 3D nanoyarn (collection of fibers in bundles) scaffolds with or without n-HA and also as a carrier for BMP-2 in a rabbit model.

6.2 Materials and Methods

6.2.1 Scaffold fabrication

Pure PLLA (300,000 Da, Aldrich Chemical Company, Inc.) and PLLA/Type I collagen (Koken Co., Tokyo, Japan) were dissolved (w/w 50:50) in 1,1,1,3,3-hexafluoro-2-propanol (HFP, Aldrich Chemical Company, Inc., St. Louis, MO). The fabrication of 3D nanoyarns was described in our previous work [267]. Briefly, a dynamic liquid system was used to create a vortex through a 5mm diameter hole at the centre of the collector basin as the water was pumped into the basin at room temperature (25 ± 1ºC) and relative humidity of 65%. The syringe loaded with the polymer solution was connected to a direct current high-voltage power supply (Gamma High Voltage Research, Ormond Beach, Florida) and the applied voltage was 15 kV. The spinneret used was a BD 27G ½ flat-tip needle and the feed rate was set at 1ml/hour (KD Scientific syringe pump, Holliston, MA). The working distance was 15 cm. The fibers were gathered on

the surface of the water and then drawn through the vortex and collected at the bottom of the water tank, which supplied the flow of water to the basin through a pump. After an hour, the nanoyarns were then collected. For non-mineralized scaffolds, the nanoyarns were immediately mounted into a mold (6mm in diameter, 17mm in length) and freeze-dried overnight. For mineralized scaffolds, the yarns were stored in DI water (no longer than 1 day) prior to n-HA mineralization.

6.2.2 Mineralization of 3D nanoyarn scaffolds

The 3D nanoyarns were chemically treated in calcium and phosphate (Ca-P) solutions. Using the same treatment conditions in our previous studies [19,21], the nanoyarns were first subjected in 0.5M of $CaCl_2$ (pH 7.2) (Aldrich Chemical Company, Inc., St. Louis, U.S.) for 10 mins, following by deionized water (DI) rinsing for a couple of mins. The nanoyarns were then immersed in 0.3M Na_2HPO_4 (pH of 8.96) (Merck & Co. Inc., N.J, U.S.) solution for 10 minutes and then rinsed with DI water. This typified 1 cycle of treatment and the PLLA/Col nanoyarns underwent 3 cycles of Ca-P treatment. After n-HA mineralization, the nanoyarns were fitted into a mold (6mm in diameter, 17mm in length) and then subsequently freeze-dried overnight.

6.2.3 Material Characterization

The morphologies of the nanoyarns were studied using a using a field-emission scanning electron microscopy (FESEM) (Quanta 200F, FEI, Oregon, U.S.) at an accelerating voltage of 10 kV or 20 kV.

6.2.4 Loading BMP-2 onto mineralized scaffolds

Human recombinant bone morphogenetic protein-2 (rhBMP-2, from ProSpec-Tany TechnoGene Ltd, Israel) was diluted with sterile saline to obtain a concentration of 0.4 mg/cm^3 [295]. 250 µL saline +BMP-2 solution (final concentration: 0.4 mg/cm^3) was added and completely absorbed into the PLLA/Col+n-HA scaffold before implantation. 0.4 mg/cm^3 was chosen as the final concentration because this was the minimum concentration that was needed to show bone repair based on radiographical evidence [295].

6.2.5 Operative procedures

Prior to implantation, all the scaffolds are sterilized in gamma irradiation conditions (Gamma Chamber 4000A, Co60 source, Isotope Group, Bhabha Atomic Research Centre/Trombay/India), at a total dose of 25 kGrays. Each scaffold was implanted in the midshaft of the rabbit ulna (n=3/material group). The material groups were 1) pure PLLA/Col, 2) mineralized PLLA/Col+n-HA, 3) PLLA/Col+n-HA impregnated with BMP-2 and 4) Blank control (n = 1). The rabbit was anesthetized using ketamine 50mg/kg (i.m) + Xylazine 10mg/kg (i.p). We also administered pre-op antibiotics and analgesic, Baytril @ 5mg/kg (i.m) + Rimadyl @ 2mg/kg (s.c). The bony defect of 15 mm was created using an oscillating saw under continuous saline cooling. The entire bone block was removed with the periosteum and the bone ends were cleaned with a bony rongeur. The defect site was then copiously irrigated with saline to remove any bone debris. Internal fixation was not considered because of the fibro-osseous syndesmosis between the ulna and radius. Post-surgery, the rabbit received Baytril @

5mg/kg (i.m) - 5 days postop+ Rimadyl at 2mg/kg (s.c) - 3 days postop. After three months implantation, the explant was removed. The explant was then fixed in 10% neutral buffered formalin.

6.2.6 X-rays

The ulna was assessed bi-weekly using X-ray radiography (Siemens Polymobil Plus, Siemens Medical, Singapore) to evaluate the extent of bone formation. The settings used were 40 kV and 0.8 mAs.

6.2.7 Microcomputed tomography (MicroCT)

The explant was scanned through 360º with a rotation step of 3º/s, at a spatial resolution of 27 µm x 27 µm x27 µm using a microCT machine (SMX-100CT X-ray CT Sys, Shimadzu, Japan). The parameters used were: X-ray voltage (47 kV), X-ray current (50 µA), detector size (9") and scaling coefficient (50). No filter was used during the scanning. The scan files were then reconstructed using a modified Feldkamp algorithm (Skyscan, Belgium), at a step size of 27 µm. The microCT software (VGStudioMax, version 1.2, Volume Graphics GmbH, Germany) was used to construct the 3D image of the explant. Bone volume values were determined by using the reconstructed 3D image where the gray value range for bone were set at 225-255 (CTAnalyser, version 1.9, Skyscan, Belgium).

6.2.8 Histological analyzes

The explant was thoroughly dehydrated prior to histological staining. Serial 5 µm paraffin sections were done using a microtome. The sections were stained with

hematoxylin and eosin (H&E), Masson's Trichrome and von Kossa stains, according to routine histology protocol. Images of the stained sections were captured using an Olympus microscope (Leica Microsystems Ltd, DFC 295 (model), Germany), at magnifications of x4, x10, x20 and x63.

6.2.9 Statistical analyzes

Student's T-test and two-way ANOVA were employed to assess statistical differences between the material groups for microCT tests. Difference was considered to be of statistically significance at $p < 0.05$.

6.3 Results

6.3.1 Morphology of 3D nanoyarns

The 3D scaffold as seen in Fig 6.1(a) was used for implantation. Both PLLA/Col (Fig. 6.1b) and mineralized PLLA/Col scaffolds (Figs. 6.1d, e, f) maintained their yarn structures (collection of nanofibers in bundles). The n-HA deposition was uniform on the fibers. Furthermore, the morphology of the mineralized nanofibers highly resemble to that of native bone fibrils [1].

(a)

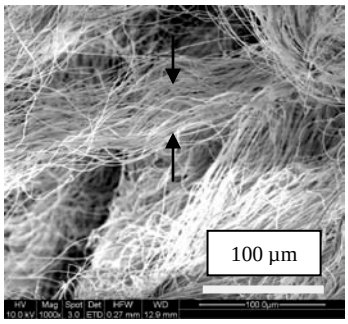

(b)

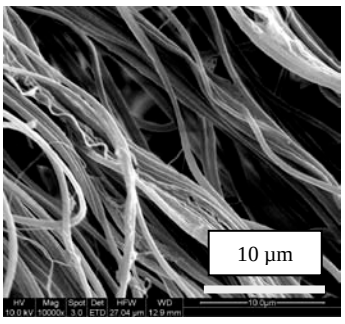

(c)

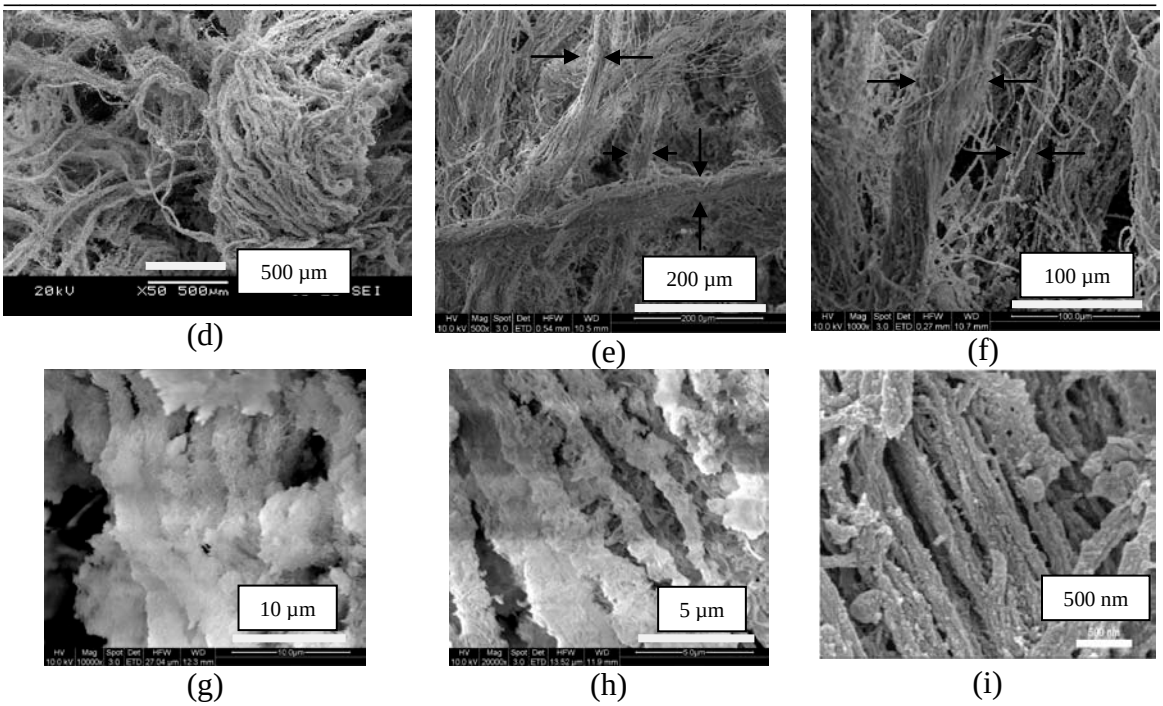

Fig. 6.1: 3D nanoyarn scaffolds. (a) Gross image of 3D scaffold used for implantation. (b)-(c) SEM micrographs of pure PLLA/Col nanoyarn scaffold, (d) to (h) SEM micrograph of mineralized PLLA/Col nanoyarn scaffold and (i) native bone fibrils [1]. Arrows denote bundles of fibers (collection of fibers in yarn formation). Note that yarn bundles remain intact after n-HA mineralization

6.3.2 X-rays analyses

Fig. 6.2 shows the X-ray images of all the groups at various time points. Surprisingly, just two weeks after surgery, all the scaffold groups showed initial bone growth from the bony ends, with the BMP-2 group leading the rest. On the contrary, this observation was not evident in the blank control group. By one month, denser callus formation was noted in the BMP-2 group, with a notable bony bridging at the proximal end of the radius. More bone growth was seen in PLLA/Col group compared to the mineralized PLLA/Col group. After one month, the blank control group showed evidence of bone formation. After six weeks, callus bridging was more prominent in the

mineralized PLLA/Col group, whereas further bone growth was not radiographically evident in the PLLA/Col, BMP-2 and blank control groups. By two months, partial bone bridging was present in all the scaffold groups except the blank control group. Interestingly, callus formation increased in the PLLA/Col and mineralized PLLA/Col groups over time, but for the BMP-2 group, the amount of bone growth did not fluctuate as seen in the X-ray images. After three months, the scaffold groups showed more bone formation compared to the blank control group, where mineralized PLLA/Col group fared the best, followed by the PLLA/Col and BMP-2 groups.

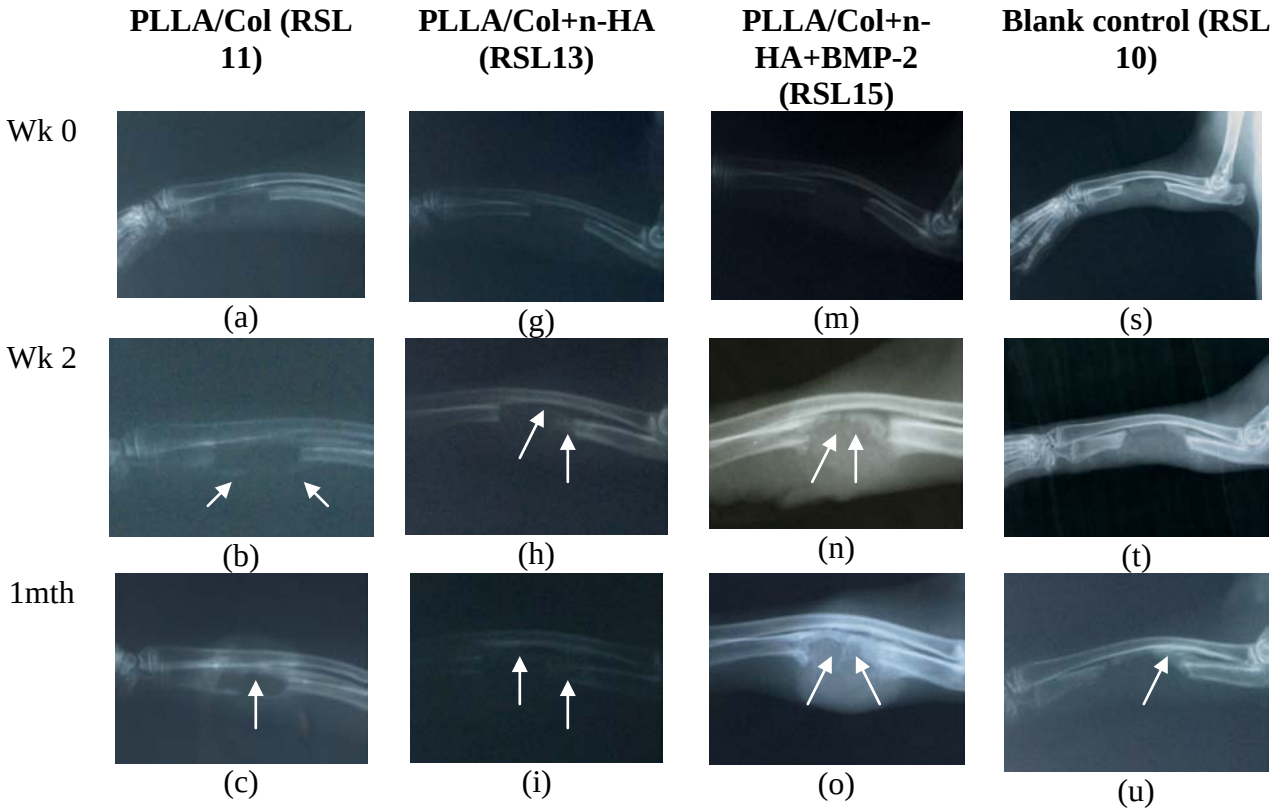

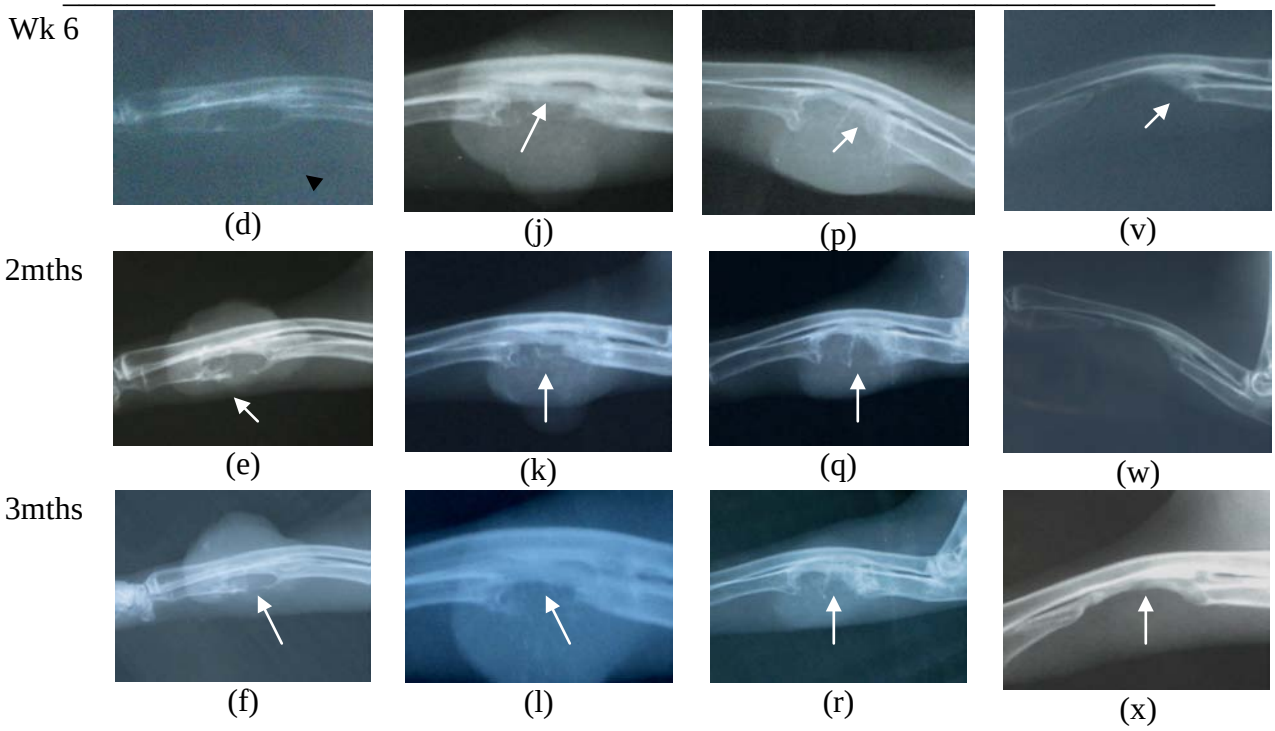

Fig. 6.2: Representative ulnar radiographs. Sequential radiographs depict bone formation immediately after implantation (Week 0), 2 weeks, 1 month, 6 weeks, 2 months and 3 months after implantation. (a)-(f) PLLA/Col, (g)-(l) PLLA/Col+n-HA, (m)-(r) PLLA/Col+n-HA+BMP-2 and (s)-(x) blank control. Arrows represent new bone formation

6.3.4 MicroCT analyzes

The 3D representative microCT images in Fig. 6.3 depict the amount of bone formation after three months of implantation. Interestingly, the blank control group did not show bone specks within the defect site. Interestingly, the mineralized PLLA/Col group exhibited bone specks uniformly within the defect site, without the presence of BMP-2. This could suggest that the presence of n-HA alone could elicit an osteoinductive bone formation process. Furthermore, the bone formation in the PLLA/Col group did not display such uniform bone specks in the defect site, but rather the growth proceeded from the bony ends of the midshaft.

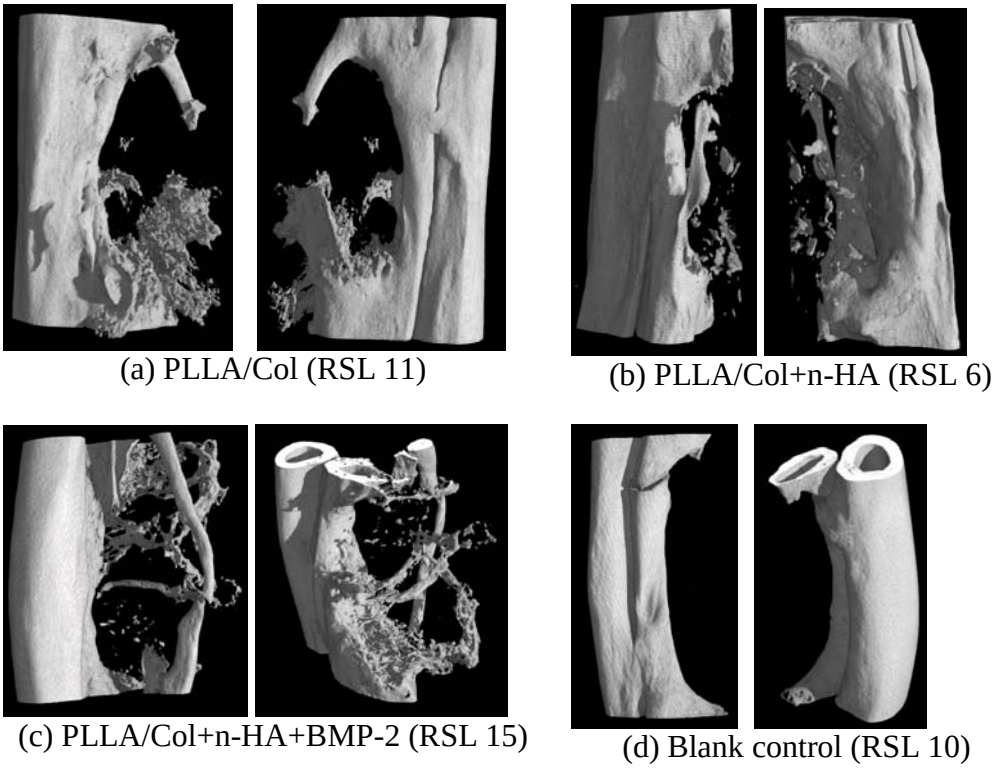

(a) PLLA/Col (RSL 11) (b) PLLA/Col+n-HA (RSL 6)

(c) PLLA/Col+n-HA+BMP-2 (RSL 15) (d) Blank control (RSL 10)

Fig. 6.3: 3D Micro-CT images after three months of implantation

Based on the microCT results, the amount of bone volume was calculated from all the groups. In Fig. 6.4, the percentage of bone formation in all the nanoyarn groups was higher than the blank control. The mineralized PLLA/Col group showed the highest bone volume, followed by the PLLA/Col group. The mineralized PLLA/Col scaffold impregnated with BMP-2 did not perform as well as expected and we suspected this could be due to the low concentration of BMP-2.

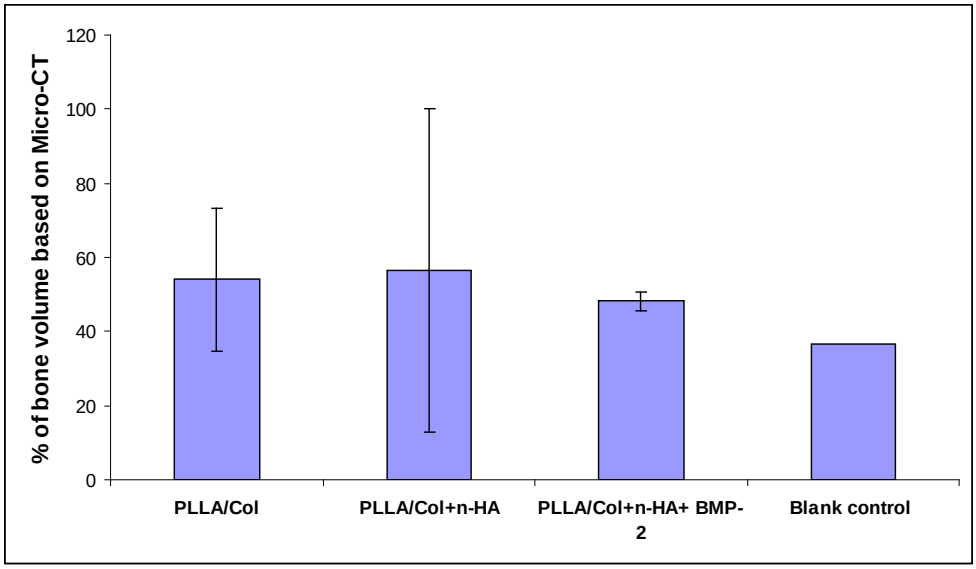

Fig. 6.4: Percentage of bone volume based on Micro-CT after 3 months of implantation

6.3.5 Histological analyzes

Histology results revealed all the scaffold groups were well-tolerated and osteoconductive. There was no evidence of infection or chronic foreign body response. Fig. 6.5 shows the histology images of our material groups. New bone formation was evident in all the groups, and confirmed by Masson Trichrome's staining, where collagen was stained blue. Even though the explants were decalcified, some minerals still remained (Fig. 6.5i).

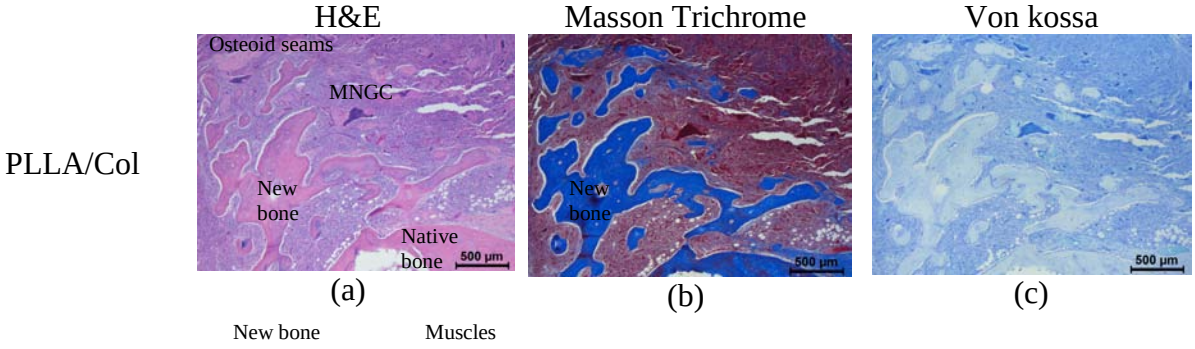

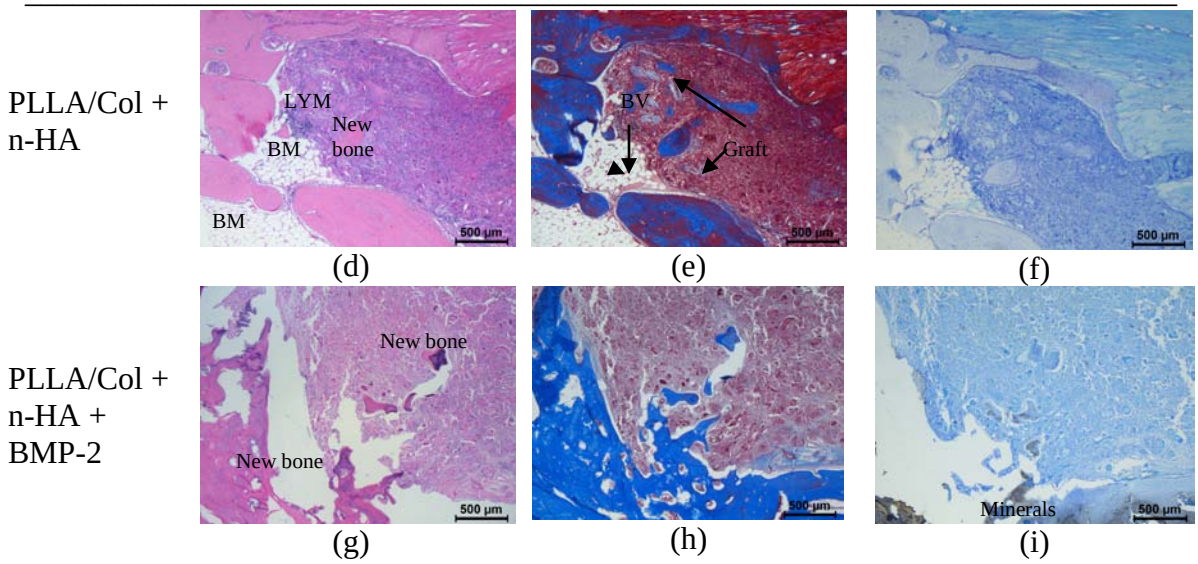

Fig. 6.5: Histology images after three months of implantation. (a) to (c) PLLA/Col, (d) to (f) PLLA/Col +n-HA and (g) to (i) PLLA/Col+n-HA +BMP-2. Note that some brown minerals were seen in (i). Abbreviations – multi-nucleated giant cell (MNGC), blood vessel (BV), lymphoid aggregates (LYM), bone marrow (BM)

Fig. 6.6 illustrates the different types of cells which were present in all our material groups. Some cartilage (a precursor of bone) was present. The hallmark of the newly formed bone matrix consisted of chondrocytes were embedded in the lacunae, surrounding by blood vessels and osteoblasts laying down new bone at the borders of the osteoid seams.

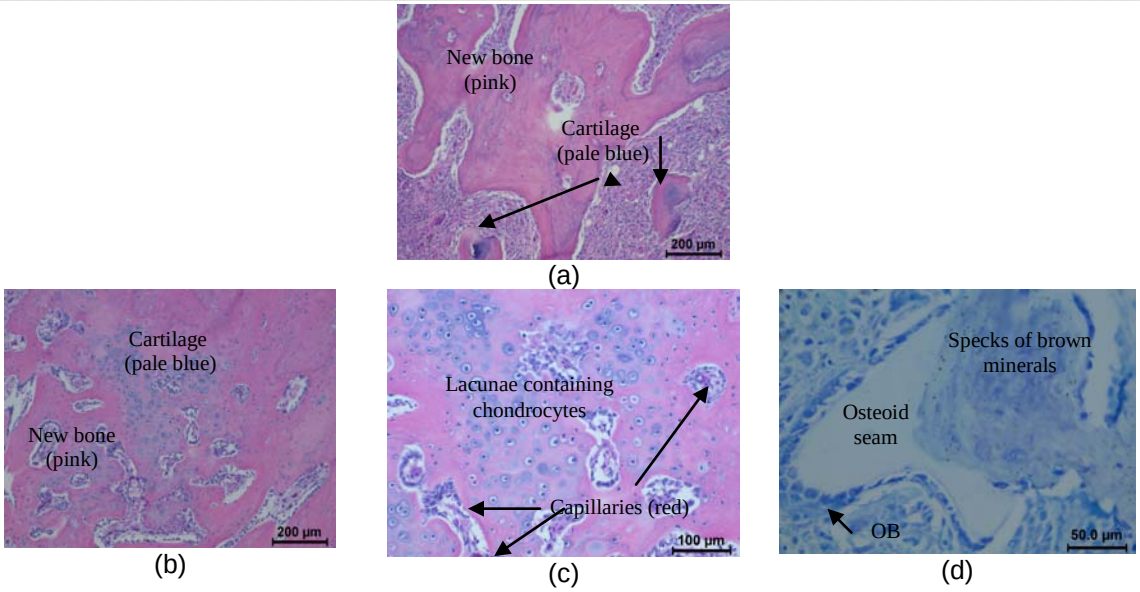

Fig. 6.6: Histology of new bone formation. (a) and (b) bone consists of mature bone (pink) and immature bone (cartilage) [H&E], (c) chondrocytes within lacunae, surrounding with blood vessels (capillaries) [H&E] and (d) mineralized bone (brown specks) surrounding with osteoid seams where osteoblasts (OB) were laying down new bone [von kossa]

As expected, our graft was slowly degraded with the aid of certain cells engulfing the material (Fig. 6.7). Macrophages (mono-macrophages and bi-macrophages) prior to forming multi-nucleated giant cells (MNGCs) was seen digesting smaller graft materials, whereas MNGCs attacked larger graft materials. In addition, lymphocytes also participated in the phagocytosis process.

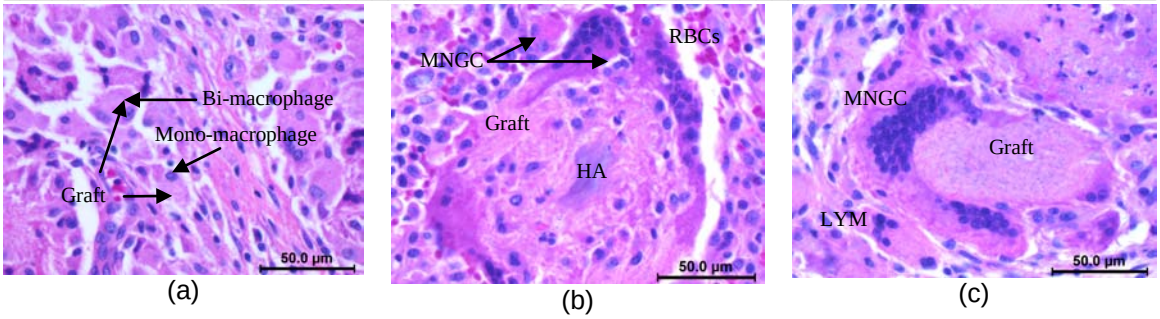

Fig. 6.7: Histology of different cell types which were present in all material groups. Note that the graft was engulfed by (a) macrophages, (b) multi-nucleated giant cells (MNGCs) and (c) lymphocytes (LYM) in the presence of red blood cells (RBCs). Hydroxyapatite (HA) from the graft could also be seen

6.4 Discussion

Our results showed that the 3D nanoyarn scaffolds were capable of inducing bone repair in segmental bone defects in a rabbit model. We hypothesized that mineralized PLLA/Col scaffolds would improve bone repair more than pure PLLA/Col scaffolds. We believed that by mimicking the scaffold closer to the native bone's morphology and composition, the n-HA particles would serve as anchorage points for osteoprogenitor and osteoblastic cells, providing a more favorable surface for cell attachment and interaction, thereby improving bone mineralization. Although the percentage of bone growth based on microCT results was not significantly different in all the groups, radiographically, mineralized PLLA/Col group performed better than pure PLLA/Col group. In addition, microCT images indicated that a greater extent of bone formation was prevalent in the mineralized scaffold group compared to the pure scaffold group. Large standard deviations were also associated with surface grafted hydroxyapatite with PLLA/PLGA (gHAP/PLGA) and hydroxyapatite/PLGA (HAP/PLGA) at 20 weeks post-surgery [296]

Surprisingly, the BMP group did not supersede the non-BMP materials groups in terms of bone formation. There could be a possibility that there was an initial burst release of BMP-2 during the early stages, as more new woven bone was formed in the BMP-2 group compared to the other scaffold groups. Moreover, the extent of new callus formation at later time points was not as impressive as one would expect since BMP-2 was loaded into the scaffold to hasten bone regeneration. We suspected that the amount of BMP-2 was too low to elicit abundant bone growth to completely fill the gap. For instance, different amounts of BMP-2 [17mg (100 mg/mL), 35mg (205.88 mg/mL) and 70 mg (411.76 mg/mL)] were loaded onto PLLA scaffolds which were then implanted in the radii of the rabbits [297]. The amount of bone formation in all the BMP groups was similar to those treated with autografts and higher BMP-2 concentrations (35 mg and 70 mg) were associated with cortices and marrow elements [297]. Besides BMP concentrations, other factors which influence bone regeneration are the defect size, presence of fixation tools, material type and so on. In a separate study, despite a lower BMP-2 concentration (10 µg) in a silica-calcium phosphate nanocomposite, bone formation was seen after 16 weeks where the defect size in the rabbit ulna was 10 mm and a fixation plate was used to secure the graft in position [298]. Although our BMP concentration and ulnar defect size were similar to that of Kokubo's study [295], the defects were radiographically repaired in Kokubo's study. One of the possibilities was that the material (PLGA-coated gelatin sponge) used was shaped into suitable sizes for specific defects with a scalpel prior to implantation [295], thus the graft could be more securely fitted into the defect site with minimal movement, preventing dislodging. Bone healing would be impaired if the graft is not in touch with the native host bone during

implantation or movement. Our graft sizes were standardized regardless of the size of the rabbits (due to animal variability even though animals were of the same age). We suspected that for some animal groups, the graft acted more as a tissue spacer than an osteoconductive graft as there were non-osseous tissues with fibrous connective tissues. If the degradation process is too fast, the osteoblasts will not have a surface to migrate to and deposit bone matrix, resulting in fibrous repair instead of osseous regeneration [299]. Without the addition of BMP-2 in PLLA grafts, fibrous tissue filled the defects [297].

In some studies, the periosteum (source of osteoprogenitor cells) was present [297]. In our study, the periosteum was completely removed, which could be one of the reasons as to why a complete union was not observed and our BMP group did not perform as well as expected as higher BMP concentrations might be needed to facilitate bone growth.

When human BM-MSCs were cultured on HA ceramics, and implanted in the patient's bone cavity, no adverse reactions were observed and new bone formation was seen after three months and complete integration with the patient's native bone was seen after a year [179]. In a separate study, spinal fusion was achieved in a rabbit model when MSCs were employed [178]. The effects of MSCs on HA and osteogenic supplements were investigated. Four out of five rabbits achieved new bone formation when MSCs cultured on type I Col gel with HA particles in the presence of osteogenic supplements were implanted, compared to only two out of six rabbits, which had fusion in the non-osteogenic MSCs group. One possible reason could be due to the inadequate osteogenic

growth factors present. Moreover, MSCs that have been directed to an osteogenic lineage prior to implantation may induce better fusion and bone formation as these differentiated MSCs are less dependent on the local growth factors. It is noteworthy to highlight that the fusion rate and level of bone formation were similar in both the osteogenic MSC+Type I Col gel+HA particles and autologous bone group. On the other hand, none of the rabbits in the HA group without MSCs had fusion but only fibrous tissue was observed. Another study showed that there was a synergistic effect on the osteogenic differentiation of BM-MSCs on type I Col gel and HA particles when BMP and fibroblast growth factor (FGF) were used [27].

Although bone growth was observed within the defect site after three months, the defect site was not completely filled up in all the groups. This could possibly be due to the lack of immobilization of the scaffold at the defect site. From our histology images, immature woven bone and bone marrow elements were evident in all the scaffold groups. Vascularization (blood vessels) and osteocytes in the regenerated bone was observed. Persuasive evidence of osteoblasts actively forming new bone was indicative of active bone. The graft remnants were observed in the newly formed bone. As the polymer undergoes resorption, the voids left behind allows the activated osteoblasts to deposit new bone and blood vessels to infiltrate into the active bone region.

No obvious abnormalities were detected. The histological evaluation showed no signs of infection or adverse inflammatory reactions in all the animal groups. Biodegradable polymers such as PLLA and PLGA undergo hydrolysis. The biodegradation of PLLA elicit the recruitment of osteoclasts during the resorption process. In a separate study, osteoclastic resorption of the material carrier was also observed [300]. Furthermore, osteons (concentric lamellar structures) were present. Macrophages and multi-nucleated giant cells (MNGCs) participate in the phagocytosis process as well [299]. MNGCs were present as part of the wound healing response. In all our groups, lymphocytes, macrophages, MNGCs, neutrophils, granulocytes were seen. A separate study involving PLLA scaffold implantation also exhibited the presence of giant cells, macrophages, granulocytes and lymphocytes. This could be due to the inflammatory response caused by the PLLA [297]. MNC infiltration was also evident in another study involving PLLA [301] and PLGA residues [295]. In addition, lymphocytes infiltration occurred at the implant region [299]. Thus, the foreign body reaction seen in this study is a common phenomenon associated with biodegradable polymers as observed in many other studies.

6.5 Conclusion

Our 3D mineralized and non-mineralized nanoyarn scaffolds aided in bone regeneration. The amount of BMP-2 loaded into a material is important as this would affect the study outcome. Future work entails evaluating the release profile of BMP-2, dissolution kinetics, torsional testing and performing large animal model studies for more in-depth evaluation of the performance of the nanoyarn scaffolds.

Chapter 7

Conclusions and Recommendations

The scope of this research encompasses the *in vitro* osteogenic differentiation of human BM-MSCs using geometric cues provided by the NFS in the absence of osteogenic supplements. A biomimetic approach of n-HA mineralization was achieved on NFS for efficient cell capture of osteoblasts and BM-MSCs. The final product is a 3D mineralized nanoyarn scaffold for bone graft applications. This product has been tested in a rabbit model, showing favorable bone healing without any adverse inflammation response.

7.1 Main conclusions

- Rapid biomimetic mineralization was possible on the NFS using the alternate dipping method, where the n-HA obtained was similar to that of natural teeth. Co-blending collagen in PLLA NFS was an effective way to enhance the mineralization of the NFS due to the nucleation sites (e.g. the amide I and II groups) of collagen. Moreover, n-HA significantly improved the hydrophilicity of PLLA/Col NFS. The n-HA on the PLLA and PLLA/Col NFS significantly enhanced osteoblast cell capture efficacy within 30 minutes.

- The osteogenic differentiation potential of human BM-MSCs was confirmed and achieved by manipulating the biochemical, physical and environmental conditions.

The nanotopographical cues of the surface of mineralized PLLA and PLLA/Col NFS induced osteogenic differentiation of BM-MSCs without any osteogenic chemical intervention. In addition, the Ca/P ratios for the mineralized PLLA and PLLA/Col NFS were 1.8 ± 0.12 and 1.7 ± 0.14 respectively, which was similar to HA (~1.67) in native bone.

- n-HA alone had a positive modulation on osteogenic differentiation of BM-MSCs as the osteocalcin expression was comparable in mineralized PLLA NFS in both normal and osteogenic media conditions. The synergistic effects of n-HA and collagen were evident as the osteocalcin expression and ARS levels were significantly enhanced in normal media but not in osteogenic media. Cell mineralization or bone nodules, an indicator of late-stage differentiation, was present on mineralized PLLA and PLLA/Col NFS in normal media at much earlier time points on day 14. The Ca/P ratios of the bone nodules ranged from 1.5 to 1.85, similar to that of natural bone. The observations in this study showed that osteoinduction was demonstrated by the material characteristics of biomimetic nanocomposites circumventing osteogenic supplements or mechanical stimulation.

- 3D mineralized NFS (deemed as mineralized 3D nanoyarn) was successfully fabricated using a dynamic electrospinning system and n-HA deposition technique. The 3D mineralized nanoyarn had shown to have a close resemblance to native bone, in terms of morphology, composition and compressive strength.

- 3D mineralized NFS has shown to be an effective carrier for rapid cell capture from bone marrow aspirate as the nanotexture features of the NFS provided nanotopographical signals and biomolecular cell signals for cell-scaffold interactions for cell attachment. The unique 3D nanostructural characteristics highly facilitated early cell capture (within less than 30 minutes), where up to 80% of the cells were captured when rabbit bone marrow was flushed through the nanoyarn. The mineralized nanoyarn enriched with bone marrow cells exhibited promising results in a critical size defect of 15 mm in the rabbit model, and may serve as an *in-situ* therapeutic bone graft option for bone regeneration.

- The 3D mineralized and non-mineralized nanoyarns were implanted in a 15 mm segmental ulnar defect in a rabbit model. Bone formation was seen after two weeks. Moreover, there were speckles of bone observed within the defect site, away from the bony ends of the fracture especially for the mineralized PLLA/Col nanoyarn group, suggesting the osteoinductivity potential of the scaffolds.

7.2 Recommendations for future work

The focus of this study lies mainly in investigating the osteogenic differentiation of BM-MSCs on 2D nanofibrous mesh. It is therefore necessary to conduct future work to understand the osteogenic differentiation of BM-MSCs on 3D nanofibrous scaffolds, so that the physical and biochemical properties of the scaffolds can be tailored to elicit specific biological responses for the effective guidance of cells to form functional tissues.

The NFS described in this project has shown promising results as an efficient carrier for cell capture and inducing osteogenic differentiation by means of geometric cues. The results of the bone healing process in a rabbit model were encouraging. However, further investigations are required to study the gene expression of the BM-MSCs under *in vitro* and *in vivo* conditions. The mechanisms of the transdifferentiation of BM-MSCs and the interactions between the differentiated BM-MSCs and surrounding cells (such as inflammatory, vascular cells etc.) in the injured site renders further considerations. The cascade of the orchestrated processes of gene expression in biological pathways render further investigation, so that the interplay between the various biomolecules and proteins can be understood and this would greatly facilitate the material selection and the choice of growth factors and biomolecules to be incorporated into the material constructs.

Extensive degradation profile of the NFS needs to be done in order to predict the complete resorption of the NFS *in vivo*. For instance, *in vivo* proteolysis analyses of the NFS can be conducted to measure the degradation behavior of the NFS in the injured site. Such information may be useful in optimizing the material characteristics for improving bone remodeling, such as supporting angiogenesis for bone healing.

Because our scaffolds are not tested in load-bearing sites in the rabbit ulna model, we would also need to conduct further animal studies for more in-depth evaluation of the performance of the nanoyarn scaffolds. Large animal studies are also closer to clinical

relevance and are often considered to be the pre-requisite for clinical trials. Other future work entails evaluating the release profile of BMP-2 and dissolution kinetics. It was said that the products of a 3D porous silica-calcium phosphate nanocomposite and the released BMP-2 provided a conducive environment at the implant site, which promoted ossification and maturation of the regenerated bone in a rabbit model [298] . Gamma scintigraphy can also be employed to detect the BMP dose that is retained at the osteotomy site at different time points after implantation, to map out the protein release profile [300]. The mechanical properties of the current nanoyarn scaffolds need to be further improved to cater for load-bearing sites. Mechanical testing of explants such as torsional testing can be also considered. Such biomechanical properties such as maximum torque to failure, torsional stiffness and energy adsorbed to failure are important parameters to determine the success of the graft material in facilitate bone healing.

Incorporation of growth factors such as BMP-2 into the NFS can be achieved by using the co-axial or core-shell electrospinning technique as seen in Fig. 7.1. The protein release rate can be manipulated by adjusted the ratio of the thickness of the shell to the core. Previous studies showed that a controlled release profile of FITC-BSA was achieved when the protein was encapsulated in the core of the core-shell nanofibers [302].

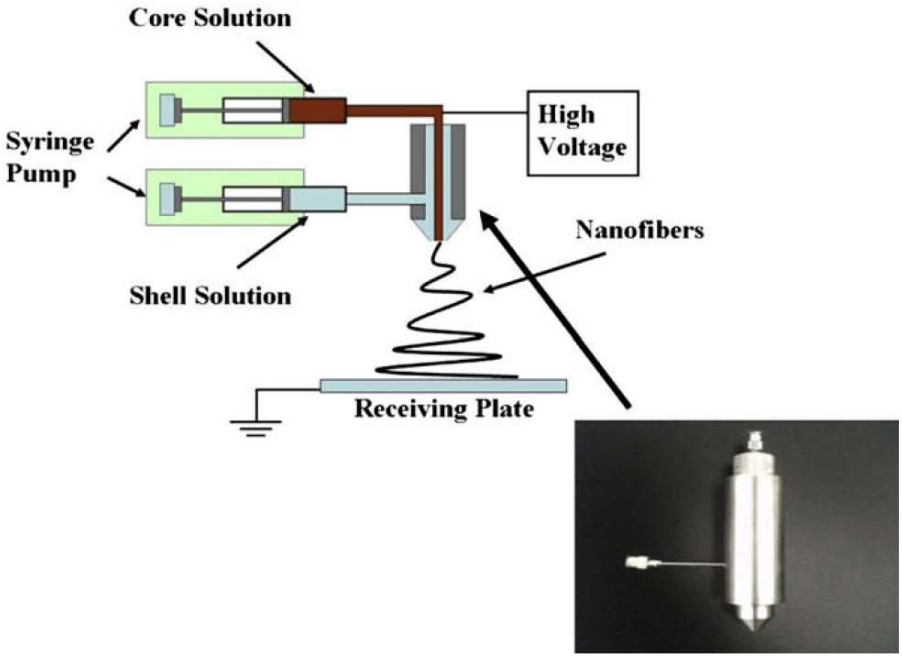

Fig. 7.1: Co-axial electrospinning setup. The inset picture shows the special apparatus (inner and outer dopes) for the fabrication of core-shell nanofibers Reprinted from [2], Copyright 2009, with permission from Elsevier Limited)

For a wider range of clinical applications, the graft can be more amenable to contouring for the implantation in different sizes and shapes of bony defects. As such, improvements of the 3D nanoyarns can be made by developing an injectable form of the nanoyarns.

References

[1] Fantner GE, Hassenkam T, Kindt JH, Weaver JC, Birkedal H, Pechenik L, et al. Sacrificial bonds and hidden length dissipate energy as mineralized fibrils separate during bone fracture. Nat Mater 2005;4(8):612-6.

[2] Su Y, Li X, Tan L, Huan C, Mo X. Poly(L-lactide-co-e-caprolactone) electrospun nanofibers for encapsulating and sustained releasing proteins. Polymer 2009;50:4212-9.

[3] Greenwald A, Boden S, Goldberg V, Khan Y, Laurencin C, Rosier R. Bone graft substitutes: facts,fictions, and applications. J Bone Joint Surg Am 2001;83:S98-103.

[4] Steinmann J, Herkowitz H. Pseudoarthrosis of the spine. Clin Orthop 1992;284:80-90.

[5] Lee K, Roper J, Wang J. Demineralized bone matrix and spinal arthrodesis. Spine J 2005;5(6):S217S-223.

[6] Frost & Sullivan. U.S. Medical Devices Market Outlook 2008. 28 2008;5:16-28.

[7] Desai B. Osteobiologics. Am J Orthop 2007;36:8-11.

[8] Muschler GF, Lane JM. Bone grafts and bone substitutes. In: Habal MB, Reddi AH, editor. Orthopaedic surgery: Philadelphia: Saunders; 1992. p. 375-407.

[9] Lutolf MP, Gilbert PM, Blau HM. Designing materials to direct stem-cell fate. Nature 2009;462(7272):433-41.

[10] Laurencin CT, Ambrosio AM, Borden MD, Cooper JA. Tissue engineering: orthopedic applications. Annu Rev Biomed Eng 1999;1:19-46.

[11] Dawson JI, Wahl DA, Lanham SA, Kanczler JM, Czernuszka JT, Oreffo ROC. Development of specific collagen scaffolds to support the osteogenic and chondrogenic differentiation of human bone marrow stromal cells. Biomaterials 2008;29(21):3105-16.

[12] Woo KM, Chen VJ, Ma PX. Nano-fibrous scaffolding architecture selectively enhances protein adsorption contributing to cell attachment. J Biomed Mater Res A 2003;67(2):531-7.

[13] Woo KM, Jun JH, Chen VJ, Seo J, Baek JH, Ryoo HM, et al. Nano-fibrous scaffolding promotes osteoblast differentiation and biomineralization. Biomaterials 2007;28(2):335-43.

[14] Reddi AH. Role of morphogenetic proteins in skeletal tissue engineering and regeneration. Nat Biotechnol 1998;16(3):247-52.

[15] Yang XB, Bhatnagar RS, Li S, Oreffo ROC. Biomimetic collagen scaffolds for human bone cell growth and differentiation. Tissue Eng 2004;10(7-8):1148-59.

[16] Jikko A, Harris SE, Chen D, Mendrick DL, Damsky CH. Collagen integrin receptors regulate early osteoblast differentiation induced by BMP-2. J Bone Miner Res 1999;14(7):1075-83.

[17] Mizuno M, Fujisawa R, Kuboki Y. Type I collagen-induced osteoblastic differentiation of bone-marrow cells mediated by collagen-alpha2beta1 integrin interaction. J Cell Physiol 2000;184(2):207-13.

[18] Kim BS, Mooney DJ. Development of biocompatible synthetic extracellular matrices for tissue engineering. Trends Biotechnol 1998;16(5):224-30.

[19] Ngiam M, Liao S, Patil AJ, Cheng Z, Yang F, Gubler MJ, et al. Fabrication of mineralized polymeric nanofibrous composites for bone graft materials. Tissue engineering. Part A 2009;15(3):535-46.

[20] Fujihara K, Kotaki M, Ramakrishna S. Guided bone regeneration membrane made of polycaprolactone/calcium carbonate composite nano-fibers. Biomaterials 2005;26(19):4139-47.

[21] Ngiam M, Liao S, Patil AJ, Cheng Z, Chan CK, Ramakrishna S. The fabrication of nano-hydroxyapatite on PLGA and PLGA/collagen nanofibrous composite scaffolds and their effects in osteoblastic behavior for bone tissue engineering. Bone 2009;45(1):4-16.

[22] Prabhakaran MP, Venugopal J, Ramakrishna S. Electrospun nanostructured scaffolds for bone tissue engineering. Acta Biomater 2009;5(8):2884-93.

[23] Shih YRV, Chen CN, Tsai SW, Wang YJ, Lee OK. Growth of mesenchymal stem cells on electrospun type I collagen nanofibers. Stem Cells 2006;24(11):2391-7.

[24] Lin L, Chow KL, Leng Y. Study of hydroxyapatite osteoinductivity with an osteogenic differentiation of mesenchymal stem cells. J Biomed Mater Res A 2009;89(2):326-35.

[25] Bernhardt A, Lode A, Boxberger S, Pompe W, Gelinsky M. Mineralised collagen--an artificial, extracellular bone matrix--improves osteogenic differentiation of bone marrow stromal cells. J Mater Sci Mater Med 2008;19(1):269-75.

[26] Lee JH, Rim NG, Jung HS, Shin H. Control of osteogenic differentiation and mineralization of human mesenchymal stem cells on composite nanofibers containing poly[lactic-co-(glycolic acid)] and hydroxyapatite. Macromol Biosci 2010;10(2):173-82.

[27] Minamide A, Yoshida M, Kawakami M, Okada M, Enyo Y, Hashizume H, et al. The effects of bone morphogenetic protein and basic fibroblast growth factor on cultured mesenchymal stem cells for spine fusion. Spine 2007;32(10):1067-71.

[28] Liao SS, Guan K, Cui FZ, Shi SS, Sun TS. Lumbar spinal fusion with a mineralized collagen matrix and rhBMP-2 in a rabbit model. Spine 2003;28(17):1954-60.

[29] Jørgensen NR, Henriksen Z, Sørensen OH, Civitelli R. Dexamethasone, BMP-2, and 1,25-dihydroxyvitamin D enhance a more differentiated osteoblast phenotype: validation of an in vitro model for human bone marrow-derived primary osteoblasts. Steroids 2004;69(4):219-26.

[30] Gupta A, Leong DT, Bai HF, Singh SB, Lim TC, Hutmacher DW. Osteo-maturation of adipose-derived stem cells required the combined action of vitamin D3, beta-glycerophosphate, and ascorbic acid. Biochem Biophys Res Commun 2007;362(1):17-24.

[31] Dalby MJ, Gadegaard N, Tare R, Andar A, Riehle MO, Herzyk P, et al. The control of human mesenchymal cell differentiation using nanoscale symmetry and disorder. Nat Mater 2007;6(12):997-1003.

[32] Buma P, Schreurs W, Verdonschot N. Skeletal tissue engineering-from in vitro studies to large animal models. Biomaterials 2004;25(9):1487-95.

[33] Gugala Z, Gogolewski S. Regeneration of segmental diaphyseal defects in sheep tibiae using resorbable polymeric membranes: a preliminary study. J Orthop Trauma 1999;13(3):187-95.

[34] Crigel MH, Balligand M. Critical size defect model on the femur in rabbits. Vet Comp Orthop Traumatol 2022;15:158-63.

[35] Chan C, Sampath Kumar T, Liao S, Murugan R, Ngiam M, Ramakrishna, et al. Biomimetic nanocomposite for bone graft applications. Nanomed 2006;1(2):177-88.

[36] Gupta D, Venugopal J, Mitra S, Giri Dev VR RS. Nanostructured biocomposite substrates by electrospinning and electrospraying for the mineralization of osteoblasts. Biomaterials 2009;30:2085-94.

[37] Francis L, Venugopal J, Prabhakaran MP, Thavasi V, Marsano E, Ramakrishna S. Simultaneous electrospin–electrosprayed biocomposite nanofibrous scaffolds for bone tissue regeneration. Acta Biomater 2010;6:4100-9.

[38] Woolf AD. The bone and joint decade 2000-2010. Ann Rheum Dis 2000;59(2):81-2.

[39] Siris ES. Paget's disease of bone. J Bone Miner Res 1998;13(7):1061-5.

[40] Engelbert RH, Pruijs HE, Beemer FA, Helders PJ. Osteogenesis imperfecta in childhood: treatment strategies. Arch Phys Med Rehabil 1998;79(12):1590-4.

[41] Rho JY, Kuhn-Spearing L, Zioupos P. Mechanical properties and the hierarchical structure of bone. Med Eng Phys 1998;20(2):92-102.

[42] Vallet-Regi M. Ceramics for medical applications. JChemSocDalton Trans 2001;100:97-108.

[43] Landis WJ, Song MJ, Leith A, McEwen L, McEwen BF. Mineral and organic matrix interaction in normally calcifying tendon visualized in three dimensions by high-voltage electron microscopic tomography and graphic image reconstruction. J Struct Biol 1993;110(1):39-54.

[44] Matsuo K, Irie N. Osteoclast-osteoblast communication. Arch Biochem Biophys 2008;473(2):201-9.

[45] Einhorn TA. The cell and molecular biology of fracture healing. Clin Orthop Relat Res 1998;(355 Suppl):S7-21.

[46] Brighton CT, Hunt RM. Early histological and ultrastructural changes in medullary fracture callus. J Bone Joint Surg Am 1991;73(6):832-47.

[47] Dimitriou R, Tsiridis E, Giannoudis PV. Current concepts of molecular aspects of bone healing. Injury 2005;36(12):1392-404.

[48] Liu P, Oyajobi BO, Russell RG, Scutt A. Regulation of osteogenic differentiation of human bone marrow stromal cells: interaction between transforming growth factor-beta and 1,25(OH)(2) vitamin D(3) In vitro. Calcif Tissue Int 1999;65(2):173-80.

[49] Beck GR, Zerler B, Moran E. Phosphate is a specific signal for induction of osteopontin gene expression. Proc Natl Acad Sci U S A 2000;97(15):8352-7.

[50] Fujita T, Izumo N, Fukuyama R, Meguro T, Nakamuta H, Kohno T, et al. Phosphate provides an extracellular signal that drives nuclear export of Runx2/Cbfa1 in bone cells. Biochem Biophys Res Commun 2001;280(1):348-52.

[51] Reyes M, Verfaillie CM. Characterization of multipotent adult progenitor cells, a subpopulation of mesenchymal stem cells. Ann N Y Acad Sci 2001;938:231-5.

[52] Atmani H, Audrain C, Mercier L, Chappard D, Basle MF. Phenotypic effects of continuous or discontinuous treatment with dexamethasone and/or calcitriol on osteoblasts differentiated from rat bone marrow stromal cells. J Cell Biochem 2002;85(3):640-50.

[53] Nuttelman CR, Tripodi MC, Anseth KS. Dexamethasone-functionalized gels induce osteogenic differentiation of encapsulated hMSCs. J Biomed Mater Res A 2006;76(1):183-95.

[54] Jørgensen N, Henriksen Z, Sørensen OH, Civitelli R. Dexamethasone, BMP-2, and 1,25-dihydroxyvitamin D enhance a more differentiated osteoblast phenotype: validation of an in-vitro model for human bone marrow-derived primary osteoblasts. Steroids 2004;69:219-26.

[55] Gupta A, Leong D, Bai H, Singh S, Lim T, Hutmacher D. Osteo-maturation of adipose-derived stem cells required the combined action of vitamin D β-glycerophosphate, and ascorbic acid. Biochem Biophys Res Commun 2007;362(1):17-24.

[56] Ngiam M, Liao S, Chan C, Ramakrishna S. Cell-based nanocomposites and biomolecules for bone tissue engineering. In: Basu B, Katti DS, Kumar A, editor. Advanced biomaterials: fundamentals, processing and applications. New Jersey: John Wiley & Sons Inc.; 2009. p. 551-588.

[57] Taira M, Nakao H, Takahashi J, Araki Y. Effects of two vitamins, two growth factors and dexamethasone on the proliferation of rat bone marrow stromal cells and osteoblastic MC3T3-E1 cells. J Oral Rehabil 2003;30(7):697-701.

[58] Shui C, Scutt AM. Mouse embryo-derived NIH3T3 fibroblasts adopt an osteoblast-like phenotype when treated with 1alpha,25-dihydroxyvitamin D(3) and dexamethasone in vitro. J Cell Physiol 2002;193(2):164-72.

[59] Luu HH, Song WX, Luo X, Manning D, Luo J, Deng ZL, et al. Distinct roles of bone morphogenetic proteins in osteogenic differentiation of mesenchymal stem cells. J Orthop Res 2007;25(5):665-77.

[60] Nordsletten L. Recent developments in the use of bone morphogenetic protein in orthopaedic trauma surgery. Curr Med Res Opin 2006;22 Suppl 1:S13-7; S23.

[61] Diefenderfer D, Osyczka A, Reilly G, Leboy P. BMP responsiveness in human mesenchymal stem cells. Connect Tissue Res 2003;44(Supp 1):305-11.

[62] Groeneveld EH, Burger EH. Bone morphogenetic proteins in human bone regeneration. Eur J Endocrinol 2000;142(1):9-21.

[63] Lane JM. BMPs: why are they not in everyday use? J Bone Joint Surg Am 2001;83-A Suppl 1(Pt 2):S161-3.

[64] Service RF. Tissue engineers build new bone. Science 2000;289(5484):1498-500.

[65] Huang YC, Kaigler D, Rice KG, Krebsbach PH, Mooney DJ. Combined angiogenic and osteogenic factor delivery enhances bone marrow stromal cell-driven bone regeneration. J Bone Miner Res 2005;20(5):848-57.

[66] Kaigler D, Wang Z, Horger K, Mooney DJ, Krebsbach PH. VEGF scaffolds enhance angiogenesis and bone regeneration in irradiated osseous defects. J Bone Miner Res 2006;21(5):735-44.

[67] Hsu HP, Zanella JM, Peckham SM, Spector M. Comparing ectopic bone growth induced by rhBMP-2 on an absorbable collagen sponge in rat and rabbit models. J Orthop Res 2006;24(8):1660-9.

[68] Welch RD, Jones AL, Bucholz RW, Reinert CM, Tjia JS, Pierce WA, et al. Effect of recombinant human bone morphogenetic protein-2 on fracture healing in a goat tibial fracture model. J Bone Miner Res 1998;13(9):1483-90.

[69] Yamamoto M, Takahashi Y, Tabata Y. Enhanced bone regeneration at a segmental bone defect by controlled release of bone morphogenetic protein-2 from a biodegradable hydrogel. Tissue Eng 2006;12(5):1305-11.

[70] Srouji S, Rachmiel A, Blumenfeld I, Livne E. Mandibular defect repair by TGF-beta and IGF-1 released from a biodegradable osteoconductive hydrogel. J Craniomaxillofac Surg 2005;33(2):79-84.

[71] Simmons CA, Alsberg E, Hsiong S, Kim WJ, Mooney DJ. Dual growth factor delivery and controlled scaffold degradation enhance in vivo bone formation by transplanted bone marrow stromal cells. Bone 2004;35(2):562-9.

[72] Maissen O, Eckhardt C, Gogolewski S, Glatt M, Arvinte T, Steiner A, et al. Mechanical and radiological assessment of the influence of rhTGFbeta-3 on bone regeneration in a segmental defect in the ovine tibia: pilot study. J Orthop Res 2006;24(8):1670-8.

[73] Sumner DR, Turner TM, Urban RM, Leven RM, Hawkins M, Nichols EH, et al. Locally delivered rhTGF-beta2 enhances bone ingrowth and bone regeneration at local and remote sites of skeletal injury. J Orthop Res 2001;19(1):85-94.

[74] Yoshida Y, von Bubnoff A, Ikematsu N, Blitz IL, Tsuzuku JK, Yoshida EH, et al. Tob proteins enhance inhibitory Smad-receptor interactions to repress BMP signaling. Mech Dev 2003;120(5):629-37.

[75] Gaur T, Lengner CJ, Hovhannisyan H, Bhat RA, Bodine PVN, Komm BS, et al. Canonical WNT signaling promotes osteogenesis by directly stimulating Runx2 gene expression. J Biol Chem 2005;280(39):33132-40.

[76] Shindo K, Kawashima N, Sakamoto K, Yamaguchi A, Umezawa A, Takagi M, et al. Osteogenic differentiation of the mesenchymal progenitor cells, Kusa is suppressed by Notch signaling. Exp Cell Res 2003;290(2):370-80.

[77] Woodruff MA, Rath SN, Susanto E, Haupt LM, Hutmacher DW, Nurcombe V, et al. Sustained release and osteogenic potential of heparan sulfate-doped fibrin glue scaffolds within a rat cranial model. J Mol Histol 2007;38(5):425-33.

[78] Babensee JE, McIntire LV, Mikos AG. Growth factor delivery for tissue engineering. Pharm Res 2000;17(5):497-504.

[79] Zhang X, Sobue T, Hurley MM. FGF-2 increases colony formation, PTH receptor, and IGF-1 mRNA in mouse marrow stromal cells. Biochem Biophys Res Commun 2002;290(1):526-31.

[80] Johnson EE, Urist MR. Human bone morphogenetic protein allografting for reconstruction of femoral nonunion. Clin Orthop Relat Res 2000;(371):61-74.

[81] Johnson E, Urist M, Finerman G. Repair of segmental defects of the tibia with cancellous bone grafts augmented with human bone morphogenetic protein. A preliminary report Clin Orthop 1998;236:249-57.

[82] Johnson E, Urist M, Finerman G. Bone morphogenetic protein augmentation grafting of resistant femoral nonunions. A preliminary report Clin Orthop 1998;230:257-65.

[83] Morone MA, Boden SD. Experimental posterolateral lumbar spinal fusion with a demineralized bone matrix gel. Spine 1998;23(2):159-67.

[84] Peterson B, Whang PG, Iglesias R, Wang JC, Lieberman JR. Osteoinductivity of commercially available demineralized bone matrix. Preparations in a spine fusion model. J Bone Joint Surg Am 2004;86-A(10):2243-50.

[85] Chan CK, Kumar TSS, Liao S, Murugan R, Ngiam M, Ramakrishnan S. Biomimetic nanocomposites for bone graft applications. Nanomed 2006;1(2):177-88.

[86] Giannoudis PV, Dinopoulos H TE. Bone substitutes: An update. Injury, Int. J. Care Injured 2005;36S:S20—S27.

[87] Kokubo T, Kim HM, Kawashita M. Novel bioactive materials with different mechanical properties. Biomaterials 2003;24:2161-75.

[88] Kim HW, Kim HE. Nanofiber generation of hydroxyapatite and fluor-hydroxyapatite bioceramics. J Biomed Mater Res B Appl Biomater 2006;77(2):323-8.

[89] Marie PJ, De Vernejoul MC, Lomri A. Stimulation of bone formation in osteoporosis patients treated with fluoride associated with increased DNA synthesis by osteoblastic cells in vitro. J Bone Miner Res 1992;7(1):103-13.

[90] de Leeuw N. Resisting the onset of hydroxyapatite dissolution through the incorporation of fluoride. J Phys Chem B 2004;108:1809-11.

[91] Ramay HRR, Zhang M. Biphasic calcium phosphate nanocomposite porous scaffolds for load-bearing bone tissue engineering. Biomaterials 2004;25(21):5171-80.

[92] Gibson LJ. The mechanical behaviour of cancellous bone. J Biomech 1985;18(5):317-28.

[93] Xia W, Zhang D, Chang J. Fabrication and in vitro biomineralization of bioactive glass (BG) nanofibres. Nanotechnology 2007;18:1-7.

[94] Zhang W, Liao S, Cui F. Hierarchical Self-Assembly of Nano-Fibrils in Mineralized Collagen. Chem Mater 2003;15:3221-6.

[95] Zhang W, Huang Z, Liao S, Cui F. Nucleation Sites of Calcium Phosphate Crystals during Collagen Mineralization. J Am Ceram Soc 2003;86(6):1052-4.

[96] Awad H, Wickham M, Leddy H, Gimble J, Guilak F. Chondrogenic differentiation of adipose-derived adult stem cells in agarose, alginate, and gelatin scaffolds. Biomaterials 2004;25(16):3211-22.

[97] Malafaya P, Pedro A, Peterbauer A, Gabriel C, Redl H, Reis R. Chitosan particles agglomerated scaffolds for cartilage and osteochondral tissue engineering approaches with adipose tissue derived stem cells. J Mater Sci Mater Med 2005;16:1077-85.

[98] Oliveira JM, Rodrigues MT, Silva SS, Malafaya PB, Gomes ME, Viegas CA, et al. Novel hydroxyapatite/chitosan bilayered scaffold for osteochondral tissue-engineering applications: Scaffold design and its performance when seeded with goat bone marrow stromal cells. Biomaterials 2006;27(36):6123-37.

[99] Solchaga LA, Yoo JU, Lundberg M, Dennis JE, Huibregtse BA, Goldberg VM, et al. Hyaluronan-based polymers in the treatment of osteochondral defects. J Orthop Res 2000;18(5):773-80.

[100] Karp JM, Sarraf F, Shoichet MS, Davies JE. Fibrin-filled scaffolds for bone-tissue engineering: An in vivo study. J Biomed Mater Res A 2004;71(1):162-71.

[101] Marolt D, Augst A, Freed LE, Vepari C, Fajardo R, Patel N, et al. Bone and cartilage tissue constructs grown using human bone marrow stromal cells, silk scaffolds and rotating bioreactors. Biomaterials 2006;27(36):6138-49.

[102] Li C, Jin H, Botsaris G, Kaplan D. Silk apatite composites from electrospun fibers. J Bone Miner Res 2005;20(12):3374-84.

[103] Ishaug SL, Crane GM, Miller MJ, Yasko AW, Yaszemski MJ, Mikos AG. Bone formation by three-dimensional stromal osteoblast culture in biodegradable polymer scaffolds. J Biomed Mater Res 1997;36(1):17-28.

[104] Xin X, Hussain M, Mao JJ. Continuing differentiation of human mesenchymal stem cells and induced chondrogenic and osteogenic lineages in electrospun PLGA nanofiber scaffold. Biomaterials 2007;28(2):316-25.

[105] Liao SS, Cui FZ. In vitro and in vivo degradation of mineralized collagen-based composite

scaffold: nanohydroxyapatite/collagen/poly(L-lactide). Tissue Eng 2004;10(1-2):73-80.

[106] Williams JM, Adewunmi A, Schek RM, Flanagan CL, Krebsbach PH, Feinberg SE, et al. Bone tissue engineering using polycaprolactone scaffolds fabricated via selective laser sintering. Biomaterials 2005;26(23):4817-27.

[107] Ciapetti G, Ambrosio L, Marletta G, Baldini N, Giunti A. Human bone marrow stromal cells: In vitro expansion and differentiation for bone engineering. Biomaterials 2006;27(36):6150-60.

[108] Gunatillake PA, Adhikari R. Biodegradable synthetic polymers for tissue engineering. Eur Cell Mater 2003;5:1-6.

[109] Liao S, Cui F, Zhu Y. Osteoblasts adherence and migration through three-dimensional porous mineralized collagen based composite: nHAC/PLA. J Bioact Compat. Polym 2004;19(2):117-30.

[110] Christenson EM, Anseth KS, van den Beucken JJJP, Chan CK, Ercan B, Jansen JA, et al. Nanobiomaterial applications in orthopedics. J Orthop Res 2007;25(1):11-22.

[111] Huang J, Jayasinghe S, Best S, Edirisinghe M, Brooks R, Bonfield W. Electrospraying of a nano-hydroxyapatite suspension. Clin Infect Dis 2004;39:1029-32.

[112] Liao S, Wang W, Uo M, Ohkawa S, Akasaka T, Tamura K, et al. A three-layered nano-carbonated hydroxyapatite/collagen/PLGA composite membrane for guided tissue regeneration. Biomaterials 2005;26(36):7564-71.

[113] Liao SS, Cui FZ, Zhang W, Feng QL. Hierarchically biomimetic bone scaffold materials: nano-HA/collagen/PLA composite. J Biomed Mater Res B Appl Biomater 2004;69(2):158-65.

[114] Liao S, Watari F, Uo M, Ohkawa S, Tamura K, Wang W, et al. The preparation and characteristics of a carbonated hydroxyapatite/collagen composite at room temperature. J Biomed Mater Res B Appl Biomater 2005;74(2):817-21.

[115] Liao S, Yokoyama A, Wang W, Zhu Y, Watari F, Ramakrishna S, et al. In-Vitro and In-Vivo behaviors of the Three Layered Nano-carbonated Hydroxyapatite/Collagen/PLGA Composite. J Bioactive Compat Polym 2010;25(2):154-68.

[116] Du C, Cui FZ, Zhang W, Feng QL, Zhu XD, de Groot K. Formation of calcium phosphate/collagen composites through mineralization of collagen matrix. J Biomed Mater Res 2000;50(4):518-27.

[117] Du C, Cui FZ, Zhu XD, de Groot K. Three-dimensional nano-HAp/collagen matrix loading with osteogenic cells in organ culture. J Biomed Mater Res 1999;44(4):407-15.

[118] Du C, Cui FZ, Feng QL, Zhu XD, de Groot K. Tissue response to nano-

hydroxyapatite/collagen composite implants in marrow cavity. J Biomed Mater Res 1998;42(4):540-8.

[119] Kikuchi T, Ikoma S, Itoh H, Matsumoto Y, Koyama K, Takakuda K, et al. M.Tanaka. Biomimetic synthesis of bone-like nanocomposites using the self-organization mechanism of hydroxyapatite and collagen. CompSciTechnol 2004;64(6):819-25.

[120] Itoh S, Kikuchi M, Koyama Y, Takakuda K, Shinomiya K, Tanaka J. Development of a hydroxyapatite/collagen nanocomposite as a medical device. Cell Transplant 2004;13(4):451-61.

[121] Kikuchi M, Itoh S, Ichinose S, Shinomiya K, Tanaka J. Self-organization mechanism in a bone-like hydroxyapatite/collagen nanocomposite synthesized in vitro and its biological reaction in vivo. Biomaterials 2001;22(13):1705-11.

[122] Rhee SH, Suetsugu Y, Tanaka J. Biomimetic configurational arrays of hydroxyapatite nanocrystals on bio-organics. Biomaterials 2001;22(21):2843-7.

[123] Rhee SH, Tanaka J. Self-assembly phenomenon of hydroxyapatite nanocrystals on chondroitin sulfate. J Mater Sci Mater Med 2002;13(6):597-600.

[124] Rhee S, Tanaka J. Synthesis of a hydroxyapatite/collagen/chondroitin sulphate nanocomposite by a novel precipitation method. J Am Ceram Soc 2001;84(2):459-61.

[125] Liao S, Cui F, Zhu Y. Osteoblasts Adherence and Migration through Three-dimensional PorousMineralized Collagen Based Composite: nHAC/PLA. J. Bioact. Comp. Pol 2004;19:117-30.

[126] Zhang S, Cui F, Liao S, Zhu Y, Han L. Synthesis and biocompatibility of porous nano-hydroxyapatite/collagen/alginate composite. J Am Soc Nephrol 2003;14(7):641-5.

[127] Jones SJ, Boyde A. The migration of osteoblasts. Cell Tissue Res 1977;184(2):179-93.

[128] Du C, Su XW, Cui FZ, Zhu XD. Morphological behaviour of osteoblasts on diamond-like carbon coating and amorphous C-N film in organ culture. Biomaterials 1998;19(7-9):651-8.

[129] Schimandle JH, Boden SD, Hutton WC. Experimental spinal fusion with recombinant human bone morphogenetic protein-2. Spine 1995;20(12):1326-37.

[130] Catledge SA, Clem WC, Shrikishen N, Chowdhury S, Stanishevsky AV, Koopman M, et al. An electrospun triphasic nanofibrous scaffold for bone tissue engineering. Biomed Mater 2007;2(2):142-50.

[131] Sui G, Yang X, Mei F, Hu X, Chen G, Deng X, et al. Poly-L-lactic acid/hydroxyapatite hybrid membrane for bone tissue regeneration. J Biomed Mater Res A 2007;82(2):445-54.

[132] Ito Y, Hasuda H, Kamitakahara M, Ohtsuki C, Tanihara M, Kang IK, et al. A composite of

hydroxyapatite with electrospun biodegradable nanofibers as a tissue engineering material. J Biosci Bioeng 2005;100(1):43-9.

[133] Li C, Vepari C, Jin HJ, Kim HJ, Kaplan DL. Electrospun silk-BMP-2 scaffolds for bone tissue engineering. Biomaterials 2006;27(16):3115-24.

[134] Fan H, Wen X, Tan Y, Wang R, Cao H, Zhang X. Compare of electrospinning PLA and PLA/b-TCP scaffold in-vitro: PRICM 5: the Fifth Pacific Rim International Conference on Advanced Materials and Processing. Mater.Sci.Forum.Part 1; ; 2005.

[135] Thomas V, Jagani S, Johnson K, Jose MV, Dean DR, Vohra YK, et al. Electrospun bioactive nanocomposite scaffolds of polycaprolactone and nanohydroxyapatite for bone tissue engineering. J Nanosci Nanotechnol 2006;6(2):487-93.

[136] Zhang Y, Ouyang H, Lim CT, Ramakrishna S, Huang ZM. Electrospinning of gelatin fibers and gelatin/PCL composite fibrous scaffolds. J Biomed Mater Res B Appl Biomater 2005;72(1):156-65.

[137] Ramakrishna S, Fujihara K, Teo W, Lim T, Ma Z. An introduction to electrospinning and nanofibers. World Scientific Publishing: Singapore; 2005.

[138] Ma Z, Kotaki M, Inai R, Ramakrishna S. Potential of nanofiber matrix as tissue-engineering scaffolds. Tissue Eng 2005;11(1-2):101-9.

[139] Subbiah T, Bhat G, Tock R, Parameswaran S, Ramkumar S. Electrospinning of nanofibers. Nurs J India 2005;96:557-69.

[140] Teo WE, Ramakrishna S. A review on electrospinning design and nanofibre assemblies. Nanotechnology 2006;17(14):R89-106.

[141] Ngiam M, Ramakrishna S, Raghunath M, Chan CK. Nanofiber patent landscape. Recent patents on nanotechnology 2007;1(2):137-44.

[142] WE T, Gopal R, Ramaseshan R, Fujihara K, Ramakrishna S. A dynamic liquid support system for continuous electrospun yarn fabrication. Polymer 2007;48:3400-5.

[143] Teo W, Liao S, Chan C, Ramakrishna S. Remodeling of three-dimensional hierarchically organized nanofibrous assemblies. Curr Nanosci 2008;4(4):361-9.

[144] Norman J, Collins J, Sharma S, Russell B, Desai T. Microstructures in 3D biological gels affect cell proliferation. Tissue Eng 2008;14(3):379-90.

[145] Tsang V, Bhatia S. Three-dimensional tissue engineering. Adv Drug Deliv Rev 2004;56:1635-47.

[146] Shieh M. Control of bone cell functions on three-dimensional tissue engineering scaffolds.

BUG J 2000;3:194-204.

[147] Hartgerink JD, Beniash E, Stupp SI. Self-assembly and mineralization of peptide-amphiphile nanofibers. Science 2001;294(5547):1684-8.

[148] Silva G, Czeisler C, Niece K, Beniash E, Harrington D, Kessler J, et al. Selective differentiation of neural progenitor cells by high epitope density nanofibers. Science 2001;303(5662):1352-5.

[149] Hosseinkhani H, Hosseinkhani M, Tian F, Kobayashi H, Tabata Y. Ectopic bone formation in collagen sponge self-assembled peptide-amphiphile nanofibers hybrid scaffold in a perfusion culture bioreactor. Biomaterials 2006;27(29):5089-98.

[150] Bhatnagar RS, Qian JJ, Gough CA. The role in cell binding of a beta-bend within the triple helical region in collagen alpha 1 (I) chain: structural and biological evidence for conformational tautomerism on fiber surface. J Biomol Struct Dyn 1997;14(5):547-60.

[151] Bhatnagar R, Wedrychowska A, Sadeghi M, Qian J, Wu Y, Smith N. Design of biomimetic habitats for tissue engineering with P- a synthetic peptide analogue of collagen. Tissue Eng 1999;5(1):53-65.

[152] Nguyen H, Qian JJ, Bhatnagar RS, Li S. Enhanced cell attachment and osteoblastic activity by P-15 peptide-coated matrix in hydrogels. Biochem Biophys Res Commun 2003;311(1):179-86.

[153] Mizuno M, Kuboki Y. TGF-beta accelerated the osteogenic differentiation of bone marrow cells induced by collagen matrix. Biochem Biophys Res Commun 1995;211(3):1091-8.

[154] DeLustro F, Condell RA, Nguyen MA, McPherson JM. A comparative study of the biologic and immunologic response to medical devices derived from dermal collagen. J Biomed Mater Res 1986;20(1):109-20.

[155] Meade KR, Silver FH. Immunogenicity of collagenous implants. Biomaterials 1990;11(3):176-80.

[156] Durrieu MC, Pallu S, Guillemot F, Bareille R, Amédée J, Baquey CH, et al. Grafting RGD containing peptides onto hydroxyapatite to promote osteoblastic cells adhesion. J Mater Sci Mater Med 2004;15(7):779-86.

[157] Ho MH, Hou LT, Tu CY, Hsieh HJ, Lai JY, Chen WJ, et al. Promotion of cell affinity of porous PLLA scaffolds by immobilization of RGD peptides via plasma treatment. Macromol Biosci 2006;6(1):90-8.

[158] Ruoslahti E, Pierschbacher MD. New perspectives in cell adhesion: RGD and integrins. Science 1987;238(4826):491-7.

[159] Saito A, Suzuki Y, Ogata SI, Ohtsuki C, Tanihara M. Prolonged ectopic calcification induced by BMP-2-derived synthetic peptide. J Biomed Mater Res A 2004;70(1):115-21.

[160] Tanahashi M, Matsuda T. Surface functional group dependence on apatite formation on self-assembled monolayers in a simulated body fluid. J Biomed Mater Res 1997;34(3):305-15.

[161] Lin X, Elliot JJ, Carnes DL, Fox WC, Peña LA, Campion SL, et al. Augmentation of osseous phenotypes in vivo with a synthetic peptide. J Orthop Res 2007;25(4):531-9.

[162] Lin X, Zamora PO, Albright S, Glass JD, Peña LA. Multidomain synthetic peptide B2A2 synergistically enhances BMP-2 in vitro. J Bone Miner Res 2005;20(4):693-703.

[163] Kofron MD, Zhang JX, Lieberman JR, Laurencin CT. Genetically modified mesodermal-derived cells for bone tissue engineering. IEEE Eng Med Biol Mag 2003;22(5):57-64.

[164] Laurencin CT, Attawia MA, Lu LQ, Borden MD, Lu HH, Gorum WJ, et al. Poly(lactide-co-glycolide)/hydroxyapatite delivery of BMP-2-producing cells: a regional gene therapy approach to bone regeneration. Biomaterials 2001;22(11):1271-7.

[165] Huang J, Wong C, George A, Kaplan DL. The effect of genetically engineered spider silk-dentin matrix protein 1 chimeric protein on hydroxyapatite nucleation. Biomaterials 2007;28(14):2358-67.

[166] He G, Dahl T, Veis A, George A. Nucleation of apatite crystals in vitro by self-assembled dentin matrix protein 1. Nat Mater 2003;2(8):552-8.

[167] Zhai Y, Cui F. Recombinant human-like collagen directed growth of hydroxyapatite nanocrystals. J Crystal Growth 2006;291:202-6.

[168] Thomson JA, Itskovitz-Eldor J, Shapiro SS, Waknitz MA, Swiergiel JJ, Marshall VS, et al. Embryonic stem cell lines derived from human blastocysts. Science 1998;282(5391):1145-7.

[169] Evans M, Kaufman M. Establishment in culture of pluripotential cells from mouse embryos. Nature 1981;292:154-6.

[170] Martin G. Isolation of a pluripotent cell line from early mouse embryos cultured in medium conditioned by teratocarcinoma stem cells. Proc. Natl Acad. Sci. USA 1981;78:7634-8.

[171] Bradley A, Evans M, Kaufman MH, Robertson E. Formation of germ-line chimaeras from embryo-derived teratocarcinoma cell lines. Nature 1984;309(5965):255-6.

[172] Bongso A, Fong CY, Ng SC, Ratnam S. Isolation and culture of inner cell mass cells from human blastocysts. Hum Reprod 1994;9(11):2110-7.

[173] Shamblott MJ, Axelman J, Wang S, Bugg EM, Littlefield JW, Donovan PJ, et al. Derivation of pluripotent stem cells from cultured human primordial germ cells. Proc Natl Acad

Sci U S A 1998;95(23):13726-31.

[174] Gentleman E, Swain RJ, Evans ND, Boonrungsiman S, Jell G, Ball MD, et al. Comparative materials differences revealed in engineered bone as a function of cell-specific differentiation. Nat Mater 2009;8(9):763-70.

[175] Pittenger MF, Mackay AM, Beck SC, Jaiswal RK, Douglas R, Mosca JD, et al. Multilineage potential of adult human mesenchymal stem cells. Science 1999;284(5411):143-7.

[176] Wang HS, Hung SC, Peng ST, Huang CC, Wei HM, Guo YJ, et al. Mesenchymal stem cells in the Wharton's jelly of the human umbilical cord. Stem Cells 2004;22(7):1330-7.

[177] Jeon O, Rhie JW, Kwon IK, Kim JH, Kim BS, Lee SH. In vivo bone formation following transplantation of human adipose-derived stromal cells that are not differentiated osteogenically. Tissue engineering. Part A 2008;14(8):1285-94.

[178] Nakajima T, Iizuka H, Tsutsumi S, Kayakabe M, Takagishi K. Evaluation of posterolateral spinal fusion using mesenchymal stem cells: differences with or without osteogenic differentiation. Spine 2007;32(22):2432-6.

[179] Morishita T, Honoki K, Ohgushi H, Kotobuki N, Matsushima A, Takakura Y. Tissue engineering approach to the treatment of bone tumors: three cases of cultured bone grafts derived from patients' mesenchymal stem cells. Artif Organs 2006;30(2):115-8.

[180] Quarto R, Thomas D, Liang C. Bone Progenitor Cell Deficits and the Age-Associated Decline in Bone Repair Capacity. Calcif Tissue Int 1995;56(2):123-9.

[181] Haynesworth SE, Goshima J, Goldberg VM, Caplan AI. Characterization of cells with osteogenic potential from human marrow. Bone 1992;13(1):81-8.

[182] Friedman MS, Long MW, Hankenson KD. Osteogenic differentiation of human mesenchymal stem cells is regulated by bone morphogenetic protein-6. J Cell Biochem 2006;98(3):538-54.

[183] Boden SD, McCuaig K, Hair G, Racine M, Titus L, Wozney JM, et al. Differential effects and glucocorticoid potentiation of bone morphogenetic protein action during rat osteoblast differentiation in vitro. Endocrinology 1996;137(8):3401-7.

[184] Boden SD, Hair G, Titus L, Racine M, McCuaig K, Wozney JM, et al. Glucocorticoid-induced differentiation of fetal rat calvarial osteoblasts is mediated by bone morphogenetic protein-6. Endocrinology 1997;138(7):2820-8.

[185] Diefenderfer DL, Osyczka AM, Reilly GC, Leboy PS. BMP responsiveness in human mesenchymal stem cells. Connect Tissue Res 2003;44 Suppl 1:305-11.

[186] Curran JM, Chen R, Hunt JA. The guidance of human mesenchymal stem cell

differentiation in vitro by controlled modifications to the cell substrate. Biomaterials 2006;27(27):4783-93.

[187] D'Ippolito G, Schiller PC, Ricordi C, Roos BA, Howard GA. Age-related osteogenic potential of mesenchymal stromal stem cells from human vertebral bone marrow. J Bone Miner Res 1999;14(7):1115-22.

[188] Lennon DP, Caplan AI. Isolation of human marrow-derived mesenchymal stem cells. Exp Hematol 2006;34(11):1604-5.

[189] Muschler GF, Nitto H, Boehm CA, Easley KA. Age- and gender-related changes in the cellularity of human bone marrow and the prevalence of osteoblastic progenitors. J Orthop Res 2001;19(1):117-25.

[190] Bruder SP, Jaiswal N, Haynesworth SE. Growth kinetics, self-renewal, and the osteogenic potential of purified human mesenchymal stem cells during extensive subcultivation and following cryopreservation. J Cell Biochem 1997;64(2):278-94.

[191] Wexler SA, Donaldson C, Denning-Kendall P, Rice C, Bradley B, Hows JM. Adult bone marrow is a rich source of human mesenchymal 'stem' cells but umbilical cord and mobilized adult blood are not. Br J Haematol 2003;121(2):368-74.

[192] Jaiswal N, Haynesworth SE, Caplan AI, Bruder SP. Osteogenic differentiation of purified, culture-expanded human mesenchymal stem cells in vitro. J Cell Biochem 1997;64(2):295-312.

[193] Gronthos S, Franklin D, Leddy H, Robey P, Storms R, Gimble J. Surface Protein Characterization of Human Adipose Tissue-Derived Stromal Cells. J Cell Physiol 2001;189(1):54-63.

[194] Kang SK, Putnam L, Dufour J, Ylostalo J, Jung JS, Bunnell BA. Expression of telomerase extends the lifespan and enhances osteogenic differentiation of adipose tissue-derived stromal cells. Stem Cells 2004;22(7):1356-72.

[195] Lee H, Cho H, Kim H, Bae Y, Baik H, Jung J. Tbx a transcriptional factor, involves in proliferation and osteogenic differentiation of human adipose stromal cells. Mol Cell Biochem 2007;296(1-2):129-36.

[196] Kern S, Eichler H, Stoeve J, Klüter H, Bieback K. Comparative analysis of mesenchymal stem cells from bone marrow, umbilical cord blood, or adipose tissue. Stem Cells 2006;24(5):1294-301.

[197] Hui JHP, Li L, Teo YH, Ouyang HW, Lee EH. Comparative study of the ability of mesenchymal stem cells derived from bone marrow, periosteum, and adipose tissue in treatment of partial growth arrest in rabbit. Tissue Eng 2005;11(5-6):904-12.

[198] Yoshimura H, Muneta T, Nimura A, Yokoyama A, Koga H, Sekiya I. Comparison of rat

mesenchymal stem cells derived from bone marrow, synovium, periosteum, adipose tissue, and muscle. Cell Tissue Res 2007;327(3):449-62.

[199] Sakaguchi Y, Sekiya I, Yagishita K, Muneta T. Comparison of human stem cells derived from various mesenchymal tissues: superiority of synovium as a cell source. Arthritis Rheum 2005;52(8):2521-9.

[200] Muraglia A, Cancedda R, Quarto R. Clonal mesenchymal progenitors from human bone marrow differentiate in vitro according to a hierarchical model. J Cell Sci 2000;113 (Pt 7):1161-6.

[201] Niemeyer P, Kornacker M, Mehlhorn A, Seckinger A, Vohrer J, Schmal H, et al. Comparison of immunological properties of bone marrow stromal cells and adipose tissue-derived stem cells before and after osteogenic differentiation in vitro. Tissue Eng 2007;13(1):111-21.

[202] Abramovitch-Gottlib L, Gross T, Naveh D, Geresh S, Rosenwaks S, Bar I, et al. Low level laser irradiation stimulates osteogenic phenotype of mesenchymal stem cells seeded on a three-dimensional biomatrix. Lasers Med Sci 2005;20(3-4):138-46.

[203] Mygind T, Stiehler M, Baatrup A, Li H, Zou X, Flyvbjerg A, et al. Mesenchymal stem cell ingrowth and differentiation on coralline hydroxyapatite scaffolds. Biomaterials 2007;28(6):1036-47.

[204] Chastain SR, Kundu AK, Dhar S, Calvert JW, Putnam AJ. Adhesion of mesenchymal stem cells to polymer scaffolds occurs via distinct ECM ligands and controls their osteogenic differentiation. J Biomed Mater Res A 2006;78(1):73-85.

[205] Calvert JW, Marra KG, Cook L, Kumta PN, DiMilla PA, Weiss LE. Characterization of osteoblast-like behavior of cultured bone marrow stromal cells on various polymer surfaces. J Biomed Mater Res 2000;52(2):279-84.

[206] Keselowsky BG, Collard DM, García AJ. Integrin binding specificity regulates biomaterial surface chemistry effects on cell differentiation. Proc Natl Acad Sci U S A 2005;102(17):5953-7.

[207] Miller DC, Haberstroh KM, Webster TJ. Mechanism(s) of increased vascular cell adhesion on nanostructured poly(lactic-co-glycolic acid) films. J Biomed Mater Res A 2005;73(4):476-84.

[208] Webster TJ, Schadler LS, Siegel RW, Bizios R. Mechanisms of enhanced osteoblast adhesion on nanophase alumina involve vitronectin. Tissue Eng 2001;7(3):291-301.

[209] McBeath R, Pirone DM, Nelson CM, Bhadriraju K, Chen CS. Cell shape, cytoskeletal tension, and RhoA regulate stem cell lineage commitment. Dev Cell 2004;6(4):483-95.

[210] Ayers R, Nielsen-Preiss S, Ferguson V, Gotolli G, Moore J, Kleebe H. Osteoblast-like cell mineralization induced by multiphasic calcium phosphate ceramic. Mat Sci Eng C

2006;26:1333-7.

[211] Thian ES, Huang J, Best SM, Barber ZH, Brooks RA, Rushton N, et al. The response of osteoblasts to nanocrystalline silicon-substituted hydroxyapatite thin films. Biomaterials 2006;27(13):2692-8.

[212] Park J, Bauer S, von der Mark K, Schmuki P. Nanosize and vitality: TiO2 nanotube diameter directs cell fate. Nano Lett 2007;7(6):1686-91.

[213] Oh S, Brammer KS, Li YSJ, Teng D, Engler AJ, Chien S, et al. Stem cell fate dictated solely by altered nanotube dimension. Proc Natl Acad Sci U S A 2009;106(7):2130-5.

[214] Engler AJ, Sen S, Sweeney HL, Discher DE. Matrix elasticity directs stem cell lineage specification. Cell 2006;126(4):677-89.

[215] Khatiwala CB, Peyton SR, Metzke M, Putnam AJ. The regulation of osteogenesis by ECM rigidity in MC3T3-E1 cells requires MAPK activation. J Cell Physiol 2007;211(3):661-72.

[216] Khatiwala CB, Kim PD, Peyton SR, Putnam AJ. ECM compliance regulates osteogenesis by influencing MAPK signaling downstream of RhoA and ROCK. J Bone Miner Res 2009;24(5):886-98.

[217] Rowlands AS, George PA, Cooper-White JJ. Directing osteogenic and myogenic differentiation of MSCs: interplay of stiffness and adhesive ligand presentation. Am J Physiol Cell Physiol 2008;295(4):C1037-44.

[218] Kundu AK, Khatiwala CB, Putnam AJ. Extracellular matrix remodeling, integrin expression, and downstream signaling pathways influence the osteogenic differentiation of mesenchymal stem cells on poly(lactide-co-glycolide) substrates. Tissue engineering. Part A 2009;15(2):273-83.

[219] Appleford MR, Oh S, Cole JA, Carnes DL, Lee M, Bumgardner JD, et al. Effects of trabecular calcium phosphate scaffolds on stress signaling in osteoblast precursor cells. Biomaterials 2007;28(17):2747-53.

[220] Zhang W, Liao S, Cui F. Hierarchical self-assembly of nanofibrils in mineralized collagen. Chem Mater 2003;15(16):3221-6.

[221] Wei G, Ma P, J. Macroporous and nanofibrous polymer scaffolds and polymer/bone-like apatite composite scaffolds generated by sugar spheres. Mater Res 78A 2006;306

[222] Wang F, Li M, Lu Y, Qi Y, Liu Y. Synthesis and microstructure of hydroxyapatite nanofibers synthesized at 37ºC. Mater Chem Phys 2006;95(1):145-9.

[223] Wang L, Li C. Preparation and physicochemical properties of a novel hydroxyapatite/chitosan-silk fibroin composite. Carbohydrate Polym 2007;68(4):740-5.

[224] Taguchi T, Kishida A, Akashi M. Hydroxyapatite Formation on/in poly(vinyl alchohol) hydrogel matrices using a novel alternate soaking process. Chem Lett 1998;8:711-2.

[225] Chen J, Chu B, Hsiao BS. Mineralization of hydroxyapatite in electrospun nanofibrous poly(L-lactic acid) scaffolds. J Biomed Mater Res A 2006;79(2):307-17.

[226] Oyane A, Uchida M, Yokoyama Y, Choong C, Triffitt J, Ito A. Simple surface modification of poly(epsilon-caprolactone) to induce its apatite-forming ability. J Biomed Mater Res A 2005;75(1):138-45.

[227] Maeda H, Kasuga T, Hench LL. Preparation of poly(L-lactic acid)-polysiloxane-calcium carbonate hybrid membranes for guided bone regeneration. Biomaterials 2006;27(8):1216-22.

[228] Webster TJ, Ergun C, Doremus RH, Siegel RW, Bizios R. Enhanced functions of osteoblasts on nanophase ceramics. Biomaterials 2000;21(17):1803-10.

[229] Zhang W, Huang K, Liao S, Cui F. Nucleation sites of calcium phosphate crystals during collagen mineralization. Acta Neurochir Suppl 2003;86(6):1052-4.

[230] LeGeros RZ. Calcium phosphates in oral biology and medicine. In: Myers H, editor. Monographs in oral science. Basel, Karger; 1991

[231] Cui W, Li X, Zhou S, Weng J. In situ growth of hydroxyapatite within electrospun poly(DL-lactide) fibers. J Biomed Mater Res 2007;82A:831-41.

[232] Klein C, Driessen A, De Groot K, van den Hooff A. Biodegradation behavior of various calcium phosphate materials in bone tissue. J Biomed Mater Res 1983;17:769-82.

[233] He W, Yong T, Teo WE, Ma Z, Ramakrishna S. Fabrication and endothelialization of collagen-blended biodegradable polymer nanofibers: potential vascular graft for blood vessel tissue engineering. Tissue Eng 2005;11(9-10):1574-88.

[234] Chesnutt B, Viano A, Yuan Y, Yang Y, Guda T, Appleford M, et al. Design and characterization of a novel chitosan nanocrystalline calcium phosphate composite scaffold for bone regeneration. J Biomed Mater Res B Appl Biomater 2009;88(2):491-502.

[235] He W, Ma Z, Yong T, Teo WE, Ramakrishna S. Fabrication of collagen-coated biodegradable polymer nanofiber mesh and its potential for endothelial cells growth. Biomaterials 2005;26(36):7606-15.

[236] Zhang Y, Zhang M. Calcium phosphate/chitosan composite scaffolds for controlled in vitro antibiotic drug release. J Biomed Mater Res 2002;62(3):378-86.

[237] Manjubala I, Ponomarev I, Wilke I, Jandt KD. Growth of osteoblast-like cells on biomimetic apatite-coated chitosan scaffolds. J Biomed Mater Res B Appl Biomater

2008;84(1):7-16.

[238] Sinha RK, Morris F, Shah SA, Tuan RS. Surface composition of orthopaedic implant metals regulates cell attachment, spreading, and cytoskeletal organization of primary human osteoblasts in vitro. Clin Orthop Relat Res 1994;(305):258-72.

[239] Chim H, Hutmacher DW, Chou AM, Oliveira AL, Reis RL, Lim TC, et al. A comparative analysis of scaffold material modifications for load-bearing applications in bone tissue engineering. Int J Oral Maxillofac Surg 2006;35(10):928-34.

[240] Lohmann C, Bonewald L, Sisk M, Sylvia V, Cochran D, Dean D, et al. Maturation state determines the response of osteogenic cells to surface roughness and 1,25-dihydroxyvitamin D3. J Bone Miner Res 2000;15(6):1169-80.

[241] Martin JY, Dean DD, Cochran DL, Simpson J, Boyan BD, Schwartz Z. Proliferation, differentiation, and protein synthesis of human osteoblast-like cells (MG63) cultured on previously used titanium surfaces. Clin Oral Implants Res 1996;7(1):27-37.

[242] Manjubala I, Scheler S, Bössert J, Jandt KD. Mineralisation of chitosan scaffolds with nano-apatite formation by double diffusion technique. Acta Biomater 2006;2(1):75-84.

[243] Wei G, Ma PX. Structure and properties of nano-hydroxyapatite/polymer composite scaffolds for bone tissue engineering. Biomaterials 2004;25(19):4749-57.

[244] Venugopal J, Low S, Choon AT, Kumar AB, Ramakrishna S. Electrospun-modified nanofibrous scaffolds for the mineralization of osteoblast cells. J Biomed Mater Res A 2008;85(2):408-17.

[245] Black J, Hastings G. Handbook of Biomaterials Properties. : London, UK; 1998.

[246] Verfaillie CM. Adult stem cells: assessing the case for pluripotency. Trends Cell Biol 2002;12(11):502-8.

[247] Yoon SJ, Park KS, Kim MS, Rhee JM, Khang G, Lee HB. Repair of diaphyseal bone defects with calcitriol-loaded PLGA scaffolds and marrow stromal cells. Tissue Eng 2007;13(5):1125-33.

[248] Quarto R, Thomas D, Liang CT. Bone progenitor cell deficits and the age-associated decline in bone repair capacity. Calcif Tissue Int 1995;56(2):123-9.

[249] Dorozhkin S. Calcium orthophosphate cements for biomedical application. J Mater Sci 2008;43:3028-57.

[250] Ichinohe N, Takamoto T, Tabata Y. Proliferation, osteogenic differentiation, and distribution of rat bone marrow stromal cells in nonwoven fabrics by different culture methods. Tissue engineering. Part A 2008;14(1):107-16.

[251] Schneider OD, Loher S, Brunner TJ, Uebersax L, Simonet M, Grass RN, et al. Cotton wool-like nanocomposite biomaterials prepared by electrospinning: in vitro bioactivity and osteogenic differentiation of human mesenchymal stem cells. J Biomed Mater Res B Appl Biomater 2008;84(2):350-62.

[252] Müller P, Bulnheim U, Diener A, Lüthen F, Teller M, Klinkenberg ED, et al. Calcium phosphate surfaces promote osteogenic differentiation of mesenchymal stem cells. J Cell Mol Med 2008;12(1):281-91.

[253] Keselowsky BG, Collard DM, García AJ. Surface chemistry modulates fibronectin conformation and directs integrin binding and specificity to control cell adhesion. J Biomed Mater Res A 2003;66(2):247-59.

[254] Klees RF, Salasznyk RM, Kingsley K, Williams WA, Boskey A, Plopper GE. Laminin-5 induces osteogenic gene expression in human mesenchymal stem cells through an ERK-dependent pathway. Mol Biol Cell 2005;16(2):881-90.

[255] Salasznyk RM, Williams WA, Boskey A, Batorsky A, Plopper GE. Adhesion to Vitronectin and Collagen I Promotes Osteogenic Differentiation of Human Mesenchymal Stem Cells. Journal of biomedicine & biotechnology 2004;2004(1):24-34.

[256] Moursi AM, Globus RK, Damsky CH. Interactions between integrin receptors and fibronectin are required for calvarial osteoblast differentiation in vitro. J Cell Sci 1997;110(18):2187-96.

[257] Mata A, Kim EJ, Boehm CA, Fleischman AJ, Muschler GF, Roy S. A three-dimensional scaffold with precise micro-architecture and surface micro-textures. Biomaterials 2009;30(27):4610-7.

[258] Stein GS, Lian JB. Molecular mechanisms mediating proliferation/differentiation interrelationships during progressive development of the osteoblast phenotype. Endocr Rev 1993;14(4):424-42.

[259] Chou YF, Dunn JCY, Wu BM. In vitro response of MC3T3-E1 pre-osteoblasts within three-dimensional apatite-coated PLGA scaffolds. J Biomed Mater Res B Appl Biomater 2005;75(1):81-90.

[260] Deligianni DD, Katsala ND, Koutsoukos PG, Missirlis YF. Effect of surface roughness of hydroxyapatite on human bone marrow cell adhesion, proliferation, differentiation and detachment strength. Biomaterials 2001;22(1):87-96.

[261] Castano-Izquierdo H, Alvarez-Barreto J, van den Dolder J, Jansen JA, Mikos AG, Sikavitsas VI. Pre-culture period of mesenchymal stem cells in osteogenic media influences their in vivo bone forming potential. J Biomed Mater Res A 2007;82(1):129-38.

[262] Hu J, Feng K, Liu X, Ma PX. Chondrogenic and osteogenic differentiations of human bone marrow-derived mesenchymal stem cells on a nanofibrous scaffold with designed pore network. Biomaterials 2009;30(28):5061-7.

[263] Liu X, Ma PX. Phase separation, pore structure, and properties of nanofibrous gelatin scaffolds. Biomaterials 2009;30(25):4094-103.

[264] Cao H, Kuboyama N. A biodegradable porous composite scaffold of PGA/beta-TCP for bone tissue engineering. Bone 2010;46(2):386-95.

[265] Cao T, Ho KH, Teoh SH. Scaffold design and in vitro study of osteochondral coculture in a three-dimensional porous polycaprolactone scaffold fabricated by fused deposition modeling. Tissue Eng 2003;9 Suppl 1:S103-12.

[266] Seitz H, Rieder W, Irsen S, Leukers B, Tille C. Three-dimensional printing of porous ceramic scaffolds for bone tissue engineering. J Biomed Mater Res B Appl Biomater 2005;74(2):782-8.

[267] Teo W, Gopal R, Ramaseshan R, Fujihara K, Ramakrishna S. A dynamic liquid support system for continuous electrospun yarn fabrication. Polymer 2007;48(12):3400-5.

[268] Karageorgiou V, Kaplan D. Porosity of 3D biomaterial scaffolds and osteogenesis. Biomaterials 2005;26(27):5474-91.

[269] Johnstone B, Hering TM, Caplan AI, Goldberg VM, Yoo JU. In vitro chondrogenesis of bone marrow-derived mesenchymal progenitor cells. Exp Cell Res 1998;238:265-72.

[270] Clarke SA, Hoskins NL, Jordan GR, Marsh DR. Healing of an ulnar defect using a proprietary TCP bone graft substitute, JAX™, in association with autologous osteogenic cells and growth factors. Bone 2007;40:939-47.

[271] McLain RF, Fleming JE, Boehm CA, Muschler GF. Aspiration of osteoprogenitor cells for augmenting spinal fusion: comparison of progenitor cell concentrations from the vertebral body and iliac crest. J Bone Joint Surg Am 2005;87(12):2655-61.

[272] Qu X, Cui W, Yang F, Min C, Shen H, Bei J, et al. The effect of oxygen plasma pretreatment and incubation in modified simulated body fluids on the formation of bone-like apatite on poly(lactide-co-glycolide) (70/30). Biomaterials 2007;28(1):9-18.

[273] Kim SS, Park MS, Gwak SJ, Choi CY, Kim BS. Accelerated bonelike apatite growth on porous polymer/ceramic composite scaffolds in vitro. Tissue Eng 2006;12(10):2997-3006.

[274] Suchanek W, Yoshimura M. Processing and properties of hydroxyapatite-based biomaterials for use as hard tissue replacement implant. J.Mater.Res 1998;13(1):94-117.

[275] Yuen Cheng Fung. Biomechanics: Mechanical Properties of Living Tissues. Springer-Verlag Inc: New York; 1993.

[276] Pountos I, Corscadden D, Emery P, Giannoudis PV. Mesenchymal stem cell tissue engineering: techniques for isolation, expansion and application. Injury 2007;38 Suppl 4:S23-33.

[277] Muschler GF, Midura RJ. Connective tissue progenitors: practical concepts for clinical applications. Clin Orthop Relat Res 2002;(395):66-80.

[278] Connolly J, Guse R, Lippiello L, Dehne R. Development of an osteogenic bone-marrow preparation. J Bone Joint Surg Am 1989;71(5):684-91.

[279] Connolly JF, Guse R, Tiedeman J, Dehne R. Autologous marrow injection as a substitute for operative grafting of tibial nonunions. Clin Orthop Relat Res 1991;(266):259-70.

[280] Neen D, Noyes D, Shaw M, Gwilym S, Fairlie N, Birch N. Healos and bone marrow aspirate used for lumbar spine fusion: a case controlled study comparing healos with autograft. Spine 2006;31(18):E636-40.

[281] Muschler GF, Nitto H, Matsukura Y, Boehm C, Valdevit A, Kambic H, et al. Spine fusion using cell matrix composites enriched in bone marrow-derived cells. Clin Orthop Relat Res 2003;(407):102-18.

[282] Muschler GF, Matsukura Y, Nitto H, Boehm CA, Valdevit AD, Kambic HE, et al. Selective retention of bone marrow-derived cells to enhance spinal fusion. Clin Orthop Relat Res 2005;(432):242-51.

[283] No.12 US5824084 muschler method of preparing a composite bone graft.

[284] No.13 US6049026 muschler apparatus and methods for preparing an implantable graft.

[285] Benoit DSW, Anseth KS. The effect on osteoblast function of colocalized RGD and PHSRN epitopes on PEG surfaces. Biomaterials 2005;26(25):5209-20.

[286] Wilson CJ, Clegg RE, Leavesley DI, Pearcy MJ. Mediation of biomaterial-cell interactions by adsorbed proteins: a review. Tissue Eng 2005;11(1-2):1-8.

[287] Tsai WB, Ting YC, Yang JY, Lai JY, Liu HL. Fibronectin modulates the morphology of osteoblast-like cells (MG-63) on nano-grooved substrates. J Mater Sci Mater Med 2009;20(6):1367-78.

[288] Moroni L, Licht R, de Boer J, de Wijn JR, van Blitterswijk CA. Fiber diameter and texture of electrospun PEOT/PBT scaffolds influence human mesenchymal stem cell proliferation and morphology, and the release of incorporated compounds. Biomaterials 2006;27(28):4911-22.

[289] Lim JY, Dreiss AD, Zhou Z, Hansen JC, Siedlecki CA, Hengstebeck RW, et al. The

regulation of integrin-mediated osteoblast focal adhesion and focal adhesion kinase expression by nanoscale topography. Biomaterials 2007;28(10):1787-97.

[290] Quarto R, Mastrogiacomo M, Cancedda R, Kutepov SM, Mukhachev V, Lavroukov A, et al. Repair of large bone defects with the use of autologous bone marrow stromal cells. N Engl J Med 2001;344(5):385-6.

[291] De Long WG, Einhorn TA, Koval K, McKee M, Smith W, Sanders R, et al. Bone grafts and bone graft substitutes in orthopaedic trauma surgery. A critical analysis. J Bone Joint Surg Am 2007;89(3):649-58.

[292] Guo X, Wang XF. Signaling cross-talk between TGF-beta/BMP and other pathways. Cell Res 2009;19(1):71-88.

[293] Medtronic INFUSE bone graft. http://www.medtronic.com/for-healthcare-professionals/products-therapies/spinal-orthopedics/bone-graft-options/infuse-bone-graft/index.htm

[294] Stryker OP-1. http://www.stryker.com/en-us/products/Orthobiologicals/Osteoinductive/OP-1/index.htm

[295] Kokubo S, Fujimoto R, Yokota S, Fukushima S, Nozaki K, Takahashi K, et al. Bone regeneration by recombinant human bone morphogenetic protein-2 and a novel biodegradable carrier in a rabbit ulnar defect model. Biomaterials 2003;24(9):1643-51.

[296] Zhang P, Hong Z, Yu T, Chen X, Jing X. In vivo mineralization and osteogenesis of nanocomposite scaffold of poly(lactide-co-glycolide) and hydroxyapatite surface-grafted with poly(L-lactide). Biomaterials 2009;30(1):58-70.

[297] Zegzula HD, Buck DC, Brekke J, Wozney JM, Hollinger JO. Bone formation with use of rhBMP-2 (recombinant human bone morphogenetic protein-2). J Bone Joint Surg Am 1997;79(12):1778-90.

[298] El-Ghannam A, Cunningham L, Pienkowski D, Hart A. Bone engineering of the rabbit ulna. J Oral Maxillofac Surg 2007;65(8):1495-502.

[299] Meikle MC, Papaioannou S, Ratledge TJ, Speight PM, Watt-Smith SR, Hill PA, et al. Effect of poly DL-lactide--co-glycolide implants and xenogeneic bone matrix-derived growth factors on calvarial bone repair in the rabbit. Biomaterials 1994;15(7):513-21.

[300] Li RH, Bouxsein ML, Blake CA, D'Augusta D, Kim H, Li XJ, et al. rhBMP-2 injected in a calcium phosphate paste (alpha-BSM) accelerates healing in the rabbit ulnar osteotomy model. J Orthop Res 2003;21(6):997-1004.

[301] Miyamoto S, Takaoka K, Okada T, Yoshikawa H, Hashimoto J, Suzuki S, et al. Evaluation of polylactic acid homopolymers as carriers for bone morphogenetic protein. Clin Orthop Relat

Res 1992;(278):274-85.

[302] Ramakrishna S, Fujihara K, Teo W, Yong T, Ma Z, Ramaseshan R. Electrospun nanofibers: solving global issues. Mater. Today 2006;9(3):49-50.

Appendices

Appendix A

Sample Preparation for Scanning Electron Microscopy Observations

SEM imaging was conducted on scaffolds with or without cells at various time points of the study.

1. Wash samples with PBS thrice.
2. Samples with cells were fixed in 4% paraformaldehyde solution for 30 minutes at room temperature.
3. Wash samples with PBS thrice.
4. Samples were dehydrated serially in various ethanol concentrations, first in 50% and incubated for 10 minutes in room temperature
5. Next, samples were subsequently incubated in 70%, 95%, 100% (twice) for 10 minutes respectively at room temperature.
6. Samples were subsequently air-dried overnight and then gold-coated prior to SEM observation

Appendix B

Haematoxylin and Eosin (H&E) Staining Method

Technique

Step	Station	Reagent	Time	Exact
1	1	Xylene	5 mins	No
2	2	Xylene	5 mins	No
3	3	100% isopropanol	2 mins	No
4	4	100% isopropanol	2 mins	No
5	5	100% isopropanol	2 mins	No
6	6	95% isopropanol	2 mins	No
7	7	70% isopropanol	2 mins	No
8	Wash 1	Water	2 mins	No
9	8	Haematoxylin	4 mins	Yes
10	Wash 5	Water	2 mins	No
11	9	Clarifier 2	2 mins	Yes
12	Wash 4	Water	2 mins	No
13	10	Bluing solution	2 mins	Yes
14	Wash 3	Water	2 mins	No
15	11	70% alcohol	2 mins	No
16	12	Eosin Y	2 mins	Yes
17	13	70% isopropanol	2 mins	Yes
18	14	95% isopropanol	2 mins	Yes
19	15	100% isopropanol	2 mins	No
20	16	100% isopropanol	2 mins	No
21	17	100% isopropanol	2 mins	No
22	18	Xylene	2 mins	No
23	Exit	Xylene	NA	NA

Results

Nuclei ---------- blue to blue black (stained by Hematoxylin)
Cytoplasm ---------- pink (stained by Eosin)

Appendix C

Masson Trichrome Staining Method

Solution Preparation

Chromotrope 2R ---------- 0.6 g
Fast green FCF ---------- 0.3 g
Phosphotungstic acid ------ 0.6 g
Glacial acetic acid ---------- 1 ml
Distilled water ---------- 100 ml

0.2% glacial acetic acid

Technique

1. Sections to water.
2. Stain nuclei with an alum hematoxylin.
3. Differentiate in acid-alcohol and blue as in the standard technique.
4. Wash well in tap water, then in distilled water.
5. Stain in the Gomori solution 5 to 20 minutes.
6. Rinse well in the acetic acid solution.
7. Blot dry, dehydrate, clear and mount as desired.

Results

Nuclei ---------- Grey-blue
Collagen ---------- Green
Muscle, cytoplasm, red blood cells, fibrin ---------- Red

Appendix D

Von Kossa Staining Method

Technique

1. Rinse slides well in deionized water.
2. Incubate slides in 5% silver nitrate under UV lights for 30 minutes.
3. Rinse slides well in deionized water.
4. Incubate slides in 5% sodium thiosulfate for 30 seconds.
5. Rinse in tap water
6. Counterstain with toluidine blue for 30 seconds.
7. Rinse well in tap water
8. Dehydrate with 95% ethanol
9. Dehydrate with 100% ethanol
10. Clear in xylene

Results

Minerals ---------- Brown